

# **A beam finite element for the analysis of structures in fire**

by Richard Shaun Walls



Dissertation presented for the Degree of Doctor of Philosophy  
in the Faculty of Engineering, at Stellenbosch University

Supervisor: Dr Celeste Viljoen

Co-supervisor: Dr Hennie de Clercq

December 2016

## **Declaration**

By submitting this dissertation electronically, I declare that the entirety of the work contained therein is my own original work, that I am the authorship owner thereof (unless to the extent explicitly otherwise stated) and that I have not previously in its entirety or in part submitted it for obtaining any qualification.

Signature:

Date:

Copyright © 2016 Stellenbosch University of Stellenbosch

All rights reserved

## Abstract

All building structures require a specified fire resistance rating and numerous procedures have been produced for ensuring this. In engineering practice designers can generally not perform detailed structural fire designs on buildings due to the high computational modelling requirements of most modern structures, and so they typically resort to conservative prescriptive methods instead. Hence, design engineer orientated methods are required to improve fire safety while providing more economical buildings. The goal of this dissertation is to provide a simple, but technically accurate, model for the analysis of structures in fire, including composite structures, which considers buildings as skeletal frames.

To achieve this end a beam finite element has been developed that has a moving, eccentric neutral axis that accounts for material properties that change as structures heat up. A composite bending stiffness, axial stiffness and resultant thermal forces are calculated for a generic cross-section. Material and geometric nonlinearity is considered. The properties of any number of materials (e.g. a steel beam, concrete slab and reinforcing steel) are represented by single beam properties. These calculated beam properties can be included in either commercially available, but simple, finite element software or advanced finite element modelling tools. The only assumption required is that Euler-Bernoulli behaviour, where plane sections remain plane, must hold. A methodology for including rebar tension stiffening at elevated temperatures has been included based on modifying an ambient temperature model.

A series of numerical case studies are presented, comparing the results of the proposed beam formulation against finite element models using shell elements. Results between these models (which includes deflections, stresses, strains and neutral axis positions) typically differ by 0-5% when Euler-Bernoulli assumptions hold. Furthermore, case studies and experimental results from real fire tests in the literature were also analysed by the proposed formulation coupled with relatively simple finite element software. The deflections of structures in fire predicted by the proposed model are well within acceptable tolerances for fire engineering systems, and typically comparable to more complex models in the literature. The model developed has been used to investigate eleven different beams consisting of steel beams, concrete slabs and composite steel-concrete beams, along with conducting a series of parametric studies. With further research and the inclusion of three-dimensional behaviour the method could become a valuable tool for the analysis of structures in fire.

## Opsomming

Alle geboustrukture vereis 'n bepaalde brandbestandheid gradering en talle prosedures bestaan om dit te verseker. Ontwerpers in ingenieurspraktyk is in die algemeen nie in staat om gedetailleerde rasionale brand ontwerpe vir strukture uit te voer nie, as gevolg van die hoë numeriese modellering vereistes vir meeste moderne strukture. Daarom gebruik ingenieurs tipies konserwatiewe voorskriftelike metodes. Dus is eenvoudiger, ontwerp-georiënteerde modellering metodes nodig om brandveiligheid te verbeter terwyl meer ekonomiese geboue verskaf word. Die doel van hierdie verhandeling is om 'n eenvoudiger, maar tegnies akkuraat, model vir die analiese van strukture, insluitend saamgestelde strukture, in brande te voorsien waarin geboue as skeletale rame beskou word.

Om hierdie doel to bereik is 'n balk eindige element ontwikkel wat 'n bewegende, eksentriese neutrale as (NA) gebruik om die veranderinge in die eienskappe van materiale in ag te neem. 'n Saamgestelde buigingstyfheid, aksialestyfheid en resulterende temperatuurkragte word vir 'n generiese dwarsnit bereken. Materiaal en geometriese nie-lineariteit is beskou. Die eienskappe van 'n aantal materiale (bv. 'n staalbalk, betonblad en bewapeningstaal) word deur enkele balk eienskappe verteenwoordig. Hierdie berekende balk eienskappe kan ingesluit word in kommersiël beskikbare, maar eenvoudige, eindige element sagteware, of gevorderde eindige element modellering gereedskap. Die enigste benodigde aanname is dat Euler-Bernoulli gedrag, waar 'n gegewe dwarsnit in 'n enkele vlak bly, moet gebruik word in die analiese. 'n Metode vir die insluiting van bewapeningstaal trekspanning verstywing by hoë temperature is ingesluit, wat ontwikkel is deur 'n wysiging van 'n kamertemperatuur model.

'n Aantal numeriese gevallestudies word aangebied. Resultate van die metode en 'n Abaqus model met gebruik van dop elemente is vergelyk. Die resultate van die modelle (wat defleksies, spanning, vervorming en NA posisies insluit) is tipies binne 0-5% van mekaar wanneer Euler-Bernoulli aannames gebruik word. Verder is gevallestudies en eksperimentele resultate uit die literatuur ook geanaliseer met gebruik van die metode gekoppel met relatief eenvoudige eindige element sagteware. Die defleksies vir brand situasies soos bereken met gebruik van die voorgestelde model is binne aanvaarbare toleransies vir brand ingenieurswese stelsels, en is tipies vergelykbaar met meer komplekse modelle uit die literatuur. Die voorgestelde model is gebruik om elf verskillende balke, wat bestaan uit staal balke, betonblaai en saamgestelde balke, te ondersoek. 'n Reeks van parametries studies is ook uitgevoer. Met verdere navorsing en die insluiting van driedimensionele gedrag kan die metode 'n waardevolle hulpmiddel word vir die analiese van strukture in 'n brande.



## Acknowledgements

I would like to thank the following people for the significant contributions made towards this work:

- My supervisors, Dr Celeste Viljoen and Dr Hennie de Clercq, for their help, assistance and unending patience during the process of this research. Their guidance made a tremendous impact on this dissertation. Also, without Hennie's crazy idea of getting fire engineering going in South Africa who knows where we would be now.
- Prof Johan Retief for his mentorship and guidance kindly provided over the past years, even before I joined Stellenbosch. He was very instrumental in setting up this PhD, as well as providing insight and assistance throughout.
- My colleagues in the Department of Civil Engineering.
- To Prof Charles Clifton for the discussions, documents and feedback over the past few years.
- To my parents for their support and encouragement over many years of study, and providing the opportunities that they did.
- To my wife, Merryn, for her unending love, patience and help over the past years, even when things got tough. Without her support I would not have been able to do this. And also to our first child who is on his/her way, making sure that there was a definite deadline for the submission of this dissertation.

“For God so loved the world that he gave his one and only Son,  
that whoever believes in him shall not perish but have eternal life.”

– Jesus (John 3:16)

# Table of Contents

Declaration .....	ii
Abstract .....	iii
Opsomming .....	iv
Acknowledgements .....	v
List of figures .....	xiii
List of tables .....	xix
List of abbreviations .....	xx
List of symbols .....	xxi
1 Chapter 1: Introduction.....	1
1.1 Background to study.....	1
1.2 Overview .....	2
1.3 Research objectives .....	4
1.4 Scope of the work.....	5
1.5 Outline of dissertation .....	5
2 Chapter 2: Literature Review .....	8
2.1 Introduction .....	8
2.2 Fire engineering and the role of structural fire design.....	8
2.2.1 Fire and society.....	8
2.2.2 Objectives of structural fire engineering .....	9
2.2.3 Fire design codes .....	10
2.2.4 Limit state design .....	10
2.3 Important concepts in fire design .....	11
2.3.1 The standard fire and fire resistance ratings .....	11
2.3.2 “Real” fire models .....	12
2.3.3 Considering “consistent levels of crudeness” .....	13
2.3.4 Prescriptive versus performance-based design.....	14
2.3.5 Active and passive protection of structures .....	15

2.3.6	Compartmentation .....	15
2.4	Structural behaviour in fire.....	16
2.4.1	Thermally induced effects .....	16
2.4.2	Temperature gradients in cross-sections.....	17
2.4.3	Real fires in real buildings.....	17
2.4.4	Full-scale fire tests.....	18
2.4.5	The Cardington fire tests .....	19
2.4.6	Composite floors in fire.....	19
2.4.7	Connection behaviour in fire .....	22
2.4.8	Composite structure modelling considerations.....	24
2.4.9	Design engineer considerations .....	26
2.5	Finite element modelling of elements in fire.....	27
2.6	Current structural fire design methodologies and software .....	28
2.6.1	General purpose finite element software .....	28
2.6.2	SAFIR.....	28
2.6.3	Stadler's analysis model .....	28
2.6.4	Vulcan.....	28
2.6.5	Other software available for fire design .....	29
2.7	Summary.....	29
2.7.1	Finite element formulation adopted in this work as compared to the literature .....	30
2.7.2	Design assumptions adopted for the FBE formulation.....	31
3	Chapter 3: Fundamental methodology and structural mechanics procedure developed for analysing structures in fire using beam elements .....	32
3.1	Introduction .....	32
3.1.1	Academic contribution .....	32
3.2	Strains in fire .....	33
3.3	Behaviour of a uni-axially loaded and uniformly heated beam.....	33
3.4	Non-uniform heating of beams and the resulting behaviour .....	36
3.4.1	Verification example .....	40

3.5	Analysing structures using multiple beam elements .....	41
3.6	Considering movable, eccentric neutral axes .....	42
3.6.1	The need for a composite finite element that accounts for changing NA position.....	42
3.6.2	Composite FE challenges encountered when eccentricities are not considered .....	44
3.6.3	Including eccentric neutral analyses in finite element models .....	45
3.6.4	Design philosophy and formulation of beam elements .....	45
3.7	Calculating resultant thermal strain effects in non-uniform sections .....	47
3.8	Design and analysis philosophy employed.....	48
3.8.1	Iterative procedure for determining member properties .....	48
3.8.2	Analysis procedure .....	49
3.8.3	Modelling formulation.....	51
3.9	Simplified implementation of the FBE formulation.....	55
3.10	Overview of the benefits and limitations of the FBE formulation .....	57
3.10.1	Advantages of the FBE formulation.....	57
3.10.2	Limitations of the proposed FBE model.....	58
3.11	Conclusion.....	59
4	Chapter 4: Formulation and verification of the analysis procedure for beams with eccentric neutral axis positions.....	61
4.1	Introduction .....	61
4.1.1	Academic contribution .....	61
4.2	Eccentric beam element formulation and analysis theory .....	61
4.2.1	Fundamental theory .....	61
4.2.2	Iterative procedure for the determination of section properties.....	63
4.2.3	Derivation of the eccentric neutral axis stiffness matrix .....	65
4.2.4	Unbalanced Forces .....	68
4.3	Methodology verification and case studies .....	69
4.3.1	Case Study A: IPE 200 cantilever with non-linear material properties .....	71
4.3.2	Case Study B: Rectangular beam with material non-linearity.....	75
4.3.3	Case Study C: Fixed-fixed IPE 200.....	78

4.3.4	Case Study D: Fixed-fixed rectangular beam with variation in material properties.....	80
4.4	Conclusion.....	83
5	Chapter 5: Developing input parameters for beam elements in fire – material models, tension stiffening and temperature profiles .....	85
5.1	Introduction .....	85
5.1.1	Academic contribution .....	86
5.2	Structural steelwork in fire .....	86
5.2.1	Elongation of structural and reinforcing steels.....	86
5.2.2	Specific heat of steelwork.....	87
5.2.3	Thermal conductivity.....	88
5.2.4	Structural properties .....	88
5.2.5	Temperatures used in analysis models .....	91
5.2.6	Reinforcing steel in fire .....	92
5.3	Concrete in fire .....	92
5.3.1	Concrete models in structural fire engineering literature .....	92
5.3.2	Structural properties of concrete.....	93
5.3.3	Thermal properties of concrete.....	97
5.3.4	Temperature profiles in concrete slabs.....	99
5.3.5	Consideration of ribbed slabs .....	101
5.3.6	Effective width of concrete flanges .....	103
5.4	Tension stiffening.....	104
5.4.1	Tension stiffening models presented in the literature.....	105
5.4.2	Tension stiffening at ambient temperature .....	107
5.4.3	Modifications to account for elevated temperatures.....	110
5.4.4	Effective / reduced tension stiffening areas.....	111
5.4.5	Illustrating the influence of tension stiffening.....	115
5.5	Conclusion.....	116
6	Chapter 6: Validation by comparison with experimental and numerical studies .....	118
6.1	Introduction .....	118

6.1.1	Academic contribution .....	119
6.2	Modelling specifications .....	119
6.3	Case Study 1: Uniformly heated simply-supported steel beam.....	120
6.3.1	Experimental setup .....	120
6.3.2	Results and discussion .....	120
6.4	Case Study 2: Single span 1200x200 concrete slab.....	121
6.4.1	Experimental setup .....	121
6.4.2	Results and discussion .....	122
6.5	Case Study 3: Unprotected composite beams – “Test 15” and “Test 16” .....	124
6.5.1	Experimental setup .....	124
6.5.2	Results and discussion .....	128
6.6	Case Study 4: Munich Test 2.....	130
6.6.1	Experimental setup and overview.....	130
6.6.2	Technical details .....	131
6.6.3	Results and discussion .....	136
6.7	Conclusions .....	138
7	Chapter 7: Parametric Investigation .....	140
7.1	Introduction .....	140
7.1.1	Academic contribution .....	141
7.2	Considering material properties and their effects .....	141
7.3	Parametric study of a steel beam .....	142
7.3.1	Temperature and temperature gradients .....	142
7.3.2	Axial / restraining forces .....	144
7.4	Parametric study of a concrete slab .....	146
7.4.1	Stress and strain profiles.....	147
7.4.2	Concrete tensile capacity and tension stiffening .....	151
7.4.3	Concrete compressive strength.....	154
7.4.4	Temperature profiles.....	155
7.4.5	Axial restraint .....	156

7.5	Parametric study of a composite beam.....	158
7.5.1	Stress and strain profiles.....	160
7.5.2	Concrete tensile capacity and tension stiffening .....	162
7.5.3	Width of the concrete flange .....	166
7.5.4	The influence of restraint.....	168
7.6	Summary of results and conclusions .....	169
8	Chapter 8: Conclusions.....	172
8.1	Overview .....	172
8.2	Consideration of objectives .....	172
8.3	Findings.....	174
8.3.1	Modelling methodology .....	174
8.3.2	Finite element formulation .....	174
8.3.3	Experimental validation study .....	175
8.3.4	The application of engineering judgment.....	176
8.3.5	Composite beam concrete flange widths.....	176
8.3.6	Restraint against thermal expansion .....	176
8.3.7	Stress-strain behaviour in beams in fire .....	176
8.3.8	Concrete tensile capacity and tension stiffening .....	177
8.4	Future research .....	177
8.5	Closing comments .....	179
9	Appendix A – Concrete heat transfer model .....	180
10	Appendix B – Additional case study data .....	181
10.1	Validation studies from Chapter 4.....	181
10.1.1	Case Study A: IPE 200 cantilever with non-linear material properties.....	181
10.1.2	Case Study B: Rectangular beam with material non-linearity.....	181
10.1.3	Case Study C: Fixed-fixed IPE 200.....	182
10.1.4	Case Study D: Fixed-fixed rectangular beam with variation in material properties.....	183
10.2	Validation studies from Chapter 6.....	183
10.2.1	Case Study 1: Uniformly heated simply-supported steel beam.....	183

10.2.2	Case Study 2: Single span 1200x200 concrete slab.....	185
10.2.3	Case Study 3: Unprotected composite beams – “Test 15” and “Test 16” .....	186
10.2.4	Case Study 4: Munich Test 2.....	188
11	References .....	191



## List of figures

Figure 1.1: Design and analysis models available for structural fire engineering showing the position of the FBE formulation (adapted from Stadler (2012) with FE model picture from Clifton (2014)).....	3
Figure 1.2: Structure adopted for dissertation to address overall objectives .....	7
Figure 2.1: Time-temperature curves of the standard, external and hydrocarbon fires .....	12
Figure 2.2: Time-temperature behaviour of a real fire .....	12
Figure 2.3: Testing and modelling regimes in fire engineering with their associated level of credibility according to Gales et al (2012). Letters in brackets cite works listed in the original paper. ....	14
Figure 2.4: Market share in the UK of various fire protection systems (Tata Steel & BCSA 2013) .....	15
Figure 2.5: Failed column and beams at the Cardington fire tests (Lamont 2001) .....	19
Figure 2.6: Change in load carrying behaviour for a composite floor exposed to increasing temperatures (Bailey 2002).....	20
Figure 2.7: Deflected shape of a composite structure considered by Clifton (2014) in the development of the Slab Panel Method (SPM).....	21
Figure 2.8: Potential failure mechanisms in slab panels with various boundary conditions (Abu & Burgess, 2010).....	21
Figure 2.9: Moment-rotation behaviour of a variety of steel connections in fire (Al-Jabri 1999) .....	23
Figure 2.10: Behaviour of an end plate connections at 450°C – experimental and numerical results (Anderson 2011).....	23
Figure 2.11: Finite element configurations commonly used in the nonlinear analysis of composite slabs (Stadler 2012).....	25
Figure 2.12: In (a) a typical simply-supported slab is shown in which tensile membrane action can easily develop. However, in (b) offset columns and irregular bay sizes are experienced which may cause problems in the development of tensile membrane action (Flint et al. 2013). ....	27
Figure 3.1: Behaviour of a uni-axially loaded beam subjected to mechanical and thermal loads.....	34
Figure 3.2: Analysis Step (a) – Rectangular beam with mechanical load applied .....	37
Figure 3.3: Analysis Step (b) – Uniform increase in temperature of a portion of the beam, with no shear strength assumed for the section.....	37
Figure 3.4: Analysis Step (c) - Upward curvature of beam due to cross-sectional restraint .....	37
Figure 3.5: Analysis Step (d) – Converting temperature effects into resultant RTSL/M forces .....	38
Figure 3.6: Analysis Step (e) – Calculation of deflections based on applied forces .....	38
Figure 3.7: Analysis Step (f) – Determination of mechanical strains from total strains .....	39
Figure 3.8: Analysis Step (g) – Calculation of mechanical stresses based on mechanical strains .....	39
Figure 3.9: Stresses in a rectangular cantilever with the lower two-fifths uniformly heated .....	40
Figure 3.10: Analysis model for a cantilever with a uniformly heated lower portion.....	41
Figure 3.11: Fixed-fixed beam with uniformly heated lower portion resulting in no deformation.....	42

Figure 3.12: Changes in neutral axis and bending stiffness of an IPE 200 due to the Young's modulus varying .....	43
Figure 3.13: Relationship between the upward thermal curvature / bowing and steel temperature of a composite beam with variable slab thickness (Bailey 1995). Note how the scenario with $h = 0\text{mm}$ (no slab) has the maximum upward deflection when in reality it should have zero deflection.....	44
Figure 3.14: Cantilever beam with the lower portion uniformly heated, an end point load and with material properties dependent on strain and temperature .....	45
Figure 3.15: Design procedure for using the eccentric beam formulation .....	46
Figure 3.16: Temperature, thermal strain, Young's modulus and ETS profiles over the height of a composite section used for determining $N_{\theta}$ and $M_{\theta}$ values. ....	48
Figure 3.17: Flowchart illustrating the iterative procedure used for determining the non-linear properties of cross-sections exposed to fire .....	49
Figure 3.18: Flowchart for the nonlinear analysis of structures subjected to mechanical and thermal loads (the latter can be neglected as required) (based on Iu & Chan (2004)) .....	50
Figure 3.19: Typical layout and details considered for the design of a composite structure.....	51
Figure 3.20: Analysis and design of slab panels independent of primary beams. Yield line patterns are used to determine the loading for subsequent steps.....	52
Figure 3.21: Analysis model of the composite system.....	53
Figure 3.22: Typical temperature profile in a composite slab exposed to fire .....	53
Figure 3.23: Analysis model showing eccentric neutral axis positions, calculated bending moments and general structural behaviour .....	55
Figure 3.24: Modelling methodology and steps for analysing beams in fire using commercial FE software... ..	56
Figure 4.1: Variation in Young's modulus and strain across a composite section, showing section discretisation to account for such behaviour.....	63
Figure 4.2: Flow diagram for the determination of the updated neutral axis and stiffness values of a beam cross-section .....	65
Figure 4.3: Layout showing how a beam is modelled along a reference axis but has an updated neutral axis about which the beam deforms.....	66
Figure 4.4: Relationship between reference axis and deformed configuration .....	66
Figure 4.5: (a) Plane element before deformations, but noting global degrees of freedom (XY axis). (b) The element after deformation and motion showing deformations in the local ( $x'y'$ ) axis (based on Cook et al (2001)).....	69
Figure 4.6: Stress-strain relationships for the theoretical material model used.....	71
Figure 4.7: Case Study A - Simple cantilever .....	72
Figure 4.8: Analysis behaviour and considerations for Case Study A .....	73
Figure 4.9: Vertical deflections of Case Study A with increasing end moment with $E_0 = 200\text{ GPa}$ .....	74
Figure 4.10: Vertical deflections of the simple cantilever with increasing end moment with $E_0 = 20\text{ GPa}$ .....	74

Figure 4.11: Vertical deflection of the simple cantilever with end moment, shear and axial forces applied....	75
Figure 4.12: Case Study B - 5x300 rectangular beam with a UDL showing the Abaqus and final FBE model	76
Figure 4.13: Stresses over cross-sections at various positions for Case Study B.....	76
Figure 4.14: Deflection with increasing load for Case Study B.....	77
Figure 4.15: Isoline strain plot for Case Study B. The central green line of zero strain represents the NA.....	78
Figure 4.16: Case Study C – Fixed-fixed IPE 200 showing structural layout and final FBE configuration.....	79
Figure 4.17: Deflected shape and maximum stresses in the Abaqus model of Case Study C.....	79
Figure 4.18: Stress profiles for Case Study C at various location.....	80
Figure 4.19: Rectangular beam with UDL. The Young's modulus is varied to create stiffer zones internally.	81
Figure 4.20: Half of the Abaqus model of Case Study D showing longitudinal strains in the section.....	82
Figure 4.21: Cross-sectional strain profile for Case Study D at different locations.....	82
Figure 4.22: Deflection of Case Study D with increasing load.....	83
Figure 5.1: Steel thermal elongation as a function of temperature.....	87
Figure 5.2: Specific heat of steel as a function of temperature.....	88
Figure 5.3: Thermal conductivity as a function of temperature.....	88
Figure 5.4: Reduction factors for various steel properties at elevated temperatures.....	89
Figure 5.5: Stress-strain curve for steelwork at elevated temperature including strain-hardening (ECCS 2001) .....	90
Figure 5.6: Equivalent thermal stress to cause thermal elongation in unrestrained steelwork.....	91
Figure 5.7: Non-uniform variation in steel temperature over the length of beams in structures (Franssen & Vila Real 2010).....	92
Figure 5.8: Stress-strain curves according to EN 2-1-1 (BSI 2004) accounting to the confinement of concrete, comparing confined and unconfined concrete samples.....	94
Figure 5.9: Stress-strain model of concrete at elevated temperatures according to EN 2-1-2 (BSI 2005a).....	95
Figure 5.10: Comparison of stress-strain and $E_{\text{secant}}$ -strain for EN 2-1-1 and EN 2-1-2 for $f_{\text{cm}} = 30\text{MPa}$ at ambient temperature.....	96
Figure 5.11: Thermal elongation of siliceous and calcareous concrete to EN 2-1-2 (BSI 2005a).....	97
Figure 5.12: Specific heat of concrete as a function of temperature according to EN 2-1-2 (BSI 2005a), with moisture contents, $u$ , of 0%, 1.5% and 3%.....	98
Figure 5.13: Upper and lower limits of thermal conductivity according to EN 2-1-2 (BSI 2005a).....	99
Figure 5.14: Comparison of temperature profiles in a 100mm concrete slab after a 30, 60 and 120 minute fire according to (a) EN 2-1-2, (b) EN 4-1-2, (c) Wickström, and (d) a FEA model developed in this research..	101
Figure 5.15: Sheet profiles for ribbed composite slabs and their equivalent thicknesses.....	102
Figure 5.16: Temperature profiles in a profiled slab, illustrating (a) the actual profiles, (b) the simplified profile adopted in this research and by Stadler (2012), and (c) an alternative formulation that could be used in this research for 2D temperature profiles.....	103
Figure 5.17: Stages of cracking in a reinforced concrete section (Deeny 2010).....	105

Figure 5.18: Tension stiffening model for concrete developed by Deeny (2010).....	106
Figure 5.19: Load-strain relationship of a reinforced concrete sample under tensile loading (fib 2010a).....	107
Figure 5.20: Effective concrete areas of reinforced elements in tension: (a) beams, (b) slabs, and (c) member in tension (fib 2010a).....	109
Figure 5.21: Load-strain relationship of a reinforced concrete sample under tensile loading, including the modified graph for cracking load exceeding the rebar yield load .....	110
Figure 5.22: Load-strain graph to illustrate changing properties with increasing temperature .....	111
Figure 5.23: Change in the tension stiffening area for rebar due to the complex strain profiles of concrete slabs in fire. ....	112
Figure 5.24: Graph of axial load to axial stiffness and rebar strain of a 100x100 concrete section in which both tension stiffening (T.S.) and no tension stiffening (No T.S.) are considered .....	116
Figure 6.1: Case study of a simply-supported steel beam subject to a UDL with varying levels of discretisation .....	121
Figure 6.2: Slab layout for tests conducted by Ali et al (2008).....	122
Figure 6.3: Deflection results of the test, Ali et al's numerical model (2008), and the proposed FBE model	123
Figure 6.4: Position of the NA from the slab soffit and magnitude of the bending stiffness ( $EI_{\theta}$ ) along the length of the slab at 60 minutes. ....	124
Figure 6.5: Experimental setup for Test 15 and 16 (reproduced from Wainman & Kirby (1988)).....	125
Figure 6.6: Temperatures of elements for Test 15.....	126
Figure 6.7: Temperatures of elements for Test 16.....	126
Figure 6.8: Finite element modelling philosophy employed by OpenSEES (Jiang et al. 2014) .....	127
Figure 6.9: Deflection vs. time results for Test 15 showing experimental results, the FBE results and results from Jiang et al (2014) .....	128
Figure 6.10: Deflection vs. time results for Test 16 showing experimental results, the FBE results and results from Jiang et al (2014) .....	129
Figure 6.11: Second Munich test experimental layout.....	130
Figure 6.12: Finite element model developed by Stadler (2012) for the Second Munich Test.....	131
Figure 6.13: Temperatures in the Second Munich Test for steel beams (Mensingher et al. 2012; Stadler 2012) .....	133
Figure 6.14: Concrete slab temperature profile at 40 minutes.....	133
Figure 6.15: Loading on beams for the Second Munich test showing yield line patterns considered.....	135
Figure 6.16: Comparison of deflections between experimental data (EXPERIM.), predictions by Stadler (2012) and the FBE formulation (FBE). All readings are vertical deflections in mm. Additional results from the FBE model are provided considering top & bottom beams as continuous (BM CONT) and the slab as discontinuous (SLAB DIS).....	137
Figure 7.1: IPE 240 used for the parametric study .....	142

Figure 7.2: Change in bending stiffness of the IPE 240 with different temperatures and temperature gradients. The average temperature of each beam is the same at each specific web temperature. ....	143
Figure 7.3: Change in bending stiffness and RTSM for the IPE 240 with varying temperature gradients and web at 400°C .....	144
Figure 7.4: Graph of bending stiffness against mechanical axial load for the IPE 240 beam. For the graph compression is negative.....	145
Figure 7.5: Concrete slab used for the parametric study with reinforcement placed on the bottom .....	146
Figure 7.6: Stress profile in a 200x500 deep reinforced concrete beam at failure .....	147
Figure 7.7: Graph showing temperature over the height of the 130mm slab when exposed to different periods of a standard fire.....	148
Figure 7.8: Graph showing the total, mechanical and thermal strains over the height of the 130mm slab for a 60 minute standard fire exposure time .....	149
Figure 7.9: Mechanical strains over the height of the 130mm slab for different standard fire exposure times. ....	149
Figure 7.10: Graph showing secant Young's modulus values over the height of the slab at different fire exposure times.....	150
Figure 7.11: Graph showing the internal stresses caused by mechanical strains over the height of the 130mm slab when exposed to different periods of a standard fire. ....	150
Figure 7.12: Graph of bending stiffness and RTSM against standard fire time for the concrete slab with no applied mechanical forces, with (a) neither tension capacity ( $f_{ctm} = 0$ MPa) nor tension stiffening (TS), (b) for $f_{ctm} = 2.6$ MPa but no TS, and (c) for both $f_{ctm} = 2.6$ MPa and TS. ....	151
Figure 7.13: Deflections of a 3m long cantilever slab with varying tensile properties when heated in a standard fire .....	152
Figure 7.14: Graph of bending stiffness and $M_{\theta}$ against applied mechanical load for the 130mm concrete slab .....	153
Figure 7.15: Graph of axial stiffness and thermal axial force against applied mechanical load for the concrete slab.....	154
Figure 7.16: Graph of bending stiffness and $M_{\theta}$ against concrete strength.....	154
Figure 7.17: Graph of bending stiffness and $M_{\theta}$ against standard fire time exposure for different temperature profiles in a 100mm thick slab .....	156
Figure 7.18: Change in bending stiffness with applied axial compressive load for the concrete slab. For the graph compression is negative.....	157
Figure 7.19: Change in RTSL, $N_{\theta}$ , with increasing applied axial load for the concrete slab .....	158
Figure 7.20: Cross-section considered for the parametric study based on a typical office block beam size... ..	159
Figure 7.21: Temperature of the top flange and bottom flange / web for the IPE 240 when exposed to a standard fire. Bare steel (Bare) and a 10mm layer of perlite passive protection (Protected) are considered. .	159

Figure 7.22: Graph showing the total ( $\epsilon_{total}$ ), mechanical ( $\epsilon_{\sigma}$ ) and thermal strains ( $\epsilon_{\theta}$ ) over the height of the composite beam when exposed to a 30 minute fire and $f_{ctm} = 0$ MPa .....	160
Figure 7.23: Graph showing the total ( $\epsilon_{total}$ ), mechanical ( $\epsilon_{\sigma}$ ) and thermal strains ( $\epsilon_{\theta}$ ) over the height of the composite beam when exposed to a 30 minute fire, a 45 kNm mechanical moment is applied and $f_{ctm} = 0$ MPa .....	161
Figure 7.24: Graph showing the change in mechanical stresses, $\sigma_{\sigma}$ , in the composite beam for mechanical moments of 0 kNm and 45 kNm respectively, with $f_{ctm} = 0$ MPa .....	161
Figure 7.25: Graph showing the total, mechanical and thermal strains over the height of the composite beam .....	162
Figure 7.26: Graph showing mechanical stress over the height of the composite beam.....	162
Figure 7.27: Graph of bending stiffness against applied mechanical moment for the composite beam with the passively protected steel beam after a 60 minute fire, with (a) neither tension capacity ( $f_{ctm} = 0$ MPa) nor tension stiffening (TS) (b) for $f_{ctm} = 2.6$ MPa but no TS, and (c) with both $f_{ctm} = 2.6$ MPa and TS. ....	163
Figure 7.28: Graph of $M_{\theta}$ against applied mechanical moment for the composite beam with the passively protected steel beam after a 60 minute fire.....	163
Figure 7.29: Graph of deflection against applied mechanical moment for the composite beam after a 60 minute fire when considered as a 3m long cantilever with an end point moment.....	164
Figure 7.30: Graph of $EI_{\theta}$ against standard fire time for the passively protected composite beam.....	164
Figure 7.31: Graph of $M_{\theta}$ against standard fire time for the passively protected composite beam.....	165
Figure 7.32: Graph of $M_{\theta}$ against standard fire time for the composite slab with varying mechanical moment and tensile properties.....	166
Figure 7.33: Graph of bending stiffness ( $EI_{\theta}$ ) and RTSM ( $M_{\theta}$ ) against width of concrete flange acting compositely with the steel beam for various values of applied mechanical moment (M).....	167
Figure 7.34: Deflection of a 3m long cantilever subjected to an end point moment of 0kNm, 61.5kNm, and 123kNm with varying width of concrete flange acting compositely.....	168
Figure 7.35: Graph of bending stiffness and $M_{\theta}$ against applied mechanical load for the composite slab with applied mechanical moments of 0.0kNm, 61.5kNm and 123kNm. For the graph compression is negative...	168
Figure 10.1: Temperature data for the rebar of Case Study 2 .....	185

## List of tables

Table 2.1: Cost of steel and passive protection for various column sizes in South Africa.....	10
Table 5.1: Concrete properties according to EN 2-1-1 (BSI 2004).....	94
Table 5.2: Parameters for stress-strain profiles for siliceous concrete in fire according to EN 2-1-2 (BSI 2005c).....	96
Table 6.1: Temperatures of elements for Test 15.....	125
Table 6.2: Temperatures of elements for Test 16.....	126
Table 6.3: Steel temperatures for the Second Munich Test.....	134
Table 7.1: Comparison of yield load against RTSL for different temperatures of the unloaded IPE 240 .....	146
Table 7.2: Summary of thermal stiffness, RTSL and axial restraint load for the 130mm slab exposed to different standard fire times.....	158
Table 10.1: Case Study A - IPE cantilever – Properties for segments at different moments .....	181
Table 10.2: Case Study B – 5x300 Beam - Segment properties for a UDL of 10 kN/m.....	182
Table 10.3: Case Study C - Fixed-fixed IPE 200 - Segment properties for a UDL of 10 kN/m .....	182
Table 10.4: Case Study D - Fixed-fixed 5x300 beam - Segment properties for a UDL of 10 kN/m .....	183
Table 10.5: Case Study 1 - Segment properties for the 4 segment beam at 300°C .....	183
Table 10.6: Case Study 1 - Segment properties for the 8 segment beam at 300°C .....	183
Table 10.7: Case Study 1 - Segment properties for the 16 segment beam at 300°C .....	184
Table 10.8: Case Study 1 - Segment properties for the 4 segment beam at 600°C .....	184
Table 10.9: Case Study 1 - Segment properties for the 8 segment beam at 600°C .....	184
Table 10.10: Case Study 1 - Segment properties for the 16 segment beam at 600°C .....	184
Table 10.11: Case Study 2 – 1200x200 concrete slab - Segment properties at 30 minutes .....	185
Table 10.12: Case Study 2 - 1200x200 concrete slab - Segment properties at 60 minutes .....	185
Table 10.13: Case Study 3 – Test 15 – Segment properties at 15 minutes.....	186
Table 10.14: Case Study 3 – Test 15 – Segment properties at 30 minutes.....	186
Table 10.15: Case Study 3 – Test 15 – Segment properties at 40 minutes.....	186
Table 10.16: Case Study 3 – Test 16 – Segment properties at 9 minutes.....	187
Table 10.17: Case Study 3 – Test 16 – Segment properties at 15 minutes.....	187
Table 10.18: Case Study 3 – Test 16 – Segment properties at 23 minutes.....	187
Table 10.19: Case Study 4 – Munich 2 – Edge left - Segment properties.....	188
Table 10.20: Case Study 4 – Munich 2 – Intermediate - Segment properties .....	188
Table 10.21: Case Study 4 – Munich 2 – Right left - Segment properties .....	188
Table 10.22: Case Study 4 – Munich 2 – Edge top left - Segment properties.....	189
Table 10.23: Case Study 4 – Munich 2 – Edge top right - Segment properties .....	189
Table 10.24: Case Study 4 – Munich 2 – Edge bottom left - Segment properties .....	189
Table 10.25: Case Study 4 – Munich 2 – Edge bottom right- Segment properties .....	190



## List of abbreviations

ASFP	Association for Specialist Fire Protection
BS	British Standard
BSI	British Standards Institution
CEC	Commission of the European Communities
CSA	Canadian Standards Association
DOF	Degree of Freedom
EN	European Norm (Eurocode document)
ETS	Equivalent Thermal Stress
EU	European Union
FBE	Fire Beam Element
FE	Finite Element
fib	Fédération internationale du béton
FEA	Finite Element Analysis
ISO	International Standards Organisation
NA	Neutral Axis
NIST	National Institute for Science and Technology
NFPA	National Fire Protection Association
RTSL	Resultant Thermal Strain Load
RTSM	Resultant Thermal Strain Moment
SABS	South African Bureau of Standards
SANS	South African National Standard
SFPE	Society for Fire Protection Engineers
SPM	Slab Panel Method
TS	Tension stiffening
UDL	Uniformly Distributed Load



## List of symbols

### Roman

$a$	Parameter 1 for calculation of EN 3-1-2 stress-strain curve of steelwork
$A$	Cross-sectional area
$b$	Breadth
$b$	Parameter 2 for calculation of EN 3-1-2 stress-strain curve of steelwork
$b_0$	Transverse spacing of shear studs
$b_{ci}$	Effective width of concrete on each side of a composite beam
$b_{eff}$	Effective concrete flange breadth
$b_i$	Geometric width of a composite slab
$c$	Distance of neutral axis from reference axis
$c$	Parameter 3 for calculation of EN 3-1-2 stress-strain curve of steelwork
$c_0$	Initial distance of neutral axis from reference axis
$c_a$	Specific heat of steelwork
$c_p$	Specific heat of concrete
$C_{y\theta}$	Steel yield load at temperature $\theta$
$d$	Effective depth of a concrete element
$E$	Young's modulus
$E_0$	Initial tangent Young's modulus
$E_{cm}$	Mean Young's modulus of concrete
$E_S$	Secant Young's modulus
$E_T$	Tangent Young's modulus
$E_\theta$	Young's modulus at temperature $\theta$
$EA$	Axial stiffness
$EA_\theta$	Axial stiffness at temperature $\theta$
$EI$	Bending stiffness
$EI_S$	Secant bending stiffness
$EI_T$	Tangent bending stiffness
$EI_\theta$	Secant bending stiffness at temperature $\theta$
$f_c$	Stress in concrete
$f_{ck}$	Characteristic cylinder strength of concrete in compression
$f_{ck,cube}$	Characteristic cube strength of concrete in compression
$f_{cm}$	Mean cylinder strength of concrete in compression
$f_{ctm}$	Mean cylinder strength of concrete in tension
$f_i$	Load vector on node $i$
$f_y$	Yield stress of steelwork
$f_u$	Ultimate strength of steelwork
$F$	Load vector
$F_m$	Force vector of mechanically applied loads
$F_R$	Resultant force vector including reactions
$h$	Height or thickness of an element
$h_{eff}$	Effective thickness of a ribbed slab

$G$	Shear modulus
$I$	Second moment of area
$I_{composite}$	Second moment of area of a composite beam based on elastic properties
$I_{eff}$	Effective second moment of area of a composite beam considering shear connectors
$I_{steel}$	Second moment of area of a steel beam
$\mathbf{k}$	Local stiffness matrix
$k_{*,\theta}$	Reduction factor of material property * at temperature $\theta$
$\mathbf{K}$	Stiffness matrix
$K_f$	Shear force shape factor
$l$	Length of beam
$J$	Polar moment of area
$M$	Bending moment
$M_\theta$	Resultant Thermal Strain Moment (RTSM)
$n$	Number of elements
$N$	Axial load
$N_r$	Tension force at which cracking occurs in a reinforced concrete element
$N_y$	Yield load of a reinforced element
$N_\theta$	Resultant Thermal Strain Load (RTSL)
$\mathbf{N}_\theta$	Vector of Resultant Thermal Strain Loads (RTSL)
$p$	Percentage of shear connection
$P$	Applied point load
$Q$	Shear force
$\mathbf{Q}$	Matrix relating initial nodal coordinate to updated coordinate system
$\mathbf{r}$	Local unbalanced restoring force vector
$\mathbf{R}_R$	Global unbalanced restoring force vector
$t$	Time
$t$	Slab thickness
$T$	Torque
$\mathbf{T}$	Transformation matrix relating local and global axis systems
$u_{1x}$	Nodal displacement (subscripts 1/2 denote start and end node, x/y denote axis)
$u$	Moisture content of concrete
$U$	Internal work of a system
$W$	External work of a system
$\mathbf{W}$	Transpose matrix relating forces in updated to initial coordinate system
$x$	Distance of the neutral axis from the top of a reinforced concrete element
$x_i$	Horizontal nodal displacement of node $i$
$y$	Distance from axis
$y_i$	Vertical nodal displacement of node $i$
$Z_{pl}$	Plastic section modulus

**Greek**

$\alpha_e$	Modular ratio
$\alpha_i$	Rotation of node $i$
$\alpha_\theta$	Coefficient of thermal expansion at temperature $\theta$
$\beta$	Slope of $E_T - \sigma$ for the non-linear material model
$\delta$	Nodal deflection
$\Delta$	Nodal deflection vector
$\Delta *$	Change in property *
$\Delta_{total}$	Total deflection of structure
$\Delta_{mech}$	Deflection due to mechanical loading
$\Delta_\theta$	Deflection due to thermal loading
$\varepsilon$	Total strain
$\varepsilon_{c1,\theta}$	Strain of concrete at maximum stress
$\varepsilon_{cracking,\theta}$	Cracking strain of concrete at temperature $\theta$
$\varepsilon_{creep}$	Creep strain
$\varepsilon_{cu1,\theta}$	Strain of concrete at failure
$\varepsilon_{tr}$	Transient strain
$\varepsilon_\theta$	Thermal strain
$\varepsilon_\sigma$	Mechanical strain
$\lambda_a$	Thermal conductivity of steelwork
$\lambda_c$	Thermal conductivity of concrete
$\theta_a$	Temperature of steelwork
$\theta_c$	Temperature of concrete
$\theta_g$	Gas temperature
$\rho$	Material density
$\rho_{s,eff}$	Effective reinforcement ratio for tension steel
$\sigma$	Stress
$\sigma_\sigma$	Mechanical stress
$\sigma_\theta$	Equivalent Thermal Stress
$\varphi$	Nodal rotation
$\emptyset$	Reinforcement bar diameter

**Subscripts**

$a$	Steelwork
$bot. fl.$	Bottom flange
$c$	Concrete
$el$	Element
$E$	Young's modulus
$max$	Maximum
$p$	Proportional limit for steelwork
$top fl.$	Top flange
$u$	Ultimate stress

<i>w</i> <sub>web</sub>	Web
<i>x</i>	Major axis
<i>y</i>	Minor axis
<i>y</i>	Yield strength
<i>θ</i>	Temperature

# 1 Chapter 1: Introduction

## 1.1 Background to study

Events such as the collapse of the World Trade Centre have increased the interest and rate of research in structural fire engineering worldwide in recent years. A report from the Federal Emergency Management Agency (2002) following this disaster stated that: “The behaviour of the structural system under fire conditions should be considered as an integral part of structural design.” The structural engineering industry is slowly moving towards rational structural fire design as a core issue of engineering responsibility rather than an addendum addressed after the main design work is complete. All buildings require some level of fire resistance, although structural engineers often lack the skills and knowledge required to correctly provide this.

It is commonly acknowledged that fires are complex events which involve high levels of uncertainty (Buchanan 2001). The structural response associated with such unpredictable circumstances is equally difficult to quantify. Hence, it is often debateable what level of accuracy is possible in structural fire designs. Furthermore, most developmental work and standards are based on a semi-arbitrary benchmark, the Standard Fire (ISO 1999), which has limited resemblance to real fires. Thus, it is not possible to claim a high level of precision when modelling structures in fire because of such variability regarding input factors and fire scenarios.

During the course of this research and especially during a trip to the United Kingdom in 2015 the author corresponded with a number of international universities and consulting companies involved in structural fire engineering. The general attitude expressed was that full structural fire analyses are rarely done in industry due to the extensive modelling and analysis times required for such designs. Generally, simplified models or prescriptive methods are utilised by consultants instead. This can lead to overly conservative and less economical solutions, although non-conservative designs are also possible. A leading fire consulting company noted that it was only for the upmarket buildings in central London that full analyses were typically done since the higher consulting fees on such projects justified the hours required to complete analyses, whereas other projects simply did not.

Structural steelwork, as a material in isolation, is particularly sensitive to elevated temperatures. Other construction materials, such as concrete, have a greater thermal capacity and are good insulators, while some materials, such as wood, can char which provides a protective coating. This may be an important reason why many engineers use concrete for multi-storey buildings in South Africa rather than steelwork, as the passive protection (e.g. intumescent paints) required for steelwork can be prohibitively expensive. However, research has shown that significant fire resistance can be obtained from steel structures using correct design procedures (Clifton 2013; Wang et al. 2012), without such structures becoming uneconomical.

From the discussions above it can be seen that there is a divide between the extensive fire engineering research and analysis tools that are available and the current needs of practitioners. By focussing on producing tools suitable for design offices rather than only for research structural fire design can make a greater impact on society by assisting practitioners in safely producing more economical buildings. Thus, there is a need to develop technically accurate analysis tools which do not require extensive modelling times to produce predictions. With the highly unpredictable nature of fire it is justifiable that there be a trade-off between high levels of precision and pragmatic considerations, otherwise tools will become neglected except for rare cases.

## 1.2 Overview

This dissertation presents a generalised beam finite element (FE) and analysis methodology for the analysis of structural frames subject to severe fires. The aim is to provide a simpler, but technically accurate, modelling tool that could be adopted within the practical structural engineering design environment. Rather than requiring shell or volume elements only beam elements are used. By providing tools that are more accessible to engineering practitioners the design of buildings in fire can be more readily carried out, thereby providing a safer and more economical built environment. The proposed formulation considers nonlinear behaviour, temperature effects, thermal curvatures and global structural interactions, which existing simplified methods generally do not. Conversely, it allows for the modelling of structures as skeletal frames, including composite structures, which simplifies the modelling process significantly.

In order to provide a convenient ‘handle’ for the approach described in this dissertation it is called the Fire Beam Element (FBE) formulation, to differentiate it from the numerous other analysis, material and thermal models discussed. The finite element formulation presented does not only apply to structures in fire, but potentially also to other types of structures such as bridge decks or wind towers. The proposed FBE is an adaptation of the well-known Euler beam. While the Euler beam typically assumes that the bending stiffness ( $EI$ ), axial stiffness ( $EA$ ) and neutral axis (NA) position remain unchanged during analysis the FBE requires (1) the calculation of the position of the NA, (2) which is used to calculate updated section stiffnesses to account for the influence of (3) generalised temperature profiles, internal forces and nonlinear material properties. Large deflections typically must be accounted for due to the deformations that occur during fires. The FBE can be included in models with varying levels of complexity ranging from (a) simplified 2D analyses using commercial software to (b) advanced models where restraint, time-dependent properties and non-linear structural interactions are explicitly considered (although additional research is required for such implementation). The procedures developed are suitable for any structural configuration provided that (i) the temperature-stress-strain behaviour of constituent materials is known, and (ii) Euler-Bernoulli assumptions of plane sections remaining plane hold. When the element is included with the analysis methodologies and techniques developed in this dissertation it is referred to as the FBE formulation.

The positioning of the research presented in this dissertation is compared to existing design methods in Figure 1.1. It can be seen that there are a variety of options available for designing structures in fire, ranging from

very simplified prescriptive methods with no consideration of overall building behaviour to advanced models where all structural elements are explicitly accounted for. The proposed prediction model can consider global building behaviour and structural interactions without requiring extensive modelling of floors and the inclusion of finite elements such as shells, rigid links or the explicit modelling of reinforcing steel. Hence, the model generally falls between the advanced and simplified analysis procedures. The design of composite floors, as opposed to composite beams, is not directly considered, and it must be combined with one of the existing tensile membrane models (Bailey & Moore 2000b; Clifton & Abu 2014; Wu et al. 2012) to consider all structural components. Details regarding the advanced methods listed in Figure 1.1 are contained in Section 2.6.

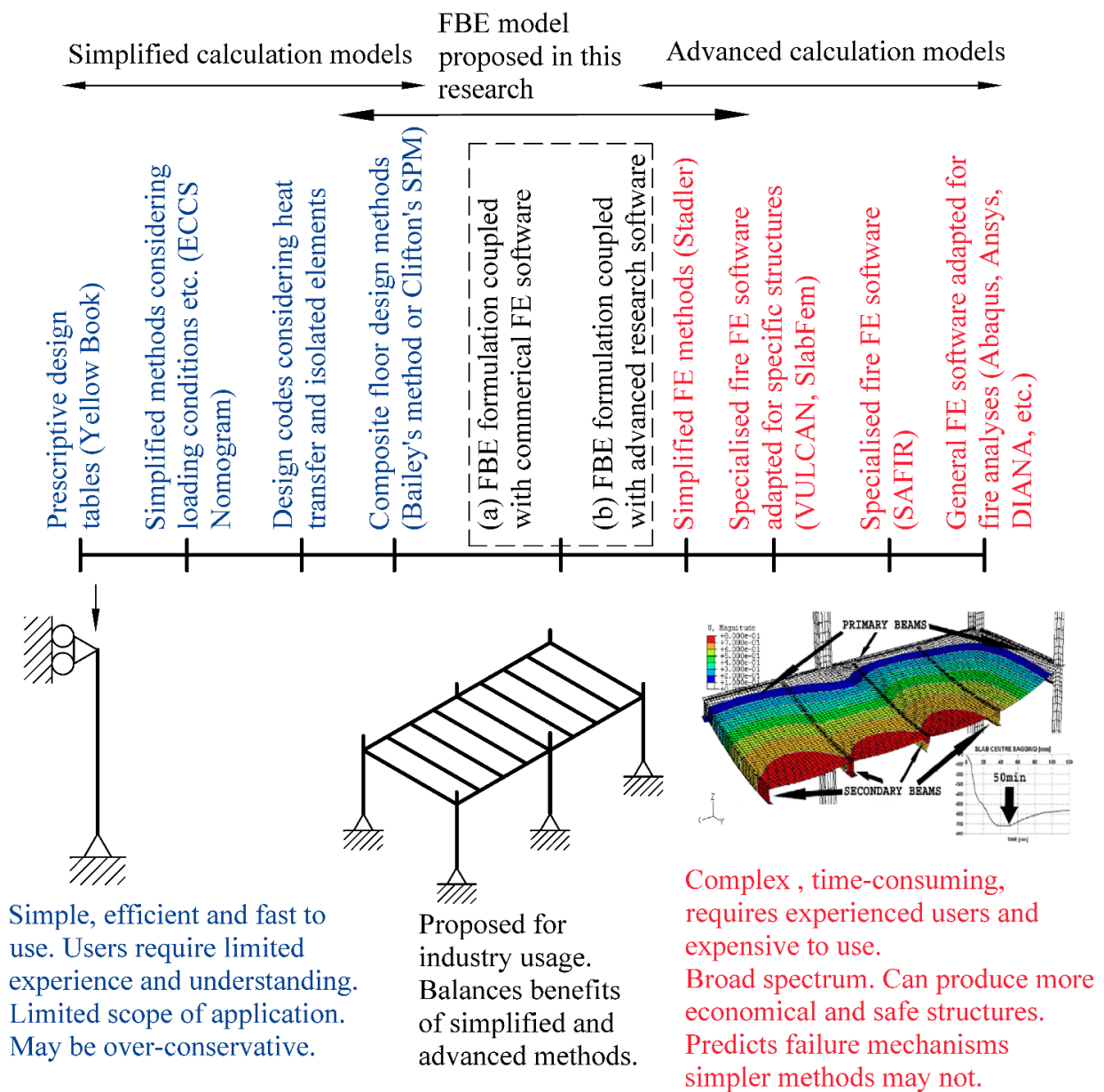


Figure 1.1: Design and analysis models available for structural fire engineering showing the position of the FBE formulation (adapted from Stadler (2012) with FE model picture from Clifton (2014))

The FBE formulation proposed in this work allows parametric investigations to be more easily carried out, enabling designers to identify parameters which have a significant influence on results. Engineering judgement can then be used to address important parameters and make decisions regarding design criteria. Furthermore, the FBE modelling procedures could allow multiple configurations to be tested in significantly less time than would be required for full three-dimensional models consisting of shell and volume elements. This would enable engineers to evaluate multiple structural configurations and determine which system would be most suitable, especially for complicated structures.

### 1.3 Research objectives

The ultimate goal of the research is to produce a simplified but technically accurate method for the analysis of structures in fire. To this end the research objectives of this dissertation can be broadly defined as:

- a) To examine, understand and explain the fundamental structural mechanics of a beam cross-section exposed to fire. Based on this understanding thermal effects can be converted into usable resultant thermal forces.
- b) The development of a mathematical finite element formulation for beam elements in fire where (a) the position of the neutral axis (NA) can change, and (b) nonlinear material behaviour occurs.
- c) To carefully consider various material and thermal input parameters for FBE models as provided in the literature and to identify those which are most suitable for predicting structural behaviour. A tension stiffening model will be incorporated, based on modifying an ambient temperature model. This is included to account for the concrete-rebar interaction that occurs, and to determine to what extent it influences calculated deflections and stresses.
- d) Implementation of the FBE procedures in a computer program to validate the methodologies associated with updating the NA and the stiffness of a member. This will be done independent of thermal considerations such that calculated strain profiles and stiffnesses can be more easily identified relative to the formulations developed.
- e) To investigate the influence of input parameters on FBE models through a parametric study, such that it may be ascertained to what extent parameters may influence validation case studies investigated. This study is also important for identifying structural behaviour that occurs due to cross-sectional interactions and thermal effects within a beam.
- f) Implementation of the FBE formulation within simple, commercially available structural analysis software to illustrate how simplified analyses can be carried out by design engineers.
- g) Validation of the FBE formulation against full-scale experimental tests. This important aspect illustrates how full systems can be considered in a manner that is efficient in terms of design engineer input requirements but still captures the behaviour of a structural system.



## 1.4 Scope of the work

The FBE formulation is presented for the analysis of generic cross-sections and structural configurations. This is done such that the methodology can be applied in a wider range of scenarios, rather than only to specific types of structures, e.g. composite buildings. However, bending about only a single axis has been considered (i.e. 2D analyses), although proposals are provided for the extension of the method to be used in 3D structures. The analysis philosophy will remain the same for the 2D and 3D systems, but the latter requires additional research regarding torsion and bending behaviour about the minor axis of floor sections (as discussed in Section 8.4). Material models have been included based on existing standards and literature. Experimental work is required for the validation of the modified tension stiffening model. Plane sections must remain plane for the methodologies presented to hold. However, it is investigated in Chapter 4 to what extent this assumption influences results if it is violated.

A nonlinear analysis programme has been developed in this research for considering the numerical validation studies conducted in Chapter 4. No thermal behaviour has been considered for these studies investigated. In Chapter 6 the FBE formulation has been used in conjunction with a commercially available software package such that it can be illustrated how designs can be carried out in a simple manner. However, additional developmental work is required to fully implement the FBE formulation in software where both iterative procedures and thermal procedures are simultaneously included.

For the parametric studies conducted in Chapter 7 only individual beam cross-sections have been considered, rather than entire structures. Parametric studies of full 3D structures can be addressed in future work. Boundary conditions in all chapters have been modelled as either being fixed or pinned, as commonly done in the literature. It would be possible to include non-linear springs to model connections, and this is a topic for future research.

## 1.5 Outline of dissertation

The objectives above are addressed in the following manner: Chapter 2 provides an overview of literature on structural fire engineering, important concepts in design, behaviour of structures in fire and other such factors.

In Chapter 3 the procedure to be followed when analysing a full structure as a skeletal frame with beam elements is presented. It is shown how stresses and strains develop in sections exposed to thermal and mechanical effects. A procedure for determining resultant thermal forces that cause the same strains as thermal effects is proposed. This is followed by the fundamental structural mechanics and design procedures used for the FBE formulation.

In Chapter 4 the finite element (FE) methodology for updating the position of the neutral axis and the calculation of resultant beam stiffnesses is developed, which is followed by a numerical validation process. This is carried out independently of temperature considerations, by developing a generic methodology.

Material models and temperature considerations required for fire are then presented in Chapter 5. A procedure for considering tension stiffening of reinforcing steel is also developed in this chapter. Various temperature profiles and material models are discussed.

Thereafter case studies consisting of numerical and full-scale experiments in the literature are investigated in Chapter 6 to validate the FBE formulation. It is shown that results from the proposed prediction model are comparable to more advanced methods in the literature, and the FBE formulation is able to predict experimentally observed deflections.

A parametric study is carried out in Chapter 7 which considers how specific input parameters influence calculated results. This highlights which parameters an analysis is most sensitive to, along with identifying how structures respond to various conditions. The change in bending stiffness, axial stiffness and resultant thermal forces for typical sections are plotted with varying input parameters. This chapter illustrates how the predicted deflections calculated in Chapter 6 may change based on the input parameters assumed.

Conclusions and recommendations for future research are presented in Chapter 8. Additional data can be found in Appendix A and B, which consist of analysis data used for case studies and temperature profiles developed for slabs. This developmental process is illustrated in Figure 1.2, where the most important content of each chapter is listed.

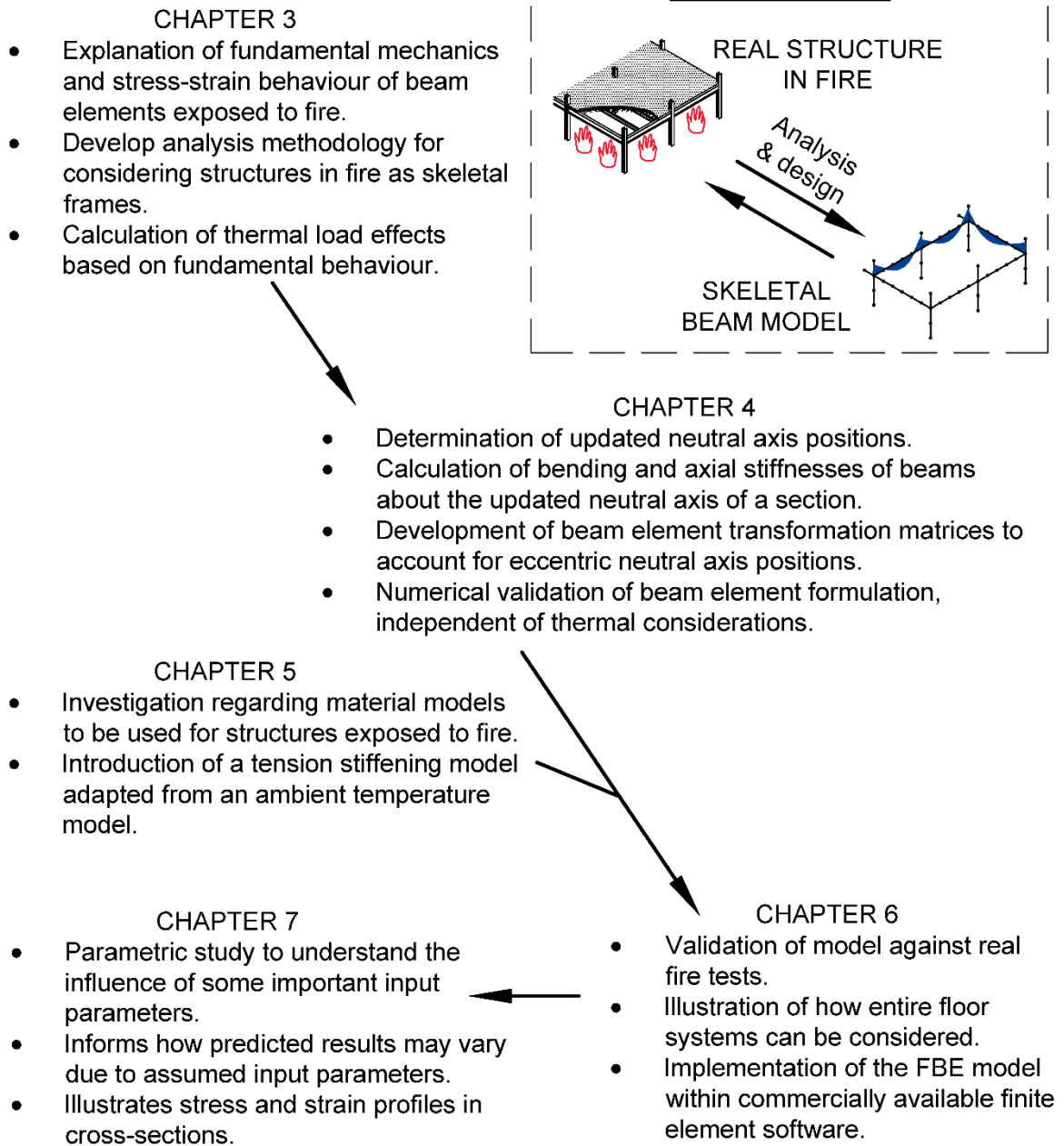


Figure 1.2: Structure adopted for dissertation to address overall objectives

## 2 Chapter 2: Literature Review

### 2.1 Introduction

This chapter provides the necessary background required to give context to the remaining chapters. It also provides an overview of the literature and state of knowledge related to structural fire engineering. Initially the fields of fire engineering and structural fire design are explained, along with important concepts related to fire design. The behaviour of structures in fire is then addressed, on the basis of fundamental structural mechanics. Well-known full-scale fire tests and case studies are presented, illustrating the current state-of-the-art of structural fire engineering and what behaviour has been observed from real structures in fire. Thereafter different design approaches and methodologies relating to fire design are discussed, addressing both prescriptive and performance based design. A brief discussion regarding finite element formulations is presented as a basis for the FBE formulation developed in Chapter 4. Software and design systems available for analysis are then addressed. It is shown how structures in fire are currently modelled, which is necessary for understanding how the research discussed in this dissertation contrasts with those systems already available. Due to the extensive treatment given to material models in fire presented in Chapter 5 the literature on material behaviour is not covered in this chapter.

### 2.2 Fire engineering and the role of structural fire design

Structural fire engineering is a broad discipline encompassing a number of specialist fields such as structural design, thermodynamics, analysis of non-linear systems, consideration of building codes, personnel safety requirements, and much more. This literature review is limited to aspects most relevant to this research topic. Refer to publications such as those of the SFPE (2008) for an in-depth discussion of the aforementioned topics.

#### 2.2.1 *Fire and society*

Fire has played a significant role in the development of societies, both positive and negative. Throughout the centuries large conflagrations have occurred across the world, often destroying thousands of homes and even ruining cities and communities. For a fascinating work on historical fire events see the work by Bankoff et al (2012). In recent times the influence of fire in developed countries has been drastically reduced due to aspects such as better building code requirements and enforcement, fire resistant construction, firefighting facilities, access to water, societal education, electrification of homes, fire breaks between buildings and other such factors. However, ensuring that structures have adequate performance in the unlikely event of a fire is still an important task to be addressed by building designers.

### 2.2.2 Objectives of structural fire engineering

Ultimately the aim of fire safety in buildings is to reduce to acceptable levels the probability of death or injury of persons, loss of property and damage to the environment (Bailey 2004b). The Commission of the European Communities (CEC) outlines the general requirements of construction works subjected to fire conditions as:

- “the load bearing capacity of the construction can be assumed for a specific period of time,
- the generation and spread of fire and smoke within the works are limited,
- the spread of fire to neighbouring construction work is limited,
- occupants can leave the works or be rescued by other means,
- the safety of rescue teams is taken into consideration.” (CEC 1988)

It is often questioned whether the significant expenses incurred to provide buildings that are safe in fire are fully justified. The following are interesting facts regarding fires in Europe, as presented by Twilt (1994): (a) The likelihood of a person being killed in a car accident is 30 times higher than being killed in a building fire. (b) In a survey of 5 European countries between 74% (Netherlands) and 85% (France) of fatal fires occurred in domestic buildings. Hence, deaths in commercial and industrial structures are rare, yet this is where structural fire analyses are used. (c) The cause of deaths in buildings due to heat and smoke is generally between 74% (Germany) and 99% (Switzerland). Thus, it must be understood that almost no deaths are caused by building collapse. (d) A survey showed that the monetary loss due to fires is in the order of about 0.2-0.29% as a portion of Gross National Product (which amounts to billions of euros or dollars in a large economy). However, of the cost of damages to buildings and businesses due to fires only between 21-32% relates to the fabric of the building whereas the rest is due to stock and indirect losses (e.g. productivity). Hence, it is often business continuity and insurance requirements that govern fire design, rather than purely safety.

Following on from such facts it must be acknowledged that often the task of structural fire engineering professionals is not simply to ensure life safety, but also to reduce the cost of infrastructure while retaining a suitable level of fire safety. With steel being particularly vulnerable to fire it is often passively protected with various products. The cost of protecting various 1m long column sizes in South Africa is shown in Table 2.1. Costing was obtained from a local supplier. It can be seen that for a two hour rating on a UC 203x203x46 column the cost of intumescent paint to protect the steelwork is 60% more than the cost of the steelwork itself. This highlights the need for safe but efficient solutions.

				Fire Protection Costing			
				60min Fire Rating		120min Fire Rating	
Section	Mass (kg/m):	$A_p/V$ ( $m^{-1}$ ):	Steel Cost (R/m):	Intumescent Paint – Nullifire S707-60	Vermiculite Spray	Intumescent Paint – Nullifire S707-120	Vermiculite Spray
UC 152x152x23	23.3	304	R 652	R772	R418	Not possible	R761
UC 203x203x46	46.2	205	R 1,294	R503	R559	R2,076	R1,019
UC 305x305x137	137	106	R 3,836	R473	R855	R1,779	R1,558

**Table 2.1: Cost of steel and passive protection for various column sizes in South Africa**

### 2.2.3 Fire design codes

To obtain a safe but economical design engineers make use of the different fire design codes available. In the USA extensive documentation on fire protection has been produced by the NFPA (National Fire Protection Association). Such guidelines are often adhered to outside America too, especially on petrochemical projects. In Europe the Eurocodes (EN documents) have a number of sections specifically dealing with structural fire design. The EN documents are typically viewed as the most technically advanced design standards in terms of fire in the world, and have been extensively drawn upon in this work. The main documents that are considered in this research are: (a) Eurocode 1-1-2: Actions on structures – Actions on structures exposed to fire (BSI 2002b); (b) Eurocode 2-1-2: Design of concrete structures – Structural fire design (BSI 2005a); (c) Eurocode 3-1-2: Design of steel structures – Structural fire design (BSI 2005b); and (d) Eurocode 4-1-2: Design of composite steel and concrete structures – Structural fire design (BSI 2005c). For a discussion regarding the compatibility between EN and South African steel codes refer to Walls & Viljoen (2016).

### 2.2.4 Limit state design

Fire scenarios are considered ‘accidental loading’ situations in terms of load factors selected (SABS 2011a). Accidental loads are those which are “not expected during the design life”, but when they do occur then structures should “not be damaged to an extent disproportionate to the original cause of the abnormal event” (Retief & Dunaiski 2009). Thus, in the case of a fire it should be expected that there will be damage, and for very severe fires structural components or the whole building may need to be replaced. Allowing some level of damage is typically more economically viable than trying to make all buildings immune to the effects of fire. At the fire limit state imposed loads are reduced because the probability of design levels of imposed loading occurring simultaneously with the highly improbable event of a fire is negligible. Imposed loads are taken at between 30% to 80% of their characteristic value depending on the building occupancy and design code used (BSI 2002b; CISC 2010).

According to British (BSI 2009), South African (SABS 2011c) and European (CEC 1988) codes structural elements are tested based on the criteria of (a) load-bearing capacity, (b) integrity (preventing smoke and hot gas flow between compartments) and (c) insulation (ASFP 2014). Columns only need to meet load-bearing

requirements whilst floor slabs need to satisfy all three. Part 20 of BS 476 limits deflections of beams during fires to  $Span/20$ , or the rate of deflection to  $Span/900d^2$  (mm/min) when deflections exceed  $Span/30$ . The value  $d$  is the effective depth from the top of a structural section to the bottom of the tensile zone (Lamont et al. 2006).

Limit state design methodologies for various construction materials in fire are often based on ambient temperature design equations modified to account for reduced material strength and stiffness. Sometimes thermally induced forces are included. For an excellent treatment of the topic of rational limit state design for fire see the book by Buchanan (2001), as well as the work by Wang et al (2012).

## 2.3 Important concepts in fire design

### 2.3.1 The standard fire and fire resistance ratings

Fire resistance ratings (FRR) are usually measured according to the length of time a structural element can withstand a standard fire, also often called the ISO 834 fire (ISO 1999) based on the code from which it comes. Ratings are typically defined in increments of 30 minutes, with a low rating being 30 minutes and a high rating being 2 hours. Tests have shown that steel members can attain 15 minutes or more fire resistance without any protection (ASFP 2014). Both structural and non-structural elements need to be fire rated to ensure that they are suitable for their application. For an in-depth discussion regarding the historical development of fire testing and design methods refer to Bisby et al (2013).

For the standard ISO 834 fire the gas temperature,  $\theta_g$ , at a time  $t$ , in minutes, is given by:

$$\theta_g = 20 + 345 \log_{10}(8t + 1) \quad (2.1)$$

The hydrocarbon fire can be used for fires with a higher fuel energy content, as might be found in the petrochemical and associated industries:

$$\theta_g = 1080(1 - 0.325e^{-0.167t} - 0.675e^{-2.5t}) + 20 \quad (2.2)$$

For structures subjected to flames emerging from a building the less intense external fire curve can be used, as given by:

$$\theta_g = 660(1 - 0.687e^{-0.32t} - 0.313e^{-3.8t}) + 20 \quad (2.3)$$

Figure 2.1 shows the time-temperature relationship for these three fires.

In fires the structural elements most affected by temperatures are typically elements above fires, rather than those underneath them. Hence, in this research all heating of structural elements is considered as occurring from below. However, this does not mean that heating from above has no influence on structural elements.

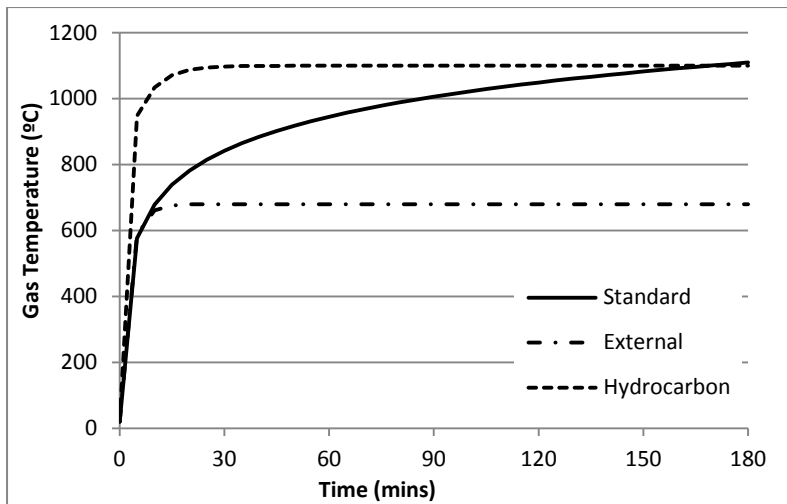


**Figure 2.1: Time-temperature curves of the standard, external and hydrocarbon fires**

### 2.3.2 “Real” fire models

In contrast to the standard fire extensive research has been carried out to characterise the behaviour of real fires, especially with pioneering work by Pettersson et al (1976) and Wickström (1985). The time-temperature relationship of a real fire is shown in Figure 2.2. After ignition there is an initial period of growth. Once sufficient heat has accumulated to cause full room involvement, flashover ensues. After the combustible material has been consumed the decay phase follows. Maximum temperatures in buildings can reach around 1000°C, although temperatures of around 1200°C are reported in the literature. In certain instances the cooling phase may result in structural failure. This is due to beams heating up and expanding, then buckling and sagging such that when beams cool it results in tension at connections. This tension can cause failure, especially in more brittle connections (Block et al. 2007). Various software models are available for producing “real” fire curves, such as OZone (Cadorin & Franssen 2003). Fire models can consider factors such as ventilation, fuel loads and room properties.

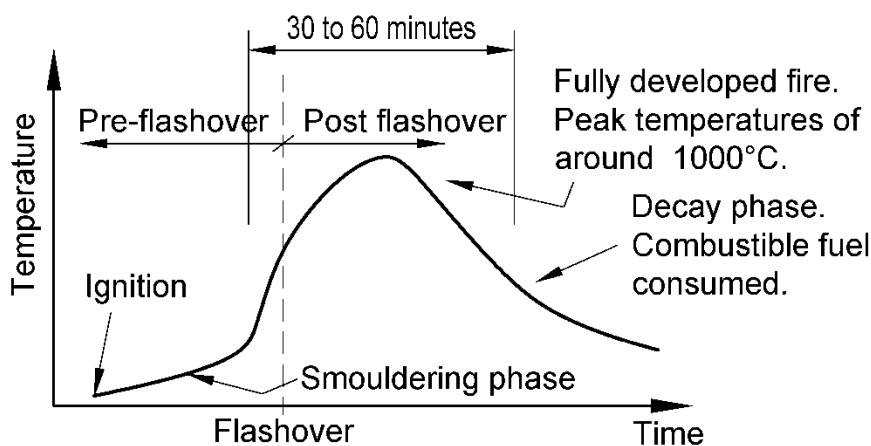


**Figure 2.2: Time-temperature behaviour of a real fire**



From observations in large, open-plan buildings it has been noted that fires often do not burn as uniform phenomena across entire floor plates, but rather move across areas as fires spread. Such fires have been termed *travelling fires* and have been subject to research by the likes of Clifton (1996), Stern-Gottfried & Rein (2012b) and Dai et al (2016). Travelling fires affect the heating regime of structural elements, potentially causing more severe temperatures in members, although this is dependent on a large number of factors, such as the size of the fire and building geometry. A review of the state-of-the-art regarding travelling fires is provided by Stern-Gottfried & Rein (2012a).

### 2.3.3 Considering “consistent levels of crudeness”

It must be understood that the standard fire discussed above does not represent a real fire, and should rather be considered a benchmark for testing. Lennon (2011) considers the standard fire to be “enshrined in national, European and international standards”, since it governs all testing and resistance requirements, even though it has only limited physical significance. When addressing the use of the standard fire Franssen & Vila Real comment:

*“If the fire and mechanical model (an isolated element) are arbitrary and do not represent the real situation, why should there be an attempt to create a more accurate model by introducing the indirect effects of actions. As mentioned by Professor A. Buchanan from Canterbury University in his talks, there must be a consistent level of crudeness.”* (Franssen & Vila Real 2010)

The idea of the consistent level of crudeness is extensively addressed in a recent paper by O’Loughlin & Lay (2015), explaining that even when innovative designs and systems are developed it is questionable to what level rational designs can be taken if they are based upon arbitrary benchmarks. Also, with the rating system being based upon either 30 or 15 minute time steps there is a relatively low number of classifications possible for buildings, possibly leading to various structures being over-engineered in terms of actual requirements.

With regards to the consideration of structural behaviour in fire Gales et al (2012) present Figure 2.3 to provide a relationship between the complexity of the fire model considered and the structural model that should be tested. The values O/R mean suitable for occasional research (i.e. for specific scenarios), and M/C means marginal credibility. It can be seen that from this that there are numerous systems where it is questionable whether results are in fact credible due to complex structural configurations being combined with simplified fire models, or vice versa. Researchers and practitioners should not be under the impression that advanced and accurate designs can be done based on very approximate and often unrealistic thermal loading scenarios.

Structural Model  Fire Model		Materials & Partial Elements	Single Elements	Sub-Frame Assemblies	Transiently Simulated Restrained Assemblies	Full-Scale Structures
Elevated Temperature Exposures (transient or steady-state)		Generate design model input data	O/R [T]	M/C	M/C	M/C [E.1-2]
Standard Fires		Generate design input data	<b>Obtain fire resistance ratings (STANDARD)</b> [T]	O/R [O]	M/C [W]	M/C [A]
Equivalent Fire Severity to a Standard Fire		Validation of fire severity concept	Obtain fire resistance ratings (using alternative metric for fire severity) [Q]	O/R	O/R	M/C [B],[G],[N]
Parametrically Defined Model Fires		Generate design input data (highly dependant time-temperature phenomenon)	O/R	O/R [K],[M],[R],[S]	O/R	O/R [E.3-5]; [H],[J],[L],[U],[V]
Localised Model Fires		Generate design input data (highly dependant time-temperature phenomenon)	O/R	O/R	O/R	O/R
Zone Model Fires		Research (highly dependant time-temperature phenomenon)	M/C	O/R	O/R	O/R [I]
Field Model Fires		Research (highly dependant time-temperature phenomenon)	M/C	M/C	O/R	O/R
Real Fires		Research (highly dependant time-temperature phenomenon) [P]	M/C	M/C [C],[D],[F]	O/R	<b>Research REAL behaviour in a REAL fire</b> [E.6]

M/C- of Marginal Credibility; O/R- used for Occasional Research

**Figure 2.3: Testing and modelling regimes in fire engineering with their associated level of credibility according to Gales et al (2012). Letters in brackets cite works listed in the original paper.**

### 2.3.4 Prescriptive versus performance-based design

In a comparison of prescriptive and performance-based approaches in structural fire design Budny and Giuliani (2010) note that the characteristics of prescriptive approaches are: (a) individual members are checked rather than systems as a whole, (b) methods are typically simplified, (c) conventional fire curves are used rather than real or natural fire curves, (d) no specialised engineering skills are required, (e) it is clear who is responsible, and (f) methods are typically not open to technical innovation. Conversely, performance based, or rational, design methods are characterised by: (a) the stability of entire systems is addressed, (b) often well-defined design procedures are not provided, (c) there is a greater computational effort and level of skills required, (d) designs can potentially be more safe and economical, (e) a variety of fire situations can be considered, and (f) modelling methods affect results.

In the UK a detailed handbook on prescriptive structural fire design has been produced by the Association for Specialist Fire Protection (ASFP), called the “Yellow Book” (ASFP 2014). This document provides extensive information regarding the design of steelwork in fire situations, including the application of various products and systems, but typically provides details for prescriptive approaches only. Conversely, in this dissertation the references cited generally are for performance based approaches.

### 2.3.5 Active and passive protection of structures

In the ‘Model Code on Fire Engineering’ (ECCS 2001) it is stated that fire safety may be achieved using the following means: (a) fire prevention, (b) active or operational measures, and (c) passive or structural measures. Active measures involve suppressing or preventing the growth of the fire by an intervention with the likes of automatic sprinklers, a fire brigade, or suppression systems. Passive measures are intended to increase the resilience of a structure and include measures such as ensuring the adequacy of escape routes, protection of structural elements, or ensuring structural robustness. Commonly available products used for fire protection include intumescent paints, gypsum boards, concrete encasement and vermiculite coatings. The market share for various fire protection systems for steelwork in the UK between 1995 and 2012 are given in Figure 2.4. It is interesting to note the significant increase in the use of intumescent paint during this period, especially when the costing listed in Table 2.1 is considered.

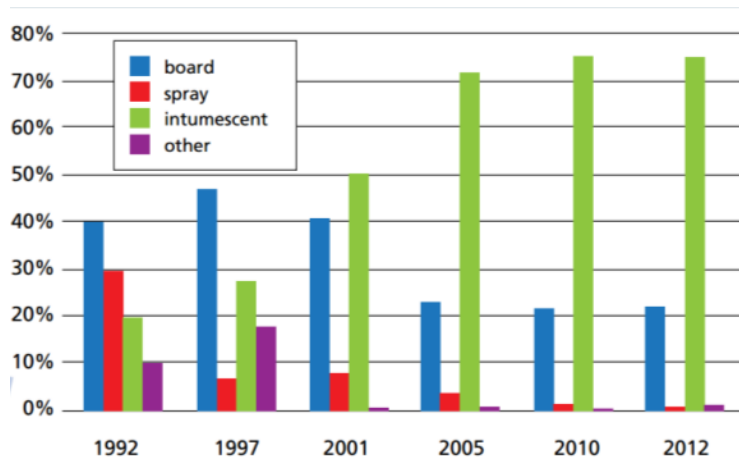


**Figure 2.4: Market share in the UK of various fire protection systems (Tata Steel & BCSA 2013)**

### 2.3.6 Compartmentation

A vital aspect that must be specifically considered during fire engineering design is that of compartmentation. The Great Fire of London, which devastated a large part of that city, helped identify the fact that to prevent fire spread there needs to be sufficient separation between adjacent buildings (Bankoff et al. 2012). This now forms part of international building codes and guidelines. Compartmentation involves the division of fire zones to limit the spread of fire. This is explicitly considered in building codes such as SANS 10400 (SABS 2011c) by limiting the maximum division area allowed in various occupancy categories. Dividing walls must

be fire rated and retain their integrity during a fire. Firewalls, fire doors and other methods are commonly used for this. For multi-storey buildings BS 9999 (BSI 2008) makes the following recommendation:

*In tall multi-storey buildings, it can be advisable for each storey to be a separate compartment capable of resisting burn-out. This can protect occupants who might have to exit past the fire storey when a fire is well developed, and can also protect fire fighters who might have to work on storeys immediately above or below a fire when it is well developed.*

Advanced design guides have started proposing details for maintaining compartmentation even when floors deflect substantially. This is done through the use of systems such as deformable ceramic blankets (Clifton 2013), which prevent compartmentation loss.

## 2.4 Structural behaviour in fire

### 2.4.1 Thermally induced effects

Chapter 3 discusses the development of stresses and strains in structural elements exposed to fire, hence in this section only general behaviour is described. Regarding thermal behaviour Sanad et al (2000) highlight that the “effect of thermal expansion is generally ignored, even though it may swamp the effects of all other phenomena in a large highly redundant building under a local fire”. This is also emphasised by Gillie et al (2001), when commenting on the first Cardington test, noting that “the response of the structure is overwhelmingly dominated by the effects of thermal expansion and that material degradation and gravity loading are of secondary importance”. In a report on the behaviour of the Cardington tests it is noted that for a restrained beam at 500°C around 90% of the deflection may be due to thermal expansion alone, which changes to around 75% at 600°C (Usmani et al. 2000). Thus, the consideration of thermally induced effects is an important factor in any potential design. However, contrary to such guidelines the following comment is made in the fire design annex of the Canadian steel design code (CSA S16-09):

*“Thermal effects due to expansion, contraction, or deflection caused by temperature changes due to the design-basis fire specified in [the clause above] can be taken equal to zero for statically determinate structures or for structures that have sufficient ductility to allow the redistribution of temperature forces before collapse” (CSA 2009).*

The exclusion of thermal forces, as proposed in this code, is feasible in statically determinate structures. However, pragmatically it is often done by engineers for indeterminate structures simply because of the difficulty associated with including thermal effects in analyses. Yet, in the majority of cases this may be a non-conservative assumption.

It is normally assumed that temperatures in a fire compartment are homogenous when thermal effects are considered. However, the work by Deeny (2010) shows that temperatures can vary substantially in a

compartment and this non-uniform distribution can influence behaviour, especially in larger firecells. Slender slabs are particularly susceptible to non-uniform temperatures which cause slab distortion. The assumption of homogenous temperature can lead to either conservative or non-conservative results, depending on the properties of a building or floor. In the case studies considered in this dissertation experimental results typically provide only a single temperature reading for the length of each structural element (bottom flange, web, top flange), meaning that uniform temperature had to be assumed.

#### 2.4.2 *Temperature gradients in cross-sections*

In a well-known fire design guide by Franssen & Vila Real (2010) the following statement is made regarding beams subjected to temperature gradients:

*A steel beam subject to a non-uniform temperature distribution can be considered as a composite beam, formed of several materials. Normally for an I-shaped beam three different temperatures are considered with simple calculation methods: the temperatures in the upper and lower flanges and the temperature in the web. In this case the beam can be considered as a three material composite beam.*

For a beam with different temperatures in each element the temperature gradient causes the member to experience thermal bowing, and it distorts based on thermally induced effects. If material properties degrade at different rates it will cause the neutral axis position of the section to shift towards the side with the higher stiffness.

#### 2.4.3 *Real fires in real buildings*

A report by Beitel and Iwankiw (2008) investigated details regarding 22 fire-induced collapses in multi-storey buildings that occurred between 1970 and 2002 in steel, concrete and masonry buildings. It is noted that of all the failure mechanisms the majority could not have been predicted by standard fire tests. Structural interactions between members and connections played pivotal roles in the modes of failure. In fact the authors note that “connections are generally recognized as the critical link in the collapse vulnerability of all structural framing systems, whether or not fire is involved.”

Of all the fires in buildings in the world the one which has received the most attention is that of the World Trade Centre (WTC), which collapsed following a terrorist attack on September 11, 2001. Extensive reports, forensic investigations and analyses have been carried out, primarily led by the National Institute for Science and Technology (NIST) in America. A detailed report on the entire event has been published by NIST (2005), whilst numerous journal papers have been published by various authors (Gurley 2008; McAllister et al. 2013; Rein 2013; Clifton 2001). One interesting point to note is that in the WTC 7 building (the 47 storey building not hit by a plane) the collapse occurred due to thermal expansion of beams and the failure of a critical connection. Based on the WTC collapse various guidelines have been proposed for future high-rise structures.



The famous Cardington tests came about as a result of the behaviour observed in the Broadgate Phase 8 fire which broke out in a 14 storey building still under construction in England in June 1990 (SCI 1991). The fire spread through this unprotected, composite building, causing £25m worth of damage. Yet, of this damage only £2m was structural, and could be rectified within 30 days. The steel frame with composite decking survived the fire extremely well, and although large deflections were observed no collapse occurred. This prompted engineers to evaluate existing approaches to fire design as they did not reflect the behaviour of real fires in real buildings.

#### 2.4.4 Full-scale fire tests

Since 1985 a number of full-scale fire experimental tests have been conducted. These were generally prompted by the realisation that individual members behave differently from entire structural systems. A report by Almand (2012) summaries various test projects such as:

1. Stuttgart-Vaihingen University Fire Test (1985). Natural fires were imposed on the third storey of an existing office building.
2. William Street Tests (circa 1992). Tests were conducted by steel producer BHP Australia on a steel framed building to demonstrate the performance of a sprinkler system and highlight structural response.
3. William Street Tests (circa 1992). Again BHP conducted tests to demonstrate that a certain steel framed structure required no beam fire protection, and the sprinkler system was sufficient.
4. Cardington Steel Building Tests (1996), as discussed below.
5. French Car Park Fire Tests (1998-2001). Through these tests the European Coal and Steel Council proved that fire protection was not required on such open car park structures.
6. Harbin Institute of Technology Tests (circa 2007 & 2010). Two tests on two-dimensional steel frames were carried out to investigate overall structural behaviour.
7. Mokrsko Fire Test (2008). The Czech Technical University in Prague tested a structure consisting of a number of different construction types and member properties.
8. FRACOF Fire Test (circa 2008). An EU funded research project which was set up to determine whether the test results from the Cardington tests were applicable to fires of longer duration, and with factors such as higher loading during fires.
9. COSSFIRE Full Scale Fire Test (circa 2008). This test was similar to that of the FRACOF tests, but investigated six different slab edge connections during a standard fire.
10. University of Ulster Fire Tests (2010). These tests were carried out in Ireland and investigated the use of cellular beams under fire conditions.
11. TU Munich Fire Tests (2010). These were large-scale non-standard tests on composite slabs where intumescent paints were also applied to certain beams.
12. Veseli Fire Tests (2011). These tests in Prague incorporated a number of innovative construction techniques on an office block.

Detailed commentaries on the above tests are also presented by Gales et al (2012) and Bisby et al (2013).

#### 2.4.5 *The Cardington fire tests*

Significant advances have been made in structural fire engineering since the series of full-scale fire tests done at the BRE's Large Building Test Facility at Cardington from 1993 to 2003, as mentioned above and discussed in a report by the European Joint Research Program (1999). A series of seven tests were conducted on a 21m x 45m x 33m high steel framed building to investigate a variety of global structural responses. Significant research and design guidelines have been produced from this research program (Bailey & Moore 2000b; Rotter et al. 1999).

These tests demonstrated that the interaction between members has a significant effect on overall structural fire behaviour (Lennon 2011). It is interesting to note that during none of the tests any structural collapse was observed, even when the atmospheric temperature reached 1200°C, and the temperature of exposed steel beams reached 1150°C (Bailey 2002). Current design codes (BS5950-8, EN1994-1-2) predict that the beams would fail at temperatures of around 680°C. Figure 2.5 shows a photo of deflected beams and a buckled column as observed at the Cardington tests.



**Figure 2.5: Failed column and beams at the Cardington fire tests (Lamont 2001)**

#### 2.4.6 *Composite floors in fire*

From the Cardington and other full-scale tests various methods have been developed for calculating the capacity of composite floors exposed to severe fires. The change in the load carrying behaviour of a composite floor with increasing temperature is shown in Figure 2.6 (Bailey 2002). Yield line patterns are used to predict capacities and analyse slab panels. It is assumed that secondary beams form part of the slab. Floors become hanging catenaries at the fire limit state, supported by passively protected primary beams around the perimeter. When a slab has restraint around its edge a compression ring may result, whilst the hanging

catenary is in tension. A background document describing the theoretical behaviour and experimental tests conducted in the validation process of the MACS+ tensile membrane floor design software has been produced by Nadjai et al (2012). The MACS+ software is based upon the tensile membrane procedure originally produced by Bailey & Moore (2000a), which is normally referred to as the Bailey-BRE tensile membrane procedure.

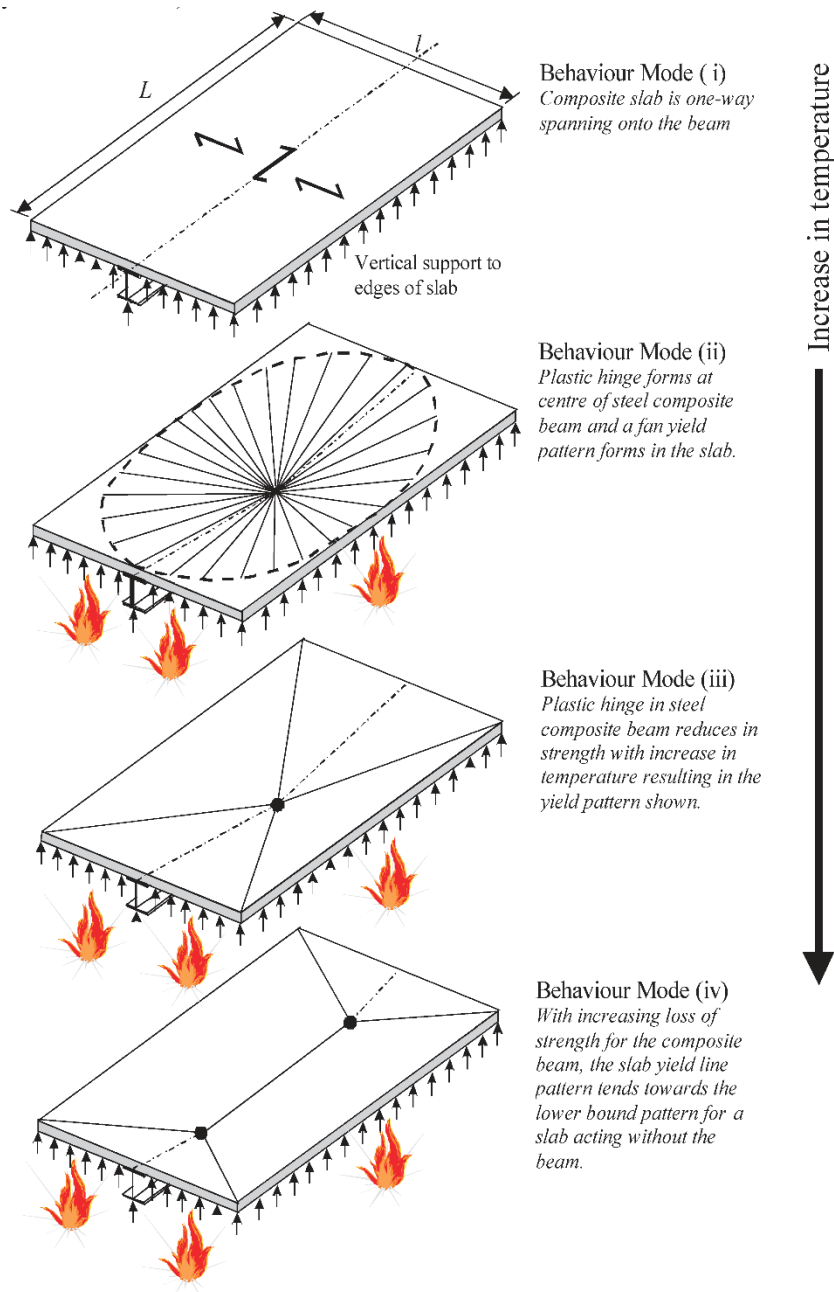


**Figure 2.6: Change in load carrying behaviour for a composite floor exposed to increasing temperatures (Bailey 2002)**

Clifton (2006; 2014) has developed the Slab Panel Method (SPM) based on the results from the Cardington tests and Bailey's tensile membrane model, along with additional research conducted. The SPM considers additional factors in comparison to methods mentioned above, and provides guidance regarding structural



detailing, rebar anchorage and more. Figure 2.7 shows a FE model that was used in the process of validating the SPM procedure. A cursory look at this model leads one to conclude that it is preferable to be able to model structures in fire using simpler methods, as extensive modelling time is required for full FE solutions.

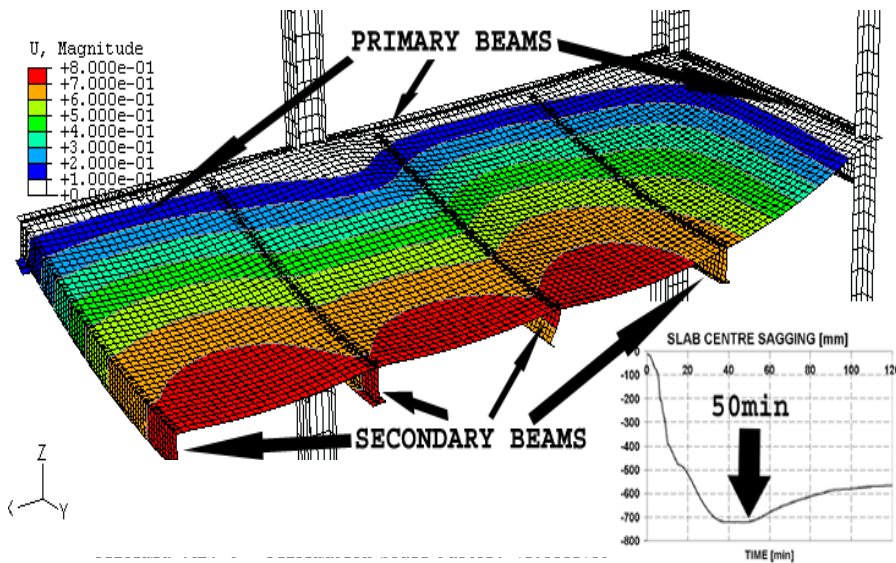


**Figure 2.7: Deflected shape of a composite structure considered by Clifton (2014) in the development of the Slab Panel Method (SPM)**

In the literature rectangular slabs with symmetrical boundary conditions are typically considered by composite floor design methods. However, Abu & Burgess (2010) discuss the fact that edge support conditions of rectangular slabs can significantly influence load capacity and the tensile membrane behaviour of structures. In Figure 2.8 various failure mechanisms that could potentially occur with different boundary conditions are shown. The mechanisms are different from the tensile membrane behaviour discussed above. From this it can be seen that typical tensile membrane compression rings may not necessarily form in structures, depending on the structural configuration.

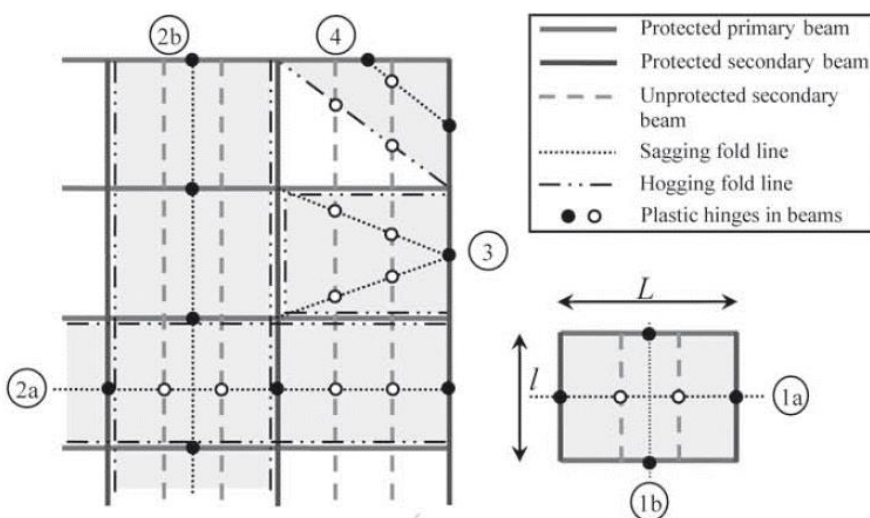


**Figure 2.8: Potential failure mechanisms in slab panels with various boundary conditions (Abu & Burgess, 2010)**

The modelling and full-scale testing of cellular beams composite with concrete floors has also been extensively researched, especially by the team at Ulster University and various groups in France (Nadjai et al. 2007; Nadjai et al. 2011; Naili et al. 2011; Bihina et al. 2013).

### ***Design of primary beams supporting slab panels***

Bailey's Method, the SPM and MACS+ explicitly model slab panels and provide suitable design methodologies for determining rebar specifications, slab thicknesses and secondary beam sizes. However, primary beams supporting slab panels must be considered after the design of slab panels is complete. The MACS+ Engineering Background document (Nadjai et al. 2012) explains that primary beams are designed based on calculating bending moments in beams using a plastic analysis, following either pattern 1a or 1b of Figure 2.8. Based on the moments calculated in beams the degree of section utilisation (i.e. ratio of fire limit state moment to ambient beam capacity) is calculated which is used to calculate critical temperatures at failure. Passive protection must then be specified to limit beam temperatures to the calculated critical temperature in a particular fire. The SPM guidelines (Clifton & Abu 2014) explain that primary beams should be designed based on applying distributed loads to beams according to the yield line patterns calculated for slab panels at failure. Recent research related to the SPM has highlighted that for exterior beams of buildings (i.e. edge beams where slabs are not continuous) the load applied to beams should be increased to ensure that primary beams do not fail plastically before slab panels reach the required fire resistance rating (Su & Zhang 2013; Gu 2016). In a draft version of a document to accompany the New Zealand steel code it is proposed that for "slab panel exterior edge beams" the fire exposure time should be increased by 1.35 times the design value (Clifton 2016).

#### ***2.4.7 Connection behaviour in fire***

The behaviour of connections in any type of building is important, but this is of particular interest when steel or composite steel structures in fire are considered. In his PhD thesis Al-Jabri (1999) discusses the behaviour of a variety of different types of steel connections and their behaviour in fire, as shown in Figure 2.9. It should be understood that connections will rarely behave as being fully pinned or fully fixed. Also, as larger rotations occur the stiffness of connections can change as components of a connection come into contact with each other. Significant research has followed Al-Jabri's work at Sheffield University (Block et al. 2013; Al-Jabri et al. 2005). In a recent study Anderson (2011) conducted extensive investigations into the behaviour of different connections in fire where various experimental setups and models were considered. Figure 2.10 is from Anderson's PhD thesis and shows numerical and experimental results from different connection configurations at 450°C. From the figures above it is clear that joint behaviour can have a significant influence on structural behaviour, although modelling such interactions is a complex task.

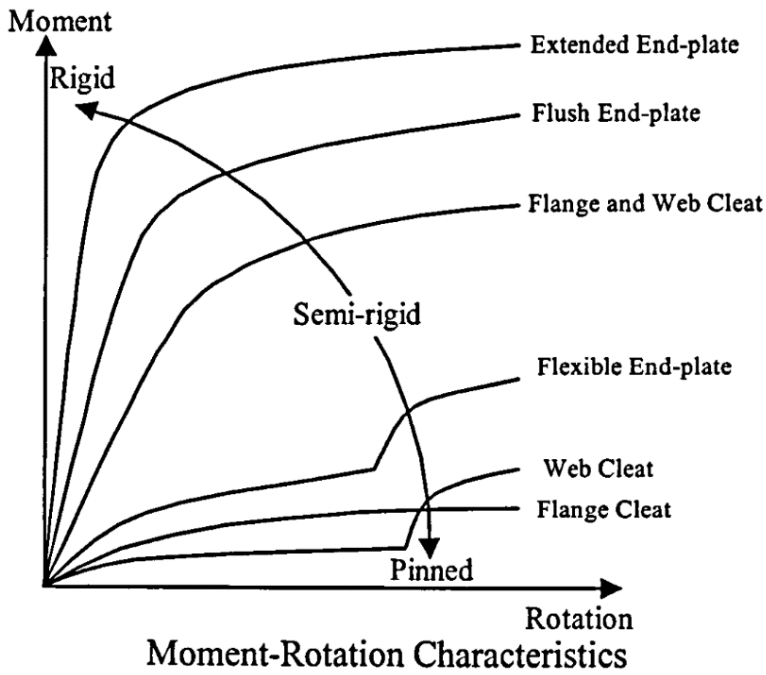
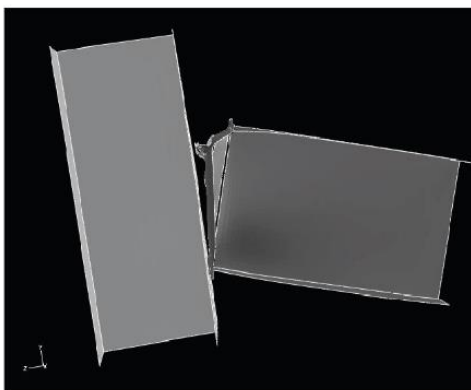


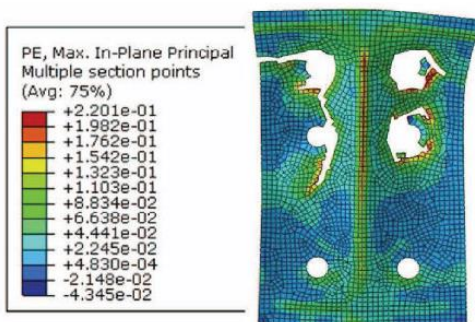
Figure 2.9: Moment-rotation behaviour of a variety of steel connections in fire (Al-Jabri 1999)



(a) Abaqus response at 450°C



(b) Experimental response at 450°C



(c) Strains in the end plate at 450°C



(d) Experimental end plate response at 450°C

Figure 2.10: Behaviour of an end plate connections at 450°C – experimental and numerical results (Anderson 2011)

Modelling bolt and connection interaction within a full 3D model is a challenging task requiring significant analysis time and computational cost. The benefit of an advanced model may be lost if boundary conditions are only crudely approximated with pinned or fixed conditions. Conversely, the benefit of using a simplified modelling tool is also lost if significant time is required to create sub-models for each connection.

#### 2.4.8 Composite structure modelling considerations

##### ***Determination of beam stiffness***

An important consideration when modelling multiple materials that contribute to the stiffness of a composite beam is how to adequately capture the combined stiffnesses of different elements without over or underestimating the stiffness contribution of constituent materials. When modelling systems in fire that experience (a) large deformations, (b) thermal gradients and (c) variable properties then factors such as membrane forces from shells and the thermal loads applied by elements become more difficult to consider than at ambient temperature. Thus, for nonlinear and high temperature analyses a single beam element has typically not been used. Rather, analysis models as shown in Figure 2.11 are commonly utilised, with typical configurations as outlined by Stadler (2012):

- a) Steelwork consisting of shell elements, connected with couplings to the concrete slab,
- b) Steelwork modelled as a beam element, connected with two couplings to the concrete slab via the top of the element,
- c) Steelwork modelled as a beam element, connected with couplings to the concrete slab,
- d) Steelwork modelled as a beam with an equivalent bending stiffness calculated about the centre of the concrete shell element, and directly linked to the nodes of concrete shell elements (as done in Vulcan (Burgess et al. 2015)).

These methods have typically performed well in the literature in a variety of scenarios and tests. However, modelling composite beams in this manner can potentially lead to the problems discussed Section 3.6.2, can require significant amounts of human time to model structures and may have a higher computational expense. Furthermore, forces calculated must be converted back into equivalent bending moments and axial forces that can be used for codified design. Hence, often design forces and bending moments need to be extracted from models through some form of post-processing of data.

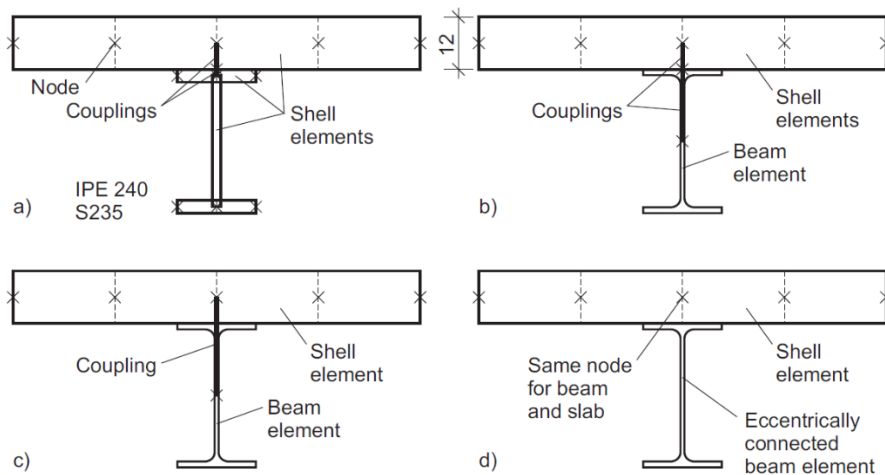


**Figure 2.11: Finite element configurations commonly used in the nonlinear analysis of composite slabs (Stadler 2012)**

### ***Interfacial slip***

In the research by Stadler (2012) the following important comment is made regarding the interfacial slip between concrete and steel beams because of shear studs: “In this work the shear studs and connection are assumed to be rigid since it delivers reasonable results compared to test data and no research results are available on this topic for the fire case”. Anderson (2011) notes that minimal information is available regarding the load-slip behaviour of shear studs. She comments that even the ductility of shear studs influences calculations and deflections, but insufficient data was available for the inclusion of such recommendations in her work. In the methodology developed by Huang et al (2000) for the analysis of three-dimensional composite structures in fire the assumption is stated that there “is no slip between the steel beam and concrete slab element”. However, slippage between composite elements in full FE models has been included by researchers such as Hozjan et al (2011), Huang et al (1999) or Ranzi & Bradford (2007). Boundary layers or non-linear springs are included between steel and concrete elements to model the slippage or partial connection between elements. This requires sophisticated models and the consideration of contact conditions. A challenge experienced with such methods is that there is often insufficient data to accurately verify results, although this is an ongoing topic of research.

Various researchers such as Shahabi et al (2016) have developed load-slip relationships between steel beams and concrete slabs. Determining such parameters in isolation is certainly possible but their inclusion in full 3D analyses introduces significant numerical challenges, where non-linear couplings or volume elements need to be included. The latter become problematic when considering other aspects of behaviour such as concrete cracking and the use of smeared crack models. Others researchers (Benedetti & Mangoni 2007) provide differential equations for predicting load-slip behaviour, but these are developed specifically for certain configurations. Hence, in general it can be seen that research results do exist for considering localised slippage

in composite beams. However, the majority of global analysis methods exclude such behaviour due numerical challenges or insufficient available data.

At ambient temperature the stiffness of a composite steel-concrete beam depends on the percentage of shear connection provided by shear studs or other such connectors. The following equation is an example of what can be used to determine the effective second moment of area of a composite beam (SAISC 2005):

$$I_{eff} = I_{steel} + 0.85p^{0.25}(I_{composite} - I_{steel}) \quad (2.4)$$

where  $I_{steel}$  is the second moment of area of only the steel beam,  $p$  is the percentage of shear connection and  $I_{composite}$  is the second moment of area of the full composite section, which has been transformed to be an equivalent steel section (i.e. concrete slab width factored by the modular ratio of  $E_{conc}/E_{steel}$ ). This equation effectively allows for slippage when calculating deflections by empirically modifying the bending stiffness of the total section. The potential application of such an empirical equation is discussed in Section 2.7

#### 2.4.9 Design engineer considerations

In research studies the floor panels analysed and tested are typically regular and rectangular. However, in practice unusual architectural features are often encountered, especially for the type of buildings that justify performance based fire design. Flint et al (2013) show that in real world structures challenges such as offset columns must be carefully considered and designed for, and such scenarios may affect the formation of compression rings, as depicted in Figure 2.12. Also, expanding internal beams may cause primary beams to experience minor axis bending and failure. Similar issues are highlighted by Law (2016) when he discusses the role of computer modelling in structural fire design. Hence, it can be understood that by providing tools which allow for entire structures to be more easily modelled such behaviour could possibly be identified and designed for. However, in any model localised failure (fracture of reinforcing steel) and buckling is difficult to predict.



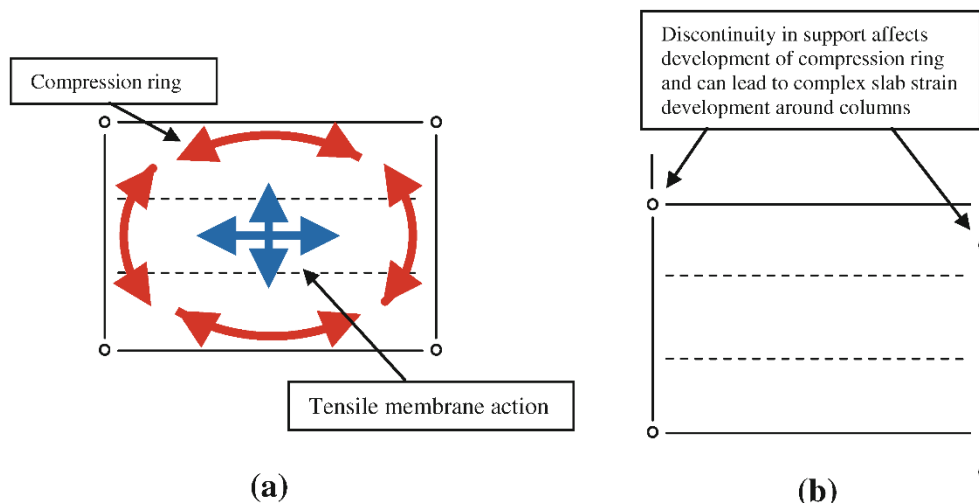


**Figure 2.12: In (a) a typical simply-supported slab is shown in which tensile membrane action can easily develop. However, in (b) offset columns and irregular bay sizes are experienced which may cause problems in the development of tensile membrane action (Flint et al. 2013).**

As an example of advanced design modelling Arup Fire in the UK reports that for the upmarket Heron Tower building in London structural robustness for a fire occurring over multiple floors was considered for the first time (Deeny, 2011). Such issues are the challenges faced by fire engineering practitioners and which modelling tools need to be able to address, rather than necessarily being more precise in very specific scenarios.

## 2.5 Finite element modelling of elements in fire

A variety of FE formulations have been used in structural fire analysis software, and could be considered for this research. The Total Lagrangian (TL) or Updated Lagrangian (UL) approaches are suitable for members with distorted axes and large deformations. The stiffness of such a member is found by integrating along its length and using polynomial shape functions. Refer to Bathe (2006) for extensive discussions regarding such methods, amongst others. However, in TL or UL literature it is always assumed that the neutral axis position of a beam element remains in the same cross-sectional position. Authors such as Gimena et al (2008) present similar methodologies for analysing distorted beam elements with variable cross-sectional properties along their lengths, but once again neutral axis positions remain fixed. Huang et al (2004) have developed a method based on the Total Lagrangian formulation for structures in fire that includes generalised cross-sections, changes in material properties and other nonlinearities. Variable neutral axes are not explicitly addressed, but are generally accounted for through the modelling of beams with multiple elements.

The corotational formulation (Iu et al. 2005) is another approach suitable for considering nonlinear behaviour, and has been selected for this work since it can be more easily adapted to meet analysis requirements. The corotational approach is based on using an updated coordinate system considering the new position of start and end nodes, and from this coordinate system member stiffnesses are determined. Local beam axis systems

do not distort to follow the path of a member between nodes, unlike the TL or UL approaches. Instead load and stiffness vectors are adjusted to account for local deformations. The overall methodology is further explained in Chapter 4. Researchers such as Crisfield (1990) have produced corotational formulations for considering nonlinear, three-dimensional beam elements. This system has been applied to structures in fire by Iu et al (2004; 2005), amongst others. Franssen (2005) incorporated the corotational approach into SAFIR, as discussed in Section 2.6.2.

## 2.6 Current structural fire design methodologies and software

A wide variety of advanced modelling tools are available for structures in fire as discussed below, and as introduced in Figure 1.1. Additional methodologies specifically relating to the modelling of the material behaviour of concrete in fire are discussed in Section 5.3.

### 2.6.1 *General purpose finite element software*

Various software tools for general finite element analyses are available, such as Abaqus (Dassault Systèmes 2013), DIANA (TNO DIANA 2016) or ANSYS (ANSYS 2016). By coupling these with specially developed subroutines for describing thermal effects and temperature-dependent material properties various authors have carried out fire analyses (Chen & Wang 2012). Often a thermal analysis has to be carried out first to obtain temperatures of all elements, followed by the mechanical analysis. .

### 2.6.2 *SAFIR*

SAFIR is possibly the most advanced of the software packages specifically tailored for fire, and was developed by Franssen (2005). Specific functions include: time-dependent temperature distributions, 2D or 3D analyses, finite element thermal analyses, non-linear material properties linked to thermal conditions, and the ability to consider large displacements and thermal expansions. It is interesting to note that connections between members are considered as either fixed or pinned, and no semi-rigid joints are considered. It appears that beam elements can only have uniform temperatures applied to them over their lengths and cross-sections.

### 2.6.3 *Stadler's analysis model*

In the PhD thesis by Stadler (2012) a novel method for analysing composite structures in fire is presented. It uses a simplified procedure where thermal effects are applied to structures through the use of pseudo temperature gradients. The model was built in Abaqus (Dassault Systèmes 2013) and linked to specially developed subroutines for the consideration of thermal and material effects. This method was tailored specifically for composite steel-concrete floor slabs. Shell elements are used for concrete slabs and for steelwork. Non-linear behaviour is accounted for by reducing member stiffnesses, but only linear-elastic analyses are employed. Additional discussions regarding this work are presented in Section 6.6.

### 2.6.4 *Vulcan*

Vulcan is a specially designed finite element software package for composite structures in fire. It has been developed by Burgess et al (2015) at the University of Sheffield. Earlier work was based on the research by



Bailey (1995), Najjer (1994) and significant other research projects. Vulcan is currently used in both industry and research. It uses shell elements for floor slabs and beam elements for steel beams. Steel beams have bending stiffnesses modified to be about the centre of the concrete, and it appears that their neutral axes remain in a fixed position. Tensile membrane action is explicitly considered.

#### 2.6.5 *Other software available for fire design*

A variety of other tools are available for the different aspects of structural fire design. Elefir-EN is a software package developed for the verification of structural members based upon the calculation methods of the Eurocodes (Franssen & Vila Real 2010). MACS+ is a free composite floor software package based on Bailey's method that uses tensile membrane action for designing composite decks (Nadjai et al. 2012).

In the FEAST software system steel beam sections are modelled using beam elements that are linked to concrete shell elements (Gillie et al. 2001). It is acknowledged that such elements do not predict the local flange buckling observed in the Cardington tests, although it has been shown that such local behaviour did not affect numerical models. Some advanced analysis FE software packages such as ADAPTIC (Izzuddin 2012) have been developed with beam elements that can account for elements in fire. However, only uniform temperatures can be applied to beam elements, similar to the aforementioned methods. In Section 6.5.1 the software OpenSEES is discussed. It is an advanced FE system that models composite slabs using layered shell elements coupled to beam elements for ribs and structural steelwork.

## 2.7 Summary

From this chapter it can be seen that significant advances have been made in the field of structural fire engineering. Various tools exist for analysing and designing buildings in fire, ranging from simple prescriptive methods to advanced modelling techniques. Many technical advances have come about through the full-scale tests that have occurred in the past decades. Fires are complex phenomena, and the response of structures to them is equally complicated. However, with the high level of uncertainty inherent in fire design it is important that designers take cognisance of the potential for assumed design variables being significantly different from actual values.

Structural fire practitioners often have to address buildings for which standard methods based on uniform layouts do not apply, necessitating rational design based upon engineering judgement. Passively protecting steelwork is very expensive and rational design can assist by providing more economically efficient structures. However, with the complexity inherent to most designs this has resulted in few rational fire designs being carried out for actual buildings.

The concept of the "consistent level of crudeness" is important when evaluating fire analyses and considering to what levels model predictions will match real world structural behaviour. In Chapter 5 the significant range of possible input variables for material and temperature models is addressed. When this is coupled with standard fire benchmarks it is questionable whether design methods can be extrapolated to provide highly

accurate predictions of actual structural behaviour in actual fires. Hence, simpler design methods which can be more easily tested in terms of sensitivity to input parameters may be preferable. Also, those methods which can be verified by approximate hand calculations may often be suitable in certain situations. The accuracy of outputs from advanced modelling techniques may be on par with simpler methods due to the inherent uncertainty regarding design variables. It is interesting to note that in Buchanan's (2001) well-known book on fire design approximate methods are presented for determining member resistance, and fundamental understanding is advocated rather than precision in design. However, it must be remembered that designs cannot be carried out purely based on intuition and understanding, as it is shown that some of the results in the parametric study of Chapter 7 are counter-intuitive.

The work presented in this dissertation provides a system for more easily determining deflections of structures in fire, assisting with identifying whether compartmentation can be maintained even when large deformations occur. However, the deflection of structures in fire is not strictly a limit state requirement when full performance-based design is carried out. In the case studies considered in Chapter 6 the ability of the FBE formulation to predict deflections is validated by comparing deflections with those measured in experiments. Such a comparison is important for investigating structural behaviour, but it must be remembered that deflections on their own may not be critically important in design, depending on the structural system utilised.

### *2.7.1 Finite element formulation adopted in this work as compared to the literature*

In Section 2.4.2 it was shown that in the literature steel beams that experience a temperature gradient can be considered as "composite" beams consisting of three materials, each with their own temperature and material properties. This concept is significantly extended in this dissertation where all cross-sections are modelled as consisting of a number of integration points, each with material properties dependent on the temperature and strain at that position. Section stiffnesses are computed by integrating material stiffnesses over the height of the section (i.e. a fine mesh discretisation is provided to characterise cross-sectional properties).

Various FE formulations exist for analysing beam elements, as discussed above. The corotational formulation has been selected as the most suitable for implementation in this dissertation. It provides the formulation that can be most easily adapted to neutral axes which are eccentric to the reference axis, while accounting for large deflections and non-linear behaviour. It has previously been included for fire analyses by Franssen (2005) and is suitable for future developmental work when 3D behaviour needs to be considered (Crisfield & Moita 1996). Members must be prismatic between nodes. For structures with significant changes in geometry across their length this can be accommodated by including a finer mesh. The work by Iu et al (2004; 2005) and Cai et al (2009) has been included in this research for calculating load vectors, for the consideration of deformations between nodes and for large deformations, as discussed in Chapter 4. Additional details regarding the implementation of the corotational approach are presented in Section 3.8.2.

Out of the finite element modelling tools currently available it can be seen that no methods provide a single beam element for considering cross-sections that are composed of multiple materials and have neutral axes

with positions that are not pre-determined. Also, it can be observed that methods are either significantly more complex in their modelling methodology or significantly simpler in their consideration of structural behaviour. However, the advanced modelling tools discussed can address certain aspects of structural behaviour, such as explicit joint modelling and catenary behaviour, which the Fire Beam Element (FBE) formulation cannot consider. Simple tabulated prescriptive methods will obviously be significantly faster to use than the FBE, but may be too conservative. Specifically, it can be seen that the design approach and FBE formulation proposed in this research does not currently exist and is a novel contribution to the field of knowledge.

### 2.7.2 *Design assumptions adopted for the FBE formulation*

Based on the discussions presented in this chapter various design parameters and procedures have been included in this research. Most importantly, the assumption of no slippage between concrete and steelwork in composite beams is adopted. With the uncertainty associated with such behaviour, lack of suitable information and the fact that similar assumptions have been used in other numerical models (discussed in Section 2.4.8) this assumption has been deemed to be justified. However, it should be noted that such an assumption may influence results calculated, although this is currently difficult to quantify. From the literature it can be observed that various researchers have included load-slip relationships in models (Hozjan et al. 2011; Ranzi & Bradford 2007). Additional research is required to include design equations that can account for such behaviour within a beam element, and this is one of the more important current limitations of the FBE formulation. For future research it may be possible to include empirical modifications to account for slippage as contained in Equation 2.4, and explained in Section 8.4.

Joints have either been assumed to be fixed or pinned in this research, following the assumption adopted in SAFIR, amongst others. However, in Section 2.4.7 it was shown that connections in fire may behave as semi-rigid elements. This is a topic requiring further research, as outlined in Section 8.4.

## **3 Chapter 3: Fundamental methodology and structural mechanics procedure developed for analysing structures in fire using beam elements**

### **3.1 Introduction**

This chapter shows how structures in fire can be modelled with modified Euler beam elements, i.e. Fire Beam Elements (FBEs), as introduced in Chapter 1. Concepts relating to the analysis of beams in fire are progressively introduced, and each section builds towards the overall analysis procedure employed in this work. Initially an explanation regarding the strains that occur in a material in fire is provided. These are then illustrated considering a cantilever which is uni-axially loaded and uniformly heated. The analysis formulation is presented for this very simple beam to highlight the methodology followed to analyse structures in fire. Thereafter a beam with non-uniform heating is considered to explain how stresses and strains vary over the height of a member due to combined thermal and external effects. This is followed by the overall procedure of analysis which is employed in this research. Only the analysis philosophy is introduced in this chapter, leaving the mathematical FE formulation and fire-specific material models to the following chapters.

Literature describing the effects of fire on beams in the manner that is explained in this dissertation is limited. Thus, in this chapter a number of key concepts are identified and defined. Furthermore, due to the complex behaviour that occurs in structures in fire this chapter seeks to illustrate such behaviour in a simple manner to assist understanding. Overall, the most important aspects of this chapter for the reader are (a) to understand how stresses and strains vary over the height of a section due to applied forces and thermal effects, (b) to become familiar with new terminology introduced in this dissertation, such as the Resultant Thermal Strain Load (RTSL) and associated terms, and (c) to appreciate the overall design procedure employed for considering complicated structures as a series of beam sections with equivalent properties.

#### *3.1.1 Academic contribution*

The primary academic contribution of this chapter is the design procedure and methodology for considering members in a structure as a series of beam elements with composite bending and axial stiffnesses, the FBE. Thermal effects are simulated through the application of pseudo-forces which cause the same strains as increasing temperatures do. The methodology presented is based upon first principles, with the only assumption required being that Euler-Bernoulli behaviour must hold, i.e. plane sections remain plane. This means that shear deformations are regarded as negligible. The proposed methodology is applicable to any structure for which temperature-stress-strain curves are available for constituent materials. For composite sections slippage between components is assumed to be negligible.

### 3.2 Strains in fire

Before considering the behaviour of entire beams it is necessary to explain material strains in fire. The total strain,  $\varepsilon$ , of a material exposed to stresses, temperature and time-dependent phenomena is given by the following, according to EN 2-1-2 (BSI 2005a):

$$\varepsilon = \varepsilon_{\theta} + \varepsilon_{\sigma} + \varepsilon_{creep} + \varepsilon_{tr} \quad (3.1)$$

This consists of thermal strain,  $\varepsilon_{\theta}$ , mechanical strain,  $\varepsilon_{\sigma}$ , creep strain,  $\varepsilon_{creep}$ , and transient strains,  $\varepsilon_{tr}$ . The transient strain can be defined as “the difference in strain between concrete that is heated under load and concrete that is loaded at elevated temperature; this strain develops during first-time heating and is irrecoverable” (Gernay & Franssen 2012). This highlights that the behaviour of certain materials, especially concrete, is different depending on whether it is heated and then loaded, or loaded and then heated. In EN 2-1-2 and EN 3-1-2 transient strain and creep are not explicitly addressed, but rather implicitly considered in the material models and reduction factors provided (see Section 5.3). Since the material models used in this work for concrete and steelwork are primarily based upon the Eurocodes strains will be considered as consisting of only thermal and mechanical components, with the excluded terms implicitly accounted for through the material models. The strain equation above is thus reduced to:

$$\varepsilon = \varepsilon_{\theta} + \varepsilon_{\sigma} \quad (3.2)$$

The mechanical strain,  $\varepsilon_{\sigma}$ , consists of components due both to externally applied mechanical loads and internally induced stresses caused by thermal effects as explained in Section 3.4.

### 3.3 Behaviour of a uni-axially loaded and uniformly heated beam

The strain behaviour explained in Equation 3.2 is illustrated in Figure 3.1 which shows an unstressed rectangular beam of length  $L$ , as shown in (a), with a compressive point load applied to it causing mechanical strains in (b) leading to a deflection of  $L \times \varepsilon_{\sigma}$ . If this beam is then exposed to a fire and uniformly heated it will elongate as in (c), resulting in the total strain now being the sum of these two strain components,  $\varepsilon = \varepsilon_{\theta} + \varepsilon_{\sigma}$ . An analysis model for considering the behaviour of the beam is shown in (d), where the beam is modelled as a two-noded bar element with each node having only translational degrees of freedom.

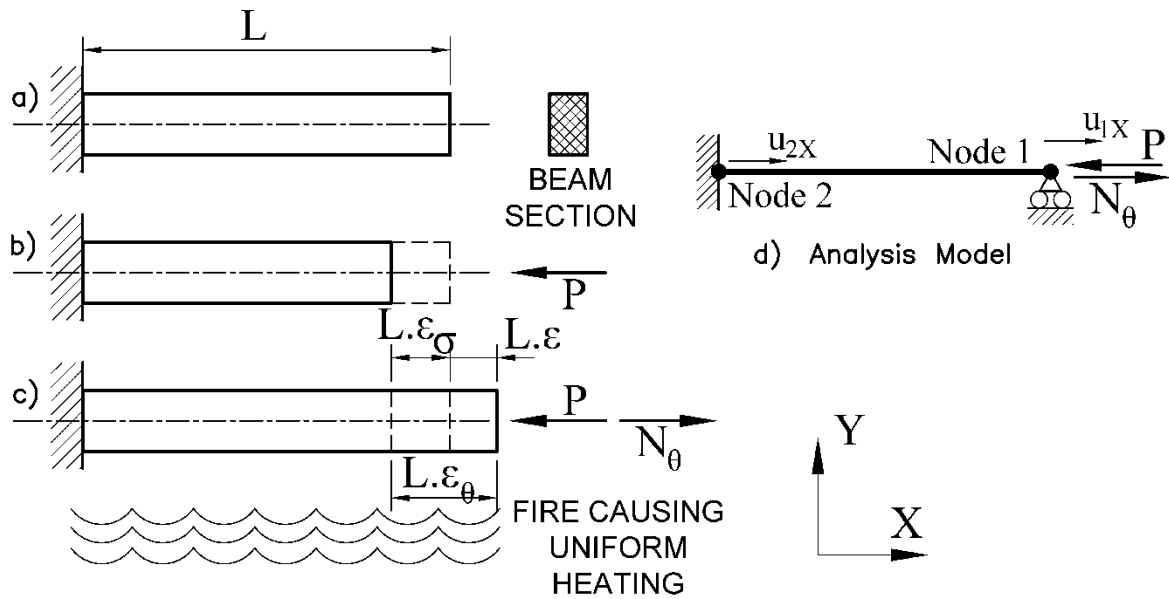


**Figure 3.1: Behaviour of a uni-axially loaded beam subjected to mechanical and thermal loads**

If the beam was fully restrained it would mean that the total strain would be zero, thus giving:  $-\epsilon_\theta = \epsilon_\sigma$ . This is an important relationship to note since in a restrained beam an increase in temperature will result in an element being in compression, with a compression strain of equal magnitude to the thermal strain. Note that throughout this research the sign convention for stresses and strains is taken as *negative for compression* (i.e. elements become shorter) and *positive for tension* (i.e. elements become longer).

In structural analysis software temperatures are typically not directly used in matrix analysis procedures, which at their most basic level directly consider (a) load vectors, (b) stiffness matrices and (c) deformation vectors (i.e.  $\mathbf{F} = \mathbf{K}\Delta$ ). Thermal effects need to be converted into equivalent thermal “forces” which cause the same deflections as the thermal strains would. These are included in the total load vector, as will be shown below. In this research the “force” which simulates the axial thermal effects will be called a **Resultant Thermal Strain Load** (RTSL), with the symbol  $N_\theta$ . This “pseudo-force” is caused by **Equivalent Thermal Stresses** (ETS), with symbol  $\sigma_\theta$ . The term RTSL is included to differentiate between these pseudo forces that are required to simulate thermal elongation and those forces that are externally applied or result due to boundary conditions. For clarity externally applied forces are referred to as **mechanical forces**. These forces can be sub-divided into *applied mechanical forces* due to external loads and *induced mechanical forces* due to boundary conditions or restraint. In complicated structures it is difficult to differentiate between these two effects. Hence, for simplicity all forces externally applied to a member will generically be referred to as *mechanical forces*.

It should be appreciated that mechanical and thermal forces affect members in different manners. A mechanical force will cause both strains and stresses in a member when applied. However, a thermal force will cause strains and no stresses in an unrestrained member, but stresses and no strains in fully restrained

member. Both mechanical and thermal load vectors are required for calculating total deflections relative to the unloaded and unheated initial configuration of a structure.

As will be explained in Section 3.4, if the RTSL is applied eccentrically in a cross-section it will result in an equivalent thermal “pseudo-moment” which will cause curvature. This occurs due to non-uniform heating of elements. The thermal “moment” which simulates curvature will be referred to as a **Resultant Thermal Strain Moment** (RTSM), with the symbol  $M_\theta$ . Once the RTSL, RTSM and mechanical forces have been calculated for a structure analyses can be performed using fundamental structural analysis procedures (e.g. Coates et al (1990)), with iterative procedures used to account for non-linear behaviour (Cook et al. 2001). By analysing elements using beam finite elements Euler-Bernoulli behaviour will always hold due to the mathematical formulation and assumptions employed. This is addressed further in this chapter.

For the example above we shall now calculate the RTSL,  $N_\theta$ , that induces the thermal strain,  $\varepsilon_\theta$ . This is given by:

$$N_\theta = A\sigma_\theta = A\varepsilon_\theta E_\theta = A\alpha_\theta \theta E_\theta \quad (3.3)$$

where  $\sigma_\theta$  is the *Equivalent Thermal Stress* (ETS) and it acts over an area  $A$ . The material has an elevated temperature  $\theta$  above ambient, a Young’s modulus of  $E_\theta$ , and  $\alpha_\theta$  is the coefficient of thermal expansion for the material. At this stage we shall assume that  $E_\theta$  and  $\alpha_\theta$  are independent of temperature or strain, and that the material remains linearly-elastic. These limitations are removed in later sections and chapters.

To mathematically calculate the deflection of the element in Figure 3.1 the following fundamental relationship is used:

$$\mathbf{F} = \mathbf{K}\Delta \quad (3.4)$$

For this relationship  $\mathbf{F}$  is the total applied load vector,  $\mathbf{K}$  is the stiffness matrix and  $\Delta$  is the resultant deflection vector. Letters in bold represent matrices or vectors. The stiffness matrices used for analysis in this research are introduced and derived in Chapter 4. Matrix procedures presented in this chapter are purely for illustration purposes, to highlight how the mathematics adopted relates to the structural behaviour described, and to illustrate how thermal forces are accounted for.

From Figure 3.1 it can be seen that the total deflection is caused by both thermal and mechanical effects. Hence, if we consider the beam as a two-noded bar element with only translational degrees of freedom in the  $x$  direction the load vector becomes:

$$\mathbf{F} = \mathbf{F}_m + \mathbf{N}_\theta = \begin{Bmatrix} -P \\ 0 \end{Bmatrix} + \begin{Bmatrix} N_\theta \\ -N_\theta \end{Bmatrix} = \begin{Bmatrix} -P + N_\theta \\ -N_\theta \end{Bmatrix} \quad (3.5)$$

where  $\mathbf{F}_m$  is a force vector of all the mechanically applied loads and  $\mathbf{N}_\theta$  is a vector of all the RTSL values. Since the beam tries to elongate in both directions  $N_\theta$  is applied at both nodes, but in opposite directions. In

such a simple system forces and deflections could be determined by inspection. However, the following illustrates the procedure that a structural analysis method would follow to calculate forces. Firstly the stiffness matrix is compiled and the following relationship is used:

$$\mathbf{F} = \begin{Bmatrix} -P + N_\theta \\ -N_\theta \end{Bmatrix} = \mathbf{K}\Delta = \begin{bmatrix} EA/L & EA/L \\ -EA/L & -EA/L \end{bmatrix} \begin{Bmatrix} u_{1x} \\ u_{2x} \end{Bmatrix} \quad (3.6)$$

Boundary conditions are now applied, i.e.  $u_{2x} = 0$ , giving:

$$\mathbf{F}' = \{-P + N_\theta\} = \mathbf{K}'\Delta' = [EA/L]\{u_{1x}\} = \frac{EAu_{1x}}{L} \quad (3.7)$$

The inverted, conditioned stiffness matrix is multiplied by the force vector to calculate the final deflections,  $\Delta' = \mathbf{K}'^{-1}\mathbf{F}'$ . From this term the horizontal deflection of the cantilever tip is determined as:  $u_{1x} = \frac{(-P+N_\theta)L}{EA}$ , as would be expected. The total deflection vector is now created by back substitution and used to determine the final resultant force vector,  $\mathbf{F}_R$ , which includes reaction forces, such that:

$$\mathbf{F}_R = \begin{Bmatrix} -P + N_\theta \\ P - N_\theta \end{Bmatrix} = \mathbf{K}\Delta = \begin{bmatrix} EA/L & EA/L \\ -EA/L & -EA/L \end{bmatrix} \begin{Bmatrix} u_{1x} \\ 0 \end{Bmatrix} \quad (3.8)$$

Now, to calculate the resultant internal forces in the element due to mechanical forces:

$$\mathbf{F}_\sigma = \mathbf{F}_R - \mathbf{N}_\theta = \begin{Bmatrix} -P + N_\theta \\ P - N_\theta \end{Bmatrix} - \begin{Bmatrix} N_\theta \\ -N_\theta \end{Bmatrix} = \begin{Bmatrix} -P \\ P \end{Bmatrix} \quad (3.9)$$

This result is trivial and intuitively correct, but the procedure illustrates a number of key aspects that are more difficult to highlight when non-linear material models and complicated geometries are included. Firstly, it must be understood that to calculate the final internal forces the  $\mathbf{N}_\theta$  vector must be subtracted from the total resultant internal force vector.

If the beam had been fully restrained at both ends, and omitting the axial load  $P$ , it would have resulted in zero deflection, i.e.  $\Delta = \mathbf{0}$ , which then leads to a zero final force vector, thus giving:

$$\mathbf{F}_\sigma = \mathbf{F}_R - \mathbf{N}_\theta = \begin{Bmatrix} 0 \\ 0 \end{Bmatrix} - \begin{Bmatrix} N_\theta \\ -N_\theta \end{Bmatrix} = \begin{Bmatrix} -N_\theta \\ N_\theta \end{Bmatrix} \quad (3.10)$$

A similar type of restraining effect occurs when the top section of a beam, say the concrete slab of a composite section, restrains a much hotter portion below it, such as a steel beam exposed to fire. This internal, cross-sectional restraint will now be explained.

### 3.4 Non-uniform heating of beams and the resulting behaviour

When bending moments and non-uniform temperatures are considered for beams the behaviour presented above becomes significantly more complex. We shall now consider the same beam but where it has a lower portion uniformly heated by temperature  $\theta$  while the upper half remains unheated, and a mechanical moment is also applied. The step-by-step methodology for determining both total deflections and final stresses in the beam is as follows, as illustrated by Figures 3.2 to 3.8, with explanations provided below each figure:



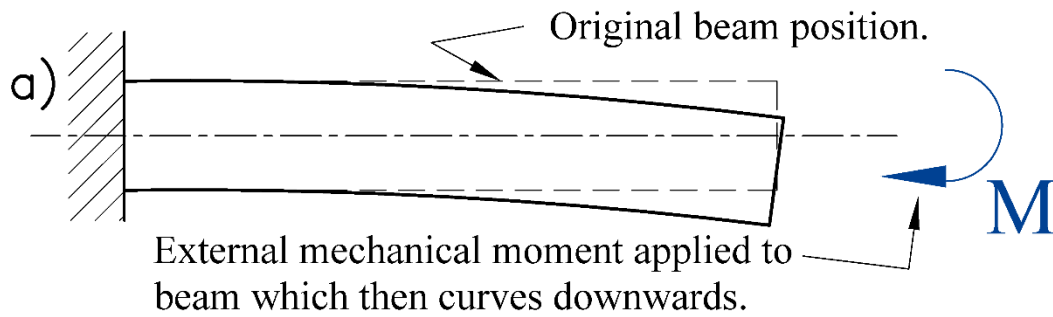


**Figure 3.2: Analysis Step (a) – Rectangular beam with mechanical load applied**

A mechanical moment  $M$  is applied causing deformations. In any real world structure the mechanical loading will be applied before fire occurs.

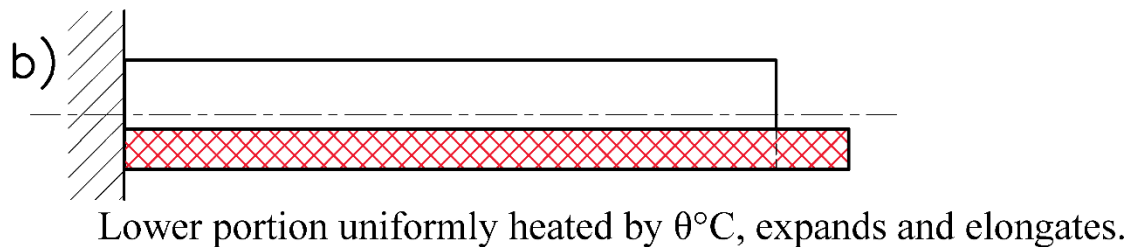


**Figure 3.3: Analysis Step (b) – Uniform increase in temperature of a portion of the beam, with no shear strength assumed for the section**

The rectangular beam has a lower portion that is now uniformly heated by  $\theta^{\circ}\text{C}$ . If the beam was to have no cross-sectional restraint, i.e. no transverse shear strength between horizontal fibres such that it is free to slip, only the heated portion would expand (mechanical deformations are not shown for clarity). Since cross-sectional restraint exists such behaviour does not occur.

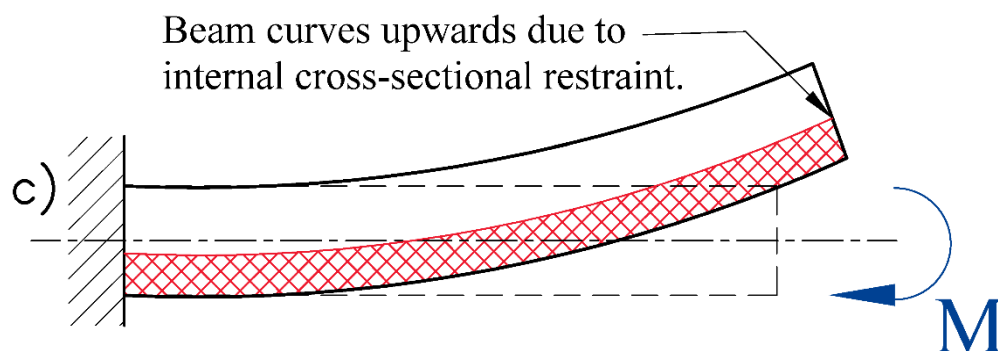


**Figure 3.4: Analysis Step (c) - Upward curvature of beam due to cross-sectional restraint**

Intuitively it can be understood that as the temperature increases the beam will tend to bow upwards due to internal cross-sectional restraint. The cooler upper section restrains the heated lower section, thus causing the upper portion to experience tension while the lower portion has compression induced in it. Internal stresses are

introduced which are independent of external mechanical loads. This process ensures that static equilibrium is maintained in each cross-section. Depending on the magnitude of  $M$  the final deflection may be upwards or downwards.

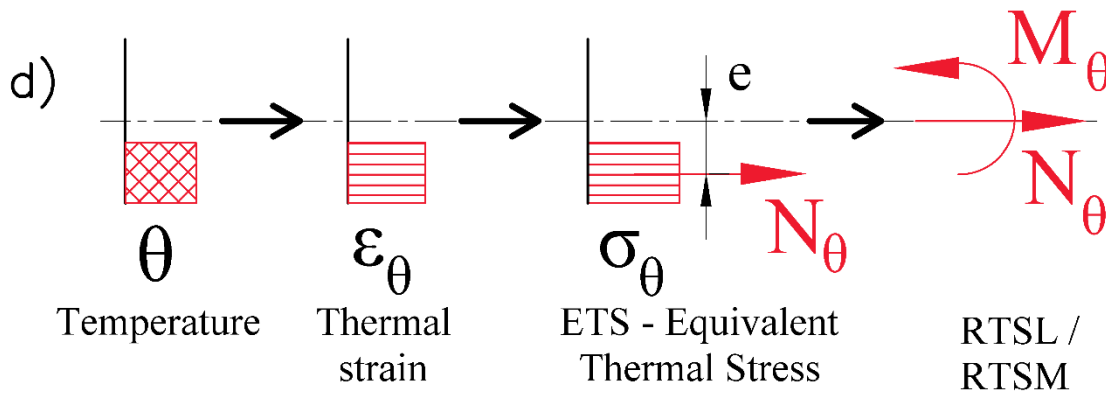


**Figure 3.5: Analysis Step (d) – Converting temperature effects into resultant RTSL/M forces**

The lower portion is at temperature  $\theta^{\circ}\text{C}$  and has a cross-sectional area  $A$ . To simulate the thermal strain an Equivalent Thermal Stress (ETS),  $\sigma_{\theta}$ , is determined based on the properties of the material. The resultant “force” of the “stress” acting over the area is:  $N_{\theta} = A\sigma_{\theta} = A\varepsilon_{\theta}E_{\theta}$ . This RTSL acts eccentrically to the neutral axis and causes a RTSM of  $M_{\theta} = N_{\theta}e$ . These two pseudo forces act about the NA. Section 3.6 describes how  $N_{\theta}$  and  $M_{\theta}$  are calculated for a generic section.

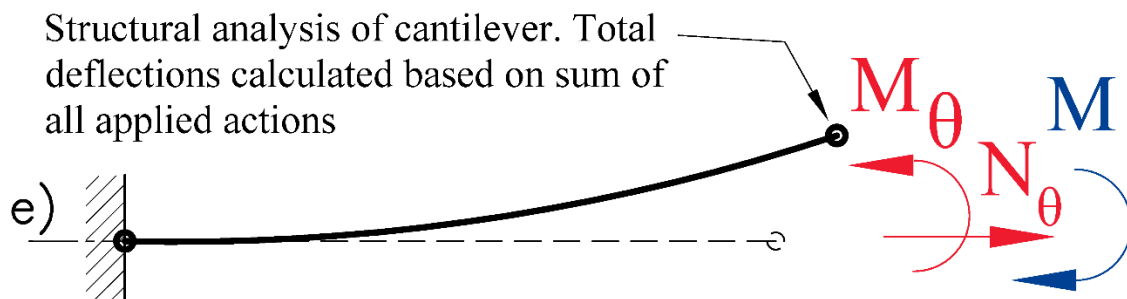


**Figure 3.6: Analysis Step (e) – Calculation of deflections based on applied forces**

A simplified analysis model of the beam is now created consisting of a two-noded element with translational and rotational degrees of freedom. Mechanical and RTSL/M forces are applied and the resulting deformations calculated based on the properties of the member. This is carried out using fundamental structural mechanics of  $F = K\Delta$  according to Equation 3.4 and the procedure above. The stiffness matrix,  $K$ , is calculated in Section 4.2. At this point only global deformation degrees of freedom have been solved for. From these global deformations total internal forces in individual members are then calculated, and converted into the local coordinate system (Cook et al. 2001). Based upon these total internal forces, with the assumption of plane sections remaining plane, total strain profiles in sections are determined. Since strains and forces consist of both thermal and mechanical components post-processing of members is needed to analyse cross-sectional

properties. Stresses in members cannot be directly calculated from deformations as this would falsely indicate that the thermal elongations result directly in mechanical stresses.

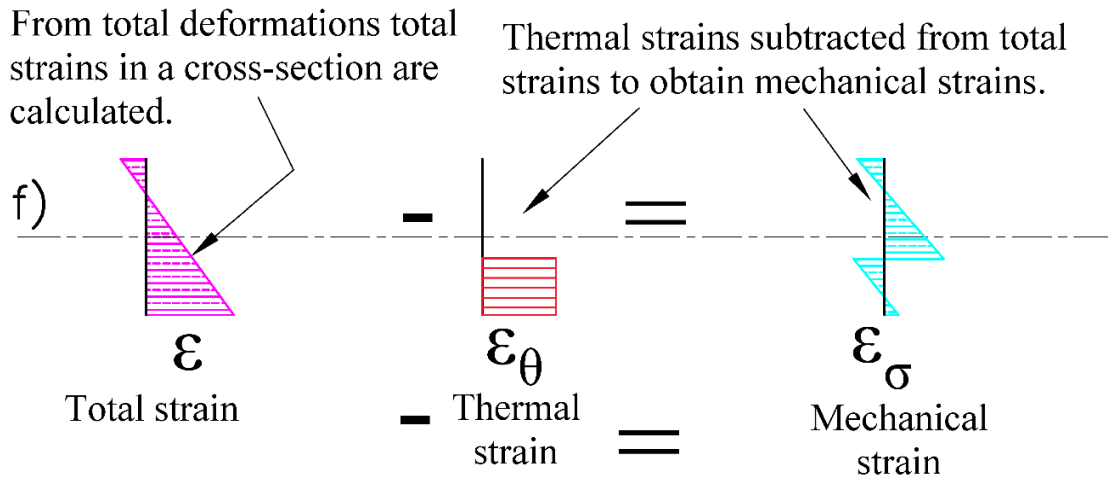


Figure 3.7: Analysis Step (f) – Determination of mechanical strains from total strains

Thus, through a post-analysis process the total strains occurring in members are determined according to:

$$\epsilon = \epsilon_{axial} + \epsilon_{bending} = \frac{(N_{\theta})}{EA_{\theta}} + \frac{(M + M_{\theta})y}{EI_{\theta}} \quad (3.11)$$

$y$  is the distance from the NA. In the same way that the thermal force was subtracted from the total force to calculate the internal mechanical force in Equation 3.9 here the thermal strains,  $\epsilon_{\theta}$ , are subtracted from the total strains,  $\epsilon$ , giving the mechanical strains,  $\epsilon_{\sigma}$ . The magnitude of this mechanical strain is influenced both by the mechanical forces and internal cross-sectional restraint forces that result from non-linear heating. The total strain has physical significance in that it can be measured and observed. However, mechanical strains cannot be directly measured but must rather be calculated. In a typical structure the influence of restraint and mechanical loading cannot be identified separately, as discussed above, so they are considered together.

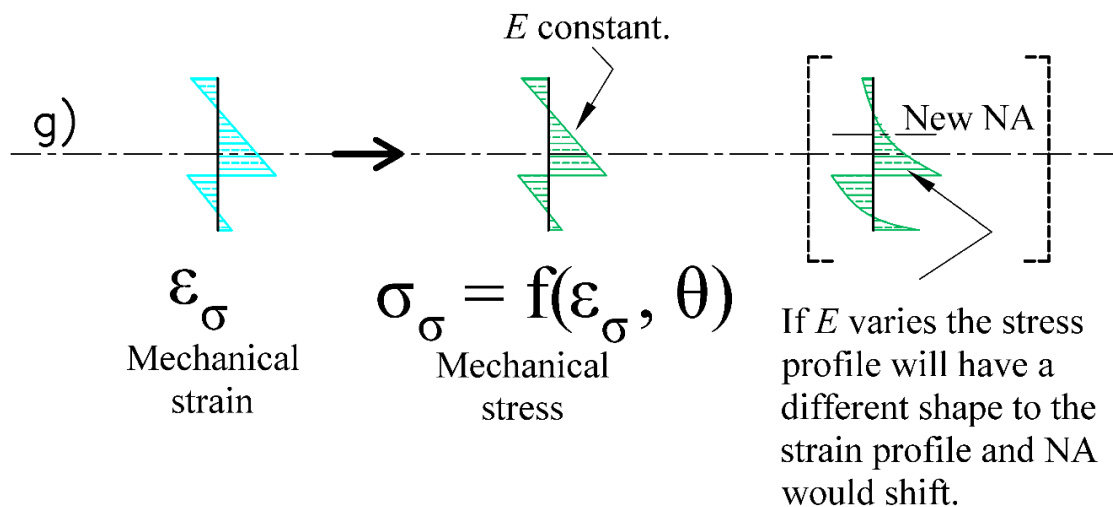
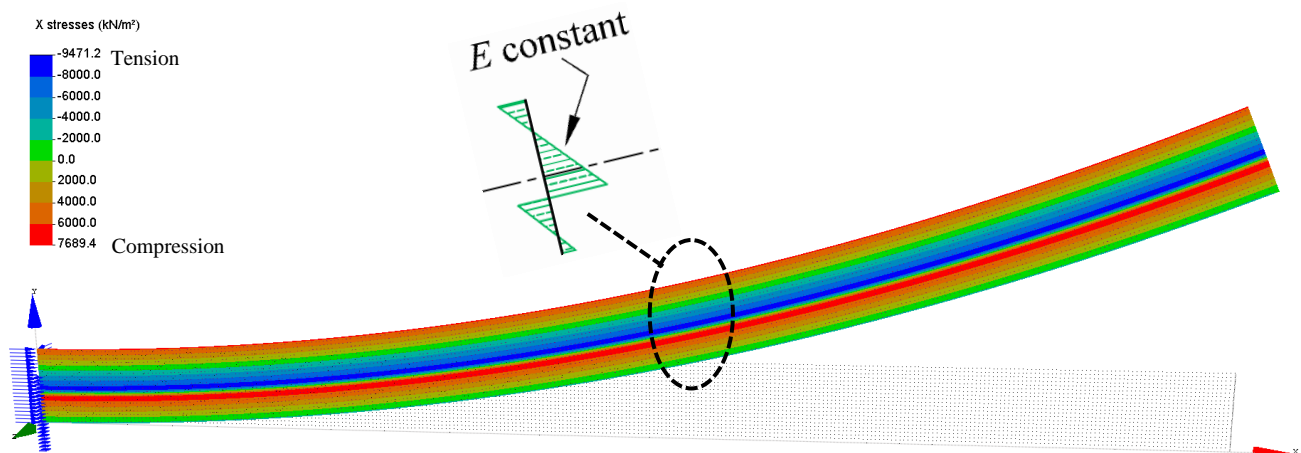


Figure 3.8: Analysis Step (g) – Calculation of mechanical stresses based on mechanical strains

From the mechanical strains the final mechanical stresses in the section are calculated. In this simplified example the stress distribution matches the strain distribution since a constant  $E$  value is used. These stresses are induced by both mechanical and thermal effects. In this example superposition could be used to independently show the influence of mechanical and thermal effects in two separate analyses. However, for non-linear stress-strain curves a more complex stress profile will be obtained, as shown in the final distribution where  $E$  varies. When this occurs the neutral axis (NA) will shift and iterative methodologies need to be adopted, as will be explained in Chapter 4. Thus, in fire analyses it cannot be directly determined what proportion of the stress is due to thermal or mechanical effects.

### 3.4.1 Verification example

Consider Figure 3.9 which has been included as a simple example to illustrate the unusual profile of mechanical stress that can occur. This figure shows the stresses determined by a finite element program for a rectangular cantilever composed of shell elements. The beam has had the bottom two-fifths uniformly heated, following the example above. No mechanical loads have been applied. Material properties are linear-elastic and not temperature or strain dependent. From the results it can be seen that the same  $\sigma_\sigma$  profile as explained in Figure 3.9 is present here along the length of the beam. At the top of the heated zone and at the very top of the beam compression occurs (the stresses in red) (in this figure the sign convention is positive for compression). Just above the heated zone maximum tension occurs (in blue), and there is some tension at the bottom fibres of the section. There is an instantaneous change in stress with height at the change in temperature. In this figure the software plots stresses at nodes as the average of stresses from adjacent elements giving the appearance that there is a transition zone (the green band at the two-fifths position) which is not the case.



**Figure 3.9: Stresses in a rectangular cantilever with the lower two-fifths uniformly heated**

### 3.5 Analysing structures using multiple beam elements

For the example presented in Section 3.4 only a single beam element was used. However, to illustrate how multiple beam segments are included consider Figure 3.10. In this case the beam shown in (a) is divided into four segments in (b) where each element has its own bending ( $EI$ ) and axial stiffness ( $EA$ ). If segment properties vary with temperature they will be called  $EI_\theta$  and  $EA_\theta$ . Here it can be seen that RTSL/M forces must be applied at the end of each segment onto the nodes. If properties are uniform it would result in all internal moments counteracting each other such that the final load vector,  $\mathbf{F}$ , would only have a non-zero moment term at the cantilever tip. If the FBE formulation was programmed into a software system users would not directly apply the RTSL/M values. The user would specify temperatures or temperature profiles and these would be converted into resultant forces by the software and applied to elements for the calculation of deflections, stresses and strains. However, a pseudo implementation of the methodology is presented in Section 3.9 below, where users can manipulate existing FE software to account for the effects of RTSL/M pseudo forces, by applying them as external loads in Euler beam models.

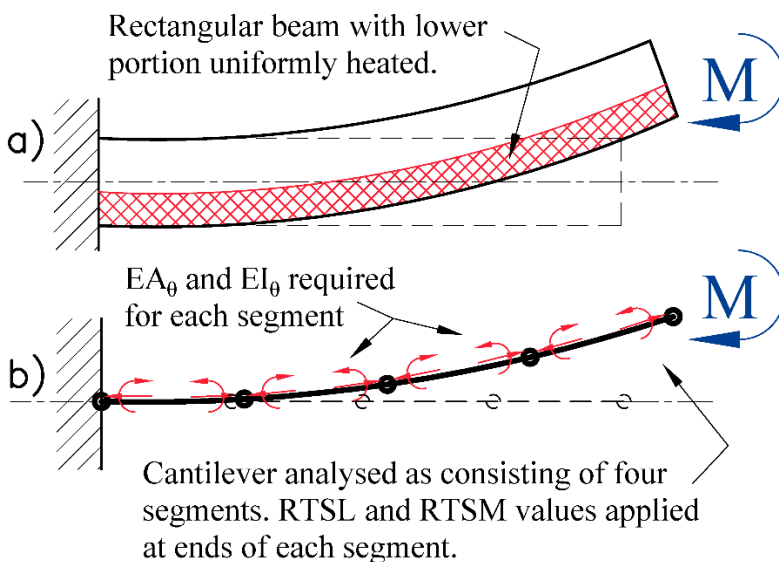


**Figure 3.10: Analysis model for a cantilever with a uniformly heated lower portion**

To illustrate the effect of restraint consider Figure 3.11 which shows the same beam, but now the boundary conditions have changed such that the beam is fixed-fixed. As before, no external mechanical loading is applied. The final load vector will only have zero terms, i.e.  $\mathbf{F} = \mathbf{0}$ , leading to the scenario where the beam will not deform, giving  $\Delta = \mathbf{0}$ . Here internal axial and bending forces will be of the same magnitude as the thermal effects. Member properties, internal forces and strains will be constant for the entire beam.

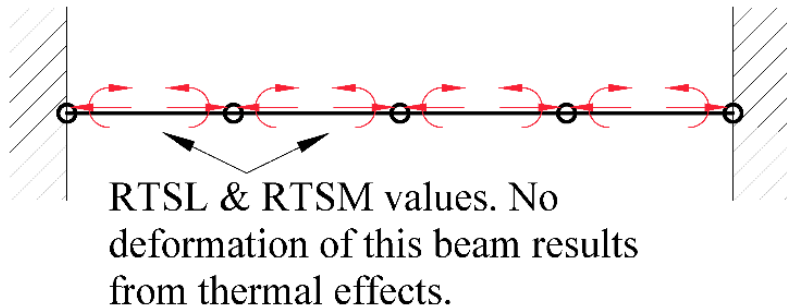


**Figure 3.11: Fixed-fixed beam with uniformly heated lower portion resulting in no deformation**

### 3.6 Considering movable, eccentric neutral axes

When a structural member is heated during a fire it typically experiences a temperature gradient. The increase in temperature causes material stiffnesses to change, where materials typically lose stiffness with increasing temperature. Materials such as concrete and steel also have non-linear stress-strain curves at elevated temperature (see Chapter 5), which implies that stiffnesses will reduce with increasing temperature and / or stress. This would cause the NA of a section to migrate towards the stiffer side of the section. The NA is defined as the position of zero strain when a cross-section is subjected to pure bending.

#### 3.6.1 *The need for a composite finite element that accounts for changing NA position*

To illustrate the effect of the change of the NA on the stiffness of a beam element an IPE 200 cross-section will be considered, as shown in Figure 3.12. The radii at the interface between the flanges and web have been ignored. In (a) the section properties are given when the Young's modulus ( $E$ ) is constant across the section, as is typically the case for most homogenous elements. In (b) the value of  $E$  is varied linearly from zero at the base to 200 GPa at the top of the section. Although such large changes are generally not found in practice, there can be large thermal gradients across a member in a fire causing stiffness variations. In certain instances brittle materials, such as concrete, can fail causing large stiffness changes in a composite member, implying changes in material stiffness over a member's height.

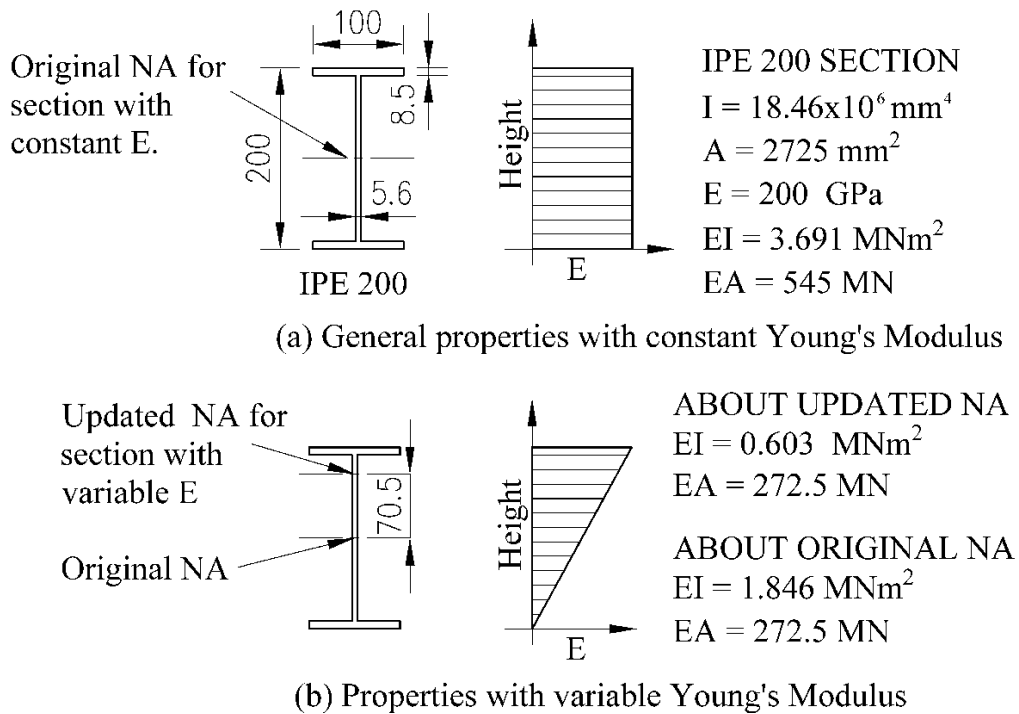


**Figure 3.12: Changes in neutral axis and bending stiffness of an IPE 200 due to the Young's modulus varying**

The original NA position of the section occurs at its mid-height, whilst the updated NA moves upwards by 70.5mm because of the varying material properties. If the bending stiffness,  $EI$ , is calculated using the variable material properties in (b) about the section's original NA the value decreases by 50.0% relative to the original value of  $3.691 \text{ MNm}^2$ . This is as expected since the average  $E$  value over the height is half that of the original value. However, if the NA is recalculated to be at the position 70.5mm above the original, and the bending stiffness is recalculated about this updated axis then the  $EI$  value decreases by 83.7% relative to the original. Thus, the difference in final bending stiffness values varies by 206% ( $0.603$  vs.  $1.846 \text{ MNm}^2$ ) depending on which axis the stiffness is calculated about. In reality the member would be bending about the updated NA, based upon fundamental structural mechanics, so the revised stiffness should be used. Note that the axial stiffness,  $EA$ , of the element is unaffected by the NA position.

Assuming that the NA position remains unaffected by changes in material properties can lead to significant inaccuracies in structural analysis, as pointed out above, especially in fire situations where temperature increases lead to large changes in material stiffness over the height of a section. Hence, it can be concluded that when calculating the bending stiffness of a beam element it is important that values are calculated about the updated NA of the entire beam element. The challenge is that this position can vary in a member as an analysis progresses, and may even change suddenly (such as when concrete cracks), and these aspects will be dealt with below.

### 3.6.2 Composite FE challenges encountered when eccentricities are not considered

In an important PhD work on the modelling of structures in fire Bailey (1995) developed a method for considering the non-linear, inelastic behaviour of elements subjected to severe fires. With further research and advances Bailey's thesis, amongst numerous other projects, has developed into the well-known finite element software named Vulcan, as discussed in Section 2.6.4. Composite slabs are modelled by creating shell elements for the concrete slab, linked to steel beams which have their stiffnesses calculated relative to the centre of the concrete slab, i.e. eccentric from the NA of the steel beam, as shown in Figure 2.11(d).

When verifying Bailey's method numerical tests were done in which different thicknesses of concrete slabs were coupled with symmetric steel beams, as shown in Figure 3.13. The steel beams were uniformly heated and the upward curvature, or thermal bowing, of the composite systems calculated. For the case where the slab has zero thickness ( $h = 0$  mm) the graph shows the system to have the maximum upward curvature. However, in reality if a symmetric beam with no slab on top was uniformly heated it would simply elongate horizontally, and no upward bowing would occur, because the NA would be, and stay at, the centre of the steel beam. Hence, from this example it can be seen that forcing the NA of a composite system to be in a fixed position can lead to error. It should be noted that geometric non-linearity which addresses this problem has since been included in Vulcan (personal correspondence with Burgess, 2015). However, the details presented above have been included to highlight the influence of not accounting for neutral axis eccentricity.

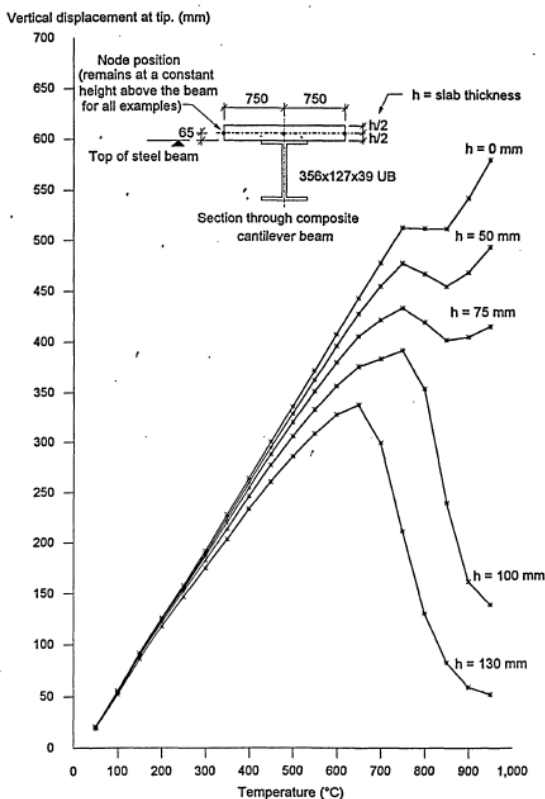


**Figure 3.13: Relationship between the upward thermal curvature / bowing and steel temperature of a composite beam with variable slab thickness (Bailey 1995). Note how the scenario with  $h = 0$  mm (no slab) has the maximum upward deflection when in reality it should have zero deflection.**



### 3.6.3 Including eccentric neutral analyses in finite element models

The methodology adopted in this dissertation for analysing a beam with an eccentric NA is shown in Figure 3.14. The distance between the reference axis (the axis on which nodes are modelled in a software package) and the actual NA of a beam is defined as the eccentricity of the section, and this topic is addressed in the next chapter. In this figure the lower portion is uniformly heated as per the previous example. An end mechanical point load is applied which causes a triangularly shaped bending moment diagram over the length. It is assumed that the material softens when exposed to high temperatures or strains. Due to the softening of the material the NA position migrates upwards. The magnitude of the NA position change increases with increasing mechanical moment due to the assumed non-linear stress-strain relationship. The value of the bending ( $EI_\theta$ ) and axial stiffness ( $EA_\theta$ ) now change over the length of the beam. The methodology for calculating the updated NA,  $EA_\theta$ ,  $EI_\theta$  and formulation for modelling the system is explained in Chapter 4. The  $N_\theta$  and  $M_\theta$  values are calculated about the updated NA and applied at the updated nodal coordinates. An iterative procedure is required to take account of such behaviour if forces and properties change with time. This is addressed further in Section 3.8.1.

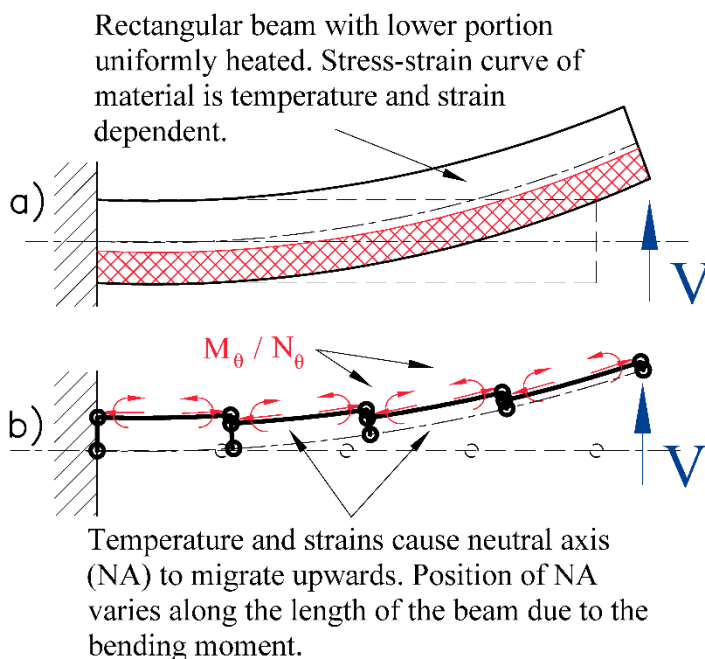


**Figure 3.14: Cantilever beam with the lower portion uniformly heated, an end point load and with material properties dependent on strain and temperature**

### 3.6.4 Design philosophy and formulation of beam elements

In this section the philosophy of the design method developed in this dissertation is explained with reference to Figure 3.15. In the figure a uniformly distributed load (UDL) is applied to a fixed-fixed ended composite beam. As the beam deflects it causes the concrete near the supports to crack, decreasing the stiffness in this area and the NA migrates downwards. At mid-span the concrete retains its full stiffness due to the sagging moment, and thus the NA stays in its original position, as shown in (b). The reference axis shown is an

arbitrary line about which the beam is modelled in the computer model, and generally placed at either the initial NA or at mid-height of a section.

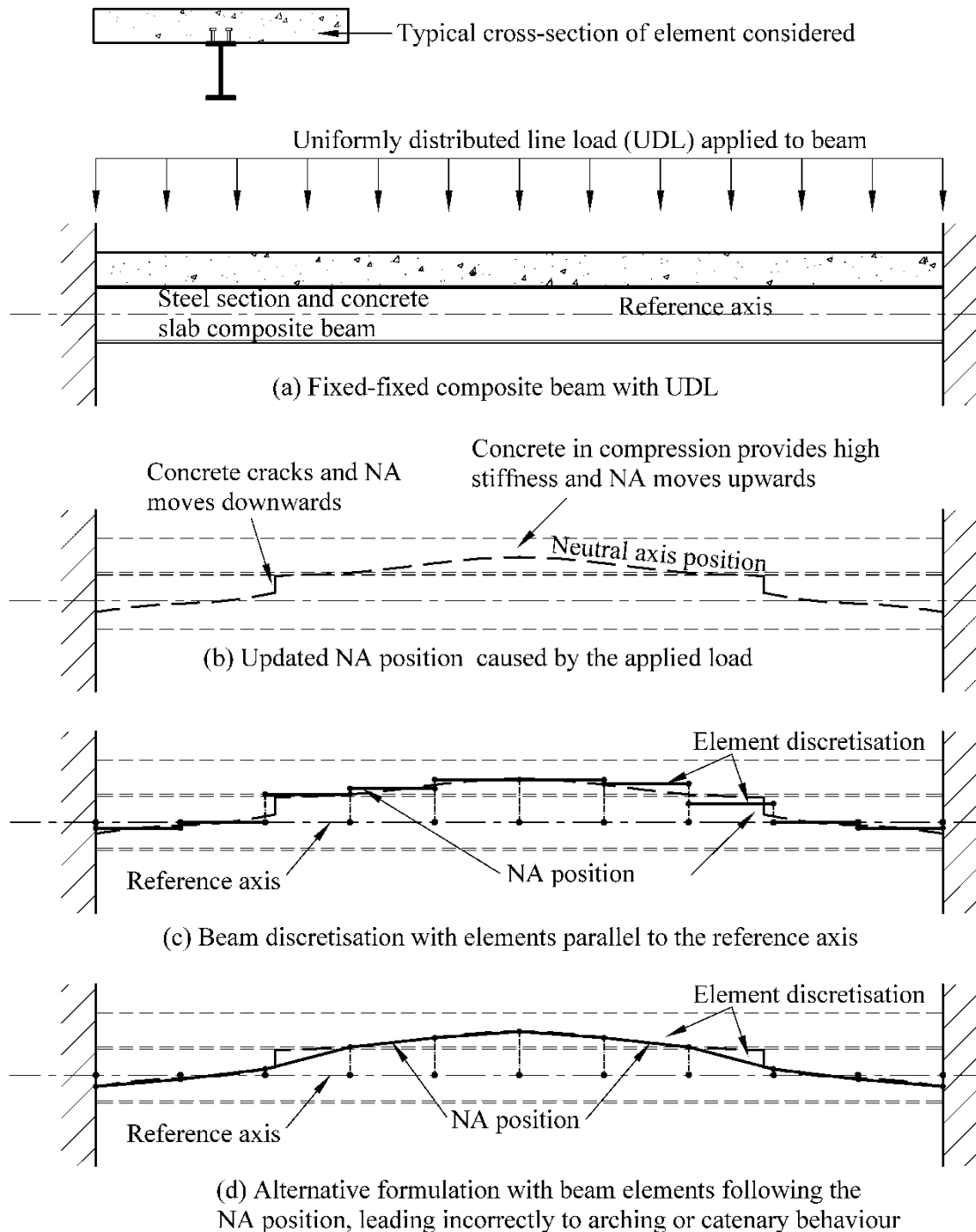


**Figure 3.15: Design procedure for using the eccentric beam formulation**

The question to be asked now is: how can the beam be discretised into a series of segments that accounts for this behaviour? There are two main alternatives as shown in (c) and (d), namely: (1) having beam elements with their axes parallel to the reference axis or (2), having diagonal elements that follow the NA. The formulation in this research adopts the first discretisation and element arrangement as shown in (c) with new

NA positions parallel to the reference axis and equal to the NA position at mid element. The reason for this is based on the numerical challenges and errors created by the formulation shown in (d), namely:

- The beam is undergoing bending. However, if elements with diagonal orientations are inserted it causes arching action to occur. This results in loads being incorrectly carried by axial forces rather than bending. Even though the NA follows an arching pattern loads are still carried in bending.
- If diagonal elements are created then section properties are not calculated as perpendicular to the member axes, so results obtained cannot be directly used for design but must be first converted back into the original axis orientation.

Arching action could potentially occur to a very limited degree in the structure shown above. In reality if there was a large increase in stiffness across a diagonal path arching behaviour would occur. However, such behaviour would be comparable to the strut-and-tie modelling philosophy (Fillo & Benko 2011), which is specifically adopted for deep concrete beams where Euler-Bernoulli assumptions are violated. This reemphasises that for basic assumptions to hold arching action and the violation of plane section assumptions cannot occur to a significant degree.

### 3.7 Calculating resultant thermal strain effects in non-uniform sections

In previous examples simple temperature profiles and material models were considered. However, in real structures thermal behaviour becomes significantly more complicated, necessitating the use of numerical procedures for calculating  $N_\theta$  and  $M_\theta$ . Figure 3.16 shows a composite beam where the NA position has migrated to the point shown within the concrete slab.

In Figure 3.16 (a) the composite cross-section has been discretised into a number of integration points. The number of integration points required will depend on the complexity of the cross-section and the desired level of accuracy. A temperature profile exists over the height of the section as shown in (b). Based on the assumed temperature-elongation relationship of materials thermal strains are calculated as shown in (c). From temperatures and strains the Young's modulus values across the section are found as presented in (d), and this is based on the assumed temperature-stress-strain relationships for the materials considered. There can be instantaneous changes in properties over the height of a section due to specified temperatures and material properties. For instance the top flange of a steel beam is often set at a different temperature to the web, or concrete may have different assumed stress-strain relationships in tension and compression. In (e) the stresses simulating thermal strains, ETSS, are calculated from:

$$\sigma_\theta = \varepsilon_\theta \cdot E_\theta \quad (3.12)$$

The change in the shape of the  $\sigma_\theta$  graph is due to the ratio of  $\varepsilon_\theta$  to  $E_\theta$ . Often at higher temperatures material stiffness degrades faster than materials elongate, meaning that a lower ETS is required to simulate larger strains. Peak ETS values do not necessarily occur at peak temperatures.

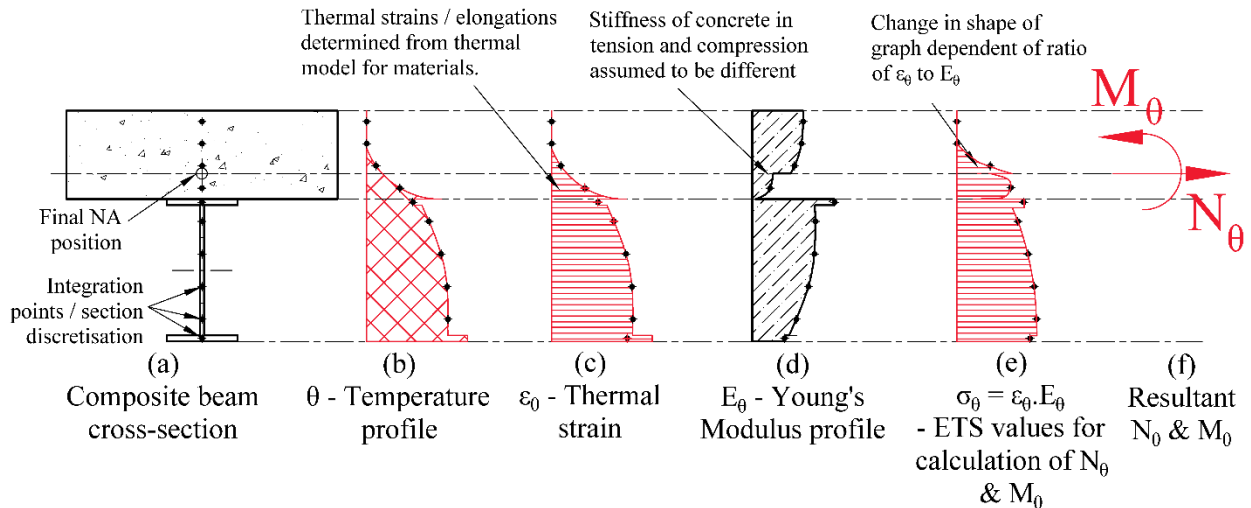


**Figure 3.16: Temperature, thermal strain, Young's modulus and ETS profiles over the height of a composite section used for determining  $N_\theta$  and  $M_\theta$  values.**

To determine the  $N_\theta$  value the following equation is used:

$$N_\theta = \int b(y)\sigma_\theta(y)dy \approx \sum_{i=1}^n A_i \sigma_{i,\theta} \quad (3.13)$$

where the integration is carried out over the height of the section, which occurs on the  $y$ -axis and the breadth at each position is given by  $b(y)$ . The area of each small integration point  $i$  is  $A_i$  and the section has been discretised into  $n$  integration points. The value of  $M_\theta$  can be calculated in the same manner with:

$$M_\theta = \int b(y)\sigma_\theta(y) y dy \approx \sum_{i=1}^n A_i \sigma_{i,\theta} y_i \quad (3.14)$$

where  $y_i$  is the distance from the NA to the centroid of integration point  $i$ . It is important to note that since the integration is carried out about the NA the calculated  $N_\theta$  and  $M_\theta$  values must be applied at the NA.

### 3.8 Design and analysis philosophy employed

The design philosophy for considering an entire structure as a skeletal frame is explained below by: (a) presenting an iterative procedure for calculating thermal forces and properties, (b) using the beam properties to carry out a global FE analysis, and then (c) presenting how to setup the model and loading based on the proposed FBE methodology.

#### 3.8.1 Iterative procedure for determining member properties

As discussed in the previous sections an iterative procedure needs to be used to calculate member properties. As the NA position changes strains will also change. Changing strains cause different material stiffnesses. The updated stiffnesses influence RTSL/M values which in turn influences the NA position. Hence, a

methodology for determining the properties of a cross-section is proposed in Figure 3.17. In the following chapter it will be explained how to calculate and consider stiffnesses and NA positions.

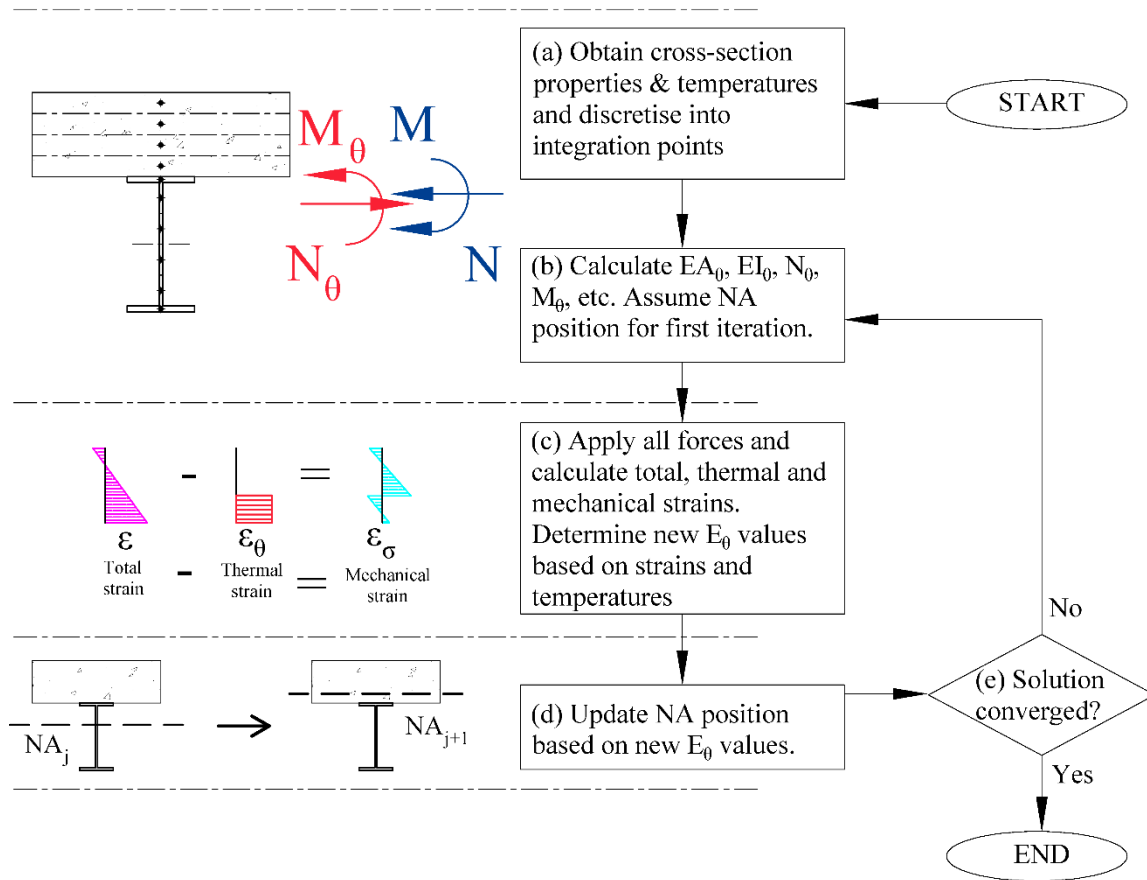


**Figure 3.17: Flowchart illustrating the iterative procedure used for determining the non-linear properties of cross-sections exposed to fire.**

The first step required for considering a cross-section is to obtain all the cross-sectional properties and specify the temperature-stress-strain curve for each material considered, as done for step (a) of Figure 3.17. Temperature profiles assumed over the height of sections must be provided, along with any mechanical loads, which may be due to external loading and/or structural restraint. For the first iteration the position of the NA is assumed and then all the necessary properties,  $N_\theta$  and  $M_\theta$  are calculated in (b). In (c) all forces are then applied to the cross-section to determine the total strains that occur, from which the thermal strains are subtracted to find mechanical strains. From these strains the stiffnesses of the beam materials are determined,  $N_\theta$  and  $M_\theta$  are modified and the NA position is updated. It is then checked whether the NA position and stiffness values have converged to within a predetermined tolerance. If convergence has not been obtained the process is repeated.

### 3.8.2 Analysis procedure

The nonlinear FE analysis procedure adopted in this dissertation is based upon a corotational approach, following the work of Iu & Chan (2004). The basis for the corotational approach is that the axis about which

member properties are calculated is determined from the updated coordinate system for each iteration, i.e. the axis migrates with the beam. A disadvantage of the corotational approach (as opposed to the Total Lagrangian or Updated Lagrangian approaches of Section 2.5) is that members must be prismatic between nodes, having constant properties. However, non-prismatic members are addressed by having a finer mesh with more beam segments. When considering changing properties along the length of a beam, which is caused by non-linear or thermally induced material behaviour, the beam effectively becomes non-prismatic. Thus, beams considered by the FBE formulation typically require a finer degree of discretisation than would be required at ambient temperature. Additional details regarding the corotational approach are discussed in Section 2.5.

The analysis procedure adopted in this work is depicted in Figure 3.18, and includes thermal and structural loadings. In this figure the thermal loading loop can be ignored if required, depending on the type of analysis considered. Based on Figure 3.18 the steps in the analysis procedure are: (1) determining the properties of a composite section, (2) creating stiffness matrices, and (3) solving for restraining forces. The steps in the procedure are illustrated in Case Study A for a simple cantilever, which may assist the reader in visualising the process.

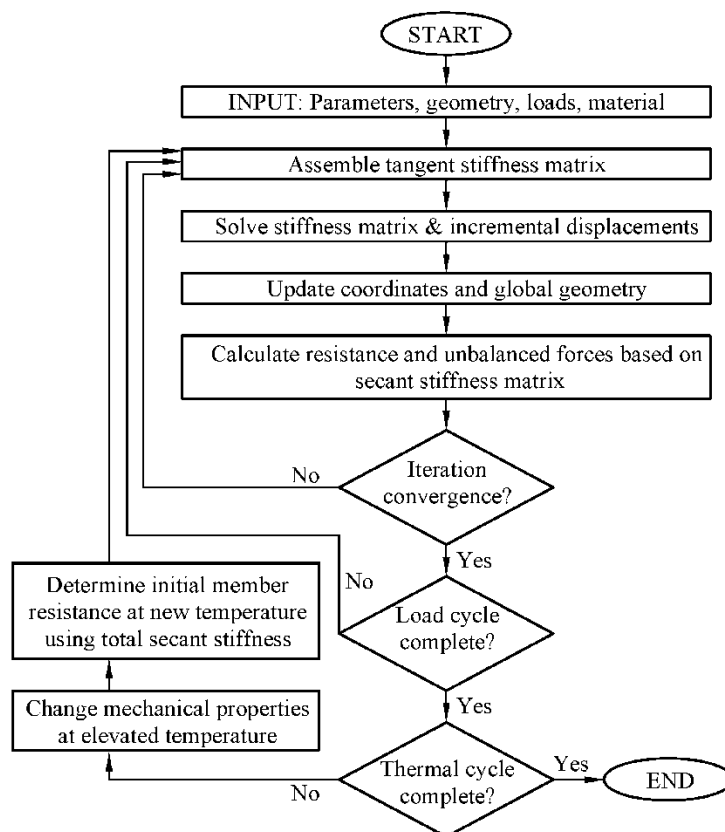


**Figure 3.18: Flowchart for the nonlinear analysis of structures subjected to mechanical and thermal loads (the latter can be neglected as required) (based on Iu & Chan (2004))**

### 3.8.3 Modelling formulation

To include a structure in the FE formulation of the previous section it must be found how to create suitable force and stiffness matrices to capture the behaviour of the structure, as will now be explained. The process is presented considering a composite steel-concrete structure as an example. A similar process could be followed for concrete, steel or other types of buildings.

(1) The relevant structural elements are shown in Figure 3.19. The structural fire design process should immediately follow the ambient temperature design during which the main structural element sizes, rebar layouts and such associated details are determined. It must also be determined what fire rating and type of fire is to be used. The member sizing, rebar layouts and passive protection for steelwork may need to be updated as the analysis progresses.

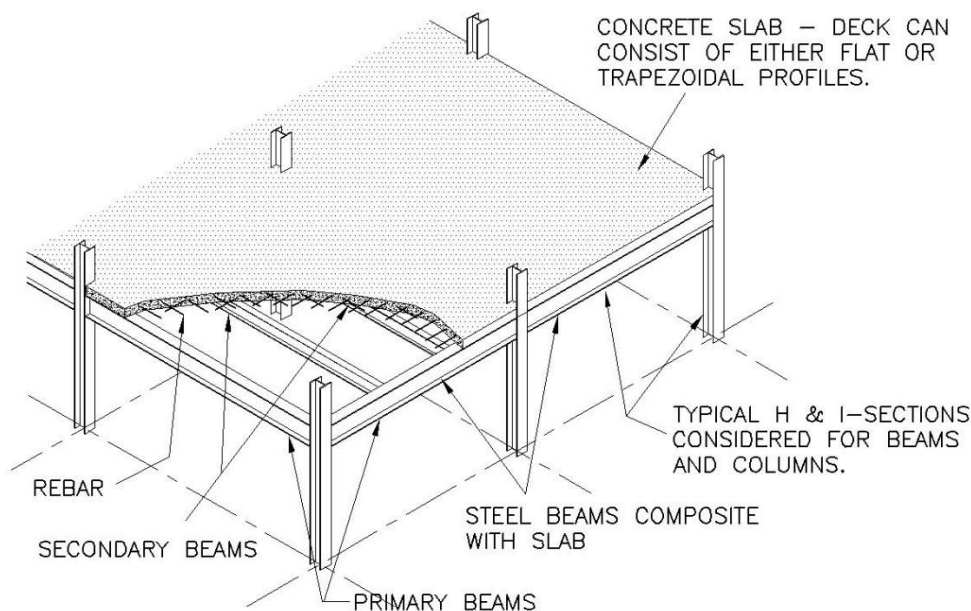


**Figure 3.19: Typical layout and details considered for the design of a composite structure.**

(2) The FBE formulation follows a philosophy similar to that used for concrete structures at ambient temperature, where slabs and beams are designed separately. For composite steel-concrete floors the slabs can be designed in isolation using methodologies such as Bailey's tensile membrane method (2004a; 2007) or Clifton's Slab Panel Method (SPM) (2006; 2012; 2014). This is illustrated in Figure 3.20. These methods determine yield line patterns using catenary action, and predict how slabs will fail and distribute loads, as discussed in Section 2.4.8. The yield line patterns are used to calculate the distributed loads applied to primary beams, which are needed in the following analysis steps. The secondary beams are considered to be part of the slabs and are not explicitly considered in this research, although, up until the point of buckling such secondary beams can be analysed with the proposed FBE procedures. Primary beams are defined as those elements that support slab panels along their perimeters and must retain structural integrity throughout a fire. Hence, they form the primary focus of the research, as secondary beams are already accounted for through the



aforementioned membrane action methods. From the discussions in Section 2.4.8 it can be understood that existing fire design methods such as MACS+ (Nadjai et al. 2012) and the SPM (Clifton & Abu 2014) also apply loads in a similar manner to that proposed in this research. Currently none of these methods include additional axial loads to account for compression ring behaviour. For edge beams additional mechanical loads (Su & Zhang 2013) or increased standard fire times (Clifton 2016) could be applied to ensure that catenary action is ensured.

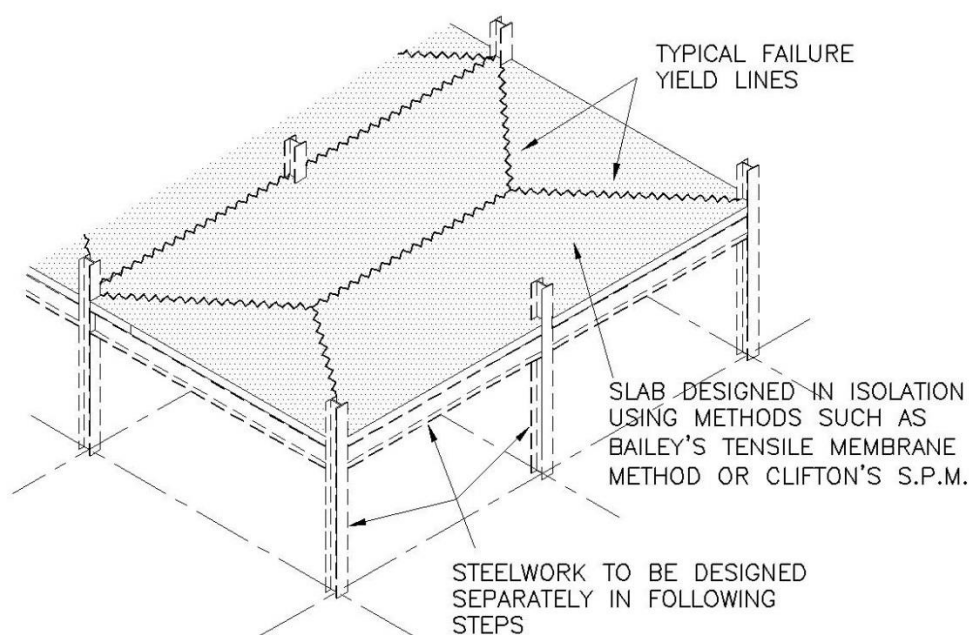


**Figure 3.20: Analysis and design of slab panels independent of primary beams. Yield line patterns are used to determine the loading for subsequent steps.**

(3) When creating the FBE analysis model only the columns and primary beams should be considered, as shown in Figure 3.21. No shell elements need to be added for floor slabs. The contribution of concrete is explicitly considered in the beam element formulation by specifying what area of concrete flange acts compositely with the steelwork. Any concrete deck profile or number of reinforcing steel layers can be included, as discussed in later chapters. Joints can be modelled as pinned, fixed/continuous or semi-rigid. The latter requires that the temperature-moment-axial force-rotation relationship of the joint be known.



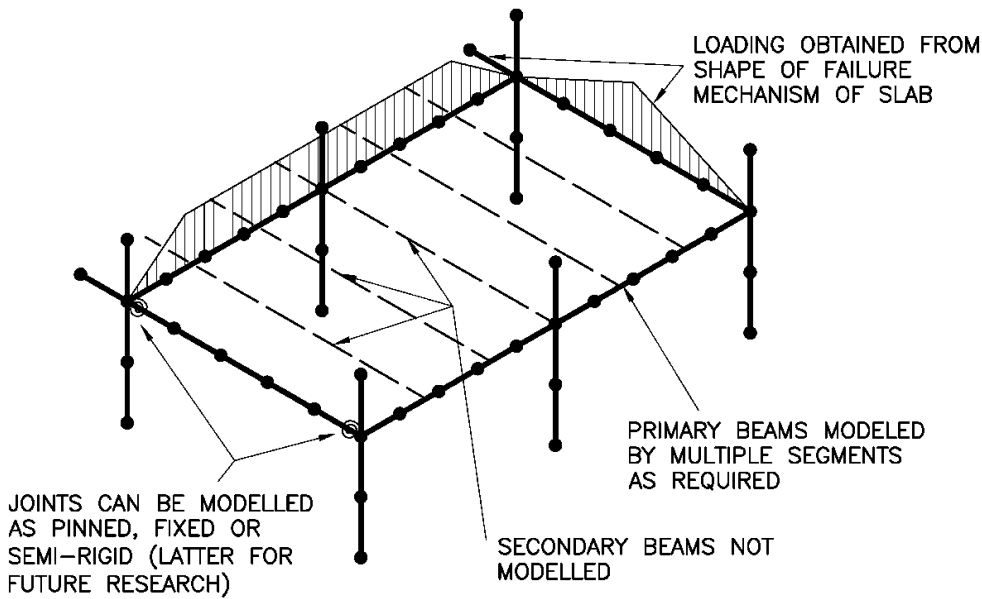


**Figure 3.21: Analysis model of the composite system**

(4) The temperatures of steelwork and concrete at each step in the analysis can be calculated from predicted fire cell temperatures, from experimental tests or from design tables (e.g. EN 4-1-2). A typical temperature profile for a composite beam is shown in Figure 3.22. Various temperature profiles could be adopted since the overall methodology is generalised. In the figure the temperature profile indicates that the steel beam has a certain amount of passive protection present, causing it to heat up more slowly than the concrete soffit. Once temperatures are known the mechanical properties of materials are calculated using a suitable temperature-stress-strain curve. Stresses and strains are updated as analyses progress. The position of the neutral axis (NA) is typically not fixed, due to changes in material stiffness and stress profiles, and is also updated as analyses progress.

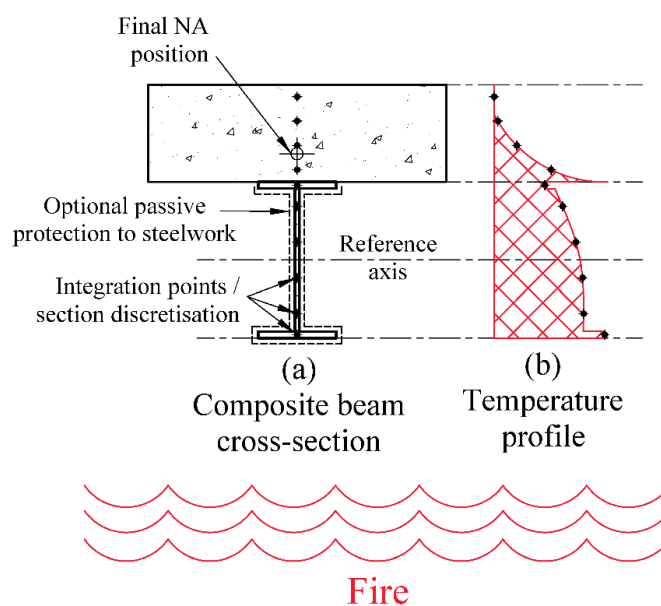


**Figure 3.22: Typical temperature profile in a composite slab exposed to fire**

To allow for the numerical procedures employed beam cross-sections must be discretised into a finite number of integration points, as shown in Figure 3.22. The stresses, strains and temperatures are calculated at all points in each iteration. The FBE methodology determines a total effective bending ( $EI$ ) and axial ( $EA$ ) stiffness based on the properties of the combined integration points. Thermal behaviour is simulated through the introduction of pseudo “forces” which cause the same elongation or curvature as thermal strains induce, as explained before.

The effective concrete slab width acting compositely with a beam must be defined by designers. The initial position of the NA must be assumed. In subsequent iterations the NA is updated based on calculated properties. To specify temperatures at integration points a number of techniques are possible:

- a) Manually specify the temperature at each integration point. This is not recommended for concrete with temperature profiles or for large numbers of integration points. However, for steel beams it is a simple task to specify the temperatures of the flanges and web in an input file.
- b) Include tabulated sets of standard fire temperature profiles for concrete, from which subroutines look up and interpolate the temperature of integration points based on the depth of a point into a slab.
- c) Define equations that set the temperature based on the position of an integration point relative to a datum or coordinate, such as by using Wickström’s equations (discussed in Section 5.3.4), which use a datum as the vertical coordinate of the slab soffit.
- d) Conduct a finite element analysis of the cross-sections to obtain temperatures at different points.

In this research finite element thermal analyses were conducted to determine temperature profiles for concrete, but steelwork temperatures were individually defined. However, to reduce computational effort, after the thermal analysis of a concrete section was completed the data was tabulated such that temperatures could easily be applied to each cross-section without needing the thermal analysis to be conducted for every mechanical analysis carried out. Based the depth of an integration point into the concrete slab the temperature was interpolated from the tabulated data.

(5) The structure is then analysed at either specific points in time or across an entire time domain by considering time-steps. In this work structures have only been considered at specific points in time, although a time history could be considered by conducting a multi-step analysis with time increments. Temperatures, structural geometry and elemental stresses would need to be updated each time step. Since non-linear structural behaviour and material properties are included (as is typically required for fire) iterative methodologies such as the Newton-Raphson, modified Newton-Raphson or other such techniques can be included (Cook et al. 2001). Structural restraint caused by either cooler adjacent structural elements or boundary conditions can be modelled. For beams with non-linear stress-strain relationships and temperature profiles the NA will shift up or down. Figure 3.23 shows the structure where the NA positions of beams have shifted. Internal forces have been calculated based on the updated member properties. If this was the final solution obtained from an analysis the beams could be designed directly from the calculated forces.

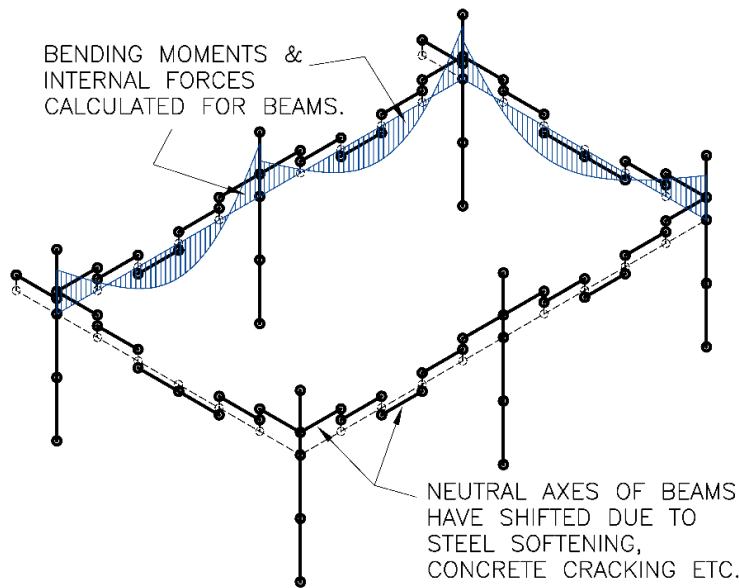


**Figure 3.23: Analysis model showing eccentric neutral axis positions, calculated bending moments and general structural behaviour**

### 3.9 Simplified implementation of the FBE formulation

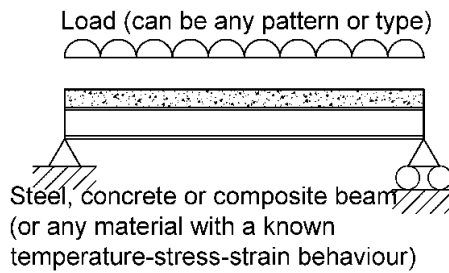
The FBE formulation provides a simplified modelling approach for doing design office analyses, as will be explained in relation to Figure 3.24. For statically determinate structures the process needs to be followed only a single time, whilst for statically indeterminate structures the process must be repeated until convergence is obtained. This process can be understood as follows:

1. After details regarding the specifications of the structure have been decided upon (based on ambient temperature design or from experimental data), then
2. The beam is discretised into a suitable number of beam segments.
3. The loading is applied and the mechanical forces calculated at the middle of each beam segment.
4. New beam properties (NA,  $EI_\theta$ ,  $EA_\theta$ ) and RTSL/Ms ( $N_\theta$ ,  $M_\theta$ ) are determined as a function of the material properties, temperatures of the elements and cross-sectional forces from Step 3. This is carried out as explained in Chapter 4, using the material models from Chapter 5, with calculations as illustrated in Chapter 6. Calculations for determining cross-sectional properties and RTSL/Ms can be carried out using independent subroutines or spreadsheets.
5. These updated structural properties and RTSL/Ms are inserted directly into the FE modelling software. Beam segments are offset from the original reference axes based on the calculated NA values. The ends of segments are connected together using rigid links. It would also be possible to use couplings or MPC constraints for this purpose, as explained in Section 2.4.8.
6. The structure is then analysed using a nonlinear solver too determine deflections in fire. To obtain final beam design forces the RTSL/Ms must be subtracted from total member forces calculated.

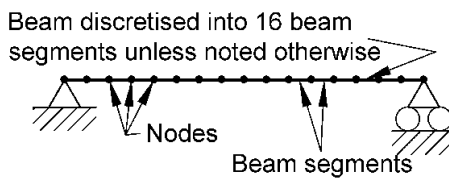
- If an iterative procedure is required for statically indeterminate structures Steps 3-6 are repeated until convergence is obtained.

**DESIGN & MODELLING STEPS**

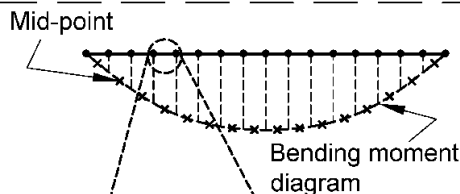
- Obtain structural information and temperature profile across beam height.



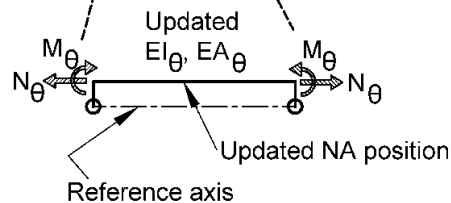
- Discretise structure into segments and apply loads.



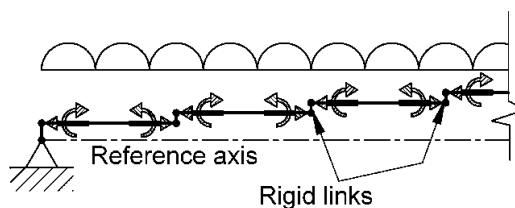
- Obtain internal forces at the mid-point of each beam section.



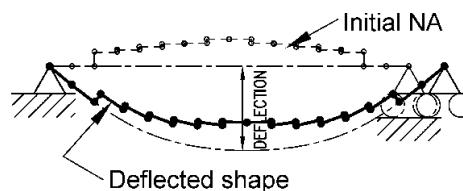
- For each beam section calculate the thermal stiffnesses ( $EA_{\theta}$ ,  $EI_{\theta}$ , NA) and resultant thermal forces ( $M_{\theta}$  /  $N_{\theta}$ ).



- Insert the updated element stiffnesses and thermal forces into the FE modelling software and analyse.



- Calculate deflections in fire using the updated properties.



For an indeterminate structure the above steps would be repeated in an iterative manner until convergence occurs.

**Figure 3.24: Modelling methodology and steps for analysing beams in fire using commercial FE software**

Hence, the proposed methodology allows structures encountered in practice to be analysed using simplified means. It is novel that a spreadsheet or sub-routines coupled with commercially available FE programs can be used for analysing structures which normally require advanced finite element models. Hence, the research in

this dissertation can be applied on two levels: (1) for statically determinate structures where analyses are carried out within standard finite element packages but coupled with independent subroutines (Chapter 6), or (2) within advanced finite element packages where restraint is considered (Chapter 4).

### 3.10 Overview of the benefits and limitations of the FBE formulation

The FBE formulation proposed is applicable for specific structural behaviour. It has both advantages, or benefits, and disadvantages, or limitations, in relation to existing analysis and design procedures.

#### 3.10.1 *Advantages of the FBE formulation*

The FBE formulation falls between advanced modelling techniques at the one end and simplified design methods at the other end, and it has advantages relative to each of these. The primary advantages of the FBE system relative to advanced design models are:

- Experimental case studies used for validation in Chapter 6 show that the FBE predicts comparable forces and deflections to those from more advanced methods.
- Modelling of structures can be done more quickly, in terms of both human and computer time. The number of degrees of freedom of a structure are significantly reduced (sometimes by orders of magnitude). Structures can be analysed as skeletal systems which structural engineers are often more familiar with.
- The NA of sections shift as cross-sectional properties change, which normal Euler beam elements do not consider.
- The formulation is based upon first principles which are relatively easy to understand and implement in a variety of scenarios. This also makes the verification of results simpler.
- The formulation allows parametric studies to be easily carried out.
- An independent finite element thermal analysis is generally not required for determining temperatures (Huang et al. 2000), although it could be included if required. Standard design equations or tables can be utilised for determining the temperature of elements.
- The proposed procedures can either be linked to simple commercial FE software, such as Prokon (2015), or advanced research software, such as Abaqus (Dassault Systèmes 2013).
- When including materials with sudden changes in stiffness, such as concrete which cracks, there can be problems with numerical stability. However, all methods which include such behaviour experience similar challenges. It is easier to isolate and address such instabilities within a beam element rather than in a fine mesh of shells or volume elements.
- In the future modifications to the formulation could be introduced that account for phenomena such as slippage between concrete and steel beams through the use of empirical factors. This is discussed further in Section 5.4.

- An advantage of considering a structure as a series of beam elements is that connections can be more easily modelled, with non-linear springs inserted between beams and columns. Spring stiffnesses can be generated from sub-models such as those shown in Section 2.4.7. The inclusion of connections in simplified models such as the FBE formulation would only be beneficial if standard moment-force-rotation curves could be used, rather than needing to be generated from sub-models each time.
- It is not necessary to know the position of the NA before an analysis starts.
- Forces calculated can be directly used for design purposes (e.g. moments and axial forces), such that minimal post-processing of results is required.

Some of the aforementioned advantages also apply in comparison to simplified design methods. The advantages of the FBE system specifically relative to simplified methods are:

- Detailed designs can be carried out to calculate forces and deflections in skeletal frames rather than individual elements.
- From the stresses calculated in members it could be determined whether a structure has failed. Also, run-away failure, where the structure can no longer sustain load, is identified when convergence of analyses is longer obtained, as discussed in Section 6.5.
- Any construction material may be included provided that temperature-stress-strain relationships are known.
- Non-linear material behaviour and cracking are explicitly accounted for.
- It would be possible to conduct time-dependent analyses accounting for both the heating and cooling phases of a fire. This is a topic for future research.

The research presented is aimed at application in structural fire analyses, but the methodologies can also be applied to other nonlinear problems such as:

- Reinforced concrete elements at ambient temperature. As concrete goes into tension it can crack, which may substantially change the position of the NA of a system, and the resulting stiffness. Such modelling procedures may be suitable for concrete wind towers where beam elements are used (Grünberg & Göhlmann 2013), bridge decks (Bapat 2009) and other similar structures.
- Structures with significant thermal gradients across elements, as experienced in certain mechanical systems and in temperature-controlled storage facilities.

### *3.10.2 Limitations of the proposed FBE model*

Various limitations exist that users or researchers should be aware of:

- Shear deformations and localised distortions are not accounted for.
- No slippage between concrete and steel elements is currently considered, based on the discussions in Section 2.4.8.

- The methodology developed is for members prior to the onset of local or global buckling. Prevention of local or global buckling must be done using the design codes selected to check member strengths based on the internal forces calculated, as commonly done for ambient temperature design.
- Floor slabs are not modelled and must be considered through separate analyses, as discussed in Section 3.8.3.
- It should be understood that the FBE formulation allows for simpler modelling of structures but the element in itself is more complicated than the Euler beam formulation. Hence, additional subroutines are required to determine the behaviour of individual sections. However, FBE analyses will be completed significantly more quickly than shell or volume element based models with much larger numbers of degrees of freedom.
- It must be pre-determined what width of material acts as part of a composite beam (e.g. the width of the concrete flange of a beam). In complex scenarios this may be challenging to define and could vary with loads. In Chapter 7 it is demonstrated that deflections are not highly sensitive to the width of concrete flange selected.
- Only 2D structures are considered in this dissertation. Future research will focus on extending the formulation to apply to 3D structures.
- Currently structures are analysed at a specific point in time, rather than over a time domain, i.e. the history of temperature is currently not considered.
- Catenary action of secondary beams is not explicitly considered, in accordance with methodologies outlined in Section 2.4.8 and 3.8.

### 3.11 Conclusion

This chapter has provided an overview of the structural mechanics and analysis procedure employed in this research, explaining the fundamental methodologies behind the FBE. Thermally induced strains and curvatures are modelled through the calculation of Resultant Thermal Strain Loads (RTSL) and Moments (RTSM). Structures are discretised into beam segments with RTSLs/Ms acting at their ends and the total deflections calculated. Final stresses in a section are both a function of the externally applied mechanical loads and internal forces caused by non-linear heating or restraint.

To analyse an entire structure it is converted into an equivalent skeletal frame. Loads are applied to beams based on the calculated failure patterns of tributary slab areas. Bending and axial beam stiffnesses are determined based on their elevated temperature material properties, with properties being calculated about the NA of a section. These stiffnesses and load vectors about the NA will be transformed from the NA to be about the reference axis of the FE model, or vice versa, in the following chapter. Hence, it can be understood that a fundamental contribution of this dissertation is the methodology for modifying the stiffness of an Euler beam and updating it to be about the reference axis, and simulating the effects of temperature through the application of RTSL/M forces.

Structural mechanics at elevated temperature can be complicated with numerous factors influencing behaviour. In this chapter only simplified examples were considered, but the procedures can be implemented for generic cross-sections and temperature profiles. The concept of changing neutral axes positions was introduced and this will be addressed in the following chapter. Thereafter the non-linear behaviour of construction materials at elevated temperatures is addressed in Chapter 5. The design philosophy developed can be implemented within commercially available finite element software or within advanced modelling software.



## 4 Chapter 4: Formulation and verification of the analysis procedure for beams with eccentric neutral axis positions

### 4.1 Introduction

In this chapter the FBE is developed by including a procedure to account for beams with eccentric neutral axes (NAs) that change during analyses. This follows the general analysis philosophy introduced in Chapter 3. In this chapter only simple material models are used and thermal loads from fires are not considered such that analyses can be more easily understood and structural behaviour identified relative to the NA procedure being developed.

Firstly, the finite element (FE) matrices used for beam elements are presented or derived in this chapter. The analysis procedure utilised is then discussed, followed by how nonlinear geometric behaviour and restraining forces are considered. Numerical case studies are provided to compare the FBE formulation developed against both analytical solutions and models employing shell elements. Case studies are included where Euler-Bernoulli assumptions do not fully hold to illustrate what level of accuracy could be expected when such assumptions are violated. Validation examples in this chapter have been analysed using a purpose-built nonlinear analysis program developed by the author. In Chapter 6 the FBE formulation is implemented within commercial software.

#### 4.1.1 Academic contribution

The academic contribution stemming from this chapter is primarily the mathematical formulation of how to analyse a beam using a finite element with an eccentric NA position that can change during an analysis. In this formulation the NA of a beam can vary along its length which other typical analysis methods do not account for. The inclusion of the iterative methodology for determining the composite stiffness of beam provides a simple technique for considering beams in fire based on first principles. It is novel that the nonlinear corotational FE formulation is extended using a modified stiffness matrix.

### 4.2 Eccentric beam element formulation and analysis theory

#### 4.2.1 Fundamental theory

The following fundamental equation describes the force-deformation relationship of a structure:

$$\mathbf{F} = \mathbf{K}\Delta \quad (4.1)$$

where the global stiffness matrix is  $\mathbf{K}$ , load vector is  $\mathbf{F}$  and deformation vector is  $\Delta$ , as introduced in Chapter 3. The global stiffness matrix is compiled based upon the inclusion of each local stiffness matrix,  $\mathbf{k}_{ij}$ , of all beams in the structure. The subscript  $ij$  denotes a beam from node  $i$  to node  $j$ . The local stiffness matrix is

modified by transformation matrix,  $T_{ij}$ , such that local coordinates correspond with the global coordinate system. Thus:

$$K = \sum T_{ij}^T k_{ij} T_{ij} \quad (4.2)$$

Local beam stiffnesses are inserted at the positions corresponding to global degrees of freedom, hence it is not a true matrix summation, but denoted as such for simplicity. The stiffness of each beam element consists of an elastic stiffness matrix,  $k_{ij,el}$ , and a geometric matrix,  $k_{ij,g}$ , to account for geometric non-linearity and buckling, such that:

$$k_{ij} = k_{ij,el} + k_{ij,g} \quad (4.3)$$

The elastic stiffness of a two-dimensional, prismatic, Euler-Bernoulli beam is given by:

$$k_{ij,el} = \begin{bmatrix} \frac{EA}{l} & 0 & 0 & -\frac{EA}{l} & 0 & 0 \\ & \frac{12EI}{l^3} & \frac{6EI}{l^2} & 0 & -\frac{12EI}{l^3} & \frac{6EI}{l^2} \\ & & \frac{4EI}{l} & 0 & -\frac{6EI}{l^2} & \frac{2EI}{l} \\ & & & \frac{EA}{l} & 0 & 0 \\ & \text{Symmetric} & & & \frac{12EI}{l^3} & -\frac{6EI}{l^2} \\ & & & & & \frac{4EI}{l} \end{bmatrix} \quad (4.4)$$

The properties of the beam are Young's modulus,  $E$ , cross-sectional area,  $A$ , second moment of inertia,  $I$ , and length,  $l$ . The geometric nonlinearity matrix,  $k_{ij,g}$ , for the corotational system is given by the following, according to Cai et al (2009):

$$k_{ij,g} = \begin{bmatrix} 0 & 0 & 0 & 0 & 0 & 0 \\ & \frac{6F}{5l} & \frac{F}{10} & 0 & -\frac{6F}{5l} & \frac{F}{10} \\ & & \frac{2Fl}{15} & 0 & -\frac{F}{10} & -\frac{Fl}{30} \\ & & & 0 & \frac{6F}{5l} & \frac{F}{10} \\ & \text{Symmetric} & & & & -\frac{10}{2Fl} \\ & & & & & \frac{15}{} \end{bmatrix} \quad (4.5)$$

where  $F$  is the axial force in the local coordinate system of a member. This is a modified form of the geometric matrix presented by Yang & McGuire (1986). The geometric nonlinearity matrix accounts for the interaction of axial force, transverse displacements and rotations. If deformations are small or structures do not experience axial loads its influence is negligible.

Once the global stiffness matrix and load vector has been assembled boundary conditions are applied and deflections solved. Resultant forces are then calculated, which include reactions. For non-linear analyses the Newton-Raphson or modified Newton-Raphson procedure can be included (Cook et al. 2001). For more details on the matrix analysis procedures presented above refer to Coates et al (1990). These stiffness matrices

will now be modified to account for changing NA positions during analyses, such that they can be applied to beams exposed to fire, after determining member stiffnesses to be included in matrices.

#### 4.2.2 Iterative procedure for the determination of section properties

When considering the cross-section of a beam which has varying Young's modulus values across the height it is essential that stiffness properties account for the variation. Figure 4.1 depicts a simplified distribution of the secant Young's modulus values and strain across a section, similar to what might be experienced for a composite beam with a thermal gradient across it in a severe fire. It can be seen that as the analysis process progresses, or as thermal or mechanical loads are applied, the position of the composite NA migrates from the original to the final positions.

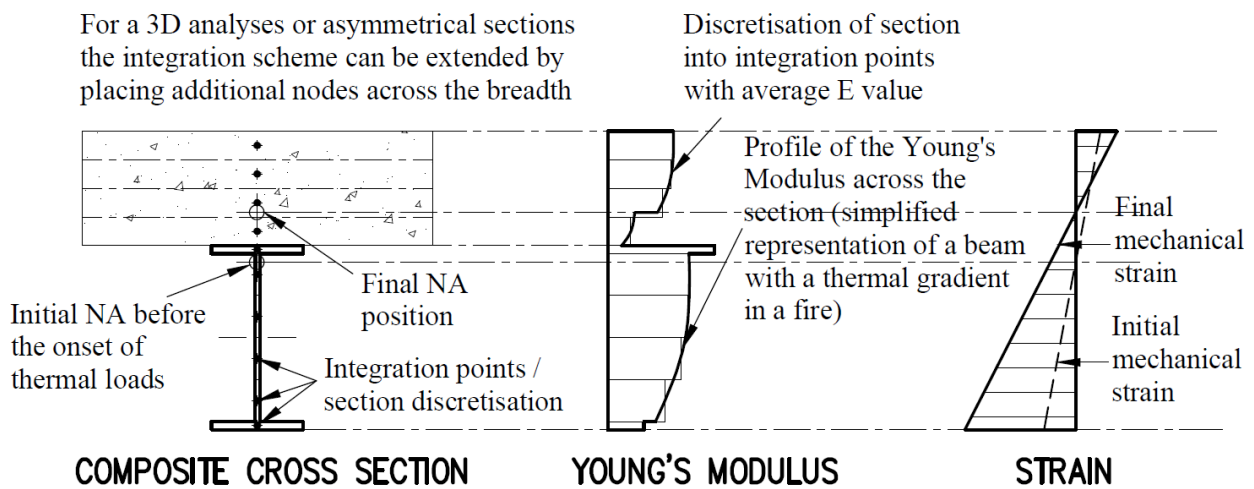


**Figure 4.1: Variation in Young's modulus and strain across a composite section, showing section discretisation to account for such behaviour**

For the first iteration the initial NA of a section, a distance  ${}^0c'$  from the reference axis (see Figure 4.3), and the bending and axial stiffnesses,  ${}^0(EI)$  and  ${}^0(EA)$ , need to be assumed (which can simply be taken as a section's initial tangent values). Based on these values the strain distribution across the section is calculated such that compatibility is maintained. From the strain profile the stresses and the Young's modulus across the section are determined, based on the assumed stress-strain relationship. The composite bending and axial stiffness of a discretised cross-section consisting of  $n$  integration points at iteration  $j + 1$  relative to the properties at iteration  $j$  is given by:

$${}^{j+1}(EI)_{S/T} = \int {}^j E_{S/T}(y) y^2 dA \approx \sum_{i=1}^n {}^j E_{i,S/T} (A_i y_i^2 + I_i) \quad (4.6)$$

$${}^{j+1}(EA)_{S/T} = \int {}^j E_{S/T}(y) dA \approx \sum_{i=1}^n {}^j E_{i,S/T} A_i \quad (4.7)$$

where  $y_i$  is the distance from the centroid of area  $A_i$  to the current NA position of integration point  $i$ , and  $I_i$  is its second moment of area. S/T refers to either secant or tangent values depending on what step of the analysis is considered. Various integration schemes can be included to improve the accuracy of the formulation and reduce the number of integration points required, although any technique used must be able to account for discontinuities. The updated NA position at iteration  $j + 1$  can now be calculated relative to the reference axis using:

$${}_{j+1}c' = \frac{\int {}^j E_S(y)y dA}{\int {}^j E_S(y) dA} = \frac{\sum_{i=1}^n {}^j E_{i,S} A_i y_i}{\sum_{i=1}^n {}^j E_{i,S} A_i} \quad (4.8)$$

This could be understood as the conventional method for calculating the NA of a section, but weighted by the  $E$  value of integration points. Note that when calculating the NA only the *secant* Young's modulus values are used as the position is based on the *total* loading and the load path encountered up until the current time. Once these values have been determined it is checked whether convergence has been obtained between the  $c'$ ,  $EI$  and  $EA$  values in the iterations. If convergence is obtained to within a predefined value the properties of the beam are set and the analysis continues. This entire process is summarised in Figure 4.2.

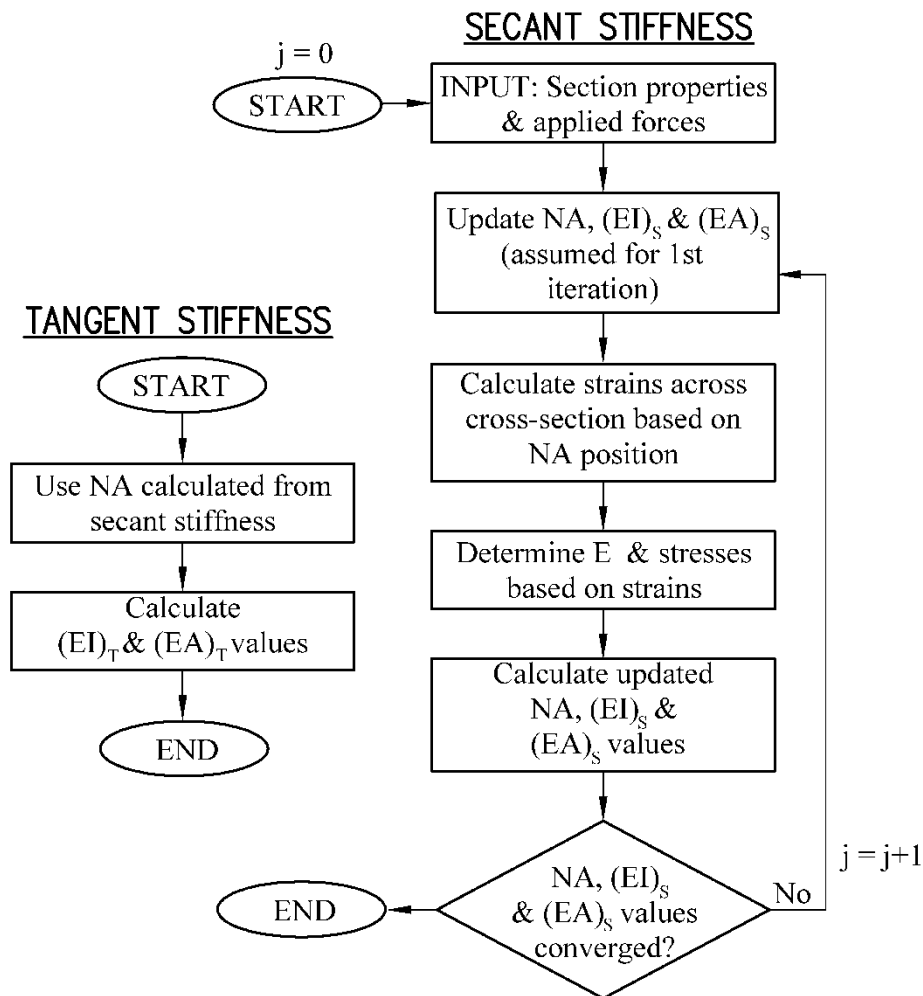


**Figure 4.2:** Flow diagram for the determination of the updated neutral axis and stiffness values of a beam cross-section

When calculating the tangent stiffness of a member the process is much simpler in that iterations are not required, except that the NA from secant calculations is required. The NA position is based on the secant calculations above, but stiffnesses are calculated by integrating over the section with tangent  $E$  values rather than secant  $E$  values. Since the tangent  $E$  value of each small element is based on the current stresses and strains in the element the NA is not recalculated with tangent values as this would create a false stress and strain distribution across the section.

#### 4.2.3 Derivation of the eccentric neutral axis stiffness matrix

To understand the overall process consider that when the NA of a Bernoulli beam is no longer at the position where it was modelled at (i.e. the nodal positions on the reference axis in the computer model) the beam will deform relative to the new position of the NA and its updated nodes, rather than relative to the reference axis. This can be visualised in Figure 4.3, where the NA has moved from its original distance,  $c_0$ , relative to a reference axis to a new position,  $c'$ . Nodes 1 and 2 occur in the computer model, and shall now be considered relative to nodes placed on the new NA, which are called Nodes A and B.

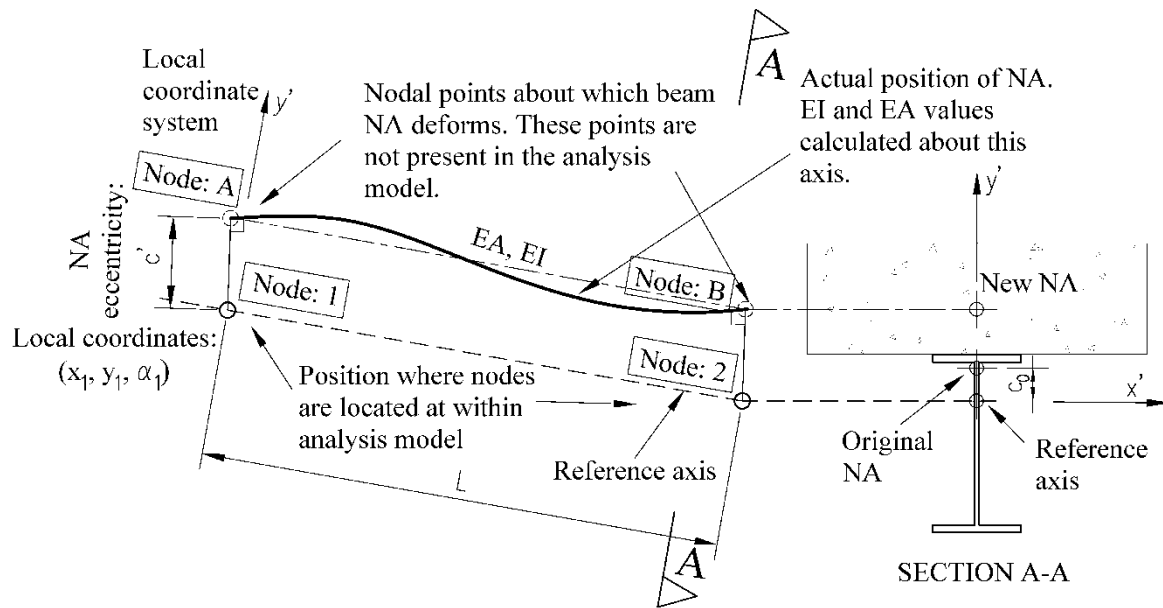


**Figure 4.3: Layout showing how a beam is modelled along a reference axis but has an updated neutral axis about which the beam deforms**

If a beam starts from an already deformed condition at time  $t$ , with a local axis system that joins the end nodes (corotational approach), and deflects by the vector  $\Delta u$  to an updated position at  $t+\Delta t$ , the layout will be as shown in Figure 4.4. The total deflection from the initial position is given by the vector  $u$ . The relationship between the local coordinate vector of Node A,  $x_A$ , and the coordinates of Node 1,  $x_1$ , is:

$$x_A = \begin{Bmatrix} x_A \\ y_A \\ \alpha_A \end{Bmatrix} = \begin{bmatrix} 1 & 0 & 0 \\ 0 & 1 & 0 \\ 0 & 0 & 1 \end{bmatrix} \begin{Bmatrix} x_1 \\ y_1 \\ \alpha_1 \end{Bmatrix} + c' \begin{Bmatrix} -\sin(\alpha_1) \\ \cos(\alpha_1) \\ 0 \end{Bmatrix} \approx \begin{bmatrix} 1 & 0 & -c' \\ 0 & 1 & 0 \\ 0 & 0 & 1 \end{bmatrix} \begin{Bmatrix} x_1 \\ y_1 \\ \alpha_1 \end{Bmatrix} + \begin{Bmatrix} 0 \\ c' \\ 0 \end{Bmatrix} = Q x_1 + \begin{Bmatrix} 0 \\ c' \\ 0 \end{Bmatrix} \quad (4.9)$$

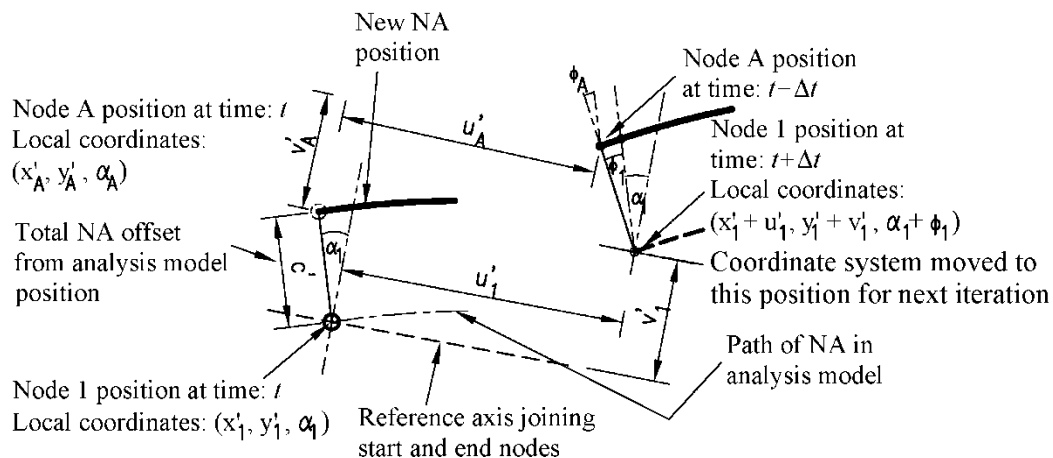


**Figure 4.4: Relationship between reference axis and deformed configuration**

Similarly, the relationship between the deflections of Node A and Node 1 is given by:

$$\Delta \mathbf{u}_A = \begin{Bmatrix} \Delta u_A \\ \Delta v_A \\ \Delta \varphi_A \end{Bmatrix} = \begin{bmatrix} 1 & 0 & 0 \\ 0 & 1 & 0 \\ 0 & 0 & 1 \end{bmatrix} \begin{Bmatrix} \Delta u_1 \\ \Delta v_1 \\ \Delta \varphi_1 \end{Bmatrix} + c' \begin{Bmatrix} -\sin(\alpha_1 + \varphi_1) + \sin(\alpha_1) \\ \cos(\alpha_1 + \varphi_1) - \cos(\alpha_1) \\ 0 \end{Bmatrix} \quad (4.10)$$

$$\approx \begin{bmatrix} 1 & 0 & -c' \\ 0 & 1 & 0 \\ 0 & 0 & 1 \end{bmatrix} \begin{Bmatrix} \Delta u_1 \\ \Delta v_1 \\ \Delta \varphi_1 \end{Bmatrix} = \mathbf{Q} \Delta \mathbf{u}_1$$

$\mathbf{Q}$  is a 3x3 matrix relating the deformations of a node on the NA to a node on the reference axis. For a beam joining A and B the matrix  $\mathbf{Q}_{AB}$  is a 6x6 matrix relating deformations of both nodes on the NA to those on the reference axis. Furthermore, the relationship between the forces in the local coordinate system of the nodes is:

$$\mathbf{f}_A = \begin{Bmatrix} f_{xA} \\ f_{yA} \\ m_{zA} \end{Bmatrix} = \begin{Bmatrix} f_{x1} \\ f_{y1} \\ m_{z1} + f_{x1}c' \end{Bmatrix} = \begin{bmatrix} 1 & 0 & 0 \\ 0 & 1 & 0 \\ c' & 0 & 1 \end{bmatrix} \begin{Bmatrix} f_{x1} \\ f_{y1} \\ m_{z1} \end{Bmatrix} = \mathbf{W} \mathbf{f}_1 \quad (4.11)$$

Equations 4.9 to 4.11 hold provided that  $\sin x \approx x$ . The same assumption is also required for finite design methods in the literature (Bailey 1995; Saab & Nethercot 1991). Now, considering the behaviour of the beam the following relationship is derived for the member joining Nodes A and B:

$$\mathbf{f}_{AB} = \begin{Bmatrix} \mathbf{f}_A \\ \mathbf{f}_B \end{Bmatrix} = \mathbf{k}_{AB} \begin{Bmatrix} \mathbf{u}_A \\ \mathbf{u}_B \end{Bmatrix} \quad (4.12)$$

with  $\mathbf{k}_{AB}$  being the stiffness matrix of a beam joining nodes A and B, as defined in Equation 4.3. Substituting Equations 4.10 and 4.11 in 4.12 we obtain:

$$\mathbf{f}_{AB} = \begin{bmatrix} \mathbf{W} & \mathbf{0} \\ \mathbf{0} & \mathbf{W} \end{bmatrix} \begin{Bmatrix} \mathbf{f}_1 \\ \mathbf{f}_2 \end{Bmatrix} = \mathbf{Q}_{AB} \mathbf{f}_{AB} = \mathbf{k}_{AB} \begin{bmatrix} \mathbf{Q} & \mathbf{0} \\ \mathbf{0} & \mathbf{Q} \end{bmatrix} \begin{Bmatrix} \mathbf{u}_1 \\ \mathbf{u}_2 \end{Bmatrix}, \quad (4.13)$$

$$\text{Therefore: } \begin{Bmatrix} \mathbf{f}_1 \\ \mathbf{f}_2 \end{Bmatrix} = \begin{bmatrix} \mathbf{W} & \mathbf{0} \\ \mathbf{0} & \mathbf{W} \end{bmatrix}^{-1} \mathbf{k}_{AB} \begin{bmatrix} \mathbf{Q} & \mathbf{0} \\ \mathbf{0} & \mathbf{Q} \end{bmatrix} \begin{Bmatrix} \mathbf{u}_1 \\ \mathbf{u}_2 \end{Bmatrix}, \quad (4.14)$$

$$\text{But: } \begin{bmatrix} \mathbf{W} & \mathbf{0} \\ \mathbf{0} & \mathbf{W} \end{bmatrix}^{-1} = \begin{bmatrix} \mathbf{Q} & \mathbf{0} \\ \mathbf{0} & \mathbf{Q} \end{bmatrix}^T \quad (4.15)$$

$$\text{Therefore: } \begin{Bmatrix} \mathbf{f}_1 \\ \mathbf{f}_2 \end{Bmatrix} = \begin{bmatrix} \mathbf{Q} & \mathbf{0} \\ \mathbf{0} & \mathbf{Q} \end{bmatrix}^T \mathbf{k}_{AB} \begin{bmatrix} \mathbf{Q} & \mathbf{0} \\ \mathbf{0} & \mathbf{Q} \end{bmatrix} \begin{Bmatrix} \mathbf{u}_1 \\ \mathbf{u}_2 \end{Bmatrix} = \mathbf{Q}_{AB}^T \mathbf{k}_{AB} \mathbf{Q}_{AB} \begin{Bmatrix} \mathbf{u}_1 \\ \mathbf{u}_2 \end{Bmatrix} \quad (4.16)$$

$$\text{So: } \mathbf{k}_{12} = \mathbf{Q}_{AB}^T \mathbf{k}_{AB} \mathbf{Q}_{AB} \quad (4.17)$$

Equation 4.17 is the fundamental methodology for transforming the stiffness of an eccentric beam to be about a specified reference axis. The updated stiffness matrix,  $\mathbf{k}_{12}$ , represents an elegant relationship that considers the eccentric position of a NA relative to an arbitrary reference axis. Note that the above relationship can also be numerically derived and verified by modelling rigid links between Nodes 1-A and 2-B, and then statically condensing out Nodes A and B (Bathe 2006). The matrix formulation provides a method comparable to the technique in FE software of slaving the deformation of specific nodes to master nodes.

A form of the eccentric stiffness matrix derived above is presented by Hartmann & Katz (2007), amongst others, but in the former work only transverse and rotational displacements are considered, not longitudinal displacements. Longitudinal displacements are necessary for considering axial loads, which are essential in

structural fire design. Furthermore, the aforementioned authors considered a time invariable NA, which is not the case in this work. Researchers such as Chan & Chan (1999) use the transformation matrix presented in Equation 4.10 to slave the nodal displacements of a beam element to shell elements to create composite beams. Hence, the matrices derived in this chapter have been used in the literature in various ways. This has been typically done for structures where the NA of a member being modelled is known before the analysis commences, and remains in a fixed position with time and along the member's length.

#### 4.2.4 Unbalanced Forces

In any nonlinear formulation it is important that the unbalanced forces due to the deformation of a member be calculated for each iteration. In the methodology presented here this is done using the total deformations that have occurred up to the time being considered, and *not* incremental forces being added together as is normally the case. When the unbalanced forces are determined for an increment they are calculated relative to a specific NA position. However, once the NA migrates there will be errors due to forces being calculated about the wrong axis. Hence, it is necessary to recalculate the total unbalanced forces in each element in each iteration relative to the updated NA positions, which is not required in typical methods. Thus, the unbalanced forces in the local ( $\mathbf{r}'$ ) and global ( $\mathbf{r}$ ) coordinate system are determined as:

$$\mathbf{r}' = -\mathbf{k}_{12,S}\mathbf{u}' \quad (4.18)$$

$$\mathbf{r} = \mathbf{T}^T\mathbf{r}' \quad (4.19)$$

$\mathbf{T}^T$  is the standard matrix transformation matrix transposed. The transformation matrix is given by:

$$\mathbf{T} = \begin{bmatrix} \cos \alpha_0 & \sin \alpha_0 & 0 & 0 & 0 & 0 \\ -\sin \alpha_0 & \cos \alpha_0 & 0 & 0 & 0 & 0 \\ 0 & 0 & 1 & 0 & 0 & 0 \\ 0 & 0 & 0 & \cos \alpha_0 & \sin \alpha_0 & 0 \\ 0 & 0 & 0 & -\sin \alpha_0 & \cos \alpha_0 & 0 \\ 0 & 0 & 0 & 0 & 0 & 1 \end{bmatrix} \quad (4.20)$$

where  $\alpha_0$  is the angle of the member in the global coordinate system, as shown in Figure 4.5. The local deflections,  $\mathbf{u}'$ , are determined from Cook et al (2001), where:

$$\mathbf{u}' = \{ 0, 0, \varphi_{12}, u'_2, 0, \varphi_{21} \}^T \quad (4.21)$$

$$\varphi_{12} = \varphi_1 - (\alpha' - \alpha_0) \quad (4.22)$$

$$\varphi_{21} = \varphi_2 - (\alpha' - \alpha_0) \quad (4.23)$$

$$u'_2 = \frac{1}{L' + L} [(2x_0 + u_2 - u_1)(u_2 - u_1) + (2y_0 + v_2 - v_1)(v_2 - v_1)] \quad (4.24)$$

$$\alpha = \arctan(y_0 + v_2 - v_1 / x_0 + u_2 - u_1) \quad (4.25)$$



These equations can be understood in reference to Figure 4.5. The equation for  $u'_2$  ensures that small differences between large numbers do not need to be calculated, although it would be possible to calculate the value directly from local displacements.

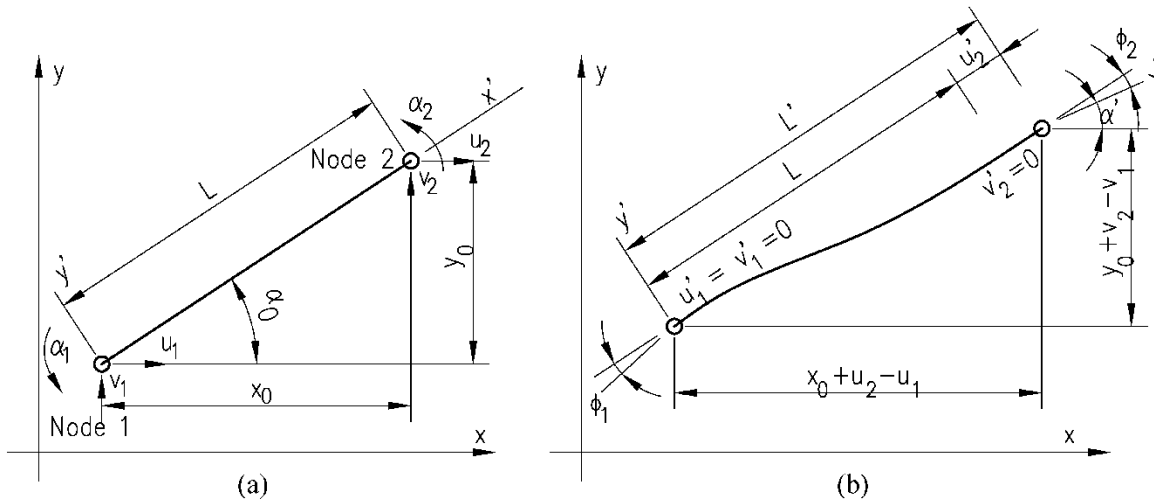


**Figure 4.5:** (a) Plane element before deformations, but noting global degrees of freedom (XY axis). (b) The element after deformation and motion showing deformations in the local (x'y') axis (based on Cook et al (2001))

Once the local unbalanced forces for each element have been obtained the global unbalanced load vector is calculated as:

$$R_R = \sum r \quad (4.26)$$

The calculation of the secant matrix and unbalanced forces is important to ensure convergence of the solution. Any numerical inaccuracies in their formulation will cause solutions to not converge or converge to incorrect results. Conversely, various tangent matrix formulations can be used (e.g. initial tangent stiffness, updated each iteration, modified tangent stiffness), but analyses will generally still converge to the same solution, although the rate of convergence will vary. Overall, the inclusion of the eccentric transformation matrices, movable NAs, and calculation procedure for restraining forces form the foundation of the FBE.

### 4.3 Methodology verification and case studies

Various studies are presented below to compare the FBE formulation derived above against FE models using shell elements. The FE models have been analysed in the modelling software Abaqus (Dassault Systèmes 2013). The Abaqus models consist of significantly more complex 3D configurations of shell elements with much greater numbers of degrees of freedom (DOFs) in comparison to the FBE formulation models used. Shell elements are modelled with S4R elements, which are 4-noded, reduced integration elements. For each model the mesh configuration is shown. The Abaqus models are included to show how the modelling philosophy and assumptions adopted by the FBE formulation compare with other models that are based on different assumptions (i.e. Euler-Bernoulli behaviour not enforced and multiple elements for each cross

section). Also, it is considered what level of inaccuracy in results may be encountered when fundamental Euler-Bernoulli assumptions are violated.

The FBE formulation has been implemented within a specially developed non-linear structural analysis programme developed by the author. It uses the Newton-Raphson procedure to account for non-linear behaviour (Cook et al. 2001). The programme considers large deflections, the material models described below, and uses the stiffness matrices for analysis as presented in this chapter. The software has been programmed in C++. The number of segments beams are discretised into is provided for each case study.

Non-beam element formulations (i.e. shell and volume element formulations), do not explicitly consider the position of the NA of a beam, rather this is implicitly accounted for through the model formulation and FE elements used. In any FE model consisting of shells or volume elements the position of zero strain for a cross-section in pure bending represents the NA. In the Abaqus models created the assumption of plane sections remaining plane is not enforced, except at boundary conditions. Shear deformations can occur in Abaqus analyses, which does account for some of the differences observed in results presented below, although this is typically limited.

By comparing stresses, strains and NA positions it can be determined whether models predict the same, or very similar, structural mechanics for a particular system under load. This chapter only addresses numerical modelling and verification of the FBE model. Experimental case studies specific to fire design are considered in Chapter 6. In this chapter material models and structural configurations have been selected to cause NAs to shift relative to their original positions. Each of the four case studies considered illustrate a different behaviour. Case Study A is a simple example comparing deflections and non-linear behaviour between the Abaqus, FBE and a closed-form equation describing deformations. Also, it is shown how results are affected when the NA of a section is not adjusted. Case Study B compares stresses, strains and NA position across the length of a beam. Case Study C is a statically indeterminate fixed-fixed beam which experiences forces due to restraint. Case Study D is of a beam with linear elastic material but with a distinct change in material stiffness along its length. This final case study illustrates behaviour when plane sections do not remain plane in a localised area, as might occur when concrete cracks. Additional details regarding the case studies are contained in Appendix B, which contains the beam stiffnesses calculated for each case study.

### ***Non-linear material model to cause NA movement***

A theoretical material model has been developed for the case studies in this chapter where the material used for beams hardens in compression and softens in tension. In bending the NA will migrate towards the side which goes into compression. In the next chapter more realistic material models are developed to allow for the consideration of the experimental case studies. The following equations describe the behaviour of the proposed material with changes in stress,  $\sigma$ :

$$E_T(\sigma) = E_0 + \beta\sigma \quad (4.27)$$

$$\epsilon(\sigma) = \frac{\ln(E_0 + \beta\sigma) - \ln(E_0)}{\beta} \quad (4.28)$$

$$\sigma(\epsilon) = \frac{E_0(e^{\beta\epsilon} - 1)}{\beta} \quad (4.29)$$

$E_0$  is the initial slope of stress-strain graph, representing the initial tangent stiffness.  $E_T(\sigma)$  is the tangent stiffness which is a function of the stress. The slope of the  $E_T - \sigma$  graph is  $\beta$  which represents the rate of change of  $E_T$  with changing stress. The material model has been implemented within Abaqus using UMAT (user material) subroutines (Dassault Systèmes 2013). Two configurations of  $E_0$  and  $\beta$  have been included. The first is with  $E_0 = 200$  GPa, and  $\beta = -1000$ , with behaviour as shown in Figure 4.6. The second configuration is  $E_0 = 20$  GPa, and  $\beta = -50$ . The latter is a much softer material that has been included to ensure that there are large deflections in systems, as would be expected in a fire. In the case studies below these material configurations are simply referred to by their  $E_0$  values.

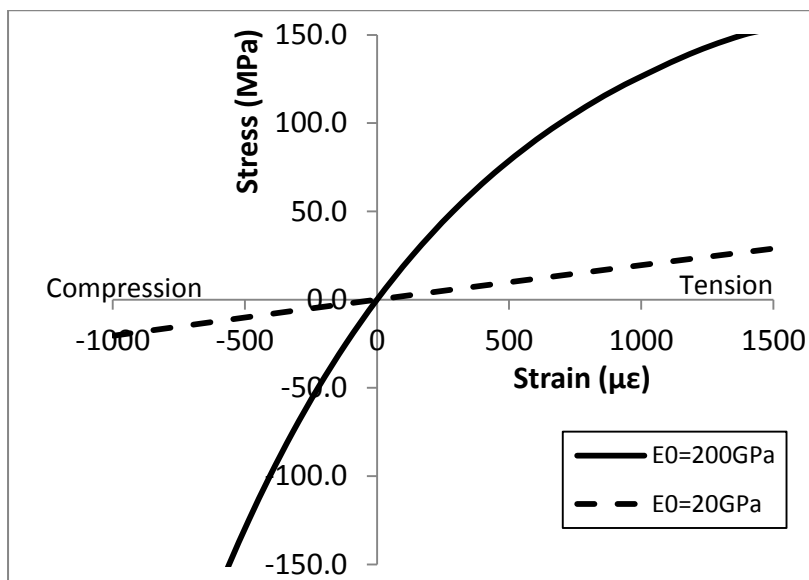


**Figure 4.6: Stress-strain relationships for the theoretical material model used**

#### 4.3.1 Case Study A: IPE 200 cantilever with non-linear material properties

The cantilever shown in Figure 4.7 consists of an IPE 200 beam, with cross-sectional dimensions as previously shown in Figure 3.12, and is made of the non-linear material discussed above with either  $E_0 = 200$  GPa or  $E_0 = 20$  GPa. This structure has been chosen because there is a closed form analytical solution to calculate deflections when only a single moment,  $M$ , is applied to the end, and the equation applies even for large deflections (Cook et al. 2001). However, the bending stiffness,  $EI$ , must be calculated about the updated NA position to account for material non-linearity when using this equation. If this is not done the same results shown in Figure 4.9 and Figure 4.10 are obtained as for the FBE case where the NA is not updated. This

analytical solution allows for validation of both the Abaqus and FBE model. If only a moment,  $M$ , is applied the maximum vertical deflection at the tip can be calculated as:

$$\delta = \frac{EI}{M} \left( 1 - \cos \left( \frac{ML}{EI} \right) \right) \quad (4.30)$$

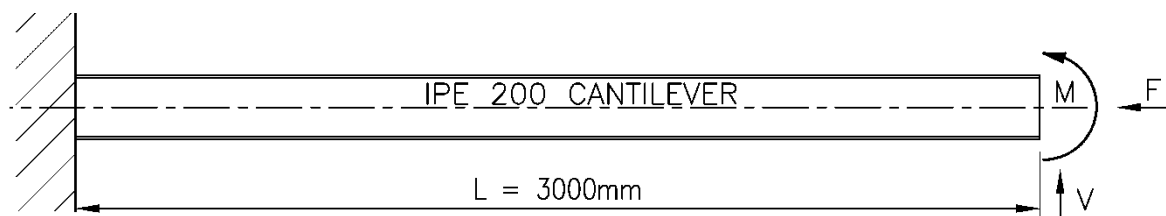


**Figure 4.7: Case Study A - Simple cantilever**

When only the moment is applied the behaviour and analysis procedure of the cantilever will be as illustrated in Figure 4.8. In (a) the structure is discretised into a number of smaller beam elements. Once the end moment is applied the cantilever deflects, causing the lower sections to go into tension, thus softening, whilst the upper sections go in compression and harden. The NA position of the system moves upwards as the load increases, as illustrated in (b). Using the eccentric transformation matrices, presented in Section 4.2, the stiffness of the beams about the updated NA is related to the reference axis, as shown in (c). Stiffness matrices are determined using this approach and the resultant global stiffness matrix and deflections calculated. The load is applied in a series of steps, the beam properties being updated in each iteration.

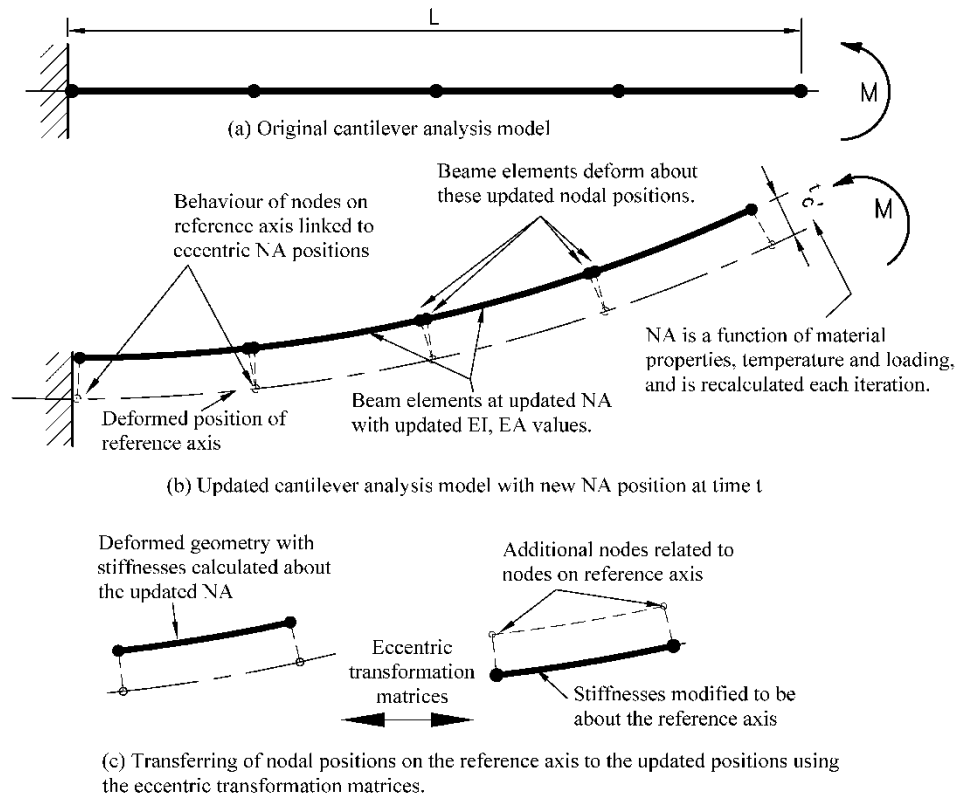


**Figure 4.8: Analysis behaviour and considerations for Case Study A**

For this case study 5 FBE sections were used with 6 degrees of freedom for each beam. This gives a total of 18 degrees of freedom (DOFs) at nodes for global analyses. Beam segments have 30 integration points, with 10 in each of the top flange, web and bottom flange. This does not influence the number of global degrees of freedom but rather defines the number of points on the stress and strain profiles for each cross-section. For the Abaqus model 1920 shell elements were used, with a total of 116886 DOFs. It was found that increasing the number of FBE beam sections provided negligible improvement in results. It is possible to reduce the Abaqus mesh size significantly with relatively small changes in results.

Figure 4.9 and Figure 4.10 show the vertical deflection of the tip of the cantilever with increasing moment for the cases with  $E_0 = 200$  GPa and  $E_0 = 20$  GPa respectively. Solutions from the analytical equation, Abaqus, and FBE formulation are compared. An additional case is included using the FBE formulation but with the NA remaining in a fixed position at its original location. This is included to demonstrate the importance of adjusting properties to suit the new NA position. For an applied moment of 30kNm the NA shifts upwards by 12.7mm for the stiffer material and by 3.3mm for the softer material.

The maximum difference in results between the Abaqus, FBE and analytical models is 0.5%, and the graphs are almost indistinguishable. This small error may be due to factors such as: integration schemes, level of discretisation, load step sizes and the Abaqus model considering shear deformations whereas the FBE method does not. Overall, differences in results can be considered negligible. However, at 30kNm the difference

between FBE results when the NA remains in a fixed position or not is -22.1% and -6.1% for the two material stiffnesses respectively. This error in calculated deflections increases with increasing load. Hence, if the NA is not adjusted the bending stiffness of the beam properties that are calculated become too high, resulting in a stiffer structure with lower deflections. A beam model calculating stiffness properties about the original NA would predict the same inaccurate deformations as the FBE model with the fixed NA position.

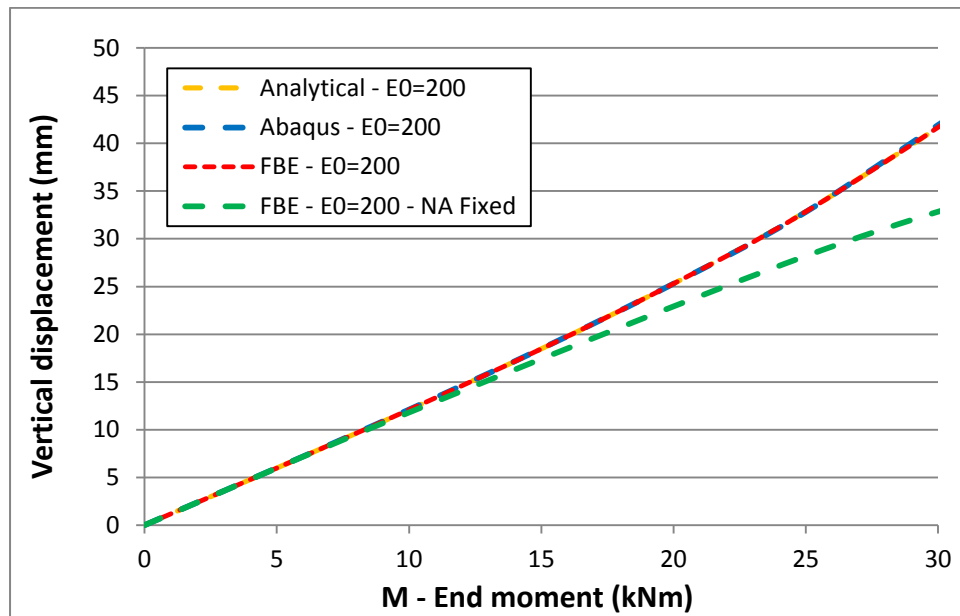


Figure 4.9: Vertical deflections of Case Study A with increasing end moment with  $E_0 = 200$  GPa

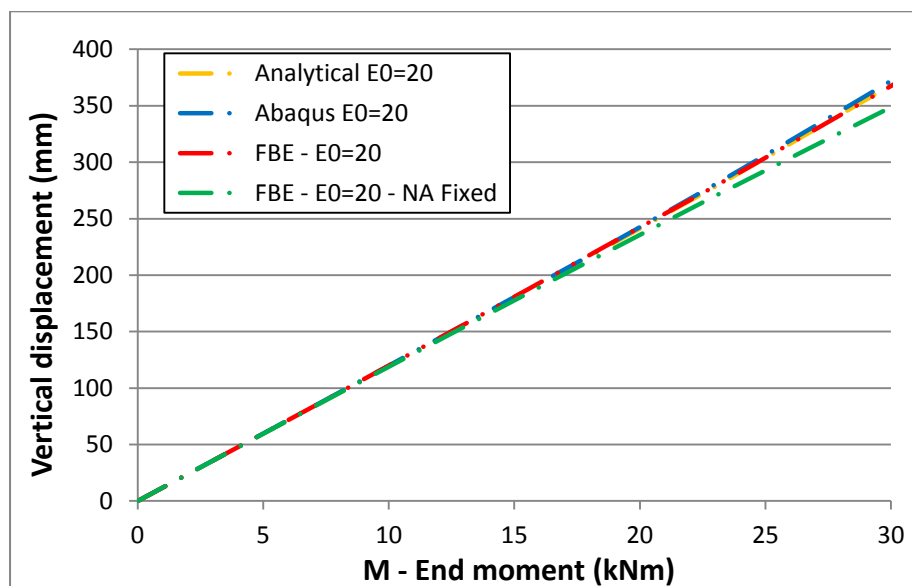
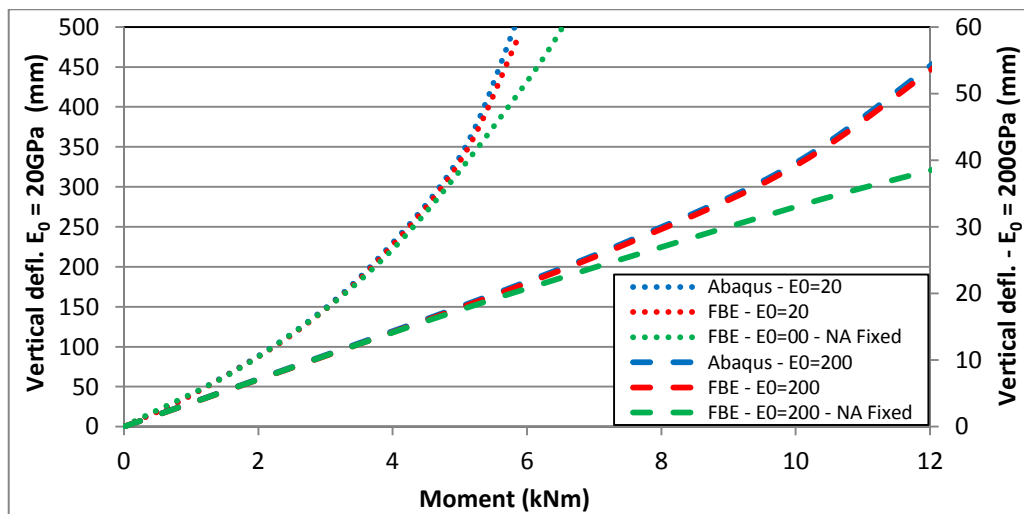


Figure 4.10: Vertical deflections of the simple cantilever with increasing end moment with  $E_0 = 20$  GPa

To create a system with a higher degree of nonlinear behaviour an axial load of  $F = \frac{30M}{L} = 10M$  kN, and a vertical end load of  $V = \frac{3M}{L} = M$  kN is now also applied to the cantilever, where  $M$  is the end moment

applied. The results are shown in Figure 4.11, with the two sets of material parameters used as above. The FBE formulation calculates deflections very similar to the Abaqus model, with differences of between 1.0% and 1.9% at maximum loads. Even though the rotations exceed small rotation theory and a deflection of  $\text{Span}/6$  is experienced for the  $E_0 = 20 \text{ GPa}$  case the results are still negligibly different. The same reasons for differences in results as mentioned above apply. Hence, the FBE formulation presented can consider large deformations and nonlinear behaviour with minimal errors between it and finite element models using shell elements. For the case with the FBE formulation being used but with the NA remaining in a fixed position deflections are significantly lower, with differences of -30.5% and -16.0% at the graph extents for the stiffer and softer materials respectively.



**Figure 4.11: Vertical deflection of the simple cantilever with end moment, shear and axial forces applied**

#### 4.3.2 Case Study B: Rectangular beam with material non-linearity

This case study compares the stress, NA and deflection profiles between the FBE formulation and an Abaqus shell element model for a rectangular 5mm thick by 300mm deep beam. The general configuration is presented in Figure 4.12, with the mesh being indicatively shown. The same material model has been used as the previous case study with  $E_0 = 20 \text{ GPa}$ . The softer material has been included to ensure that larger deflections and NA shifts occur. A UDL of  $10 \text{ kN/m}$  is applied. A relatively fine mesh of 16 elements per cross-section height has been used in the Abaqus model to ensure that there are sufficient points for comparing stresses and strains. However, a coarser mesh of 8 elements across the height provides approximately the same overall deformation behaviour. For the FBE analysis the beam has been discretised into 32 segments, to provide a number of points at which stresses can be compared. Lateral buckling has been prevented in the Abaqus model by applying boundary conditions in the model. The thickness of the shells has been selected to ensure that shells remain relatively thin in comparison to elemental dimensions.

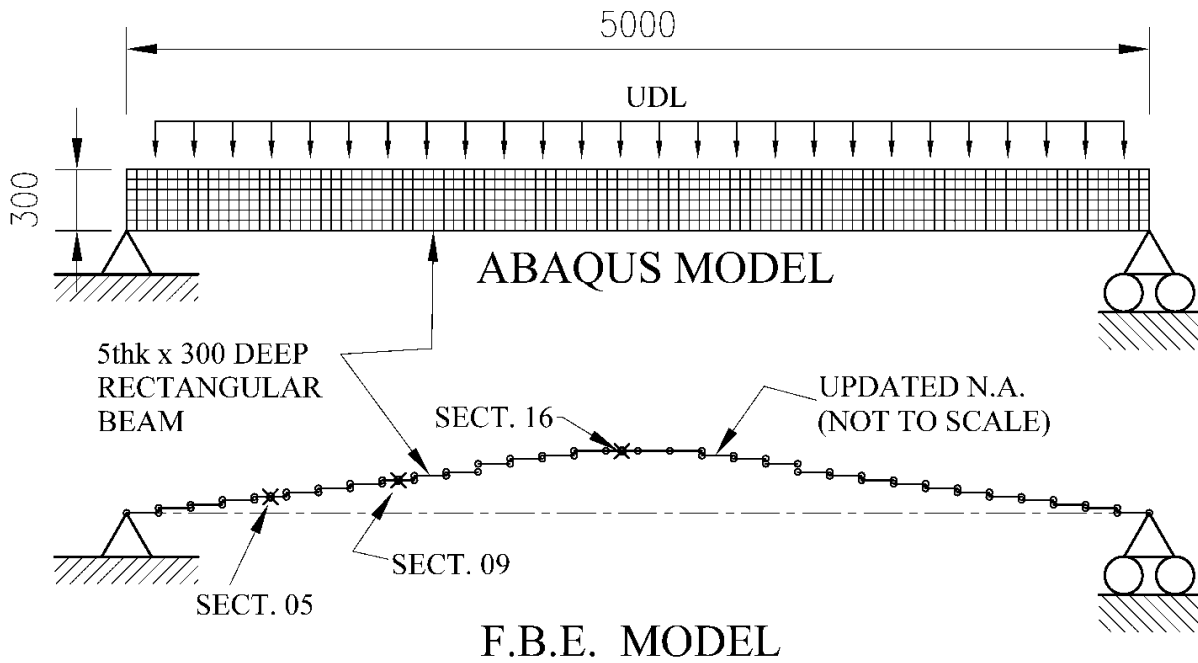


**Figure 4.12: Case Study B - 5x300 rectangular beam with a UDL showing the Abaqus and final FBE model**

A comparison of the stresses in the Abaqus and FBE models at a load of 10 kN/m is shown in Figure 4.13. This is done at the mid-point of three beam sections numbered 05, 09 and 16. The stress profiles are almost identical throughout, demonstrating that loads are carried in the same manner. The difference in results for Section 16 at maximum compressive stress (negative value) is 3.0%, and throughout differences are generally within this range. Strains follow linear distributions over the height of sections in both models. Overall it can be seen that even though a very different modelling approach is used for the two analyses the FBE scheme of determining material properties about an updated NA provides accurate stress and strain calculations.

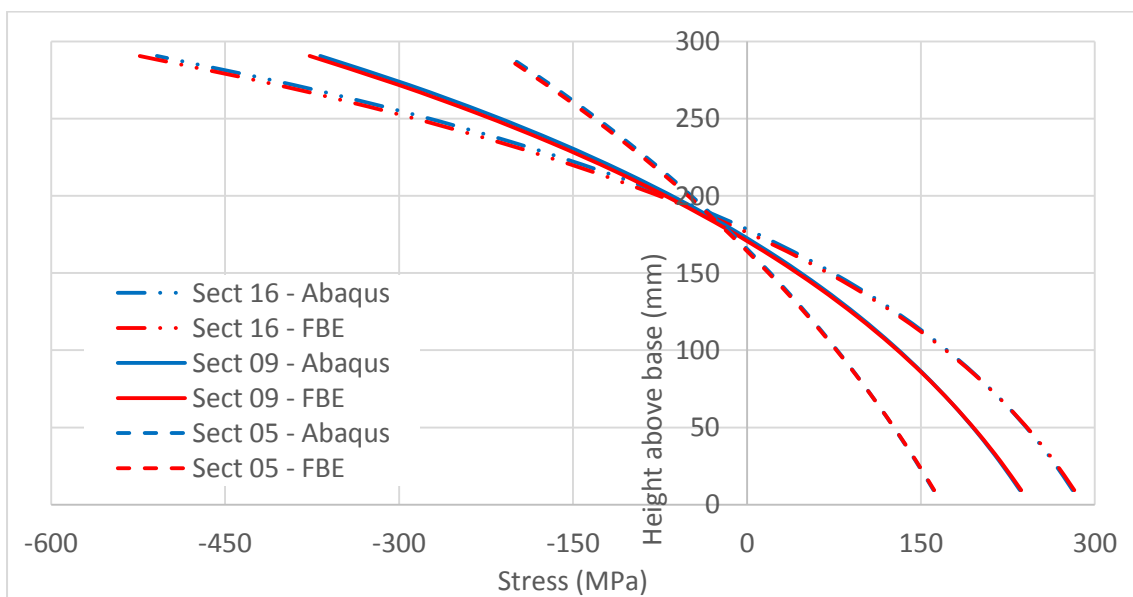


**Figure 4.13: Stresses over cross-sections at various positions for Case Study B**



The change in deflection with increasing load is shown in Figure 4.14. The scenario where the NA is fixed has also been included again. From the results it can be seen that initially the three cases predict the same deflections. As loads increase and material non-linearity becomes pronounced the difference in predicted deflections between the two FBE models increases from 0.1% at 1 kN/m to 11.8% at 10 kN/m, and 22.1% and 20 kN/m. In general the Abaqus and FBE models predict approximately the same deflections, with a difference of 0.4% at a load of 10 kN/m.

An isoline strain plot of half the beam is shown in Figure 4.15, as generated by the Abaqus model. The central green line is for zero strain, representing the NA. It can be seen that at the midspan it moves upwards in the section. At mid-span the NA is calculated as being 176.3mm above the base by Abaqus and 178.4mm above the base by the FBE model. The prediction of the NA position between the two models differ by approximately 2.0 to 2.5mm for the inner 4m of the beam. At the supports shear deformations and the influence of boundary conditions cause a localised perturbation as seen on the left hand side of the figure. This does not influence deflections but does cause a localised difference in stresses and strains.

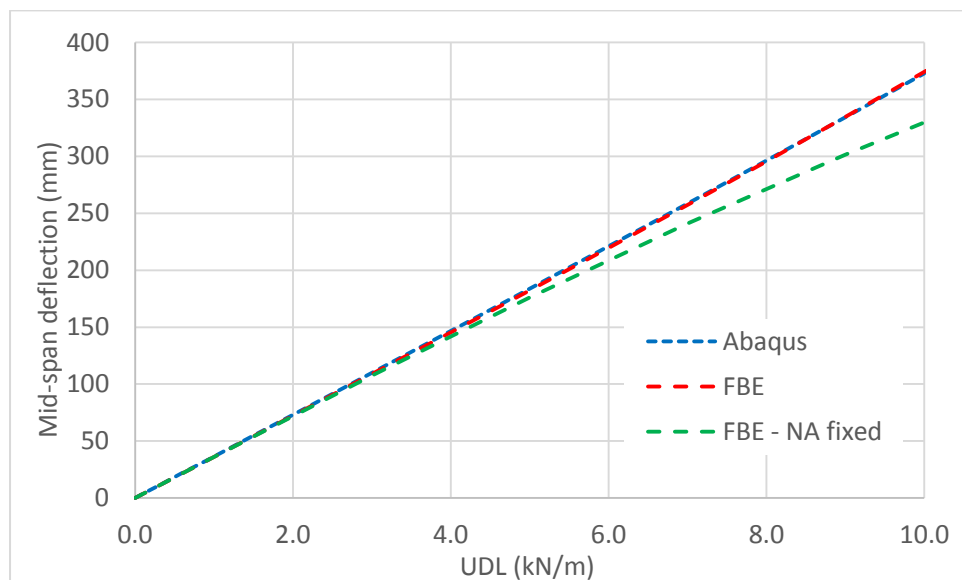


**Figure 4.14: Deflection with increasing load for Case Study B**

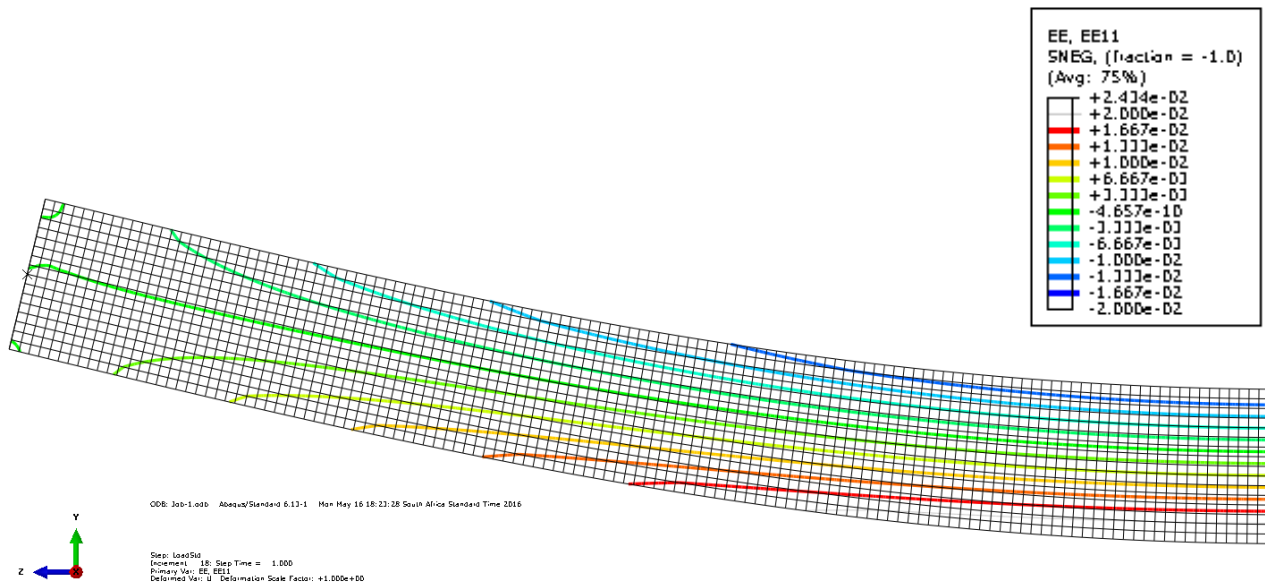


**Figure 4.15: Isoline strain plot for Case Study B. The central green line of zero strain represents the NA.**

### ***Computational effort***

It is interesting to note the difference in computational times required for the two analyses, both conducted on an Intel i7 2.60GHz laptop with 8GB of RAM. The FBE code, programmed in C++, took 0.827 seconds, while the Abaqus model required 82 seconds, which is two orders of magnitude more. It is acknowledged that neither analysis was optimised for speed and the performance of both could easily be improved. However, this information is simply provided to give a ballpark comparison of computational effort required.

#### ***4.3.3 Case Study C: Fixed-fixed IPE 200***

To illustrate the influence of static indeterminacy and bending moment diagram shape the IPE 200 considered in Case Study A is now analysed with it spanning 5m and carrying a uniformly distributed load (UDL) of 10 kN/m, with fixed-fixed boundary conditions. The layout is shown in Figure 4.16. The nonlinear material model with  $E_0 = 200$  GPa is used. For the FBE model the beam is discretised into 32 equal segments. The final, fully loaded FBE model with updated NA positions is shown by the exaggerated layout of beam elements in the lower portion of Figure 4.16. The mesh used in the Abaqus model is shown in Figure 4.17, along with maximum stresses under loading.

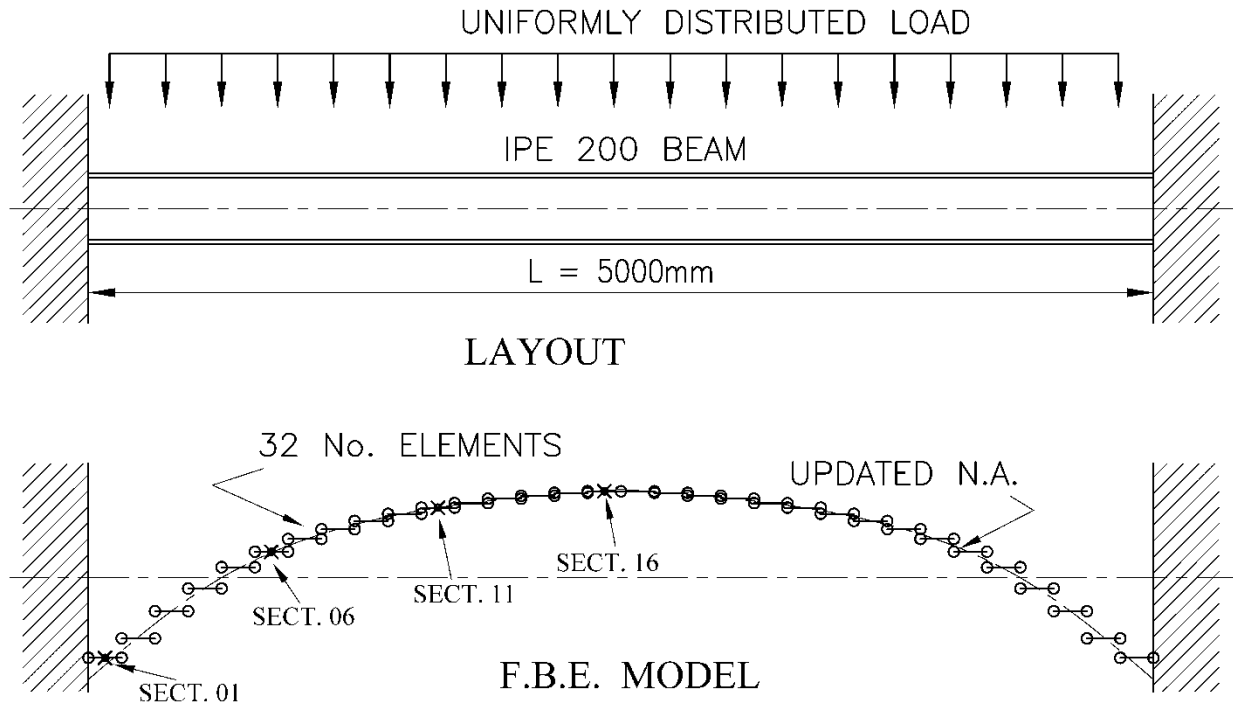


Figure 4.16: Case Study C – Fixed-fixed IPE 200 showing structural layout and final FBE configuration

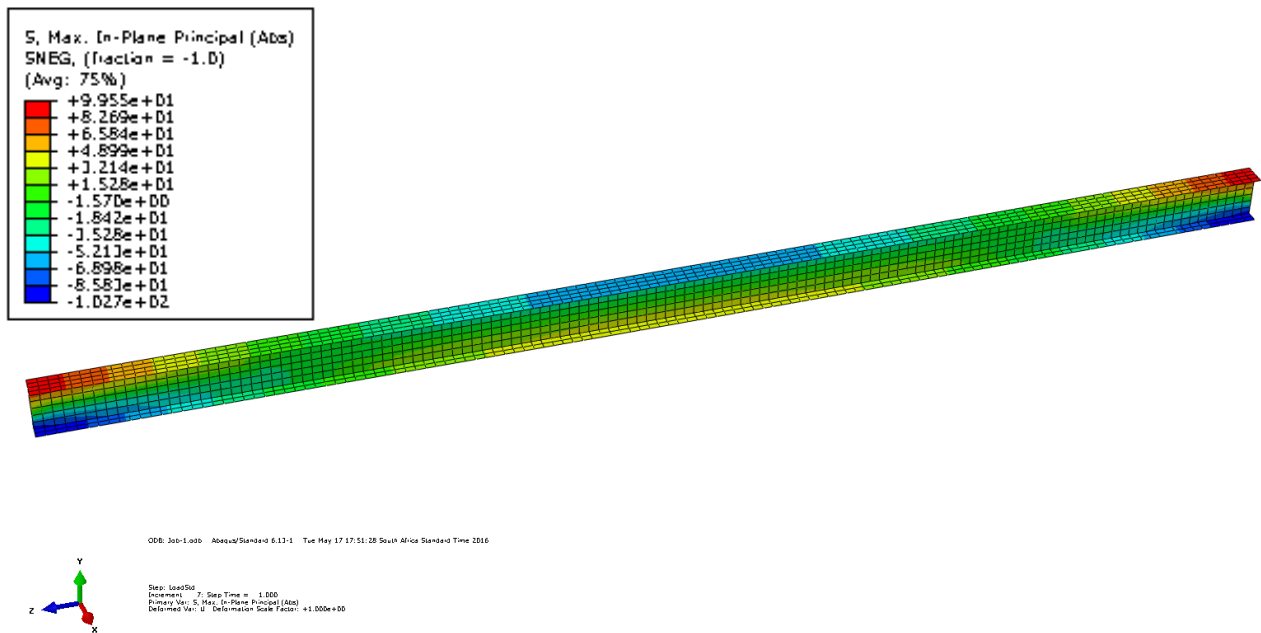
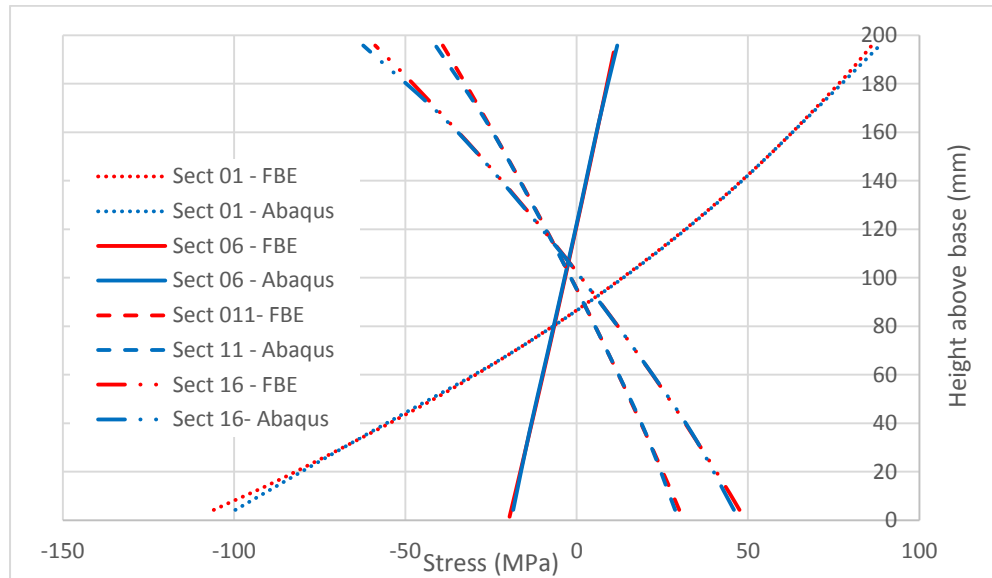


Figure 4.17: Deflected shape and maximum stresses in the Abaqus model of Case Study C

A comparison between stresses calculated at the mid-point of Sections 01, 06, 11 and 16 is shown in Figure 4.18. There is good agreement between the stress profiles showing that the structural mechanics of the two systems are similar. Strain profiles show this same level of consistency. For Section 01 the maximum difference in stresses is 6.3% in the bottom flange, while for Section 16 it is -5.6% at the top flange. With the

compression flange becoming stiffer than the remainder of the section it results in a certain amount of cross-sectional distortion to maintain equilibrium, thus leading to this discrepancy as plane sections do not remain fully plane. Overall, it can be observed that the behaviour of the system has been captured by the FBE formulation, and differences are mostly due to Euler-Bernoulli assumptions not fully holding, although differences are small.



**Figure 4.18: Stress profiles for Case Study C at various location**

For the FBE model the NA varies from 17.1mm below its centreline at the support (Sect. 01) to 9.32mm above the centreline at mid-span (Sect. 16). A 26.4mm change in NA position is substantial for a section that is only 200mm deep. The axial stresses induced by deformations result in the position of the NA not being the position of the zero strain in the Abaqus model. The positions of zero strain compare favourably, as shown in Figure 4.18. The calculated deflection at midspan is 4.34mm according to the FBE model and 4.66mm according to the Abaqus model. This 6.9% difference in results is due to cross-sectional distortion, as discussed above.

#### 4.3.4 Case Study D: Fixed-fixed rectangular beam with variation in material properties

The previous case studies have addressed beams where there is a progressive and gradual change in bending stiffness across the length of a member. Case Study D seeks to answer the question: how does the FBE system perform when there is a sudden change in stiffness over a short distance? Such behaviour can occur when a concrete slab or composite beam experiences cracking. It is important to know not only the applications of a method but also its limitations and to what extent results become inaccurate when assumptions are violated. The rectangular 5x300 beam from Case Study B is used but with fixed-fixed end conditions and two distinct materials, as shown in Figure 4.19. The same load of 10kN/m is applied for determining stresses and strains. The general material stiffness has been taken as  $E = 50$  GPa. For the outer quarters the upper half has a

stiffness of  $E = 10$  GPa, which was used as a simplified way of simulating the cracked portion of a concrete slab in the hogging region. Strains are plotted at beam sections 01, 04, 08 and 09.

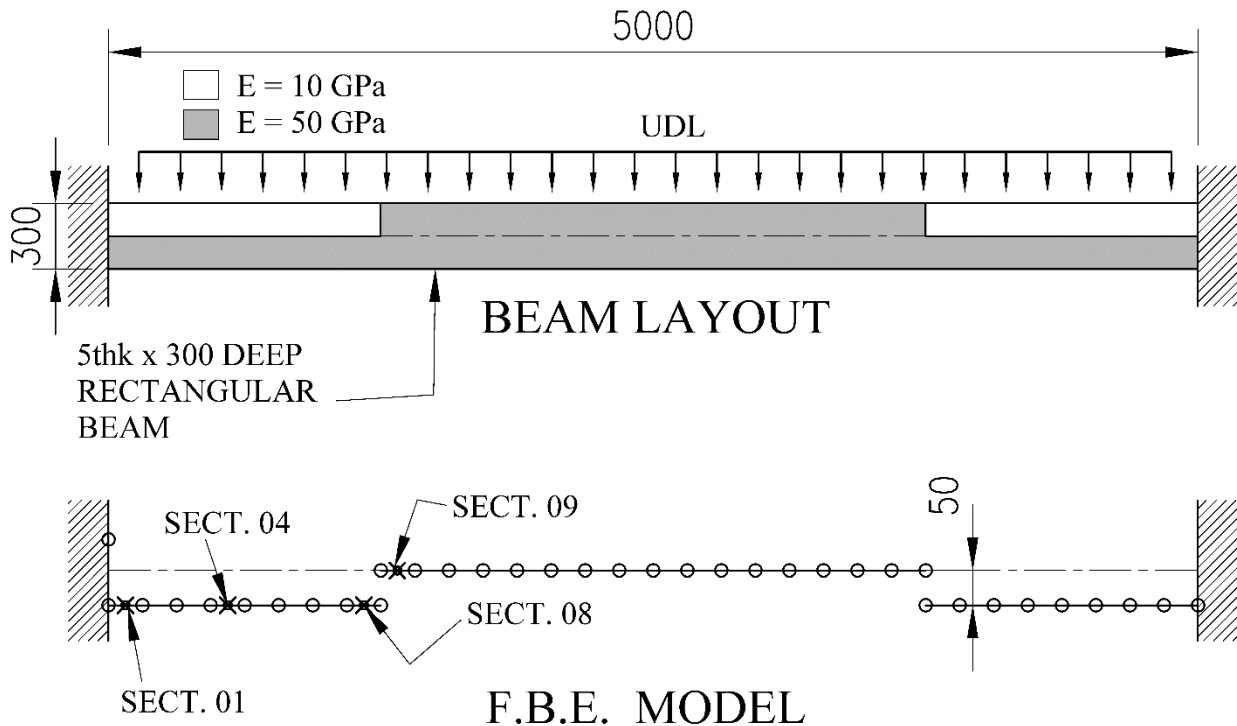


**Figure 4.19: Rectangular beam with UDL. The Young's modulus is varied to create stiffer zones internally.**

The sudden change in NA position causes localised perturbations in uniform stress patterns, which is required to ensure that in a FE solution cross-sectional compatibility is maintained. At the position of a sudden stiffness change FE models typically show that plane sections cannot remain plane due to non-linear strains. It must be understood that existing fire analysis models identified in Chapters 2 and 5 typically rely on the assumption of plane sections remaining plane and no slippage. If such an assumption is violated a number of the methods identified in the literature along with the FBE system will start becoming less accurate. Hence, it is necessary to understand how the methodology proposed in this dissertation and various other methods will be influenced by assumptions being violated. Furthermore, it must be remembered that design codes (e.g. EN 1993-1-2, 1994-1-2, SANS 10100-1) for structural design are also based on the assumption of plane sections remaining plane.

The longitudinal strains calculated by the Abaqus model for half of the beam are presented in Figure 4.20. The change in strain patterns at the discontinuity in material stiffness can easily be identified. Cross-sectional strain profiles calculated by Abaqus and the FBE model at the mid-points of various beam sections are shown in Figure 4.21. The most important sections to note are those before and after the change in material properties, namely 08 and 09. It is interesting to note that Section 08, which is composed of two materials, has a more linear strain profile than 09, which is composed of the single stiffer material. This is due to the fact that it takes a longer distance from the material stiffness step for linear strain profiles to be regained in the stiffer

section, i.e. a greater amount of shear lag. In general it can be observed that the Abaqus and FBE models predict approximately the same strains, except at Section 09. The extent of the strain transition zone relative to the overall size of the beam will influence the extent to which there would be differences in FBE and FE solutions.

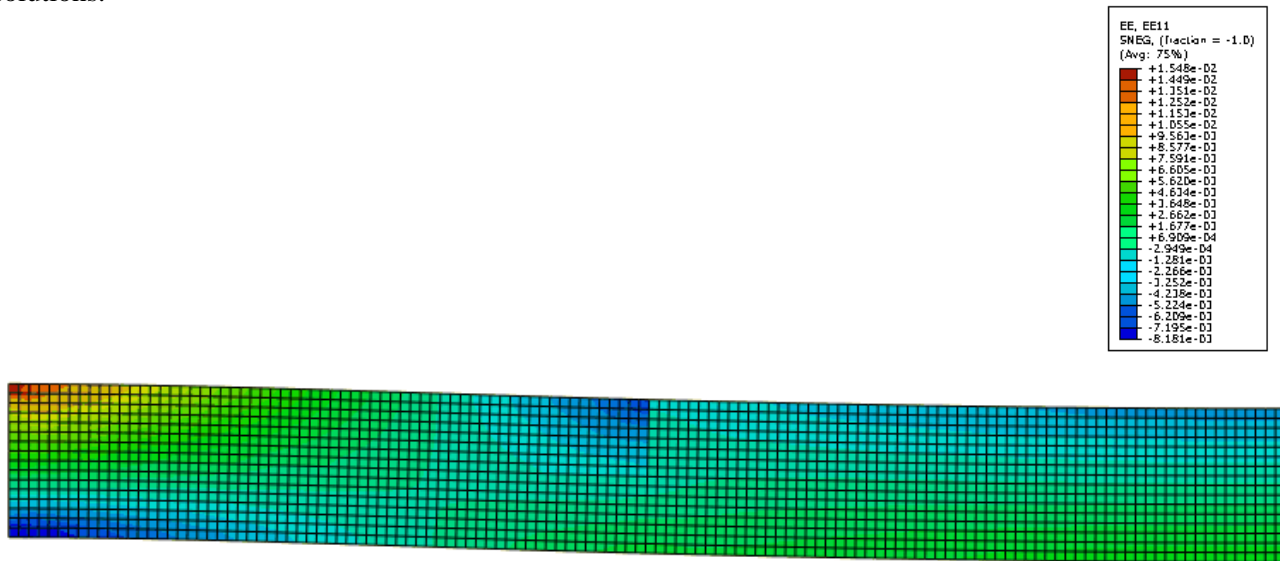


**Figure 4.20: Half of the Abaqus model of Case Study D showing longitudinal strains in the section**

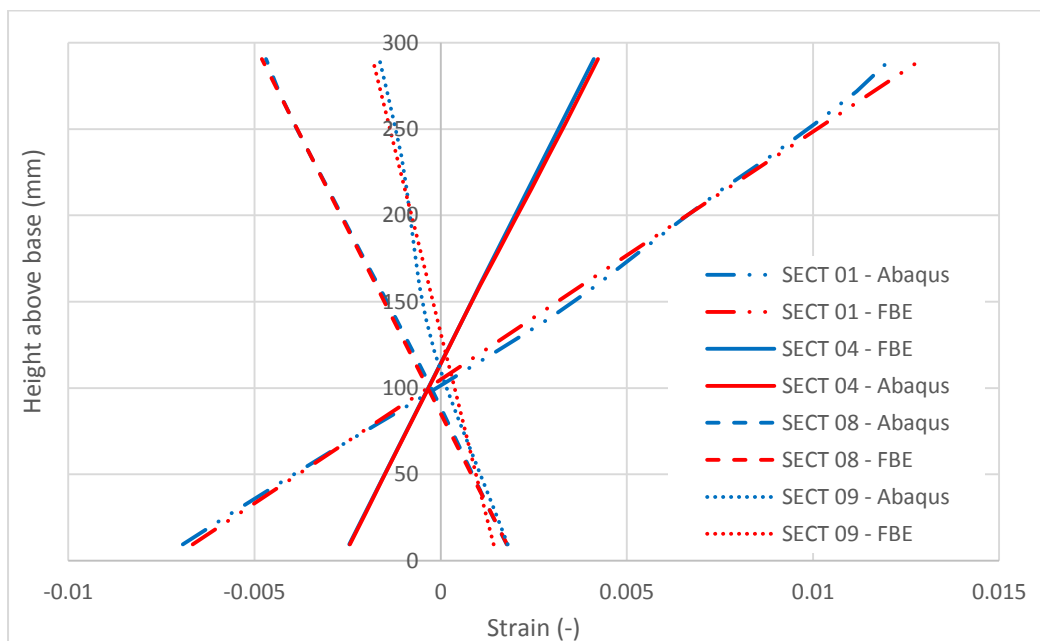


**Figure 4.21: Cross-sectional strain profile for Case Study D at different locations**

The deflection of the beam with increasing load as predicted by the Abaqus and FBE models is shown in Figure 4.22. In this case unrealistically high magnitudes of UDLs have been applied to ensure that large deformations and catenary action occurs. It can be seen that the trend of two graphs is approximately the same, with the FBE method predicting lower deflections. The differences between the deflections are 6.1% at

10 kN/m, 3.2% at 100 kN/m and 5.1% at 200 kN/m. The FBE formulation calculates that at the maximum UDL of 200kN/m the tensile load in the beam ranges between 776 kN and 822 kN along its length. Thus, catenary action is contributing to the load carrying capacity of the beam. This causes the non-linear load-deflection curve. Overall the graph demonstrates that even with large deformations and discontinuities in material properties, as might occur in a fire, the FBE formulation makes a fair prediction of expected behaviour. The level of error will be dependent upon the extent of fundamental assumptions being violated – i.e. Euler Bernoulli assumptions and  $\sin x \approx x$  in Equation 4.10. In this case where a large, sudden change in stiffness occurs results differ by only up to 6.1% in deflection. However, once again localised differences in stresses at discontinuities will be significantly in excess of this.

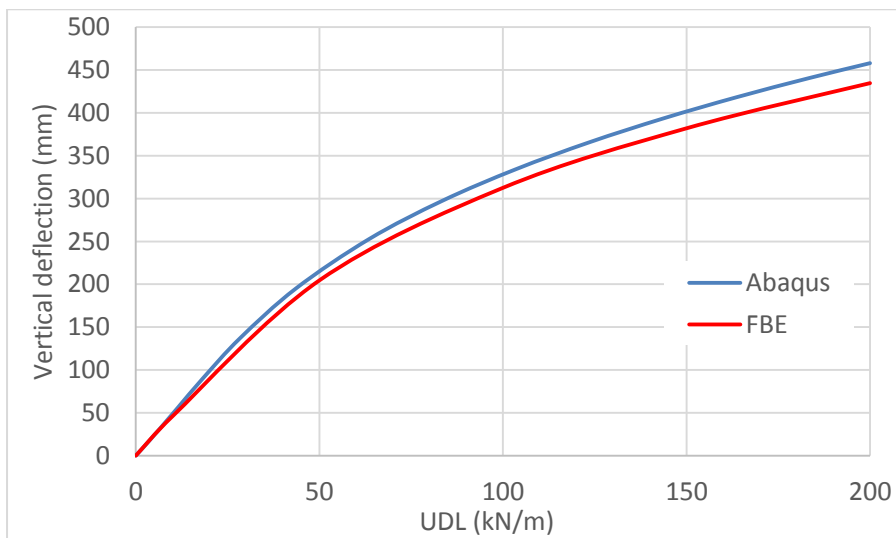


**Figure 4.22: Deflection of Case Study D with increasing load**

#### 4.4 Conclusion

This chapter has presented a method for considering beams with eccentric, movable NAs. The derivation of stiffness matrices used to account for the behaviour is shown, along with an iterative methodology for determining the position of the updated NA at each load step. The method has been implemented on a number of case studies with results being compared to analytical solutions and those from shell element models. In general there is good agreement between the models. Both large deformations and non-linear material behaviour can be accounted for by the FBE formulation.

In Case Studies A and B, which consider statically determinate structures, the difference in model results is negligible. For Case Studies C and D where Euler-Bernoulli assumptions are partially violated the difference between the Abaqus and FBE results increase, although differences are still in the range of generally less than 6%. The FBE formulation will tend to underestimate deflections when Euler-Bernoulli assumptions are violated. This is due to the fact that shear deformations and localised effects are ignored. Even when fundamental Euler-Bernoulli assumptions are violated in a beam the results obtained by the FBE formulation

still compare well with models that consider shear deformations. In the region of a discontinuity there will be different stresses and strains calculated locally between the FBE formulation and models consisting of shell or volume elements, but overall deflections calculated are relatively unaffected. As zones of discontinuity occur over larger proportions of a beam or structure all methods assuming that plane sections remain plane will become less accurate, as will be the case for the FBE formulation.

Based on the above it has been shown that the FBE theory developed produces reliable and consistent results. Also, it can be seen to what extent results may be influenced by Euler assumptions being violated. In the next chapter this formulation will now be extended to include thermal effects and more realistic material behaviour.



## **5 Chapter 5: Developing input parameters for beam elements in fire – material models, tension stiffening and temperature profiles**

### **5.1 Introduction**

This chapter presents (a) the material models used for determining temperature-stress-strain curves for concrete, steel and reinforcing steel, (b) investigates various temperature profiles in concrete slabs, and (c) proposes a modified tension stiffening model. In any FE model the constituent material models used for calculating member stiffnesses are vital, and significantly influence the results obtained. At ambient temperature material models can be relatively simple with constant Young's moduli for materials, provided that material stresses remain within linear-elastic stress limits. In fire conditions materials exhibit highly non-linear behaviour and require stress-strain relationships across a wide temperature range. Typically, stiffness of materials decrease as temperatures increase.

Steel in fire has been extensively studied and the material models presented in this work are primarily based on those from EN 3-1-2 (BSI 2005b). Concrete is a significantly more complicated material with a greater variation in properties. Hence, a number of resources have been consulted for determining which model parameters to include, although stress-strain curves are primarily based upon EN 2-1-2 (BSI 2005a). The consideration of reinforced concrete presents additional challenges to that of unreinforced concrete. In this work reinforced concrete behaviour has been explicitly dealt with through the inclusion of an elevated temperature tension stiffening model.

It must be understood that the fire testing of structural systems is a complex task, both in the experimental setup and in the recording of data. Even when using the standard fire test (ISO 834) there can be variability between furnaces and experimental results. During tests on identical samples at TNO Delft (Netherlands) and Warrington Fire (UK) there was a 30% variation in fire resistances, showing that the one test sample was subjected to significantly higher heat fluxes than the other (Thomson & Preston 1996). This highlights the fact that there can easily be a large scatter in results obtained from tests, and this is one of the reasons why there are differences in the material models in the literature. Furthermore, it is important to note how a range of input parameters used in FE models can vary significantly depending on the material model selected or due to physical characteristics inherent to the material tested. Input parameters addressed in this chapter which may readily vary include: (a) temperatures of structural elements, (b) actual strengths versus characteristic strengths used, (c) whether strain-hardening occurs in steel, (d) confined versus unconfined concrete, (e) concrete stiffness varying due to the aggregate used, (f) concrete thermal properties, (g) different methodologies for considering profiled slabs, (h) effective widths of concrete slabs acting compositely with

steel beams not being known precisely, (i) the influence of tension stiffening, (j) the presence of concrete spalling (beyond the scope of this research) and other such factors including (k) slip in composite sections. Hence, it is important that designers understand to what extent experimental results may differ from prediction models, simply due to variability inherent to input parameters. Prediction model uncertainty further add to this variability.

It is important to note that since this research seeks to compare predicted structural behaviour with experimental data *average* strengths and *average* material properties have been used in models rather than *characteristic* or *nominal* values. This is consistent with guidance from the JCSS Probabilistic Model Code (2001). Structural properties should replicate those found in experiments as closely as possible, rather than seeking to be conservative, as would be required in design scenarios. In the literature it is noted that certain researchers have used characteristic values when seeking to reproduce results.

This chapter first introduces the material models used for steel and concrete, along with the associated temperature profiles used for concrete slabs. This is followed by the development of heat transfer models to define temperature profiles through concrete slabs. An elevated temperature tension stiffening model is then developed.

### 5.1.1 Academic contribution

The inclusion of the tension stiffening model at elevated temperature presents an adaptation of an existing ambient temperature model. The methodology for addressing challenges encountered with numerical convergence in the tension stiffening model is novel. The influence of the tension stiffening model is tested in the parametric studies conducted in Chapter 7. The comprehensive treatment of the variability of parameters and multiple material models is important, although this is primarily an investigation regarding existing literature rather than an academic contribution.

## 5.2 Structural steelwork in fire

Throughout this document the Eurocode EN 3-1-2 (BSI 2005b) guidelines have been adopted to describe the temperature-stress-strain relationship of steelwork (except for Case Study 1 of Section 6.3). Kodur et al (2008) reviewed the steel in fire guidelines of the Eurocodes and ASCE codes (American Society of Civil Engineers), amongst others, and concluded that the Eurocode equations were typically more suitable than those of the ASCE and others. Also, in the literature most researchers base models upon the Eurocode equations. The proposed draft South African structural steel fire design code guidelines (SANS 10162-1, Annex K), will also adopt the EN 3-1-2 material property equations (SABS 2016).

### 5.2.1 Elongation of structural and reinforcing steels

The thermal elongation ( $\varepsilon_{\theta_a}$ ), or thermal strain, of steel at elevated temperatures can be determined by:

$$\varepsilon_{\theta_a} = -2.416 \times 10^{-4} + 1.2 \times 10^{-5} \theta_a + 0.4 \times 10^{-8} \theta_a^2 \quad \text{for } 20^\circ\text{C} < \theta_a \leq 750^\circ\text{C} \quad (5.1)$$

$$\varepsilon_{\theta_a} = 11 \times 10^{-3} \quad \text{for } 750^\circ\text{C} < \theta_a \leq 860^\circ\text{C} \quad (5.2)$$

$$\varepsilon_{\theta_a} = -6.2 \times 10^{-3} + 2 \times 10^{-5}\theta_a \quad \text{for } 860^\circ\text{C} < \theta_a \leq 1200^\circ\text{C} \quad (5.3)$$

where  $\theta_a$  is the steel temperature. This behaviour is illustrated in Figure 5.1. The plateau at  $750^\circ\text{C}$  is due to a phase change in the steelwork. It is important to note this fact as it can cause irregularities in results, evidenced by a perturbation in temperature-deflection graphs. This is clearly shown in Figure 5.6.

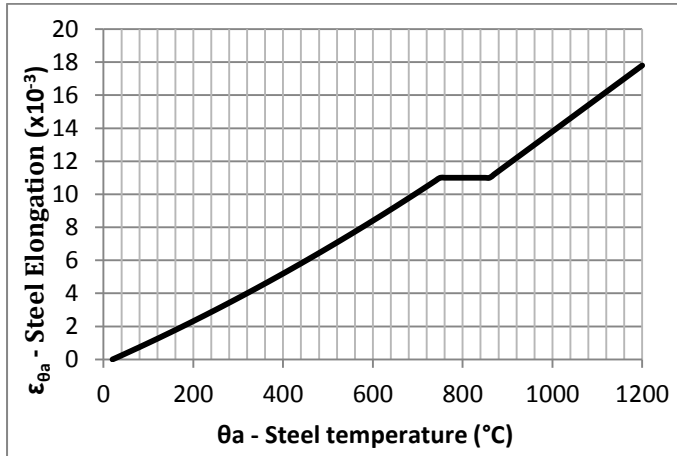


**Figure 5.1: Steel thermal elongation as a function of temperature**

### 5.2.2 Specific heat of steelwork

The specific heat of a steel,  $c_a$ , is the amount of energy required to heat 1kg of the material by 1 degree Kelvin or Celsius. It is important because it greatly influences the rate at which steelwork heats up. It is calculated by:

$$c_a = 425 + 7.73 \times 10^{-1}\theta_a - 1.69 \times 10^{-3}\theta_a^2 + 2.22 \times 10^{-6}\theta_a^3 \quad [\text{J/kgK}] \quad \text{for } 20^\circ\text{C} < \theta_a \leq 600^\circ\text{C} \quad (5.4)$$

$$c_a = 666 + \left(\frac{13002}{738-\theta_a}\right) \quad [\text{J/kgK}] \quad \text{for } 600^\circ\text{C} < \theta_a \leq 735^\circ\text{C} \quad (5.5)$$

$$c_a = 545 + \left(\frac{17820}{\theta_a-731}\right) \quad [\text{J/kgK}] \quad \text{for } 735^\circ\text{C} < \theta_a \leq 900^\circ\text{C} \quad (5.6)$$

$$c_a = 650 \quad [\text{J/kgK}] \quad \text{for } 900^\circ\text{C} < \theta_a \leq 1200^\circ\text{C} \quad (5.7)$$

The graph of specific heat is shown in Figure 5.2. The spike in the middle is due to a phase change in the steelwork, mentioned above, whereby additional energy is absorbed without an increase in the temperature of the steelwork.

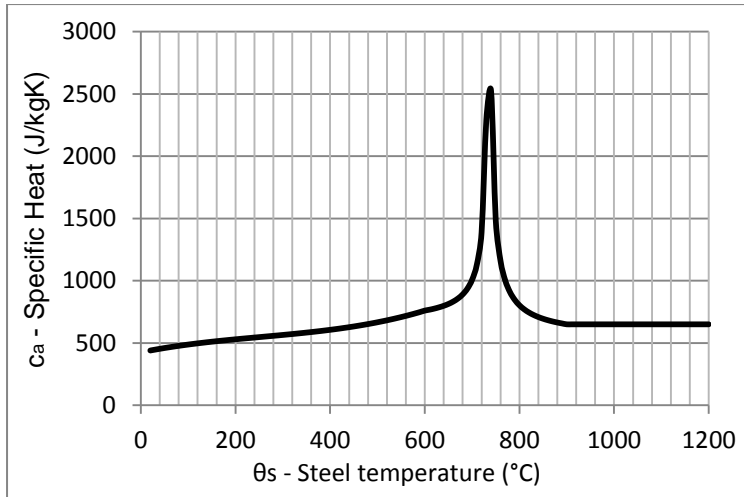


**Figure 5.2: Specific heat of steel as a function of temperature**

### 5.2.3 Thermal conductivity

The thermal conductivity of steelwork,  $\lambda_a$ , influences the rate at which steelwork heats up during a fire and also transfers heat to cooler parts of the structure. It is given by:

$$\lambda_a = 54 - 3.33 \times 10^{-2} \theta_a \text{ [W/mK]} \quad \text{for } 20^\circ\text{C} < \theta_a \leq 800^\circ\text{C} \quad (5.8)$$

$$\lambda_a = 27.3 \text{ [W/mK]} \quad \text{for } 800^\circ\text{C} < \theta_a \leq 1200^\circ\text{C} \quad (5.9)$$

The graph of thermal conductivity against temperature is shown below. After the phase change the thermal conductivity remains constant.

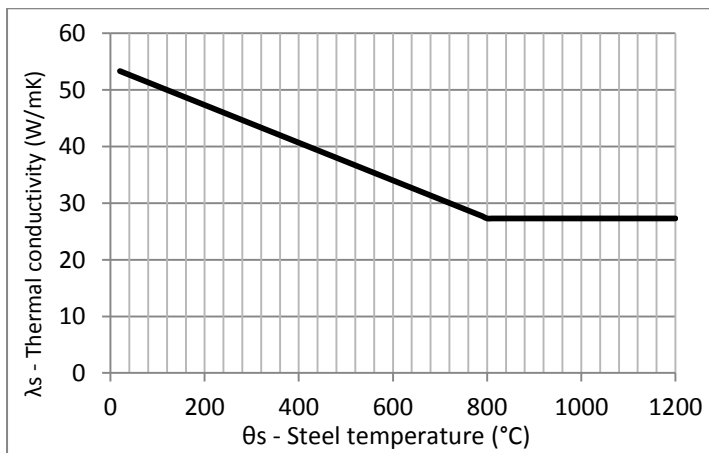


**Figure 5.3: Thermal conductivity as a function of temperature**

### 5.2.4 Structural properties

The Eurocodes use the concept of a reduction factor,  $k$ , by which the original material strength or stiffness is multiplied to reduce a specific steel property at elevated temperature. The reduction factors given below, and shown in Figure 5.4, for steelwork at temperature  $\theta_a$  are:

$k_{u,\theta}$  Reduction factor of ultimate steel strength relative to yield strength.

$k_{y,\theta}$  Reduction factor for the steel yield strength.

$k_{E,\theta}$  Reduction factor for the Young's modulus.

$k_{p,\theta}$  Reduction factor for the determination of the proportional limit from yield stress, i.e. when stress-strain curves become non-linear.

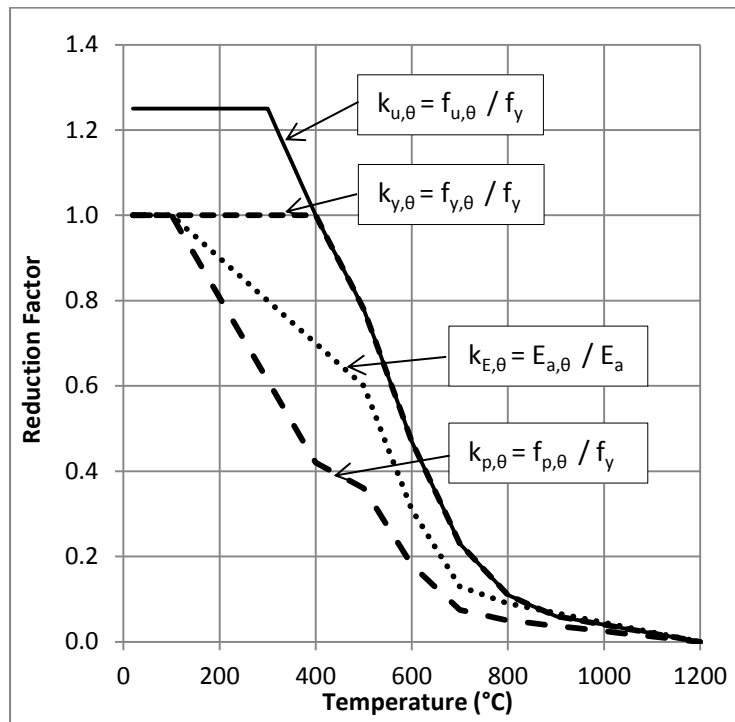


**Figure 5.4: Reduction factors for various steel properties at elevated temperatures**

The stress-strain curve, which relies upon the above-mentioned reduction factors, is as shown in Figure 5.5. The behaviour of steel with increasing strain is as follows: (a) initially the material behaves elastically up to the proportional strain limit,  $\epsilon_{p,\theta}$ . (2) This is followed by a transition phase until the yield stress and strain,  $\epsilon_{y,\theta}$ , are reached. (3) A yield plateau is then followed, until (4) the limiting strain for yield strength,  $\epsilon_{t,\theta}$ , is reached. (5) Thereafter a linear descending branch is followed until the ultimate strain,  $\epsilon_{u,\theta}$ . Annex A of EN 3-1-2 permits steelwork under 350°C to achieve an increased ultimate stress, allowing for strain-hardening, and this has been implemented in this work. Strain-hardening can be included provided that “local instability is prevented” (ECCS 2001) which is true for the case studies considered. In a design scenario it would be conservative to neglect strain-hardening.

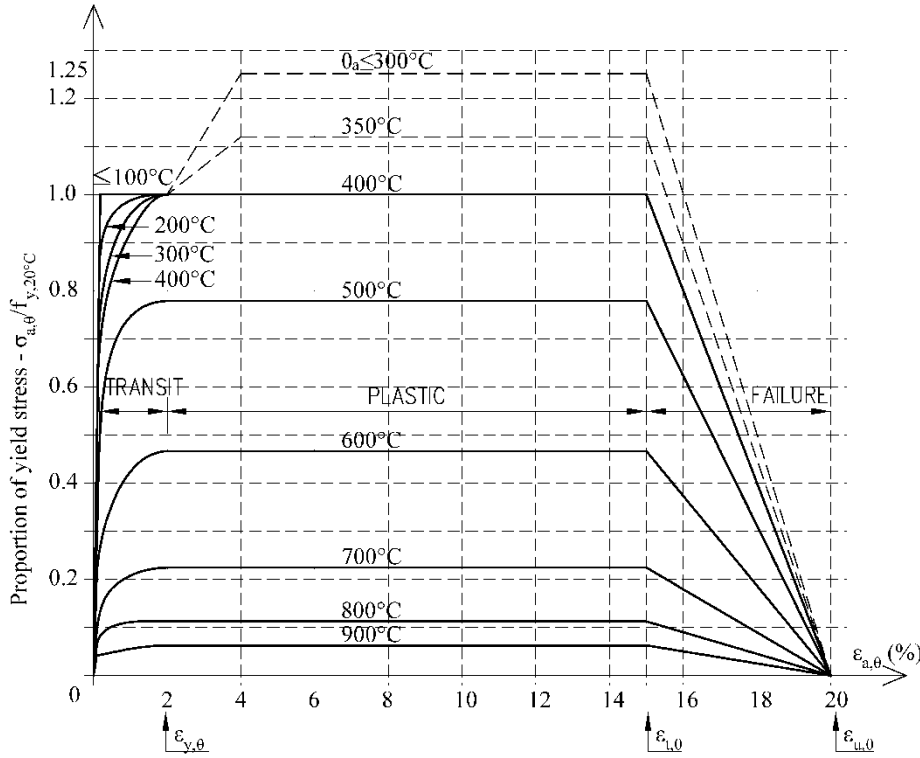


**Figure 5.5: Stress-strain curve for steelwork at elevated temperature including strain-hardening (ECCS 2001)**

The stress for each zone of Figure 5.5 is determined as follows:

$$\sigma = \varepsilon E_{s,\theta} \quad \text{for } \varepsilon \leq \varepsilon_{p,\theta} \quad (5.10)$$

$$\sigma = f_{p,\theta} - c + \left(\frac{b}{a}\right) \left[ a^2 - (\varepsilon_{y,\theta} - \varepsilon)^2 \right]^{0.5} \quad \text{for } \varepsilon_{p,\theta} < \varepsilon \leq \varepsilon_{y,\theta} \quad (5.11)$$

$$\sigma = f_{y,\theta} \quad \text{for } \varepsilon_{y,\theta} < \varepsilon \leq \varepsilon_{t,\theta} \quad (5.12)$$

$$\sigma = f_{y,\theta} \left[ 1 - (\varepsilon - \varepsilon_{t,\theta}) / (\varepsilon_{u,\theta} - \varepsilon) \right] \quad \text{for } \varepsilon_{t,\theta} < \varepsilon \leq \varepsilon_{u,\theta} \quad (5.13)$$

$$\sigma = 0.0 \quad \text{for } \varepsilon > \varepsilon_{u,\theta} \quad (5.14)$$

The parameters required to define the above are:  $\varepsilon_{p,\theta} = f_{p,\theta} / E_{a,\theta}$ ,  $\varepsilon_{y,\theta} = 0.02$ ,  $\varepsilon_{t,\theta} = 0.15$ , and  $\varepsilon_{u,\theta} = 0.20$ , and:

$$a^2 = (\varepsilon_{y,\theta} - \varepsilon_{p,\theta})(\varepsilon_{y,\theta} - \varepsilon_{p,\theta} + c / E_{a,\theta}) \quad (5.15)$$

$$b^2 = c(\varepsilon_{y,\theta} - \varepsilon_{p,\theta})E_{a,\theta} + c^2 \quad (5.16)$$

$$c = \frac{(f_{y,\theta} - f_{p,\theta})^2}{(\varepsilon_{y,\theta} - \varepsilon_{p,\theta})E_{a,\theta} - 2(f_{y,\theta} - f_{p,\theta})} \quad (5.17)$$

An understanding of the stress-strain behaviour is important for understanding the parametric studies conducted in Chapter 7. Once the proportional limit is reached materials no longer behave elastically and material stiffness decreases.

In the FBE formulation temperatures are modelled as RTSL/M forces, as explained in Chapter 3. If steel is unrestrained against elongation when heated the equivalent thermal stress (ETS) that would need to be applied to it to produce the correct strain can be calculated as:

$$\sigma_{\theta} = \varepsilon_{\theta a} E_{\theta} = \varepsilon_{\theta a} \times k_{E,\theta} E_{20^{\circ}C} \quad (5.18)$$

The change in equivalent thermal stress (ETS) with increasing temperature is shown in Figure 5.6. The peak is reached at 500°C after which point the decrease in steel stiffness exceeds the rate of steel elongation. This behaviour results in a non-linear change in overall RTSMs and axial forces as structures are subjected to increasing elevated temperatures. It is important that such behaviour be understood when considering the trends shown in Chapter 7, where localised peaks are attained on graphs when steelwork reaches around 500°C.

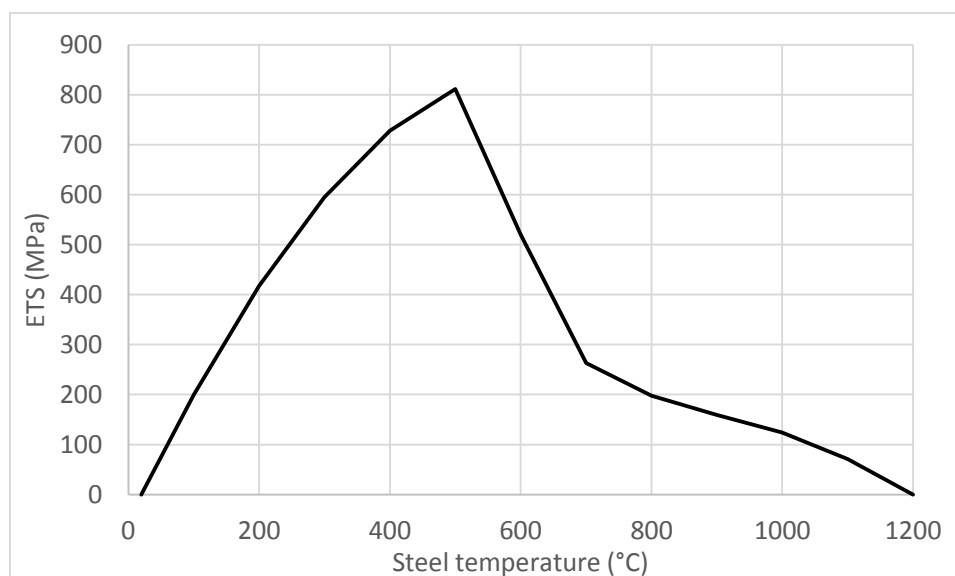


**Figure 5.6: Equivalent thermal stress to cause thermal elongation in unrestrained steelwork**

### 5.2.5 Temperatures used in analysis models

In the modelling of structural steelwork in fire the temperature of beam components is pivotal for the accurate determination of material properties and thermal behaviour. However, in an experimental fire test there will be variations in temperature both along the length of a beam, and across the height of the web or flange (Wainman & Kirby 1988; Mensinger et al. 2012). Assuming a constant web temperature is an approximation, since at the bottom of a web the temperature will be closer to that of the bottom flange, and the same will occur for the top flange. Franssen & Vila Real (2010) illustrate in Figure 5.7 that near to column supports the temperature of beams is lower, primarily due to the increased material mass and shielding that occurs in such zones. In experiments of isolated structural elements such variation in the temperature along the length of a member is typically not observed or recorded, due to either too few experimental readings being taken or due to columns and connections not being included in tests. Hence, the assumption of temperature being constant along the length of a beam section is adopted in this research based on the experimental data available.

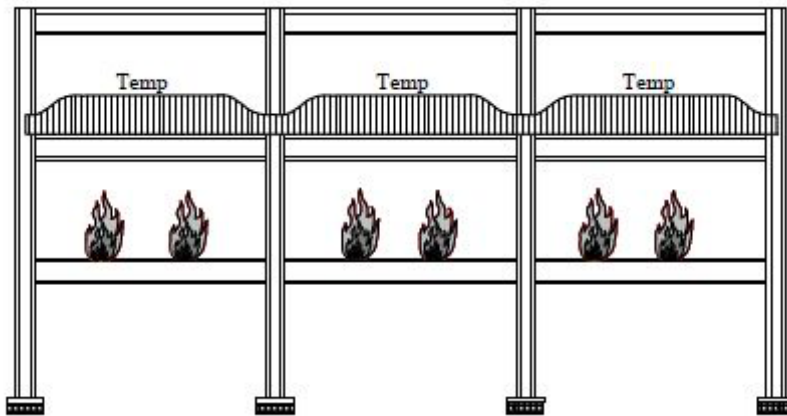


**Figure 5.7: Non-uniform variation in steel temperature over the length of beams in structures (Franssen & Vila Real 2010)**

### 5.2.6 Reinforcing steel in fire

Reinforcing steel for concrete behaves in an almost identical manner to the behaviour described above for structural steel. In this work the guidelines of EN 2-1-2 (BSI 2005a) have been adopted for reinforcing steel. However, strain hardening has been neglected following the provisions in EN 2-1-2.

## 5.3 Concrete in fire

The development of a model used to describe the behaviour of concrete is significantly more complicated than that for steel. Various experimentally verified temperature-stress-strain relationships for concrete have been developed and could be used (BSI 2005a; fib 2010b; Mensinger et al. 2012). Each model may have slightly different experimental data sets from which they are formulated, or may be based on different assumptions. Hence, it is not surprising that there are variations in the prediction model results from the literature discussed below. This section will first address modelling approaches for concrete presented in the literature, followed by possible input values of concrete properties for models and then temperature-stress-strain curves. Composite slabs often have ribbed profiles so a method for converting ribbed slabs into equivalent rectangular sections is also provided.

### 5.3.1 Concrete models in structural fire engineering literature

Researchers in structural fire engineering have taken different approaches when considering concrete. The developers of Vulcan (Burgess et al. 2015; Huang et al. 2003; Najjar & Burgess 1996) address the stiffness of concrete with varying profiles (such as ribbed decks) using layered shell elements with averaged effective thicknesses. The concept of an average effective thickness is also adopted in this work. The properties of concrete are taken as linearly inelastic before crushing or cracking occurs, and tension in concrete is ignored.

Tesar (2008) has included the non-linear Eurocode stress-strain curves in his SlabFem modelling software, also using layered shell elements for concrete slabs. Other specialised FE software available for fire design is SAFIR (Franssen 2005) and ADAPTIC developed at Imperial College (Izzuddin 2012). These include various



techniques for modelling concrete (e.g. trilinear concrete curves, constant confinement models, variable confinement models). Sanad et al (2000) developed moment-curvature relationships for composite beams in fire using Abaqus. Stress-strain curves for concrete were used as defined in EN 2-1-2. For zones in tension only the tensile capacity of reinforcing mesh was considered, not that of the concrete. Authors such as Liao & Huang (2015) incorporate concrete behaviour into their 3D finite element system using a bi-axial relationship that provides a stress envelope to predict when crushing or cracking failure of elements occurs. Cracking is explicitly incorporated in the volume elements developed by these authors. It appears that tension stiffening behaviour should be captured by the modelling philosophy employed, although this not clearly stated. Such a model would require extensive operator time and input to set up.

Advanced modelling tools such as SAFIR, SlabFem, Abaqus and others are excellent research tools which can consider generic shapes and structural forms. However, for all these packages the need to carry out two separate simulations (thermal and mechanical) increases computational and modelling costs significantly, whilst requiring extensive input data. In the majority of building design scenarios such a high level of complexity is not required or feasible, and the use of standard temperature profiles is often preferable, as discussed in Section 5.3.4.

### 5.3.2 *Structural properties of concrete*

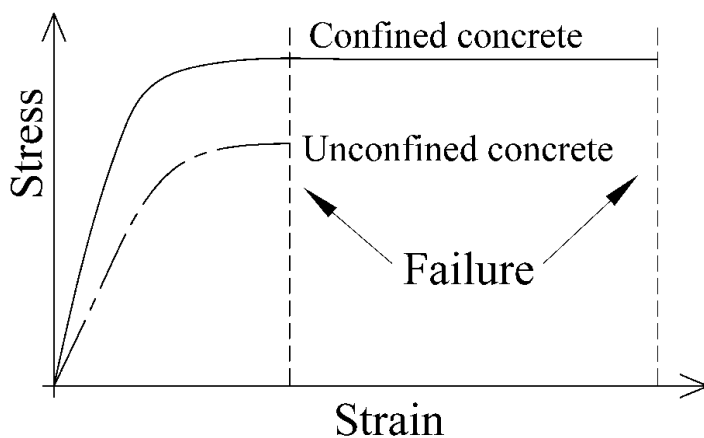
In most experimental fire test literature concrete characteristic strengths are provided, e.g. C25/30. Often researchers then use these characteristic values for analysis models, which contradicts the aim of making best estimate predictions (Section 5.1) for which average values are appropriate. If cube or cylinder tests have not been done to verify concrete strengths, and typical concrete mixes have been used, then the average strength will typically be higher than the characteristic strength in the order of 8MPa (BSI 2004). In this research average material properties will be used throughout.

Table 5.1 presents concrete properties for various concrete grades according to EN 2-1-1 (BSI 2004). The table contains details regarding: characteristic cylinder  $f_{ck}$  and cube  $f_{ck,cube}$  strengths, average cylinder strengths  $f_{cm}$ , average tensile strengths  $f_{ctm}$ , and average Young's moduli  $E_{cm}$ . This table is used for predicting average strengths and stiffnesses in the case studies in Chapter 6. Empirical equations are also provided in EN 2-1-1 for calculating material properties relative to characteristic strengths.

GRADE	$f_{ck}$ (MPa)	$f_{ck,cube}$ (MPa)	$f_{cm}$ (MPa)	$f_{ctm}$ (MPa)	$E_{cm}$ (GPa)
C12/15	12	15	20	1.6	27
C16/20	16	20	24	1.9	29
C20/25	20	25	28	2.2	30
C25/30	25	30	33	2.6	31
C30/37	30	37	38	2.9	33
C35/45	35	45	43	3.2	34
C40/50	40	50	48	3.5	35
C45/55	45	55	53	3.8	36
C50/60	50	60	58	4.1	37
C55/67	55	67	63	4.2	38
C60/75	60	75	68	4.4	39
C70/85	70	85	78	4.6	41
C80/95	80	95	88	4.8	42
C90/105	90	105	98	5.0	44

**Table 5.1: Concrete properties according to EN 2-1-1 (BSI 2004)**

In the literature the concrete strength taken for the crushing of concrete in models is normally based upon the cylinder strength. A further variable to be considered is the fact that concrete which is part of a larger element will have rebar positioned perpendicular to the direction of the load (as is the case with most beams and slabs), additional concrete surrounding it and possibly perpendicular stresses. Thus, such concrete will experience a level of concrete confinement. EN 2-1-1 allows for increased material ductility due to confinement, as illustrated in Figure 5.8. From this it can be seen that confined concrete can resist higher strains and stresses before load carrying capacity is lost, depending on the extent of confinement that occurs. However, parameters for calculating the level of confinement cannot easily be quantified, which leads to confinement being conservatively excluded in general research and this work. In the case studies of Chapter 6 the influence of confinement may be one of various reasons for the discrepancies between theoretical and experimental results.

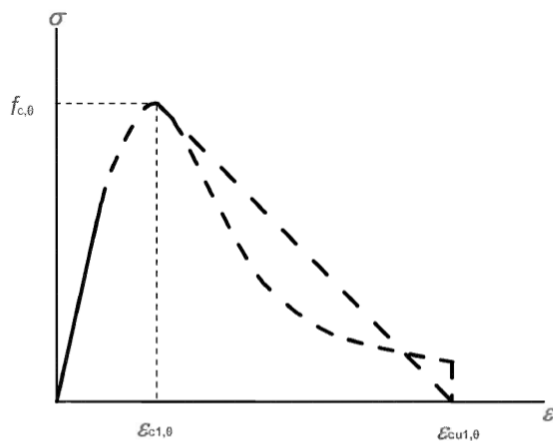


**Figure 5.8: Stress-strain curves according to EN 2-1-1 (BSI 2004) accounting to the confinement of concrete, comparing confined and unconfined concrete samples**

The Young's modulus of concrete plays an important role in the determination of beam deflections. It must be understood that this property varies substantially depending on various factors. The type of aggregate used in any mix design is a dominant factor with regards to determining stiffness. Alexander (1985) conducted extensive testing on concretes in South Africa and showed that for a 30MPa characteristic cube strength concrete the elastic modulus can vary between 16 GPa for lightweight aggregates to 36 GPa for high stiffness aggregates. The average elastic moduli values provided in EN 2-1-1 are higher than the average values recommended by Alexander. This is presumably due to the different aggregates commonly used in each geographical area.

### Concrete in compression

The behaviour of concrete in compression in fire is defined in EN 2-1-2 (BSI 2005a) as shown in Figure 5.9. The parameters  $f_{c,\theta}/f_{ck}$ ,  $\epsilon_{c1,\theta}$  and  $\epsilon_{cu1,\theta}$  are provided in Table 5.2. It should be noted that when the stress-strain curves of EN 2-1-1 (BSI 2004) for ambient temperature concrete are compared with the guidelines of EN 2-1-2 (normally used for elevated temperatures but does include an ambient temperature curve) at 20°C there is a significant difference in calculated properties. Figure 5.10 shows the stress-strain and  $E_{secant}$ -strain curves for concrete at ambient temperature with  $f_{cm} = 30\text{MPa}$  for both EN 2-1-1 and EN 2-1-2. At initial low levels of strain there is a 78% difference in the secant moduli. One of the main contributing factors to this may be that the material model from EN 2-1-2 implicitly considers transient creep in its formulation (Gernay & Franssen 2012). This difference in properties leads to the higher estimated strains and lower secant moduli at elevated temperature when EN 2-1-2 is used.



Range	Stress $\sigma(\theta)$
$\epsilon \leq \epsilon_{c1,\theta}$	$\frac{3\epsilon f_{c,\theta}}{\epsilon_{c1,\theta} \left( 2 + \left( \frac{\epsilon}{\epsilon_{c1,\theta}} \right)^3 \right)}$
$\epsilon_{c1(\theta)} < \epsilon \leq \epsilon_{cu1,\theta}$	For numerical purposes a descending branch should be adopted. Linear or non-linear models are permitted.

Figure 5.9: Stress-strain model of concrete at elevated temperatures according to EN 2-1-2 (BSI 2005a)

Temp., $\theta$ (°C)	$f_{c,\theta}/f_{ck}$ (-)	$\epsilon_{c1,\theta}$ (-)	$\epsilon_{cu1,\theta}$ (-)
20	1.00	0.0025	0.0200
100	1.00	0.0040	0.0225
200	0.95	0.0055	0.0250
300	0.85	0.0070	0.0275
400	0.75	0.0100	0.0300
500	0.60	0.0150	0.0325
600	0.45	0.0250	0.0350
700	0.30	0.0250	0.0375
800	0.15	0.0250	0.0400
900	0.08	0.0250	0.0425
1000	0.04	0.0250	0.0450
1100	0.01	0.0250	0.0475
1200	0.00	-	-

**Table 5.2: Parameters for stress-strain profiles for siliceous concrete in fire according to EN 2-1-2 (BSI 2005c)**

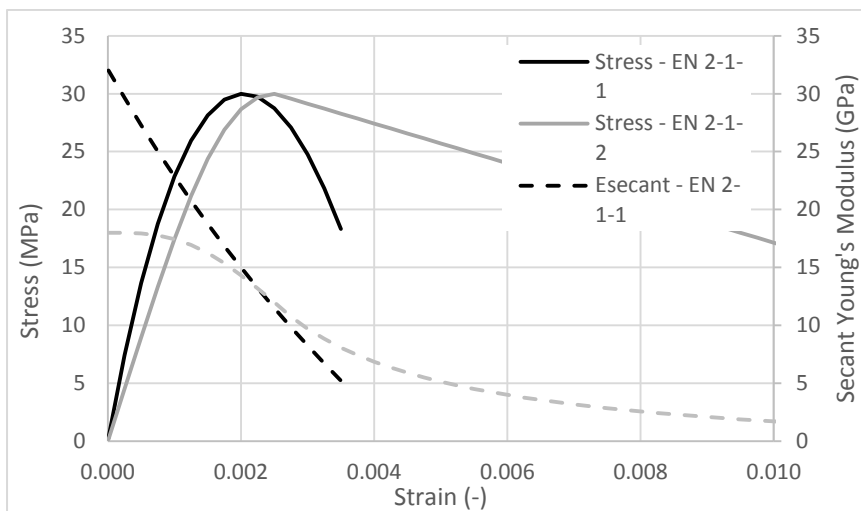


**Figure 5.10: Comparison of stress-strain and  $E_{\text{secant}}$ -strain for EN 2-1-1 and EN 2-1-2 for  $f_{cm} = 30\text{MPa}$  at ambient temperature**

A challenge presented by the difference in the Eurocode material models is that in the analysis of many concrete slabs the upper sections could be at ambient temperature, thus still suitable for EN 2-1-1. The upper zones at lower temperature often carry the highest concrete stresses and contribute significantly to the total stiffness of a beam. If the ambient temperature concrete in a slab were to behave as described by EN 2-1-1 it could theoretically result in a decrease in deflection of up to 30-50% in comparison to EN 2-1-2, especially for lower mechanical strain levels in the concrete. However, since transient strains do occur in fire scenarios the EN 2-1-2 guidelines have been adopted for all concrete elements.

### **Concrete in tension**

EN 2-1-2 provides a method for calculating the strength of concrete in tension using the following reduction factors for tensile capacities:

$$k_{c,t}(\theta) = 1.0, \quad \text{for } 20^\circ\text{C} \leq \theta_c \leq 100^\circ\text{C} \quad (5.19)$$

$$k_{c,t}(\theta) = 1.0 - \frac{\theta - 100}{500}, \quad \text{for } 100^\circ\text{C} < \theta_c \leq 600^\circ\text{C} \quad (5.20)$$

These equations provide a linear reduction in strength between 100°C and 600°C. In the case studies investigated the fire exposed sides of concrete slabs may easily exceed 600°C and such areas will lose all strength in tension. Tian (2014) implemented the above in a model for considering irregularly shaped slab panels in fire, where it appears to have functioned well.

### 5.3.3 Thermal properties of concrete

The thermal properties of concrete have a significant influence on the temperature of elements during a fire. The details below are based upon EN 2-1-2 (BSI 2005a). Details are provided for both siliceous and calcareous aggregates. In South Africa calcareous aggregates (e.g. limestone) are used less commonly in structural applications than siliceous aggregates (e.g. quartzite, granite), although this varies geographically (C&CI 2001). Furthermore, it is more conservative to assume siliceous behaviour concretes since such aggregates perform more poorly in fire (BSI 2005a). Hence, in this research siliceous aggregate has been assumed throughout as the experiments used for verification often failed to report on the type of aggregate used.

#### **Thermal elongation**

The thermal elongation, or thermal strain  $\varepsilon_c(\theta)$ , is the measure of strain that will occur when concrete is heated. It is determined by the equations below and illustrated in Figure 5.11.

$$\varepsilon_{\theta_c} = -1.8 \times 10^{-4} + 9 \times 10^{-6}\theta + 2.3 \times 10^{-11}\theta^3 \quad \text{for } 20^\circ\text{C} \leq \theta_c \leq 700^\circ\text{C} \quad (5.21)$$

$$\varepsilon_{\theta_c} = 14 \times 10^{-3} \quad \text{for } 700^\circ\text{C} < \theta_c \leq 1200^\circ\text{C} \quad (5.22)$$

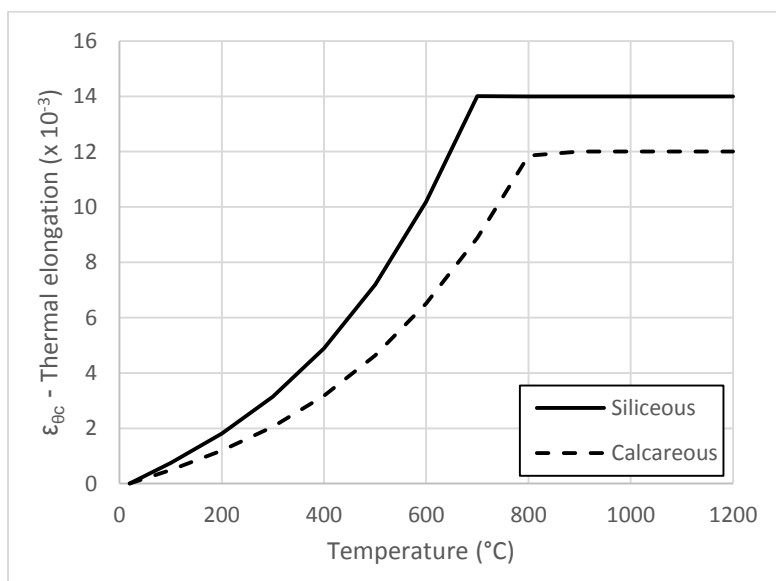


**Figure 5.11: Thermal elongation of siliceous and calcareous concrete to EN 2-1-2 (BSI 2005a)**

### Specific heat

The specific heat of concrete with a moisture content ranging from  $u = 0\%$  (dry) to 3% is given below (BSI 2005a). In the case studies investigated in Chapter 6 experimental tests were typically carried out at around 28 days after casting at which time moisture contents would still have been relatively high. Hence, a moisture content of 3% has been assumed for the heat transfer models in Section 5.3.4. At temperatures between 100°C and 115°C the specific heat increases as the water boils off.

$$c_p(\theta) = 900 \text{ (J/kgK)} \quad \text{for } 20^\circ\text{C} \leq \theta_c \leq 100^\circ\text{C} \quad (5.23)$$

$$c_p(\theta) = 900 + (\theta - 100) \text{ (J/kgK)} \quad \text{for } 100^\circ\text{C} < \theta_c \leq 200^\circ\text{C} \quad (5.24)$$

$$c_p(\theta) = 1000 + (\theta - 200)/2 \text{ (J/kgK)} \quad \text{for } 200^\circ\text{C} < \theta_c \leq 400^\circ\text{C} \quad (5.25)$$

$$c_p(\theta) = 1100 \text{ (J/kgK)} \quad \text{for } 400^\circ\text{C} < \theta_c \leq 1200^\circ\text{C} \quad (5.26)$$

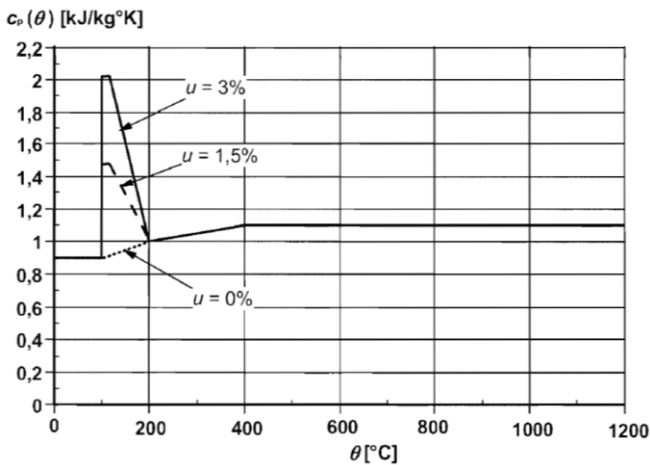


Figure 5.12: Specific heat of concrete as a function of temperature according to EN 2-1-2 (BSI 2005a), with moisture contents,  $u$ , of 0%, 1.5% and 3%

### Density

Concrete density,  $\rho$ , changes with increasing temperature due to water loss. Density affects the amount of energy that needs to be absorbed for each 1°C temperature change, and hence has been included in the thermal model developed in Section 5.3.4. It is calculated as:

$$\rho(\theta) = \rho(20^\circ\text{C}) \quad \text{for } 20^\circ\text{C} \leq \theta_c \leq 115^\circ\text{C} \quad (5.27)$$

$$\rho(\theta) = \rho(20^\circ\text{C}) \cdot (1 - 0.02(\theta - 115)/85) \quad \text{for } 115^\circ\text{C} < \theta_c \leq 200^\circ\text{C} \quad (5.28)$$

$$\rho(\theta) = \rho(20^\circ\text{C}) \cdot (0.98 - 0.03(\theta - 200)/200) \quad \text{for } 200^\circ\text{C} < \theta_c \leq 400^\circ\text{C} \quad (5.29)$$

$$\rho(\theta) = \rho(20^\circ\text{C}) \cdot (0.95 - 0.07(\theta - 400)/800) \quad \text{for } 400^\circ\text{C} < \theta_c \leq 1200^\circ\text{C} \quad (5.30)$$

### **Thermal conductivity**

According to EN 2-1-2 the thermal conductivity of concrete varies between an upper and lower limit depending on a variety of factors, and is calculated using Eq. 5.31 for the upper limit and 5.32 for the lower limit. The change with temperature is shown in Figure 5.13. The thermal conductivity influences how fast heat is transferred through a slab. The lower limit has been used for calculating temperatures in slabs in this work, as it provided temperature results more consistent with existing EN temperature profiles. Additional details are discussed in Appendix A.

$$\lambda_c = 2 - 0.2451(\theta/100) + 0.0107(\theta/100)^2 \text{ (W/mK)} \quad \text{for } 20^\circ\text{C} \leq \theta_c \leq 1200^\circ\text{C} \quad (5.31)$$

$$\lambda_c = 1.36 - 0.136(\theta/100) + 0.0057(\theta/100)^2 \text{ (W/mK)} \quad \text{for } 20^\circ\text{C} \leq \theta_c \leq 1200^\circ\text{C} \quad (5.32)$$

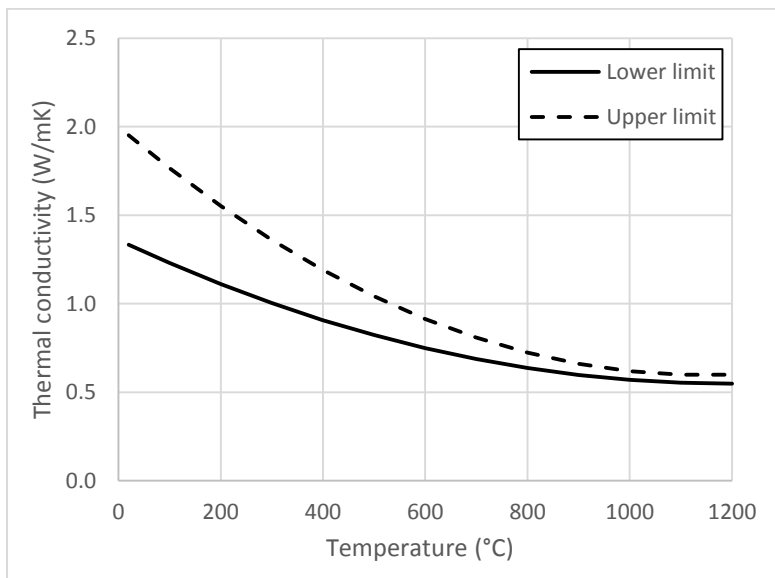


**Figure 5.13: Upper and lower limits of thermal conductivity according to EN 2-1-2 (BSI 2005a)**

#### *5.3.4 Temperature profiles in concrete slabs*

For most experiments in the literature, and almost all real world design scenarios, the temperature profile across the depth of concrete elements is not available. Such temperatures significantly influence mechanical properties and resulting thermal forces. Hence, it is necessary to use one of the various models that are available for predicting the temperature of concrete. The following are potential options:

- EN 2-1-2 temperature profiles, which are based on tests on a 200mm thick slab
- EN 4-1-2 temperature profiles, which are based on tests on a 100mm thick slab
- Empirical equations provided by Wickström (1986)
- Finite element models using heat transfer equations

- Various additional models in the literature. For a comparison of a variety of models see the work by Gao et al (2014).

The influence of different temperature profiles is investigated in the parametric studies in Chapter 7. A one-dimensional, finite element analysis (FEA) model of concrete in a standard fire has been developed in this work to generate temperature profiles for different fire exposure times and slab thicknesses. This has been necessary for the case studies investigated in Chapter 6 because the case studies typically involve results at less than 30 minutes, and are for slab thicknesses different to those which the EN codes provide guidance for. At times less than 30 minutes the EN 2-1-2 or 4-1-2 temperature profiles cannot be confidently extrapolated to suit, necessitating the development of such a heat transfer model. Stadler (2012) conducted a finite element heat transfer analysis using the data from the First Munich Test (see Section 6.6) to verify a numerical model developed in ANSYS (2016). It was concluded that by using the parameters from the Eurocode the experimental results could be correctly simulated, showing that the thermal and mechanical properties provided in the Eurocodes are reasonable for such work.

For a more detailed explanation on the heat transfer equations and material properties selected for the FEA model, based on the EN 2-1-2 data above, refer to Appendix A. By adjusting the various input variables within allowable ranges different results could be obtained, relative to those shown below. Moisture content, thermal conductivity, initial density, radiation in and out of the slab, fire and surface emissivity and configuration factors are all parameters that can be varied. The most difficult parameters to define are those relating directly to the fire and heat transfer to the surface of the concrete, namely radiation, emissivity and configuration factors.

A comparison of the temperature profile methods listed above is presented in Figure 5.14, with the fourth graph (FEA) being the prediction model developed in this work. Temperatures in a 100mm slab are provided after a standard fire exposure time of 30, 60 and 120 minutes. From this graph it can be seen that there is typically fair agreement between the model trends. It should be noted that for a 30 and 60 minute fire the difference above 60mm can be large for all the models, and this is where the majority of the load carrying concrete in a composite slab normally occurs. Significantly higher thermal forces would be calculated using EN 2-1-2 in comparison to Wickström, especially at 80-100mm. After 60 minutes at 100mm into the slab EN 2-1-2 predicts a temperature of 100°C compared to 20°C for Wickström's method, thus giving an 80°C and 0°C increase respectively. Thus, there would be substantially different forces calculated in certain instances depending on the temperature model selected.



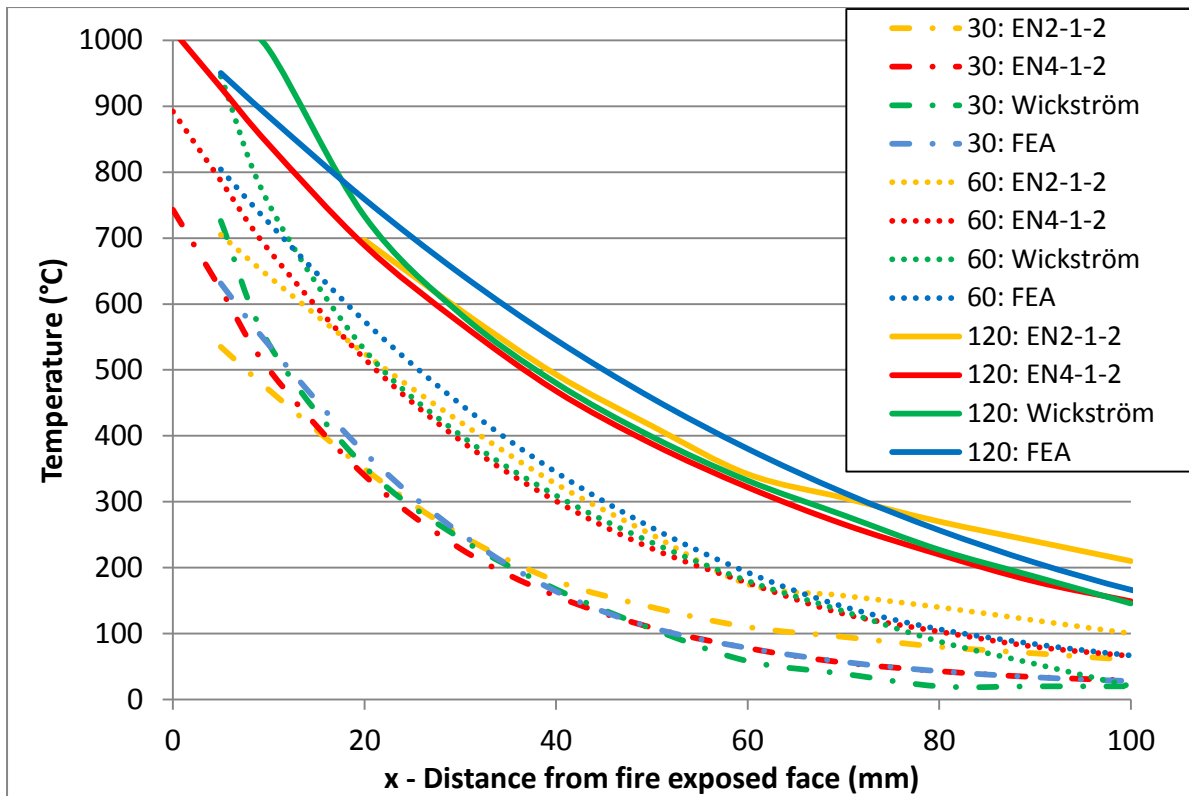


**Figure 5.14: Comparison of temperature profiles in a 100mm concrete slab after a 30, 60 and 120 minute fire according to (a) EN 2-1-2, (b) EN 4-1-2, (c) Wickström, and (d) a FEA model developed in this research.**

The different temperature profile curves may have been influenced by the thickness of slab tested, the aggregates used, amount of rebar, experimental setup and other such factors. Hence, it cannot be said that one model is necessarily superior to another, especially since input variables for each structure designed will vary.

### 5.3.5 Consideration of ribbed slabs

As discussed in Section 5.3.1, ribbed slabs have been considered by researchers in different ways. Ribs can be considered by: (a) explicitly modelling them (e.g. SAFIR), (b) adding ribs as beam elements linked to slab shell elements (Jiang et al. 2014), (c) converting ribbed slabs into equivalent rectangular slabs according to EN 4-1-2 (Stadler 2012), and various other methods using finite element formulations. Option (c) is adopted in this work where ribbed slabs are converted into flat slabs of an equivalent thickness, and as shown in Figure 5.15. Irrespective of the modelling technique adopted it must be noted that irregular temperature profiles occur in ribbed slabs, as shown in Figure 5.16 in the following section. This is a challenge for any model to consider and results are highly dependent upon the heat transfer scenarios selected.

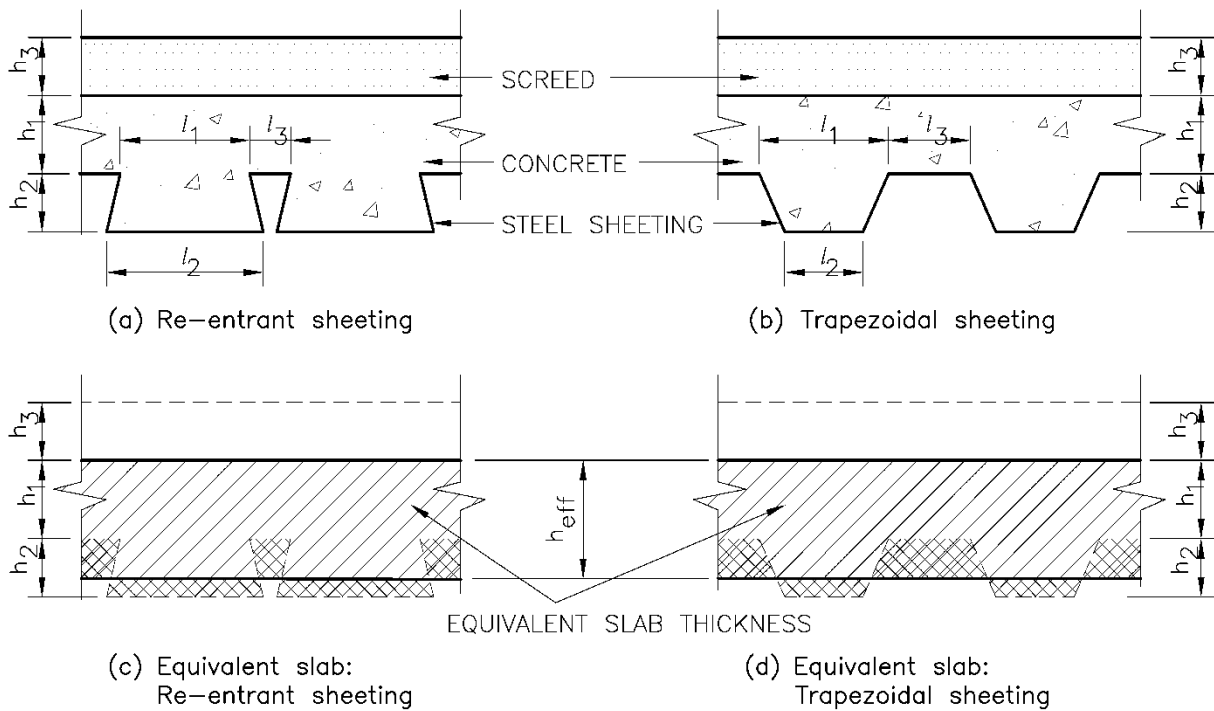


**Figure 5.15: Sheeting profiles for ribbed composite slabs and their equivalent thicknesses**

Annex D of EN 4-1-2 (BSI 2005c) provides a method for converting a ribbed slab into an equivalent rectangular slab according to the following equations and as illustrated in Figure 5.15.

$$h_{eff} = h_1 + 0.5h_2 \left( \frac{l_1 + l_2}{l_1 + l_3} \right) \quad \text{for } h_2/h_1 \leq 1.5 \text{ and } h_1 > 40 \text{ mm} \quad (5.33)$$

$$h_{eff} = h_1 \left[ 1 + 0.75h_2 \left( \frac{l_1 + l_2}{l_1 + l_3} \right) \right] \quad \text{for } \frac{h_2}{h_1} > 1.5 \text{ and } h_1 > 40 \text{ mm} \quad (5.34)$$

### ***Implications of using a transformed slab***

The above methodology has both advantages and disadvantages that researchers should be aware of. On the positive side the conversion can be done easily and subsequently allows the use of well-established temperature profiles and design procedures for rectangular slabs. The conversion equations are fairly intuitive to understand in that they simply keep the total area constant by redistributing material. Furthermore, in a severe fire the outer sections of slabs typically lose all their strength and are ineffective in any case, resulting in a final load carrying area closer to that of a rectangular slab than the original profile, although this varies. The upper sections which carry the majority of the load typically remain intact in both instances.

The negative aspects to be considered are factors such as the assumption of constant temperature and mechanical properties at each level, which is only an approximation. Ribbed slabs have significantly different stiffnesses in the span and transverse directions, and models must take cognisance of this. Irregular temperature profiles cannot be easily considered. These factors could be addressed as discussed below.

### Alternative methodology for ribbed profiles

Figure 5.16 illustrates (a) the typical temperature profile observed in a ribbed slab, (b) the simplified, equivalent flat slab considered in this research, and (c) an alternative formulation that could be introduced in the FBE model to address the negative factors identified above. In the latter formulation a two-dimensional integration scheme would be able to account for non-uniform heating profiles, although this would require significant amounts of input data and the improvement in overall accuracy of results would be based upon the accuracy of the temperature profile. An independent thermal analysis will have to be performed in most cases, making the modelling process more complex. Overall, the benefit of the simplified modelling techniques of the FBE formulation may be lost by including such considerations, and more advanced models may then become suitable when explicitly considering such behaviour.

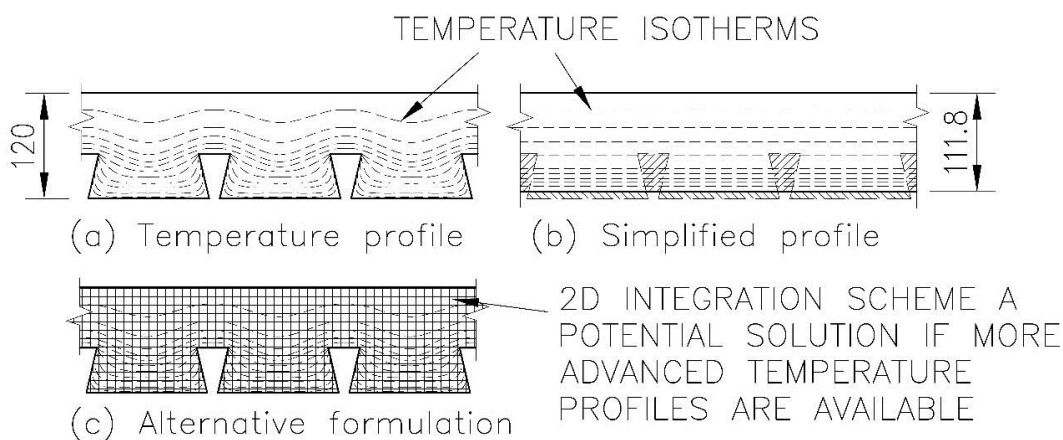


**Figure 5.16: Temperature profiles in a profiled slab, illustrating (a) the actual profiles, (b) the simplified profile adopted in this research and by Stadler (2012), and (c) an alternative formulation that could be used in this research for 2D temperature profiles**

A two-dimensional integration scheme would permit the calculation of minor-axis bending stiffness and torsional stiffness, essential for three-dimensional analyses. To maintain both the benefits of the simplified FBE modelling procedure and allow for the extension of the formulation to suit three-dimensional analyses it would be possible to combine the simple temperature profiles with the two-dimensional integration scheme. Thermal forces and member properties can be calculated in the same manner.

In Figure 5.16 the original dimension of 120 mm and effective thickness of 111.8 mm are from Case Study 4 in Chapter 6, and are provided to illustrate the magnitude of change of slab thickness that can occur. In this instance the change is relatively small, but for trapezoidal decks differences are much larger.

#### 5.3.6 Effective width of concrete flanges

At elevated temperatures EN 4-1-2 (BSI 2005c) stipulates that the effective width of concrete,  $b_{eff}$ , acting compositely with a steel beam is to be calculated in accordance with ambient temperature guidelines to EN 4-1-1 (BSI 2011). For simply-supported beams, as investigated in Chapter 6, this can be calculated as:

$$b_{eff} = b_0 + \sum b_{ci} \quad (5.35)$$

$$b_{ci} = \min(\text{Span}/8, b_i) \quad (5.36)$$

where  $b_{ci}$  is the effective width of concrete on each side of the web,  $b_0$  is the transverse shear stud spacing and  $b_i$  is the geometric width. The latter is calculated as the lateral distance between shear connectors and the mid-point between steel beams. SANS 10162-1 (SABS 2011b) recommends that the effective concrete flange width be taken as:

$$b_{eff} = \min(\text{Span}/4; \text{Average transverse beam spacing}) \quad (5.37)$$

These two code guidelines actually calculate the same values except that EN 4-1-1 also includes the shear stud spacing. However, in Case Study 3 no shear stud spacing is provided and in Case Study 4 the studs are in a single line. Hence, the guidelines above are used except that shear stud spacing is neglected.

In the Slab Panel Method (SPM) guidelines Clifton (2006) states that the effective width of a concrete flange in fire conditions should be taken as 60% of that calculated at ambient temperature. This is due to concerns regarding: (a) additional compression being present due to the tensile membrane action, and (b) transverse displacements from slab deformation inducing stresses, whereby both could potentially reduce the strength contribution of a slab. However, it is noted that there “is no clear evidence from the development work undertaken... that the effect is significant, however it is a factor that should be considered in design of slab panel support composite beams” (Clifton 2006). In a design office scenario the author would agree with this assumption of using conservative flange width values. However, when predicting experimental behaviour it becomes difficult to accurately define this parameter. The parametric study conducted in Chapter 7 highlights that due to the combined effect of RTSMs and  $EI_{\theta}$ s increasing proportionally with changing flange widths the overall effect of assuming different widths is significantly less than one might originally expect. Hence, the FBE formulation is not highly sensitive to this parameter, which is beneficial, and the EN 4-1-1 assumptions above are suitable for prediction models.

#### 5.4 Tension stiffening

In conventional finite element models tension stiffening cannot easily be accounted for, meaning that concrete is often modelled as either uncracked (full stiffness) or cracked (zero stiffness). To address this challenge the following section explains how a tension stiffening model has been developed and incorporated. It is based upon the existing *fib* Model Code tension stiffening model (fib 2010b). However, additional research is required to determine whether the same equations apply at elevated temperatures. Tension stiffening can be understood as explained below and illustrated in Figure 5.17:

- a) As reinforced concrete has tension placed upon it the stresses will increase until the tension capacity of the concrete is reached.

- b) When this capacity is reached the first crack will open, transferring all load in the concrete to the reinforcing steel.
- c) The steel then elongates until equilibrium is re-established, or more cracks open.
- d) As strains continue to increase additional cracks open up without additional load being carried.
- e) The concrete will crack until numerous cracks at regular intervals open up. Once the section has cracked to a certain level additional load is then carried by the steel alone.
- f) At this point the concrete between cracks does provide some stiffness to the rebar, giving the overall system a higher stiffness than that of the steel alone.

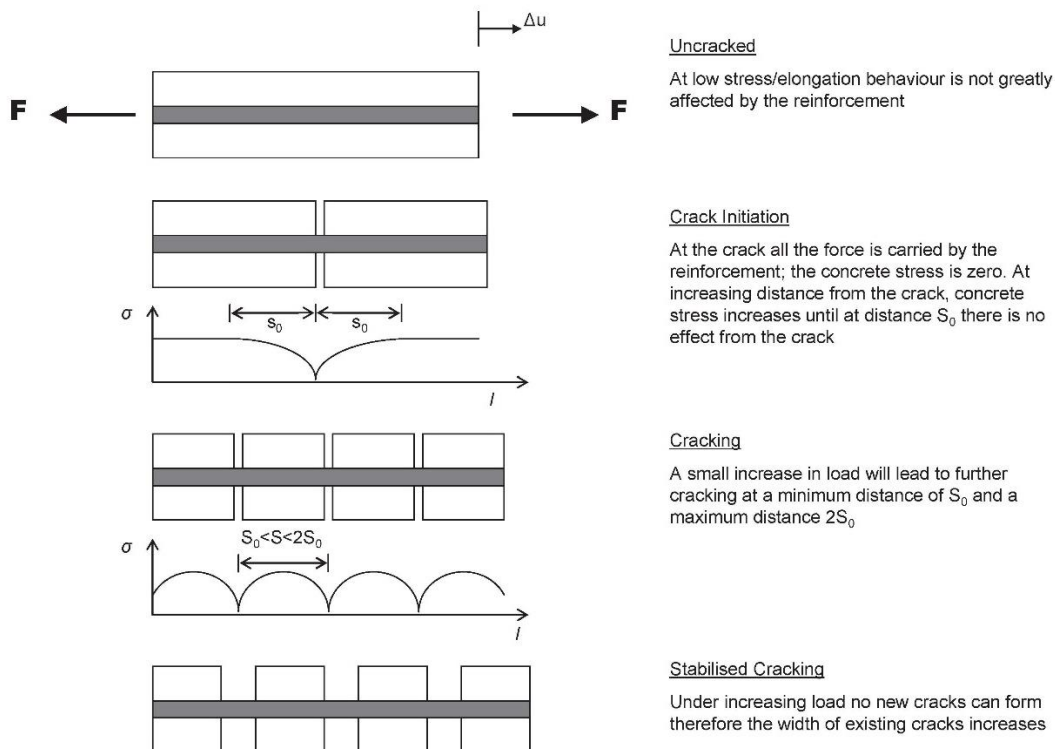


**Figure 5.17: Stages of cracking in a reinforced concrete section (Deeny 2010)**

Normal tension stiffening models are based upon semi-empirical data. The inclusion of empirical data in most general finite element models running non-linear analyses can lead to convergence problems, as the interaction of rebar and concrete becomes difficult to model. However, this work demonstrates how material models that cannot easily be included in standard finite element packages can be included in the FBE model with relative ease. This potentially opens the way for including other structural considerations such as slippage between concrete and steel, as explained in Section 2.4.8.

#### 5.4.1 Tension stiffening models presented in the literature

Various formulations are presented in the literature to account for tension stiffening (Stramandinoli & La Rovere 2008; fib 2010b; Zilch & Zehetmeier 2010; Grünberg & Göhlmann 2013), although few have been applied at elevated temperatures. In her PhD thesis Deeny (2010) included tension stiffening in a model for

composite floors in fire by adjusting the stress-strain curve of concrete. The descending branch (or post-peak stress branch) of the concrete curve had an increased slope applied to it to account for the increase in stiffness that rebar provides, as shown in Figure 5.18. The concrete had a constant tangent stiffness,  $E_T$ , up until the concrete tensile stress capacity,  $f_{T,t}$ , after which the descending branch applied. A parametric study was conducted to investigate the influence of different degrees of stiffening. It appears the final level of tension stiffening used was based on finding a level which improved numerical stability and FE model convergence, rather being based on a particular model or concrete property. It was noted that the “introduction of some tension stiffening which is a real effect can have the additional benefit or alleviating some of the numerical difficulties associated with softening behaviour” (Deeny 2010). The softening behaviour referred is that of concrete having lower stiffness when cracking occurs. It appears that the tension stiffening behaviour was applied to all concrete, irrespective of its proximity to rebar.

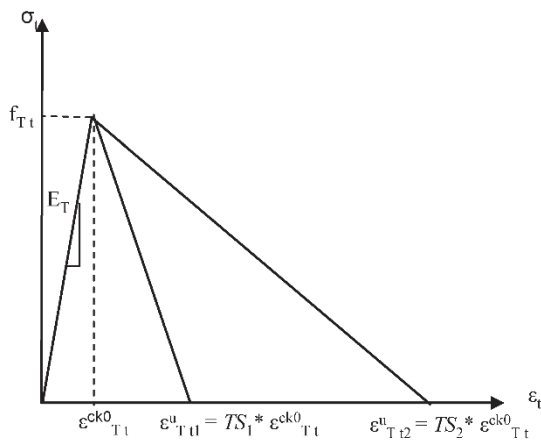


**Figure 5.18: Tension stiffening model for concrete developed by Deeny (2010)**

Stadler (2012) modified the ambient temperature tension-stiffening model developed by Zilch & Zehetmeier (2010). The procedure employed was: (a) the effective stiffness of the cracked concrete slab in tension was calculated at ambient temperature, and then (b) multiplied by a lumped global fire reduction factor to account for the reduced stiffness of only the concrete in fire. This method is fairly simple to employ and test. However, the factors which govern the stiffness of a reinforced concrete section (rebar  $f_y$  and  $E_s$ , concrete  $f_{cm}$  and  $E_c$ ) deteriorate at different rates as a section heats up, and sections may not heat up uniformly. As an example of the different rates of deterioration: at 400°C siliceous concrete in tension has lost approximately 60% of its strength, whereas the rebar is still at full strength. Concrete in tension reaches 0% strength at 600°C, whilst rebar reaches 0% at 1200°C. Hence, applying a lumped factor based on concrete properties alone will typically decrease the strength of the rebar more than has actually occurred.

In this research the *fib* guidelines from the Model Code 2010 (fib 2010b) have been modified to suit elevated temperatures. The *fib* Model Code is an authoritative guide for concrete design, although other models are available as listed above.

#### 5.4.2 Tension stiffening at ambient temperature

The ambient temperature concrete tension stiffening model adopted in this work (fib 2010b) will firstly be explained, and then this will be extended in the next section to account for fire conditions. The load-strain relationship of a reinforced concrete sample experiencing tension stiffening can be simplified to be as shown in Figure 5.19 below. The stages of the graph are:

- 1) Uncracked stage. Load is below the tensile capacity of the concrete.
- 2) Crack formation stage. As the tensile capacity of the concrete is exceeded it causes local yielding of the rebar, with a number of cracks forming along the length of a sample. This line will not be totally horizontal in reality but it is sufficiently accurate to simplify it to be horizontal i.e. the steel elongates without additional load being carried.
- 3) Stabilisation cracking stage. Once the load has caused the sample to have discontinuities along its full length, i.e. the concrete is effectively fully cracked, the increasing load is carried by the rebar alone in tension.
- 4) Naked steel. This is the path that a sample would follow if there was no concrete causing tension stiffening.
- 5) Yielding of reinforcement.

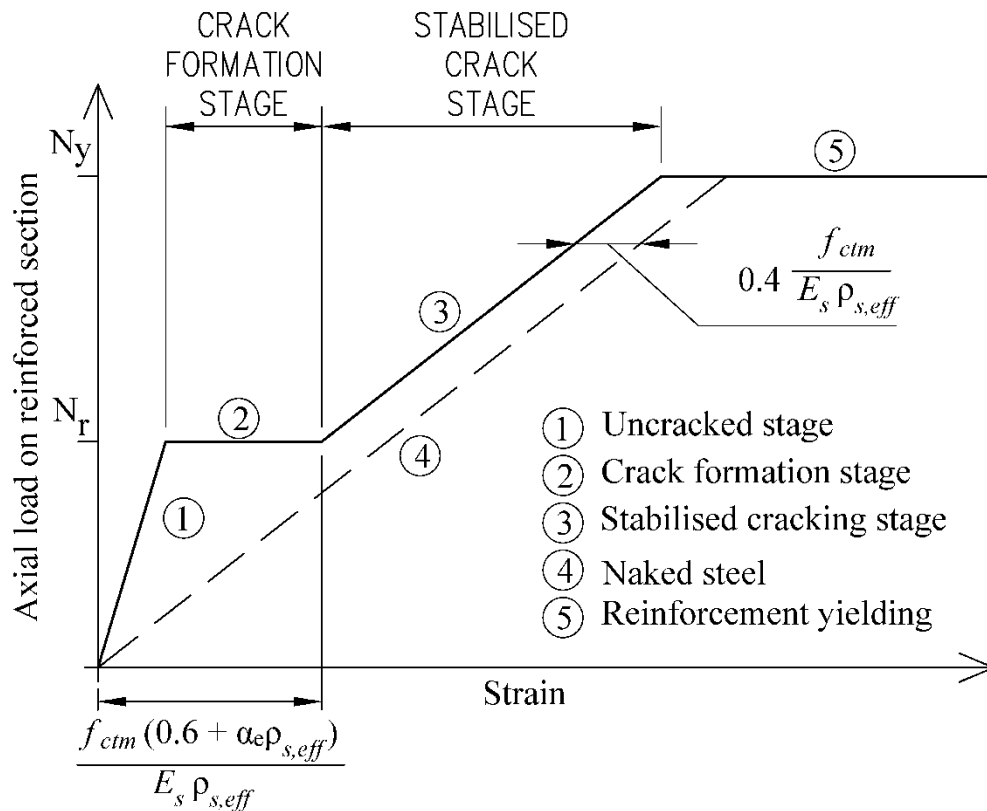


**Figure 5.19: Load-strain relationship of a reinforced concrete sample under tensile loading (fib 2010a)**

The cracking force for an element in uniaxial tension is calculated as:

$$N_r = A_c f_{ctm} (1 + \alpha_e \rho_{s,eff}) \quad (5.38)$$

When the applied load reaches the cracking load the crack formation stage commences, where the sample elongates without additional load being carried as more and more cracks open. This phase continues while the strain satisfies the following constraints:

$$\epsilon \leq \frac{f_{ctm}(0.6 + \alpha_e \rho_{s,eff})}{E_s \rho_{s,eff}} \quad (5.39)$$

Where:

$\alpha_e$  = modular ratio =  $E_s/E_c$

$\rho_{s,eff}$  = effective reinforcement ratio for tension steel

$N_r$  = tension force at which cracking occurs

During the stabilised cracking phase it can be viewed that the stiffness of the combined rebar-concrete system is that of rebar alone, but offset by the value  $0.4 \frac{f_{ctm}}{E_s \rho_{s,eff}}$ . The rebar yields when the yield load,  $N_y$ , is reached as given by:

$$N_y = A_s f_y \quad (5.40)$$

### **Effective concrete area**

For reinforced concrete in tension the effect of concrete-stiffening is typically only due to the concrete in the vicinity of the rebar, rather than the entire gross cross-sectional area being involved. According to the *fib* Model Code the concrete tension area is calculated as shown in Figure 5.20. This can be summarised as the thickness of concrete causing tension stiffening being defined as:

- a) Beams – Lesser of  $2.5(h - d)$  and  $(h - x)/3$
- b) Slabs – Lesser of  $2.5(c + \phi/2)$  and  $(h - x)/3$
- c) Tension elements – Lesser of  $2.5(c + \phi/2)$  and  $t/2$

where  $\phi$  is the diameter of a bar,  $c$  is the concrete cover to a bar and  $x$  is the distance of the NA from the top of the section. For a concrete slab in isolation (e.g. Case Study 2) the slab guidelines will be used. For a composite beam (e.g. Case Study 3 & 4) the effective depth of sections increases significantly, changing the stress distribution in concrete due to the change of NA. This will result in a concrete flange behaving somewhere between that of a tension element (for deep steel beams) and a slab (for shallow steel beams). Based on the depths of beams in Case Studies 3 & 4 the stress distribution in the slab will be closer to that of a member in tension so the guidelines as in (c) will be used.



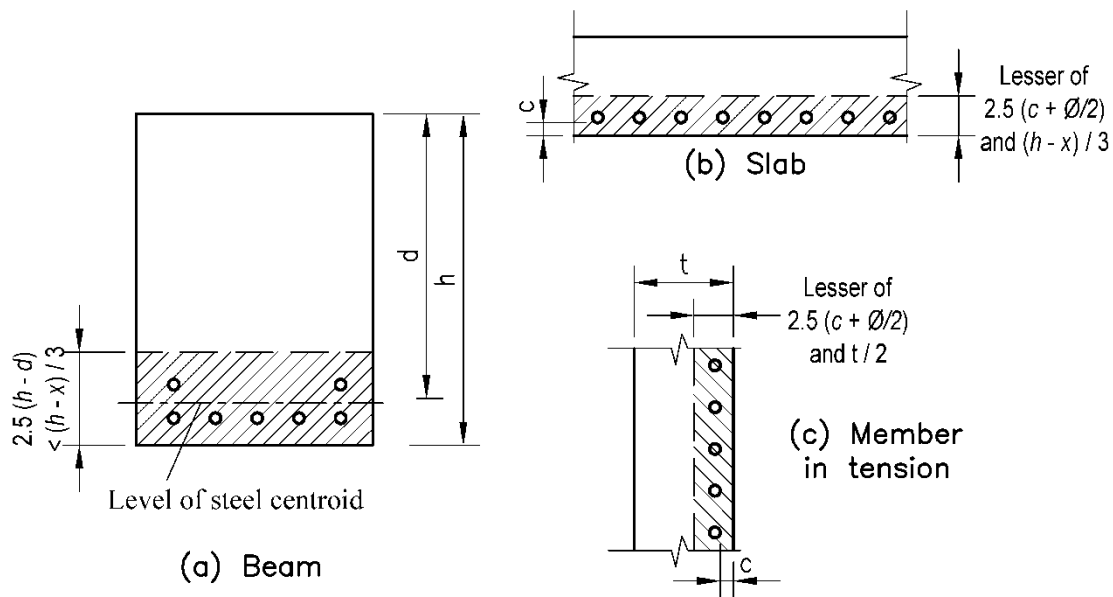


**Figure 5.20: Effective concrete areas of reinforced elements in tension: (a) beams, (b) slabs, and (c) member in tension (fib 2010a)**

### ***Concrete tensile load exceeding the rebar yield load***

Before adjusting equations to account for elevated temperatures it is necessary to consider the case where the cracking force is greater than the rebar yield load, i.e.  $N_r \geq N_y$ . This is not directly addressed in the model code, but is possible for lower ratios of reinforcement, as is often the case with composite slabs. In this situation as the first crack forms the full load of the concrete in tension is transferred to the rebar. At this point the load must either reduce immediately or fracture will occur. For composite slabs the load will redistribute to be carried by other elements of the structure, typically to the steel beam. Hence, the load-strain formulation has been updated to be as shown in Figure 5.21 when the cracking load is exceeded by the applied load. The load-strain graph does follow the graph shown with a sudden change in load with strain. A displacement controlled experimental test is required to produce such a graph. This scenario should be cautiously considered as it is possible for fracture of reinforcing steel to occur if localised strains at cracks are too high (Grünberg & Göhlmann 2013).

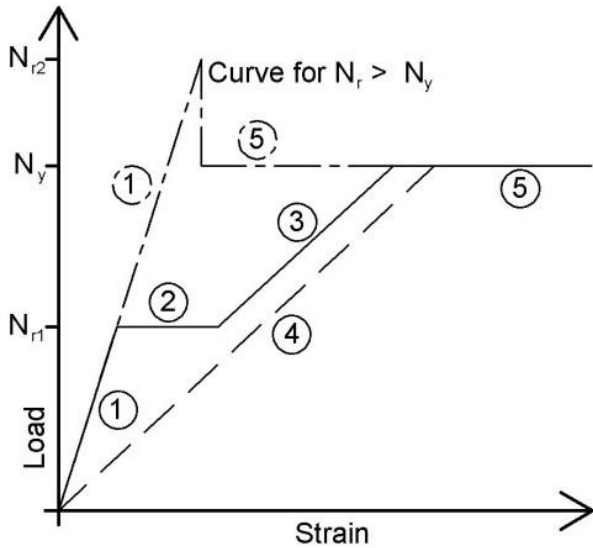


**Figure 5.21: Load-strain relationship of a reinforced concrete sample under tensile loading, including the modified graph for cracking load exceeding the rebar yield load**

#### 5.4.3 Modifications to account for elevated temperatures

To account for fire and the reduced strength and stiffness of both concrete and steel each individual property is adjusted based on the reduction factors in EN 2-1-2 (BSI 2005a) or EN 3-1-2 (BSI 2005b). Hence, the tension stiffening equations of the *fib* Model Code become:

$$N_r = A_{c,\theta} f_{ctm,\theta} (1 + \alpha_{e,\theta} \rho_{s,ef}) \quad (5.41)$$

$$\epsilon_\theta \leq \frac{f_{ctm,\theta} (0.6 + \alpha_{e,\theta} \rho_{s,ef})}{E_{s,\theta} \rho_{s,ef}} \quad (5.42)$$

Where:

$A_{c,\theta}$  = concrete area effective in tension stiffening in fire (see Figure 5.20)

$\alpha_{e,\theta} = \frac{E_{s,\theta}}{E_{c,\theta}} = \frac{k_{E,s} E_s}{k_{E,c} E_c}$ . Modular ratio at temperature  $\theta$

$N_{r,\theta}$  = tension force at elevated temperature at which cracking occurs (kN)

$f_{ctm,\theta} = k_{c,t}(\theta) f_{ctm}$ . Reduced tensile strength of concrete.

From the above it can be seen that each material property is addressed independently rather than applying a lumped factor based on only one property.

#### **Example calculation**

The following example calculation is provided to illustrate the change in stiffness of a system with changing temperature. A 1000mm wide by 120mm thick slab with Y10 bars at 200mm centres is considered. The cover to the rebar is 30mm, with properties  $f_y = 450\text{MPa}$  and  $E_s = 200\text{GPa}$ . Concrete properties are  $E_c = 33\text{GPa}$  and

$f_{cm} = 3\text{MPa}$ . Figure 5.22 shows the changing load-strain relationship for the system as the temperature increases from 20°C to 600°C.

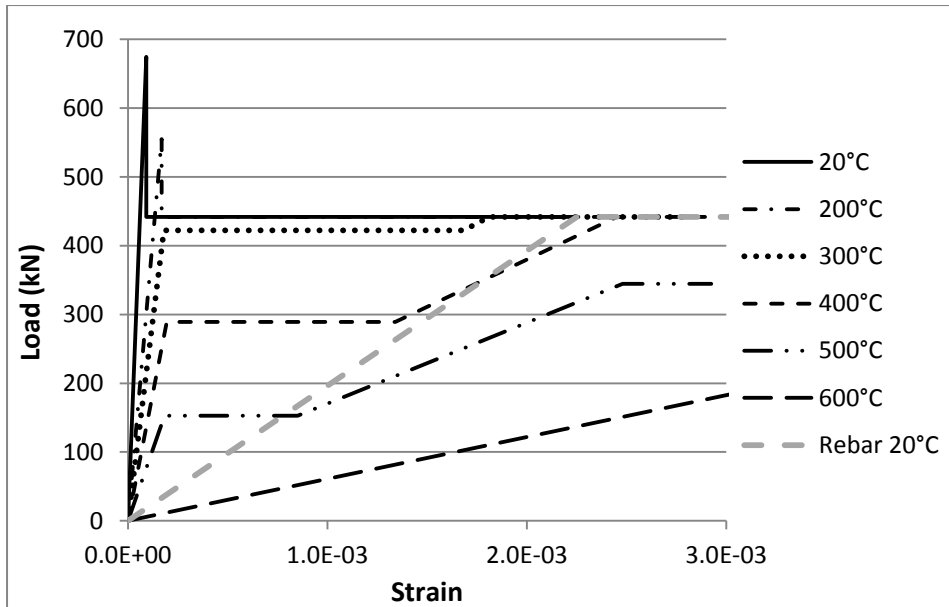


**Figure 5.22: Load-strain graph to illustrate changing properties with increasing temperature**

From this figure it can be observed that initially the cracking load is in excess of the rebar yield load. After the first crack occurs the system cannot sustain the load, and the stress drops to that at the yield load. At 300°C the concrete tensile strength has dropped more rapidly than the steel yield strength meaning that the concrete cracking load is below the rebar yield load. The length of the crack stabilisation stage varies with increasing temperature. After 400°C the steel yield strength starts decreasing resulting in the total ultimate load capacity reduced.

Depending on the total load or the strain applied to the system it can be seen that the tangent or secant stiffness of the combined concrete-rebar element can be significantly different to that consisting of only rebar, as shown by the grey dashed line in the figure.

#### 5.4.4 Effective / reduced tension stiffening areas

Two challenges are experienced when implementing tension stiffening in concrete beams and slabs, namely:

- The tension stiffening zone area layouts shown in Figure 5.20 have been developed based on the assumption that the entire area calculated cracks in tension. However, due to temperature profiles in members in fire some slab sections within the stiffening zone may have significantly higher thermal strains, which causes them to still be in compression. This would result in such sections not contributing towards overall tension stiffening behaviour.
- When a section cracks the RTSM exerted by the section decreases. It is possible to find situations where beams oscillate within an iteration between being cracked and uncracked in cross-sectional

analyses, as caused by thermal forces decreasing when a section cracks leading to total forces being under the cracking force required.

For the two challenges identified above the former may lead to an over-estimation of stiffness while the latter leads to convergence problems in FE analyses. A novel method is proposed in this work to address these challenges and provide a model which has greater numerical stability. The fundamental principle is that of all the concrete within the zone that could contribute to the stiffness of a bar only those areas which have cracked within the zone are considered, not those still in tension due to thermal expansion. This is illustrated in Figure 5.23 and explained below. It must be understood that when areas are referred to, these are represented by all the small zones or areas a cross-section has been discretised into, i.e. the integration points of a section, as per Figure 3.16, where each integration point has an associated area.

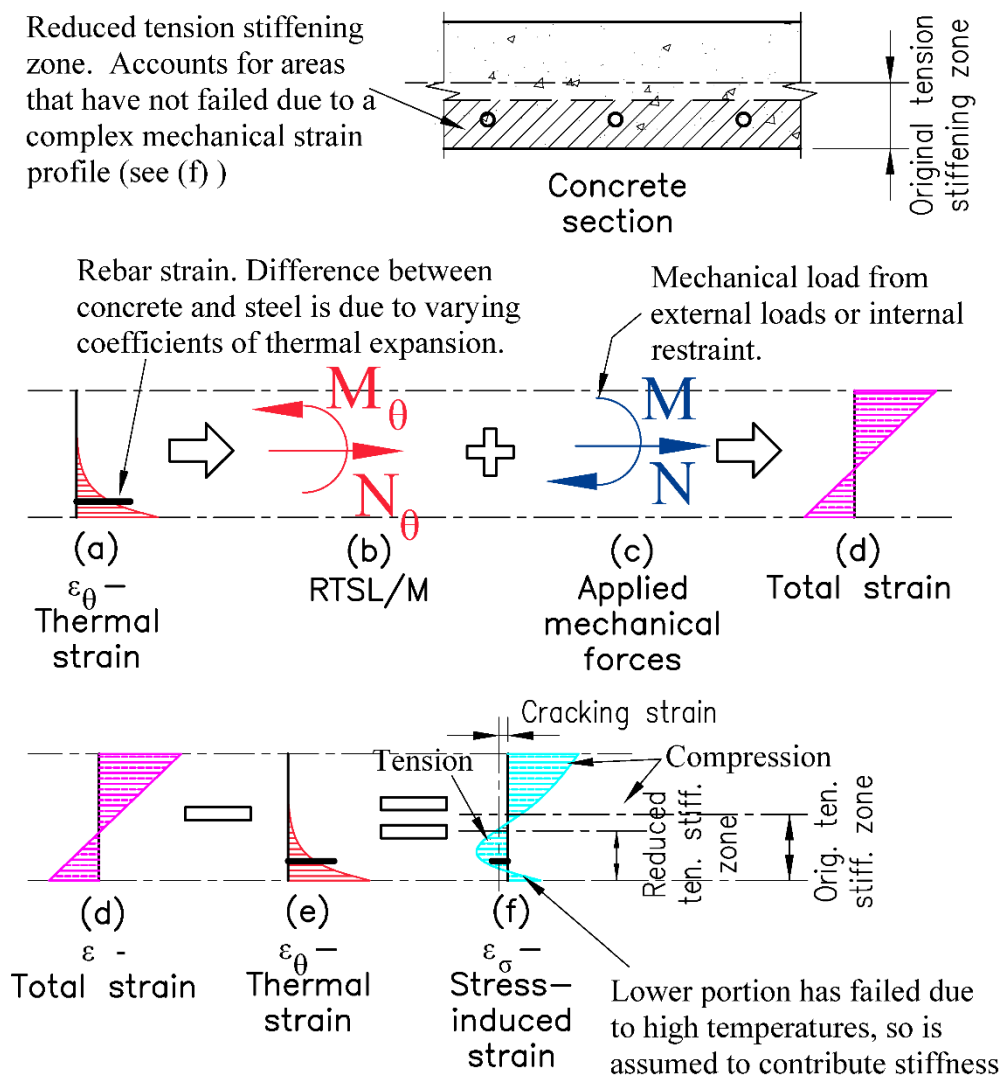


Figure 5.23: Change in the tension stiffening area for rebar due to the complex strain profiles of concrete slabs in fire.

For the concrete section shown in Figure 5.23 which is exposed simultaneously to a temperature gradient and mechanical forces the following will occur:

- (a) A thermal strain will be created over the height of the section. At the height of the reinforcing steel the concrete and steel will be at the same temperature and have the same total strain. However, due to the different thermal elongations of the concrete and the steel there may be differences in thermal strains, with the reinforcing steel having elongated either less or more. It is important that tension stiffening will only occur when the *concrete strain* exceeds the cracking strain, and not the rebar strain. This is an important issue when developing FE models as it leads to convergence problems when not correctly considered.
- (b) The elevated temperatures will induce RTSMs and RTSLs in the slab.
- (c) These thermal forces act on the beam along with the applied mechanical moments and axial forces. If there is restraint present in a structure the restraint will induce extra forces.
- (d) When both the mechanical and RTSL/MS are applied to the slab cross-section it will cause the total strain profile shown.
- (e) By subtracting the thermal strains from the total strains it will give the resultant mechanical strains in the cross section, as shown in (f).
- (f) The total mechanical strain over the height of the section now follows a complex profile with tension and compression at different positions. The zone typically contributing to tension stiffening now experiences both tension and compression. Also, some areas in tension are still below the cracking strain and thus will not have cracked yet. The uppermost section of the tension stiffening zone that is still in compression will generally still have structural resistance and may be carrying load. Hence, the original tension stiffening zone is now decreased to the reduced tension stiffening zone shown, excluding the aforementioned area. The lowest section in the beam is still in compression but will typically have failed due to the high temperatures experienced, resulting in it carrying no load and being available for tension stiffening. Since this lowermost zone is often narrow its inclusion in calculations has a relatively small influence on overall performance, which is beneficial due to the lack of certainty regarding behaviour. Experimental results are required to verify whether this assumption is correct.

From the discussion above it can be seen that assuming the concrete tension stiffening area at ambient temperature and at the fire limit state to be the same would typically be inaccurate. It is necessary to reduce the concrete area contributing to the fire limit state by only including tension stiffening zone areas which satisfy at least one of the following criteria:

- 1) Concrete strains in tension must exceed the cracking strain. This is to ensure that the application of all loads has indeed caused the elemental area to crack in tension.

- 2) If a concrete area has had material strength properties being reduced to 0%, i.e. it has crushed or experienced high temperatures. This is because it would have failed but still be connected to the adjacent concrete and provide some restraint to rebar, although it has cracked or crushed.

This can be calculated as:

$$A_{c,\theta} = \sum_{i=0}^n A_i. \text{ Subject to each element } i \text{ meeting the following criteria:} \quad (5.43)$$

$$\epsilon_{\sigma,i} \leq \epsilon_{cracking,\theta} \text{ OR} \quad (5.44)$$

$$f_{ctm,\theta,i} = 0 \text{ MPa if in tension, OR } f_{cm,\theta,i} = 0 \text{ MPa if in compression} \quad (5.45)$$

Where:

$A_i$  = cross-sectional area of element number  $i$

$n$  = number of elements / layers in the tension stiffening zone

$\epsilon_{\sigma,i}$  = mechanical strain at temperature  $\theta$  of element  $i$

$\epsilon_{cracking,\theta}$  = cracking strain of concrete at temperature  $\theta$

$f_{ctm,\theta,i}$  = reduced tensile strength at temperature  $\theta$  of element  $i$

$f_{cm,\theta,i}$  = reduced compressive strength at temperature  $\theta$  of element  $i$

As explained previously, this methodology requires experimental tests to verify the behaviour of concrete in fire and to what extent tension stiffening occurs. The benefit of the method is that it follows a simple flow of logic based on fundamental structural mechanics. The aspects which are currently the most difficult to verify are:

- 1) Does concrete at elevated temperature contribute to tension stiffening in the same manner as at ambient temperature?
- 2) Does concrete which has cracked in tension or failed at high temperatures in compression fully contribute to tension stiffening or has it cracked to such a level that no stiffness is provided? If the latter is true the reduced tension stiffening area calculated above would simply be reduced further by excluding the failed concrete in tension, i.e. the clause described by Equation 5.43 would fall away. In Chapter 7 it is shown that the influence of tension stiffening has limited influence on predicted deflections, although it may influence internal forces calculated.

### ***Addressing challenges affecting convergence***

As mentioned above, there can be cross-sectional analyses where a section fluctuates between iterations from being cracked to becoming uncracked again, which leads to convergence problems. A similar convergence challenge was experienced by Deeny (2010). This behaviour is due to: (a) RTSL/Ms being created which cause a section to crack when applied, and (b) the cracked section has reduced RTSL/Ms resulting in the

section becoming uncracked again. Although not commonly experienced in case studies this condition does occur.

It was found that the simplest and most logical way to address the challenge is to:

- (a) Allow the iterative process of determining the total stiffness of a cross-section to continue until a predefined number of iterations has occurred without convergence, which is normally between 200 and 300 iterations, although lower iteration limits could be set. A typical cross-sectional analysis requires 2-20 iterations, whereas for a complicated section with significant amounts of cracking the analysis requires around 40-60 iterations.
- (b) Once this number of iterations had been reached the number of integration points contributing to tension stiffening is reduced by a specified amount at predefined intervals (typically a reduction of 1-5 integration points depending on the size of area per integration point). These are not specific points that are removed (i.e. either at the top or bottom), but rather the total area used in Equation 5.43 is reduced by a specified number of integration point areas. The cross-sectional analysis is then given another 5-10 iterations to converge. If convergence has still not occurred after this time another portion of the tension area is ignored. In this way the area of tension is progressively reduced until convergence occurs.
- (c) Ultimately, if no intermediate solution is found the system will revert to a beam in which no tension stiffening is allowed (i.e. area of concrete contributing to tension stiffening becomes zero).

It has been found that even in highly complicated elements with unusual strain profiles convergence can be successfully obtained in this way. The advantage of using beam elements is that it is easier to identify specific cross-sections where convergence becomes problematic. In structures consisting of shells or volume elements with fine meshes it is more difficult to identify where convergence issues occur.

#### 5.4.5 *Illustrating the influence of tension stiffening*

As an example of the influence that tension can play in the stiffness of a section Figure 5.24 presents a graph showing the change in both axial stiffness ( $EA$ ) and rebar strain with applied axial load. Two cases are considered: (a) full tension stiffening (T.S.), and (b) no tension stiffening (No. T.S.). The section considered is a 100x100 concrete square with material properties according to Case Study 3. A single 16mm diameter bar is placed at the centre with a yield strength of 520 MPa. The section is uniformly heated to 200°C. At this temperature the unrestrained thermal strain of the steel would be 2318  $\mu\epsilon$  whereas the concrete is 1804  $\mu\epsilon$ , meaning that the concrete is restraining the steel and the steel is exerting a tensile force on the concrete.

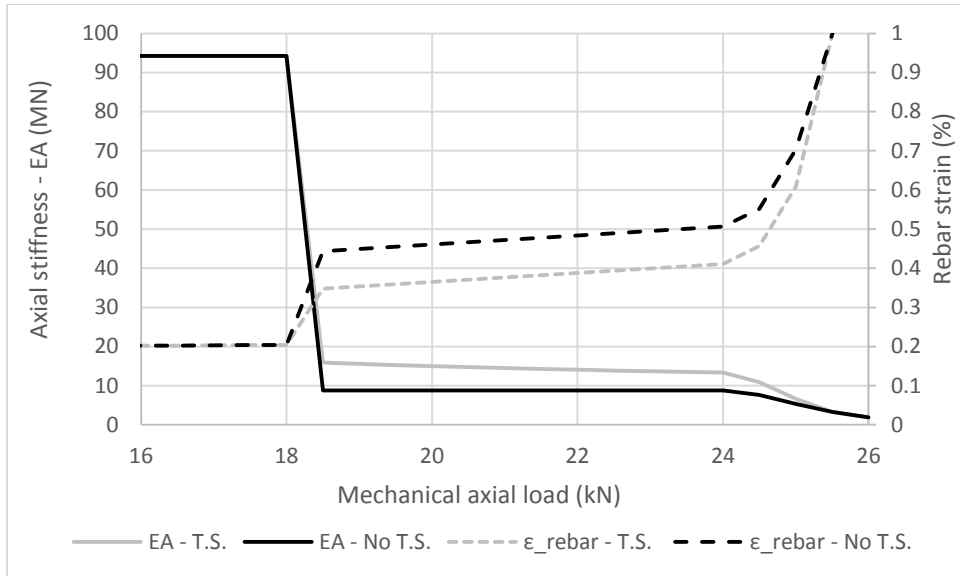


**Figure 5.24: Graph of axial load to axial stiffness and rebar strain of a 100x100 concrete section in which both tension stiffening (T.S.) and no tension stiffening (No T.S.) are considered**

The behaviour of the section is identical in compression and up to 18kN in tension whether tension stiffening is included or not, so only tensile behaviour is shown here. At a tensile load of 18kN the mechanical force coupled with the RTSL causes the concrete to fail in tension, resulting in the sudden decrease in axial stiffness and increase in rebar mechanical strain. For the case with no tension stiffening the rebar elongates more due to the more significant reduction in stiffness. After the onset of cracking the difference in axial stiffness between the two systems starts at 82% at 19kN, and then progressively diminishes. Hence, it can be seen that the inclusion of tension stiffening can increase the stiffness of an individual bar by 82%. This increase will vary depending on the area contributing to tension stiffening and the temperature of elements.

## 5.5 Conclusion

This chapter has outlined the material models and temperature profiles used in this research. The behaviour of steel at elevated temperatures is relatively well defined and the EN 3-1-2 guidelines have been followed. It can be readily observed that concrete in fire has a much higher variability than steelwork. The following factors directly influence the behaviour of concrete at elevated temperatures and have been considered:

- Compressive strength – this is influenced by whether characteristic or average properties are used and by the level of confinement. Average values according to EN 2-1-1 will be employed, unless cube or cylinder tests are reported in the literature considered, in which case these characteristic values will be adjusted to average value (see Section 5.1).
- Material stiffness – this property is significantly influenced by the material model used (e.g. whether EN 2-1-1 vs. 2-1-2 at ambient temperature), the type of aggregate, and the relationship between strength and stiffness. Since deflections are the result typically recorded during full-scale fire experiments it is important to understand that predicted deflections are strongly dependent on material



stiffness, except where increases in material stiffness are counteracted by increases in thermal forces (see Chapter 7).

- (c) Temperature profile selected - four different temperature models have been contrasted. A heat transfer model has been developed in this research to allow the case studies presented in Chapter 6 to be considered. Existing models did not provide temperatures sufficient for the slab thicknesses and fire exposure times required. Temperature profiles are influenced by the thickness of slabs tested, the thermal properties of concrete and properties related to fires such as radiation coefficients. The heat transfer model developed in this work accounts for these.
- (d) The modelling of ribbed slabs has been considered. Ribbed slabs will be converted into equivalent flat slabs, according to EN 4-1-2, and as done by other fire analysis procedures.
- (e) The width of flange assumed to be acting compositely with a beam has been addressed. Ambient temperature recommendations will be used, although this is a topic for future research as limited guidance is currently available in the literature.

An elevated temperature tension stiffening model has been presented in this chapter. It is based upon the *fib* Model Code with material behaviour being extrapolated to elevated temperature. The formulation is based on individually modifying parameters of the ambient temperature model. Experimental testing is required to verify the results obtained. The inclusion of such semi-empirical models in an analysis system highlights that additional complex behaviour could potentially be included in the beam element formulation presented. A procedure for considering the complex strain state of slabs in fire and numerical challenges regarding model convergence had been proposed. The advantage of modelling structures using beam elements is that the behaviour leading to such numerical challenges can be more easily identified and addressed. The adaptations to the *fib* tension stiffening model are novel, although the fundamental behaviour is based upon information in the literature.

The material models developed in this chapter are included with the beam element formulation of Chapter 4 to investigate experimental tests in the following chapter. From the discussions above it can be seen that there is a relatively high level of uncertainty inherent in fire design involving concrete elements, although structural steel still also has significantly variable behaviour depending on the material temperatures selected as these are often difficult to define. This variability in input parameters necessitates the use of parametric studies when designing elements, as engineers should understand the influence of design variables chosen. This will be addressed in Chapter 7.

## 6 Chapter 6: Validation by comparison with experimental and numerical studies

### 6.1 Introduction

This chapter applies the FBE formulation developed in this dissertation to case studies as validation of the proposed model and to illustrate various aspects of structural behaviour. The composite beam properties and RTSL/Ms are calculated as discussed in the preceding chapters and are inserted directly into a commercially available structural analysis package, called Prokon Frame (Prokon SCL 2015), to calculate the deflection of beams. This software has been chosen as it is a commonly available and relatively simple FE modelling tool, used extensively by consulting engineers in South Africa. By demonstrating how results from experiments, or much more advanced software can be matched by a relatively simple FE modelling program coupled to sub-routines or spreadsheets, the efficiency and use of the proposed FBE formulation can be demonstrated. It also illustrates how the methodologies could be more easily adopted by consulting engineers. It must be understood that implementing the FBE formulation within Prokon Frame is limited to statically determinate structures. Indeterminate structures require iterative procedures coupled to analysis systems. Future research will focus on developing the FBE formulation within existing FE software (such as Abaqus) or as a stand-alone software system.

The following case studies from the literature were selected to illustrate the use of the FBE formulation on both composite and non-composite structures:

1. Uniformly heated steel beam (Bailey 1995) (this is the only numerical test, all the remaining tests are based upon experimental data)
2. Single span concrete slab (Ali et al. 2008).
3. Two simply-supported composite steel beams, called “Test 15” and “Test 16” (Wainman & Kirby 1988).
4. Seven composite beams which form part of a full-scale composite slab in the “Second Munich Test” (Stadler 2012).

For each case study the experimental setup and design parameters are supplied as obtained from published work. Where information is lacking it has been estimated based on reasonable pre-analysis assumptions. For any additional information the references cited can be consulted. Results for each case study are presented along with a discussion thereof. In total eleven different beams are analysed as validation of the FBE formulation.

The case studies build upon each other. In the first one only a simple steel beam with an increasing uniform temperature is considered, which highlights the accuracy of the methodology relative to other existing FE methods. Large deflections and low stiffnesses are considered. A case study on a simply-supported concrete slab follows this in which concrete properties, tension stiffening and thermal profiles are included. The behaviour of concrete and steel is then combined with the analysis of two simply-supported composite beams in the third case study. The final structure investigated is an entire floor consisting of primary and secondary beams. Catenary action of slab panels occurs. The deflection of primary beams is specifically addressed.

It should be understood that with the number of variables that are utilised within analyses, especially when concrete is considered, it would have been possible to manipulate results to match experimental values more closely. However, in all the case studies the input parameters have been kept consistent, based as far as possible upon the data supplied. Reasons for differences in experimental and numerical results are discussed. Appendix B provides extensive details regarding the properties calculated for beams from which the results in the sections below can be verified.

#### *6.1.1 Academic contribution*

The primary academic contribution of this chapter is a validation of the FBE formulation developed throughout this research, highlighting that the formulation predicts behaviour similar to that observed in experimental tests. The consideration of an entire composite floor in Case Study 4 using beam elements is novel and illustrates the potential application of the method. Furthermore, the fact that analyses are carried out using simple software, which can easily be interrogated (see Appendix B), assists engineers with understanding structural behaviour.

## 6.2 Modelling specifications

Structures are modelled using the procedure explained in Section 3.9, where member properties are determined based on calculated bending moments and then inserted into a commercial finite element software package named Prokon Frame (Prokon SCL 2015). In Prokon Frame a non-linear analysis has been utilised with a minimum of 16 segments per beam analysed. In the functioning of the software all the loads on the structure, including both mechanical and thermal effects, are applied in uniform load increments until convergence is obtained. A minimum of 50 load steps were used as it was found that consistent results could then be obtained, even in structures with larger loads and low stiffnesses. Case Study 1 addresses a challenge faced when stiffness values become very low.

Since the structures considered in this research are statically determinate the overall process followed only needs to occur once. However, it would be possible to analyse indeterminate structures using the same methodology but coupled to an iterative procedure. As forces change throughout the structure the beam stiffnesses and thermal loadings must be continually adjusted until convergence is obtained.

## 6.3 Case Study 1: Uniformly heated simply-supported steel beam

### 6.3.1 Experimental setup

In this first case study a simply-supported, uniformly heated steel beam will be considered, as presented by Bailey (1995) and shown in Figure 6.1. This simple example is provided to demonstrate the following aspects: (a) a comparison of the proposed model with previously developed and validated methods, (b) an investigation into the effect of the number of beam segments selected for a beam (convergence study), and (c) to illustrate how discretisation can influence results.

For this case study the material model is based upon the Ramberg-Osgood stress-strain curve (Burgess et al. 1991), as selected by the original author. A yield stress of 275MPa and Young's modulus of 205GPa is used. Burgess et al (1991) analysed the same structure and produced almost identical results to those from Bailey shown below, hence it was not necessary to show these results as well. Bailey's method uses beam elements that have 22 degrees of freedom in the global coordinate system, and consider buckling and shear distortion in addition to typical rotational and translational degrees of freedom.

To gain an approximate understanding of the problem the following values quantify the behaviour assuming the development of a fully plastic section at mid-span:

- Maximum moment:  $M = \frac{\omega l^2}{8} = 91.6 \text{ kNm}$
- Beam plastic section modulus:  $Z_{pl} = 568 \times 10^3 \text{ mm}^3$
- Stress at max moment:  $\sigma = M/Z_{pl} = 161.3 \text{ MPa}$
- EN 3-1-1 temperature at which load cannot be sustained: 524°C

Hence, using the reduction factors in EN 3-1-1 the structure would no longer be able to sustain load at a temperature of around 524°C. The Ramberg-Osgood model has a similar stress-strain curve initially to EN 3-1-1, but no descending branch and instead the stress keeps increasing, albeit slowly, with increasing strain. Thus, the references above do report deflections at temperatures higher than possible with a Eurocode material model, although deflections increase rapidly with increasing temperature as discussed below.

### 6.3.2 Results and discussion

Figure 6.1 shows the deflection curves calculated by Bailey when the beam was discretised into 4 and 16 segments. Another graph for 8 segments was also produced but this is almost identical to that for 16 segments, so is not presented again here. The FBE formulation gives the data points shown for when the beam was discretised into the same number of segments as Bailey. It can be seen that there is good agreement between the curves, especially the model with 4 segments, with it being almost identical to the finer discretisation from Bailey. This highlights a consistent consideration of structural mechanics between the methods. The maximum deflection shown is span/6.4, significantly higher than the typical code deflection limits in fire.

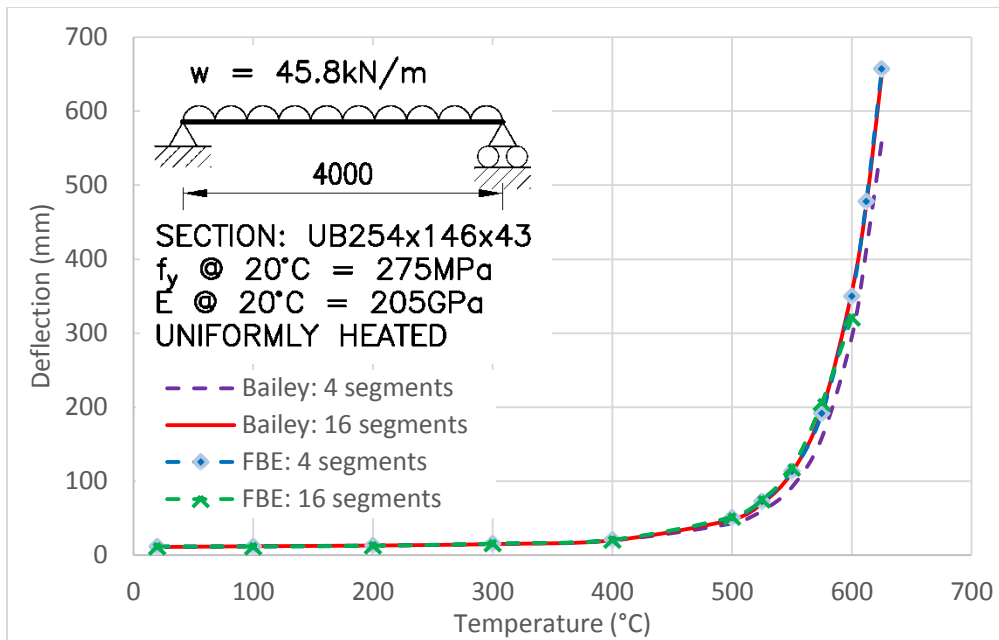


**Figure 6.1: Case study of a simply-supported steel beam subject to a UDL with varying levels of discretisation**

The model with 16 segments starts experiencing numerical errors in the commercial software at temperatures in excess of 600°C. This occurs because the moment used to calculate beam properties is taken at the mid-span of the beam segments, giving the beam with a finer discretisation a slightly higher moment for the middle segment. For the material model a small increase in stress is accompanied by a large increase in strain, leading to this situation where the slightly increased moment leads to a significantly decreased stiffness. At a temperature of 625°C the secant modulus of the material has reduced to 0.8% of its original value (i.e. from 205GPa to 1.6GPa), and the effective radius of curvature is 1.1m. At this stage it is unreasonable to assume that Bernoulli assumptions still hold due to the high levels of curvature and deflection.

Overall this case study highlights the consistency in results between the methods, with negligible difference at typical levels of stiffness. When stiffnesses become unrealistically low convergence becomes a problem in the FE software used, which is a simple design office tool. This could be addressed by using more advanced software tools, such as Abaqus (Dassault Systèmes 2013), which include improved solvers for large deflections and nonlinear analyses. The next case study now introduces material non-linearity and temperature gradients.

## 6.4 Case Study 2: Single span 1200x200 concrete slab

### 6.4.1 Experimental setup

The concrete slab shown in Figure 6.2 was tested in a standard furnace test for up to an hour. Three identical slabs, named S1 to S3, were simultaneously tested and documented by Ali et al (2008; 2010) to investigate deformation and spalling. An additional three slabs exposed to a hydrocarbon fire were also tested, but are not addressed here due to the added uncertainty of the extensive spalling that occurred during the tests. A

prediction model significantly more advanced than the FBE formulation was developed by Ali et al in DIANA for numerical analyses. Results from this model were first reported in the 2008 reference, followed by updated results reported in the 2010 paper, although reported deflection results for S1-S3 appear similar. These models included 3D twenty-noded solid brick elements, the explicit modelling of reinforcing bars, trial and error procedures to address cracking that influenced convergence, smeared crack models, separate thermal analyses and the consideration of transient strain. The 2008 model contained 6896 nodes and 1372 elements, whilst the 2010 model contained 2679 nodes and 792 elements.

The concrete properties selected for this dissertation are as defined by the original authors, having an average compressive strength of 42 MPa and tensile strength of 4.1 MPa. The characteristic strength of the rebar was given as 460 MPa, although it was not tested so will be taken as 520 MPa (two standard deviations above the specified characteristic strength (JCSS 2001) of 460 MPa, as explained in Chapter 5). The temperature of the rebar used was as provided by experimental readings (see Appendix B), whereas the concrete temperature was estimated using the FEA model from Section 5.2.5. The effective depth acting to provide tension stiffening was calculated as 50mm, using the procedure described in Section 5.4.2.

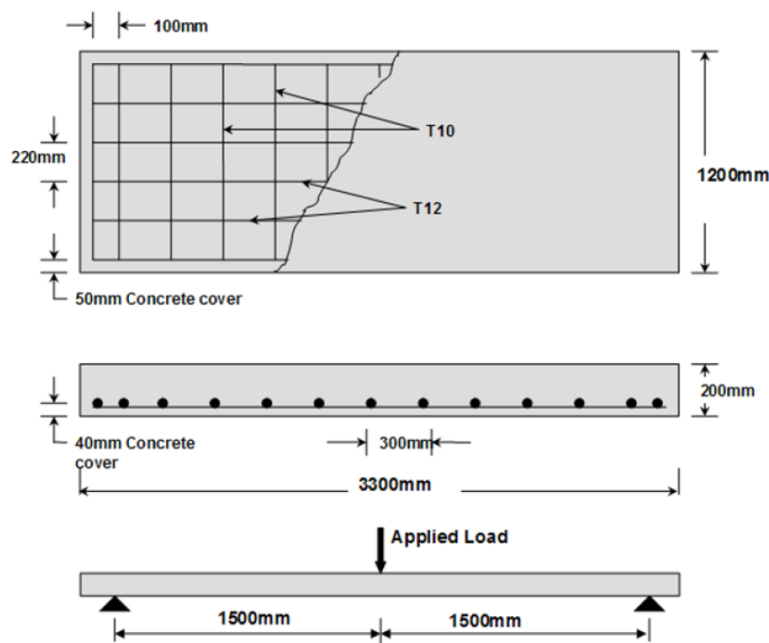


**Figure 6.2: Slab layout for tests conducted by Ali et al (2008)**

#### 6.4.2 Results and discussion

A comparison of the deflections recorded during (a) experiments S1-S3, (b) predictions by the investigators, Ali et al, using the DIANA models, and (c) the FBE formulation are shown in Figure 6.3. It can be observed that the general trend of the deflections has been well captured by the FBE formulation, with the average difference with experimental results at 60 minutes being between 4.7% and 16.9%. Deflections increase with time as the stiffness of the slab reduces and RTSMs increase. At 60 minutes the FBEs have stiffnesses of

between only 14% and 21% of their original value. At this time the maximum  $M_{\theta}$  value is 106.4 kNm, which is 4.0 times the maximum mechanical moment of 26.7 kNm. Thus, it can be observed that the thermal gradients are the dominant cause of the deflection in this case study.

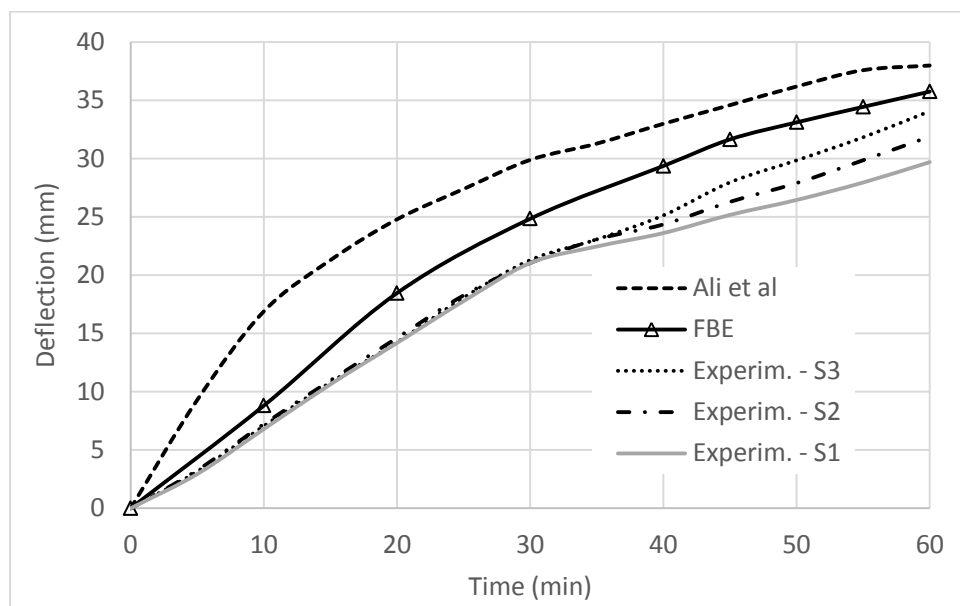


**Figure 6.3: Deflection results of the test, Ali et al's numerical model (2008), and the proposed FBE model**

During the experiments it was noted that the following occurred which would have influenced deflections: spalling of concrete, moving heat and moisture fronts through the slab, a brief drop in the temperatures at around 4 minutes, and cracking in the slab. All these factors are reasons that theoretical predictions for both models do not precisely align with experimental results. Furthermore, even the results from the three identical tests differ at 60 minutes, primarily due to differing amounts of spalling. The original authors note that due to the highly complex nature “of the moisture migration phenomenon and vapour pressure build up in concrete, these are not considered in the model” (Ali et al. 2010). It is possible that the FEA temperature prediction model used in this dissertation is conservative compared to actual experiments readings, but insufficient data is available to confirm this. Another potential reason for the difference in results between the FBE formulation and DIANA model is that in this dissertation the rebar temperatures were directly specified from measured temperature results so matched experimental conditions exactly, whereas Ali et al determined rebar temperatures from a thermal FE model (as is typically the case for advanced analysis models). Due the complex behaviour associated with the thermal effects mentioned above it meant that at certain times there were differences between experimental and FE values for rebar temperatures in analyses. It should be acknowledged that in real world designs experimental results of material temperatures are typically not available so need to be generated from FE models or standard tables.

The position of the NA above the slab soffit and the value of the bending stiffness ( $EI_{\theta}$ ) of the slab along its length are shown in Figure 6.4 at 30 and 60 minutes. The central regions have higher mechanical moments

resulting in the rebar being more highly stressed, thus decreasing the secant stiffness and causing the NA position to migrate upwards towards the concrete. The NA stays in approximately the same position over time, varying by 0.7% on average between 30 and 60 minutes, whereas the bending stiffness decreases by 18.5% over this time period. Concurrently the average RTSM increases by 14.0%. This shows that variations in NA and  $EI_{\theta} / M_{\theta}$  are not necessarily linked. The influence of the latter two parameters cause the predicted deflection to increase from 24.9 mm at 30 minutes to the maximum of 35.8 mm at 60 minutes.

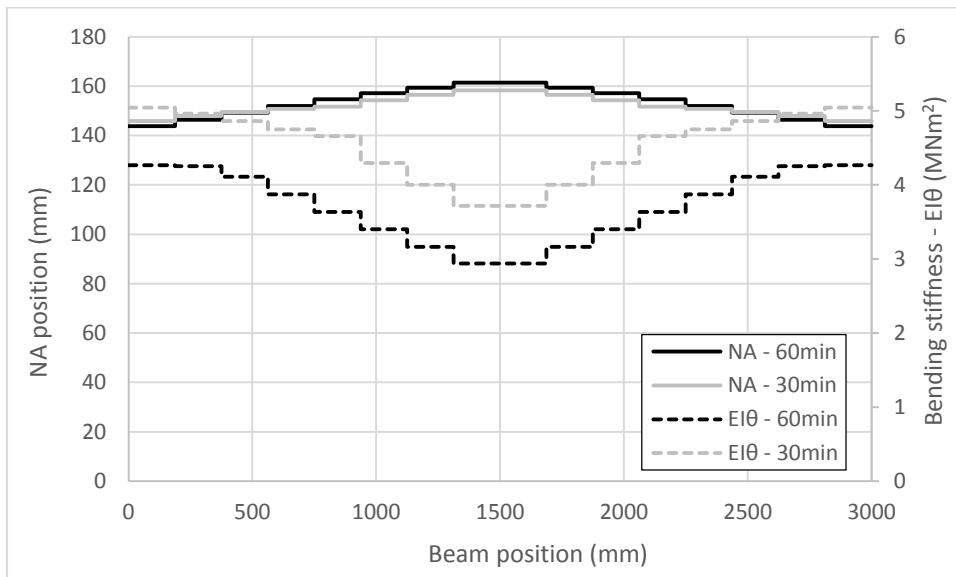


**Figure 6.4: Position of the NA from the slab soffit and magnitude of the bending stiffness ( $EI_{\theta}$ ) along the length of the slab at 60 minutes.**

## 6.5 Case Study 3: Unprotected composite beams – “Test 15” and “Test 16”

### 6.5.1 Experimental setup

The series of fire tests conducted by Wainman & Kirby (W&K) (1988) have become somewhat of a benchmark in the development of analysis methods for composite beams in fire. In a series of 83 tests conducted on various structural configurations, Test 15 & 16 were conducted on simply-supported composite beams. The tests were conducted to “provide data for researchers in the field of ‘fire resistance of steel structures’ particularly in the development of accurate calculation methods, for the determination of high temperature performance and fire resistant design” (Wainman & Kirby 1988). These two tests have been analysed by numerous researchers such as Jiang et al (2014), Cedeno et al (2011), Benedetti & Mangoni (2007) and Kassem (2009). In this work results have been compared with those of Jiang et al whose model results were generally more accurate than shown in the other papers, although there is a scatter of results in the literature. These two experiments illustrate the following: (a) the effect of thermal gradients across the height of a section, and (b) validation of the proposed model for composite beams against a full-scale test.



The experimental setup and material properties provided in the report are shown in Figure 6.5. Furnace, top flange, web and bottom flange temperatures are listed in Table 6.1 and Table 6.2, and plotted in Figure 6.6 and Figure 6.7 respectively. It should be noted that the temperature of the top flange was typically lower than that of the web and bottom flange, due to the heat sink effect of the concrete slab. All temperatures are lower than the furnace temperature, which generally followed the ISO 834 test, except for some localised variations. There was equipment malfunction for the first 9 minutes of Test 15, resulting in the lack of data readings. Test 16 was subjected to a much heavier load, hence failed earlier.

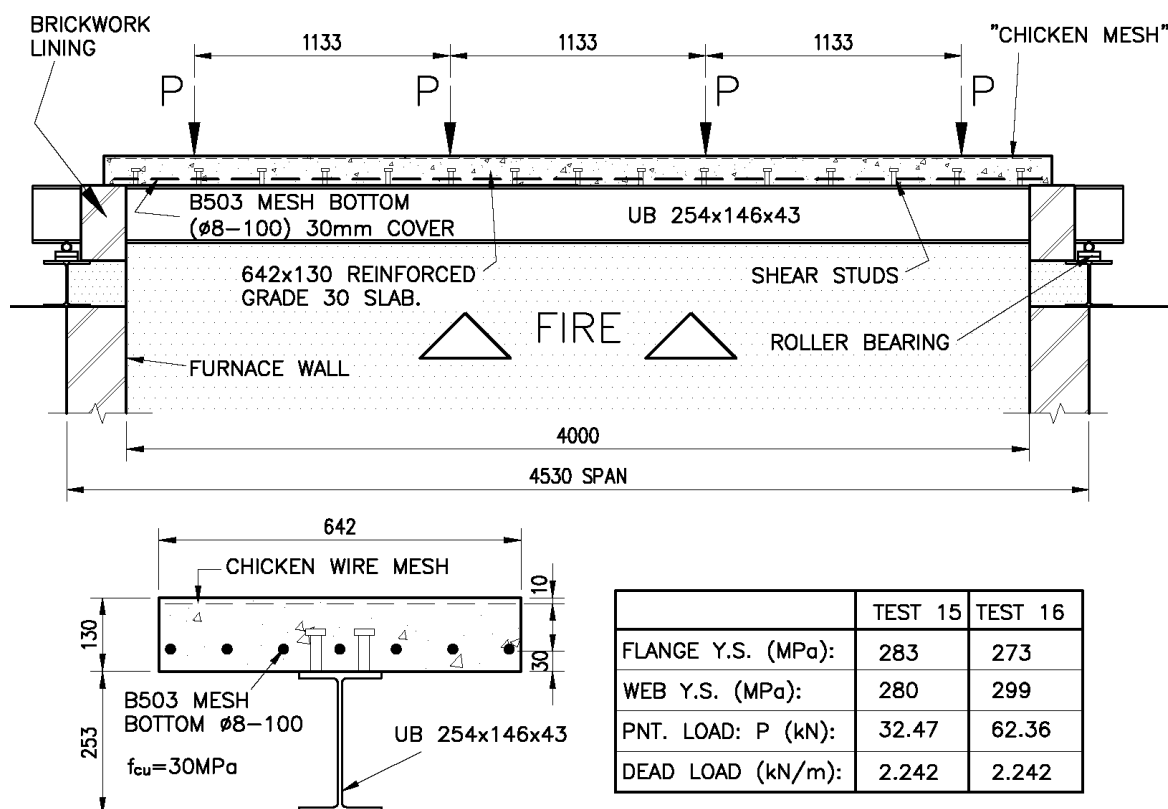


Figure 6.5: Experimental setup for Test 15 and 16 (reproduced from Wainman & Kirby (1988))

Time (min)	Temperature (°C)															
	0	3	6	9	12	15	18	21	24	27	30	33	35	36	39	40
Upper flange					221	272	318	364	407	449	492	530	533	565	594	606
Web					473	540	592	632	657	679	700	718	728	731	745	749
Lower flange					455	535	598	644	674	697	716	729	737	741	756	762
Furnace					689	723	747	761	768	779	801	806	819	819	834	838
Std. Fire curve	20	493	594	654	696	730	757	780	800	817	833	847	856	860	872	876

Table 6.1: Temperatures of elements for Test 15

Time (min):	Temperature (°C)									
	0	3	6	9	12	15	18	21	22	23
Upper flange	20	137	185	239	300	353	400	448	469	488
Web	20	183	285	388	476	542	590	625	636	647
Lower flange	20	153	248	359	462	544	602	642	654	666
Furnace	20	546	586	640	678	717	736	762	780	785
Std. Fire curve	20	497	598	658	700	734	761	784	791	797

**Table 6.2: Temperatures of elements for Test 16**

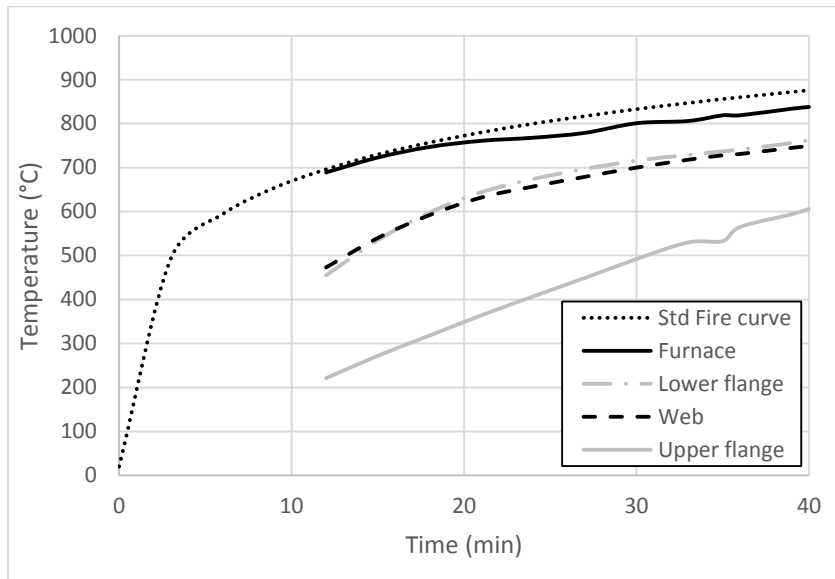


**Figure 6.6: Temperatures of elements for Test 15**

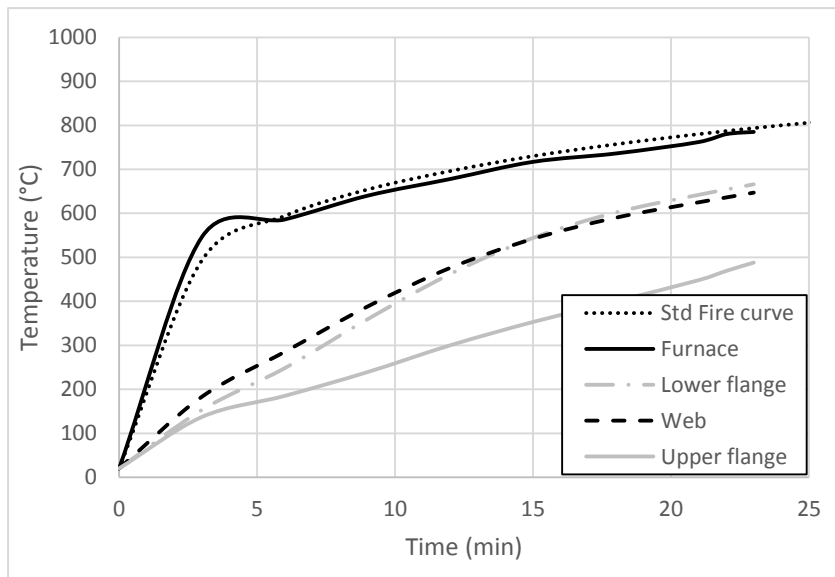


**Figure 6.7: Temperatures of elements for Test 16**

A B503 mesh was placed with 30mm cover above the top of the steel beam. The mesh is described as “The size of the mesh measured 200mm x 100mm x a bar diameter of 8mm, and was placed with the 100mm bar spacing transverse to the longitudinal axis of the test beam”. Based on this there should be 7 bars in the bottom of the slab. However, this is slightly ambiguous and contradicts that shown by authors such as Jiang et al (2014), who show 4 bars with a 200mm spacing. Overall this difference in the number of bars does not make a significant difference to the FBE formulation deflections (approximately 1% at 40 minutes). W&K make reference to the mesh being “cold worked, high yield bar to BS4461”. The yield strength of the rebar was not tested by the investigators but the code current at the time, BS4461 of 1969, gives the characteristic strength of bars up to 16mm in the UK as 460MPa. Hence, as discussed previously an average value of 520MPa is selected for this research. It is noted that a “chicken wire mesh” was placed 10mm below the upper concrete surface to reduce cracking. It is assumed that this mesh had negligible influence on the behaviour, and it is ignored.

A concrete of Grade 30 was cast for the slab, based on cube strengths. The designers used the 30 MPa strength for ambient temperature member sizing design calculations. Hence, it appears that this strength is a characteristic strength, and it is assumed for such a project that standard mix designs would have been used. Thus, based on characteristic cube strengths the analysis parameters have been determined from EN 2-1-1 (BSI 2004) as  $f_{cm} = 33\text{MPa}$ ,  $f_{ctm} = 2.6\text{MPa}$ , and  $E_c = 31\text{GPa}$ . Insufficient data is provided in the literature to make accurate assertions regarding concrete properties.

The software used by Jiang et al (2014), to which results below are compared, is called OpenSEES and has been adapted for use in fire at Edinburgh University. Figure 6.8 illustrates how OpenSEES models composite systems with multiple shell and beam elements. Composite action is simulated using rigid links between beam and slab elements. The advantage of this method is that the ribs of concrete decks can be explicitly considered, along with two-way spanning slabs. The system uses significantly more advanced three-dimensional finite elements and heat transfer equations than presented in this research. However, it utilises similar non-linear behaviour for constituent materials based upon the Eurocode models, except that in this work tension stiffening is included.

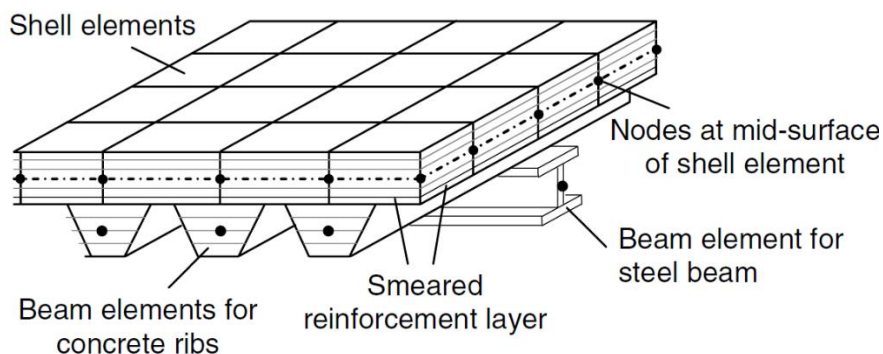


**Figure 6.8: Finite element modelling philosophy employed by OpenSEES (Jiang et al. 2014)**

### 6.5.2 Results and discussion

Graphs showing deflection against time are presented in Figure 6.9 and Figure 6.10 for the two tests respectively. These figures show the experimental deflections, those predicted by the FBE formulation and those predicted by OpenSEES (Jiang et al. 2014). It should be noted that even though the OpenSEES formulation is significantly more advanced, and would presumably require more operator and computational time, the results are comparable. For Test 15 the results obtained by the FBE model and OpenSEES are very similar, differing by only 3.2% on average. With the methods being based on comparable input values and material models this is to be expected. The main difference is the number of reinforcing bars, although due to their positioning they do not make a significant overall contribution (around 1% at 40 minutes). The decrease in deflection rate for both models at 35 minutes can be understood by observing Figure 6.6 which shows the temperature of the upper flange staying approximately constant at this time, which is unexpected. This may have been due to experimental error, equipment error, or from some form of temperature fluctuation within the furnace. It is unlikely to be due to the phase change in steel as this occurs at around 750°C. Overall, the two models predict deflections between 14% and 37% higher than experimental results.

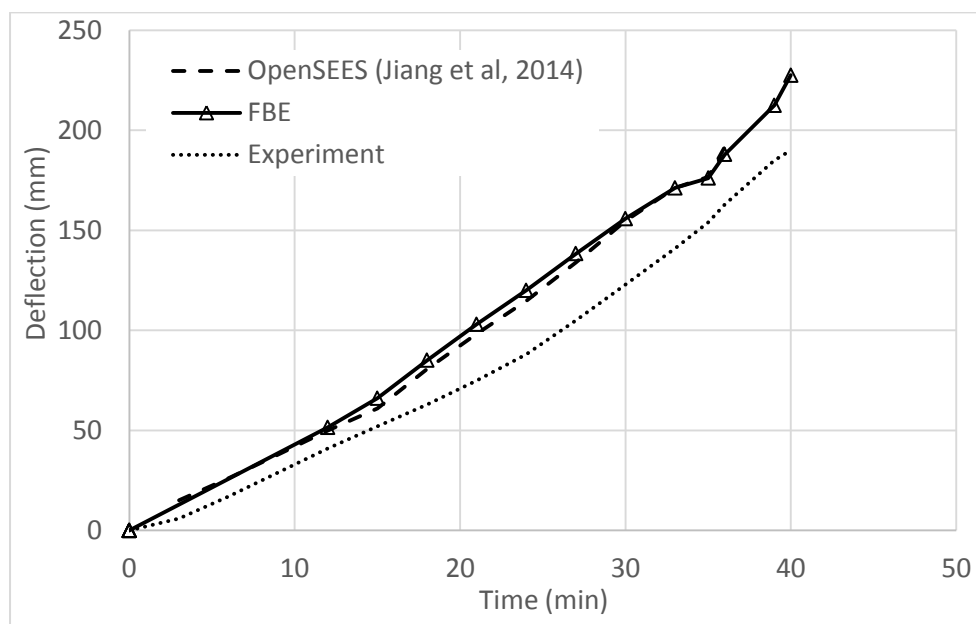


**Figure 6.9: Deflection vs. time results for Test 15 showing experimental results, the FBE results and results from Jiang et al (2014)**

The results from Test 16 are shown in Figure 6.10 and demonstrate that very similar results are obtained between OpenSEES and the proposed model once again, differing by around 5%. An aspect to note is that the FBE model predicts the run-away failure that starts occurring at around 23 minutes, with the model estimating failure to occur at the same time as observed in the experiment. It is important to note that the FBE formulation appears to be able to predict failure loads to a reasonable level of accuracy, and not only deflections. Failure is identified when model convergence can no longer be obtained, either for cross-sectional properties or for global analyses.

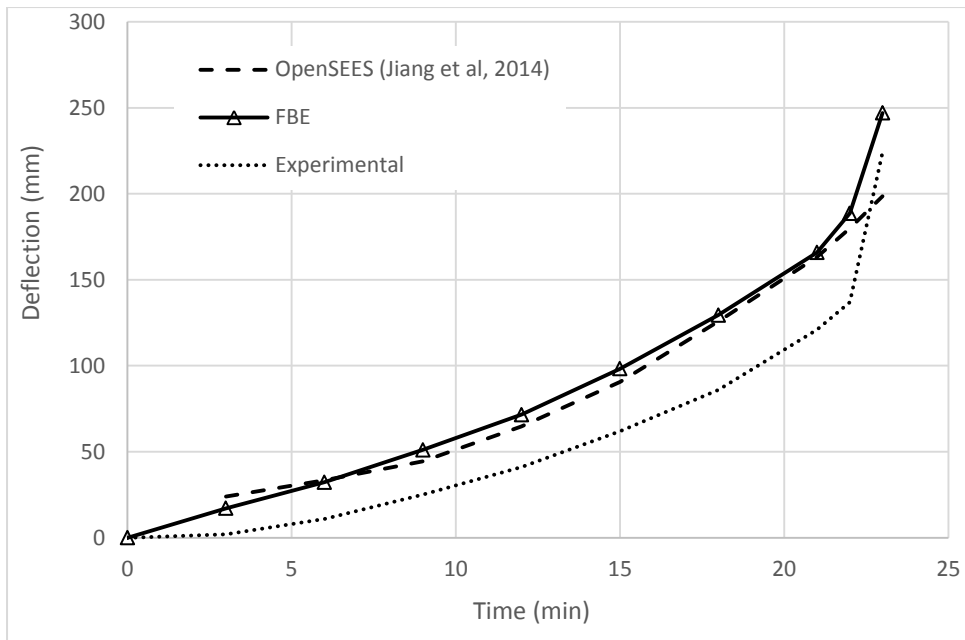


**Figure 6.10: Deflection vs. time results for Test 16 showing experimental results, the FBE results and results from Jiang et al (2014)**

Both models predict higher deflections than the experimental results. This may be due to factors such as:

1. the accuracy of temperature readings during original tests,
2. assumed concrete parameters selected (in the literature it is assumed that characteristic values are provided, and these have been adjusted to be average values in lieu of further information),
3. the influence of boundary conditions (if any amount of restraint did influence tests),
4. non-uniform heating along the lengths of beams,
5. slippage between steel and concrete (No details were reported in the test. Slippage can decrease RTSMs because internal restraint is reduced, thus potentially reducing overall deflections),
6. temperature profiles assumed for concrete slabs in the FBE formulation being different to experimental values (currently temperatures based on the FEA model of Section 5.3.4),
7. the degree to which tension stiffening occurred in experiments, and
8. the stress-strain curves of concrete and steel selected relative to those that tested.

For the items listed above some may cause lower deflections (e.g. reduced temperatures), while others may even increase deflections (e.g. lower concrete stiffnesses predicted by stress-strain curves). There is insufficient data available to make further recommendations how parameters should be updated. The fact that the predicted deflections are slightly higher than the experimental values appears to be consistent with Case Study 2. The numerical results from the case studies relating to changing NAs in Section 4.3 typically indicate that the FBE formulation would under-estimate deflections if the problem is that of Euler-Bernoulli assumptions not holding. However, it is hypothesised that an exception to this may be if RTSL/M forces significantly reduce when sections distort or slippage occurs.

Overall, based on the high level of uncertainty and degree of accuracy obtained by other researchers the FBE results are considered acceptable, and by no means worse than more advanced methods.

## 6.6 Case Study 4: Munich Test 2

### 6.6.1 Experimental setup and overview

Full scale fire tests on composite floors were conducted within a DAST project in Germany in 2010 with detailed information contained in the report by Mensinger et al (2012). The aim of the project was to provide data for developing and calibrating numerical analysis procedures. Real fires were used rather than the ISO 834 standard fire. The test referred to as the Second Munich Test is considered in this research, with the experimental setup as shown in Figure 6.11. This is an excellent setup for demonstrating how the entire design process of a composite floor in fire can be addressed by: (1) an independent floor analysis based upon tensile membrane behaviour (see Chapter 1) followed by (2) the consideration of primary beams using the FBE formulation. Hence, only the primary beams are analysed and considered in this research. Secondary beams are considered to form part of slab panels.

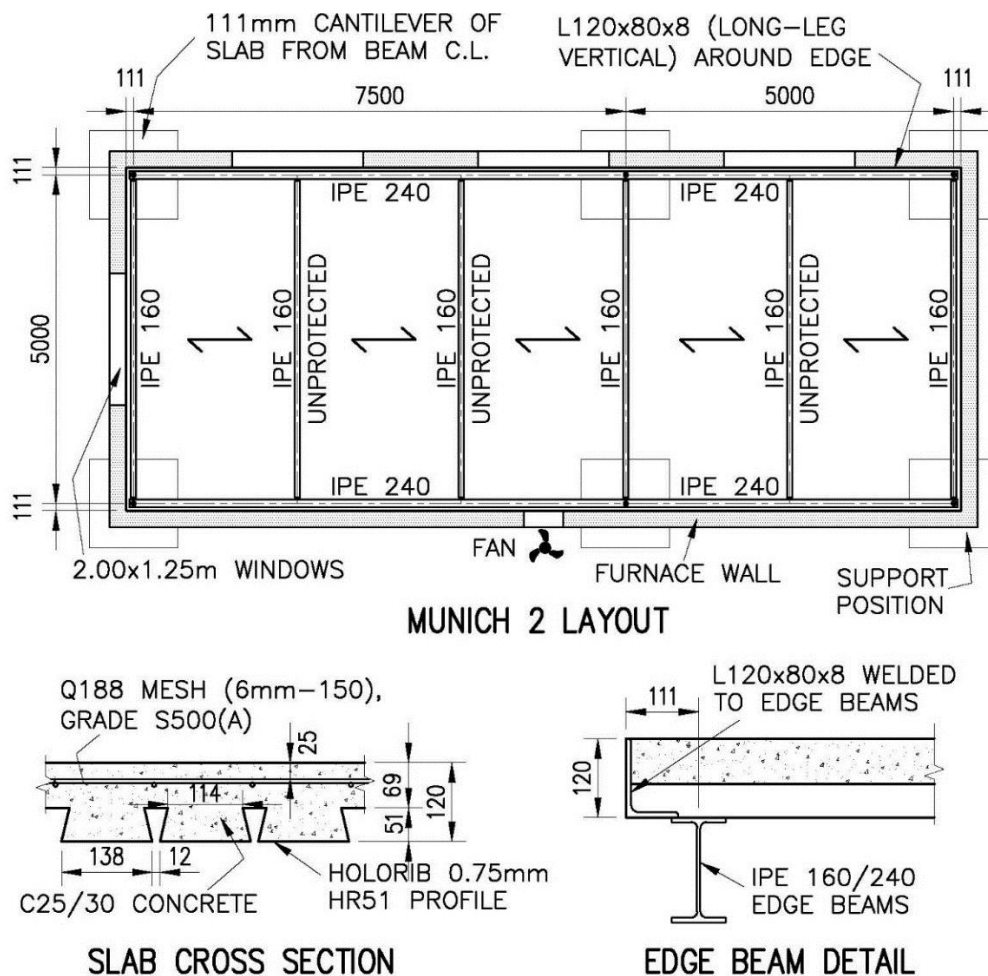
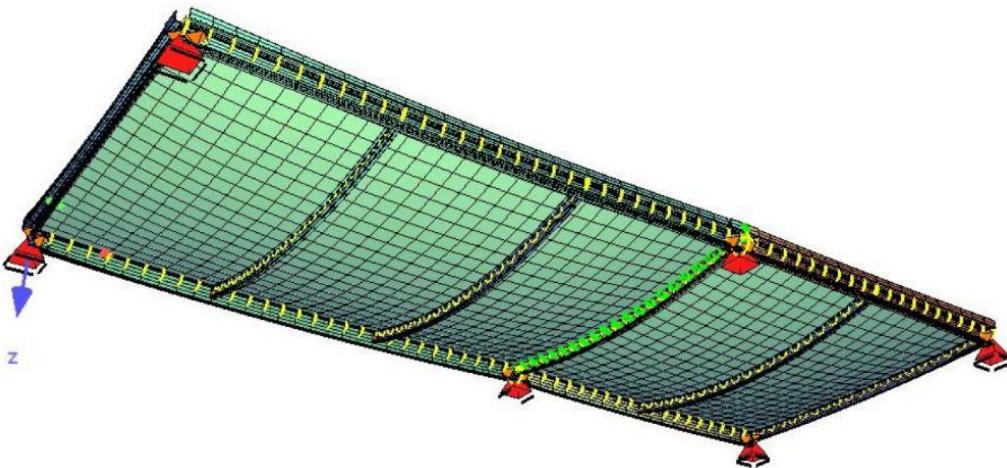


Figure 6.11: Second Munich test experimental layout



These Munich experiments have been analysed by Stadler (2012) in his PhD dissertation, where he developed a simplified analysis model. In this model specially developed shell elements were coupled together to form the composite system. Tension stiffening was included as per Section 5.4. Temperatures were introduced through the use of equivalent thermal loadings. The model was built in Abaqus (Dassault Systèmes 2013) using various specially developed subroutines. Although Stadler's work has provided useful insight for developing this research there are now significant differences in the method formulations, especially since in this work (a) a single beam element is used, (b) thermal forces are applied as RTSL/M forces rather than as pseudo temperature gradients, (c) non-linear analyses can be included, and (d) member stiffnesses are calculated based on a single section rather than having shell elements combined with beam elements. Stadler applied thermal loading to structures by back calculating an equivalent linear thermal gradient that would cause the same thermal curvature as the heated beam system, and then applied this temperature gradient in the FE model rather than loads. Thermal loads were calculated for either concrete or steel elements independently, not systems combined. Material models were converted to equivalent linear elastic stress-strain curves, which is not done in this work. The finite element model developed by Stadler for analysing the system is shown in Figure 6.12.



**Figure 6.12: Finite element model developed by Stadler (2012) for the Second Munich Test**

### 6.6.2 Technical details

For the Second Munich Test a 120mm thick slab acts compositely with steel beams. An equivalent rectangular concrete slab thickness of 111.8mm is calculated, according to EN 4-1-2 (BSI 2005c) and explained in Section 5.3.5. Technical details regarding the setup are summarised in the sections below. The steel decking, *Holorib* HR51, has been ignored in the analysis of the beams as it will rapidly lose strength in the fire and is expected to have negligible influence.

#### **Steel beams:**

The floor consists of IPE 160 and IPE 240 beams with measured yield strengths of 315MPa and 329MPa respectively. The primary beams are passively protected by a layer of intumescent paint giving a 60 minute

standard fire resistance. Shear studs of 16mm diameter and 100mm long were welded in a single line to beams at spacings of between 150 and 300mm. Long fin plates were used for the IPE 240 to IPE 240 connections, whereas end plates were employed for IPE 160 to IPE 240 connections. All bolts are M12 grade 8.8.

For the FBE formulation it is necessary to specify boundary support conditions for all beams, which in general were taken as being pinned. This is also true of the connection between the IPE 240 beams at the top and bottom of Figure 6.11 where connections can be most closely approximated as pinned, rather than assuming that the beams are continuous. Significant rotation can occur in such fin-plates before connections behave as continuous (Al-Jabri et al. 2005), even when considering the slab continuity over the top. However, to illustrate the influence of beams being continuous, or not, a separate analysis has been included with results, as discussed below. Beams are referenced to as being on the “top”, “bottom” or “left” relative to the plan layout shown in Figure 6.11. This naming convention has been adopted to be consistent with the original authors.

### **Formwork**

As formwork an L120x80x8 angle was welded to the edge beams, as seen in Figure 6.11. This angle provided significant additional stiffness and was included in the modelling of the beams, both by Stadler and in this work. The temperature of the angle leg connected to the beam was taken to be the same as the temperature of the top flange, and for the upright section the temperature was taken as the minimum value between the top flange and the concrete slab temperature profile. The latter is necessary for edge protected beams where the steelwork was at a lower temperature than the concrete slab, and the exposed angle would most likely not have achieved the maximum concrete temperature as it would have been partially protected by the beam.

### **Concrete:**

A C25/30 concrete was placed into *Holorib* HR51 panels to provide the deck. The concrete had a measured compressive cylinder strength of  $f_{cm} = 39.4$  MPa. Based on the EN 2-1-2 (BSI 2004) guidelines the tensile strength and elastic modulus were calculated as  $f_{ctm} = 3.59$  MPa and  $E_c = 36.9$  GPa. The width of concrete flange acting compositely with beams was determined based on EN 4-1-2 (BSI 2005c), as presented in Section 5.3.6. This was determined to be 1.05m for the 7.5m spanning edge beams, 0.74m for the 5m spanning edge beams, and 1.25m for the intermediate protected beam. However, as will be discussed in Section 7.5.3 a change in the width of effective flanges generally does not have a large influence on calculated results, except when concrete failure or mechanical loads are dominant.

### **Reinforcement:**

A layer of Q188 welded mesh (6mm bars at 150mm each way) of grade S500(A) was provided with a 25mm cover to the top of the slab. Thus, as per the other case studies, an average yield strength of 560MPa was assumed. The thickness of concrete effective in providing tension stiffening was calculated as  $h_{eff} = 2.5c = 62.5$  mm.



**Fire loading and temperatures:**

A fire load of 548 MJ/m<sup>2</sup> was provided in the form of 33.8 kg/m<sup>2</sup> of timber. The gas temperature and temperatures measured on the various steel beams are shown in Figure 6.13. The mean gas temperature was used in the heat transfer procedure of Section 5.3.4 to calculate concrete temperatures, with the predicted temperature profile shown in Figure 6.14. The upper 60mm of the slab is below 100°C, and this is the zone of the concrete that carries the majority of the load. The lower sections typically fail due to significantly reduced strengths.

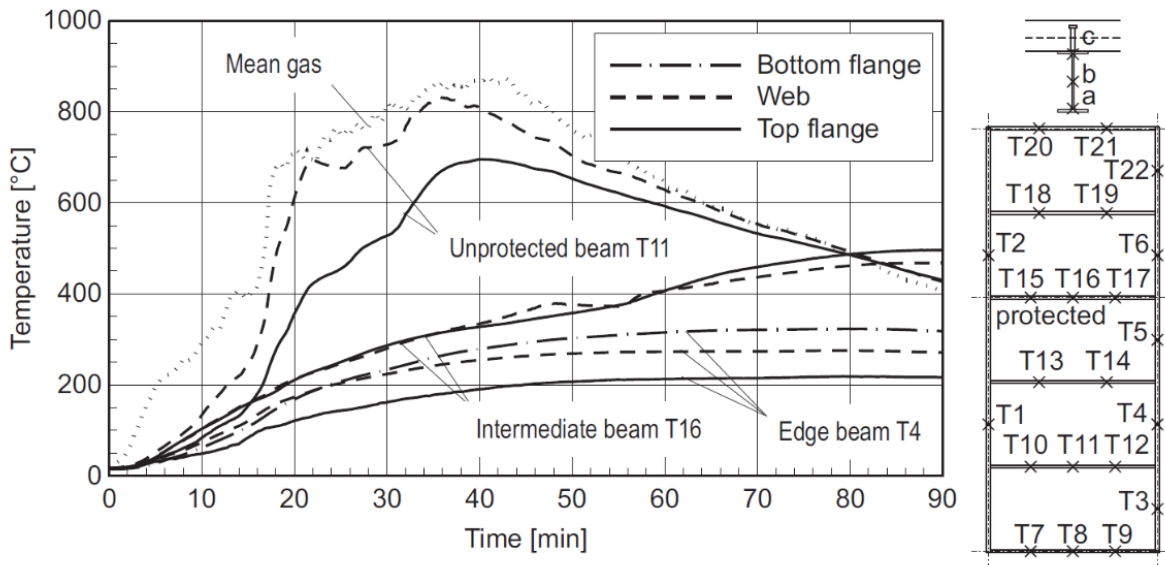


**Figure 6.13: Temperatures in the Second Munich Test for steel beams (Mensinger et al. 2012; Stadler 2012)**

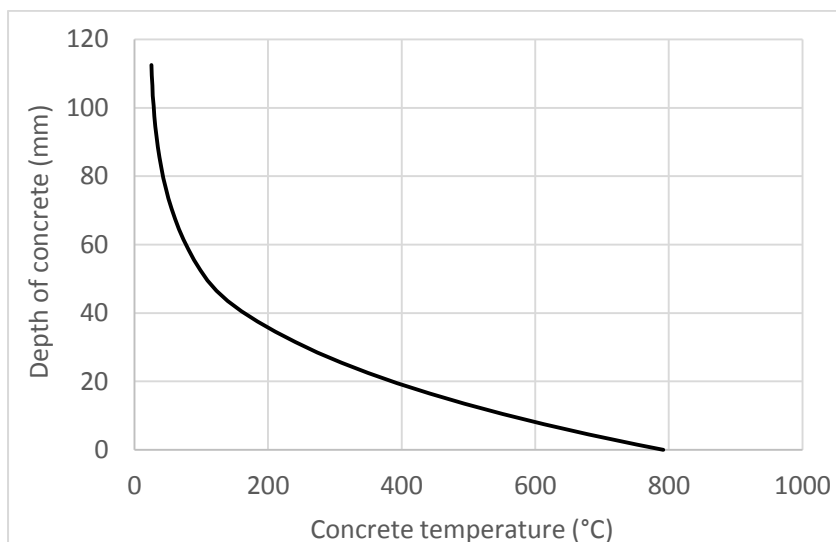


**Figure 6.14: Concrete slab temperature profile at 40 minutes**

The measured temperature of the flanges and web for the various beams are summarised in Table 6.3. It should be noted that even for identical beams with the same exposure, such as the top and bottom right beams, the bottom flange temperatures differed by up to 81°C, or 31%. Hence, even in a small experiment there can

be fluctuations with regards to measurements on identical structural elements with identical passive protection. Such behaviour can also be linked to intumescent paints delaminating during tests.

Beam	Profile	Top flange (°C)	Web (°C)	Flange Bottom (°C)
Edge left	IPE160	244	284	306
Intermediate	IPE160	311	317	389
Edge right	IPE160	233	270	291
Edge top left	IPE240	176	234	257
Unpr. 2nd very left	IPE160	670	809	809
Edge bottom left	IPE240	192	255	280
Edge top right	IPE240	234	311	342
Unpr. 2nd right	IPE160	684	826	826
Edge bottom right	IPE240	179	237	261
Unpr. 2nd left	IPE160	683	825	825

**Table 6.3: Steel temperatures for the Second Munich Test**

### ***Mechanical loading:***

The total load on the floor was 5.1kPa which includes both permanent and imposed load. This is based upon an imposed load of 2.1kPa which was calculated by the original research team as a fire load for an office according to the Eurocode guidelines, and this was applied uniformly using sandbags. Cracks appeared above the intermediate primary beam at 20 minutes and opened up to a few millimetres.

In this research the loading was transferred to primary beams using yield line theory, as presented in Chapter 3. The calculated beam loads and the yield line pattern selected is shown in Figure 6.15. The loading from the short cantilevered section of 111mm was added on as a UDL to the edge beams. It is not immediately clear to what the extent continuity of the slab over the support was lost due to cracking. However, since the rebar did not fracture and cracks commonly open up in concrete under load it is assumed that slab continuity was maintained, and this was used for the primary yield line pattern considered. If the rebar did yield to the point where continuity was lost, a separate yield line pattern has been considered as well to illustrate the change in predicted deflections that can be expected due to change in loading patterns. The results discussed below show that deflections based on the pattern which assumes that continuity has not been lost are closer to the experimental results, and also this is the more probable load transfer system.

With regards to yield line patterns it should be noted that the presence of both the secondary beams and the profiled deck influence predicted patterns. For any slab an increased stiffness in one direction causes a greater proportion of the total load to be carried in that direction. In the experiment the profiled deck has significantly less stiffness perpendicular to the direction of the ribs, but the secondary beams provide additional stiffness in this direction. However, with the high temperatures experienced by the secondary beams their effectiveness is greatly reduced and also cause significant thermal curvature. The challenge of accurately determining yield

line patterns at elevated temperatures is a topic for future research, and conventional layouts have currently been assumed, although two possible configurations have been included. In more complicated beam/slab layouts it would be conservative to consider a number of feasible yield line patterns and design each beam for the worst case loading from the set. For details regarding yield line design refer to Kennedy & Goodchild (2004).

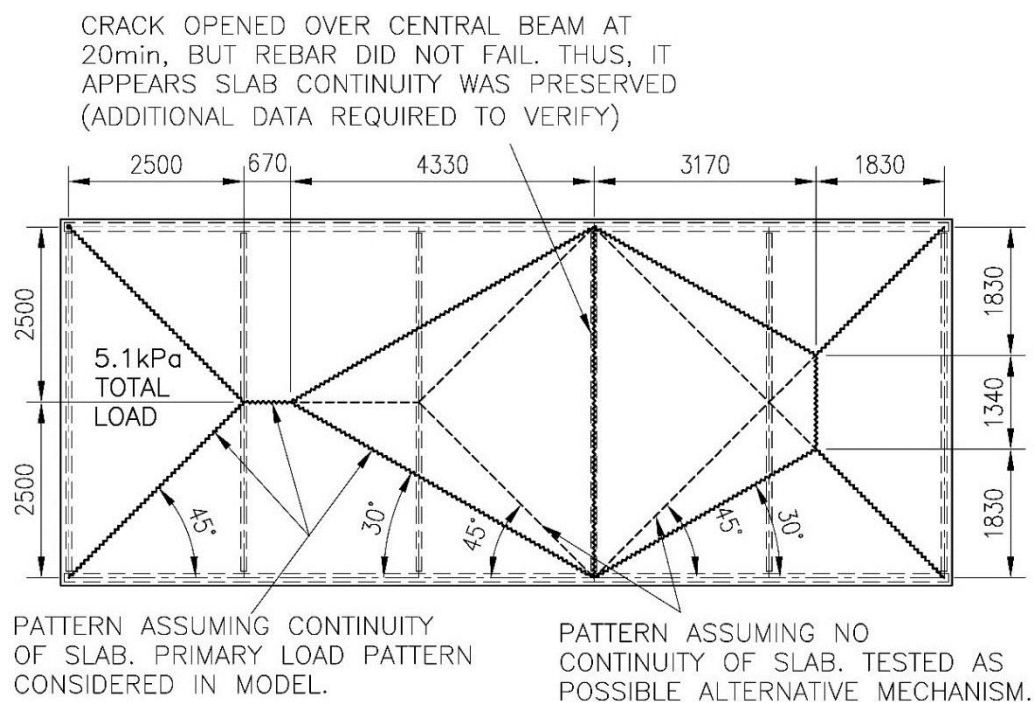


**Figure 6.15: Loading on beams for the Second Munich test showing yield line patterns considered**

### ***Experimental considerations:***

During the testing it was noted that some of the intumescent paint “partly detached” from the beams, although it appears that this was not significant enough to distort temperature readings. The system for measuring deflections was fixed to the walls of the furnace so all deflection readings are relative to the walls. It was noted that there may have been wall deformations that could have affected these readings which could introduce some amount of experimental error. After around 20 minutes of testing a crack of “several millimetres” appeared above the intermediate beam, as discussed above.

After the test it was noted that a layer of the steel decking had delaminated and a void was detected between the steel and concrete. Also, in a separate position the decking had melted through. This makes it extremely difficult to accurately calculate temperature profiles in the concrete, due to varying parameters related to conductive and radiative heat transfer. The decking provides some amount of protection to radiative heat transfer, so positions where the decking lets radiation through would be hotter.

The reason that the First Munich Test was not considered was the number of experimental challenges experienced during this fire test. These challenges included deflection readings being taken from a girder

which was affected by the heat, intumescent paint coming off beams, gaping cracks opening up which allowed smoke and heat to escape, and rebar failure. Such issues are mentioned to reiterate that the modelling of systems in fire is done in the presence of significant uncertainties. Approximate methods could thus be considered desirable, as increased modelling complexity may not add sufficient improvement in accuracy in the presence of high levels of underlying input uncertainty to justify the extra effort.

### ***Temperature profiles***

The profile of the deck used in this test leads to non-uniform temperatures across the slab, where the rebar will be hotter above the flutes and cooler above the ribs. In any FEM system this is challenging to model and would be time-consuming to accurately implement. Hence, in this work the slab was converted into an equivalent flat slab, as discussed above, and constant average mechanical and thermal properties were assumed, as was also done by Stadler.

#### *6.6.3 Results and discussion*

The experimental (EXPERIM.) vertical deflections in millimetres are shown in Figure 6.16 and compared with:

1. Deflections as predicted by Stadler's (2012) model (STADLER). The deflections at the centres of the slabs where catenary action occurred have been included for completeness. In this research these central positions have not been considered as such zones experience a bi-directional load carrying mechanism, which is outside of the scope of this work.
2. Deflections as estimated by the FBE formulation (FBE) using the parameters discussed above. With the boundary conditions playing such a significant role two additional modelling scenarios have been included to illustrate the issues introduced previously, namely:
  - Analysing the top and bottom beams as being fully continuous (BM CONT) over the intermediate support.
  - Assuming no continuity of the slab (SLAB DIS) and allocating loading as shown by the second yield line pattern in Figure 6.15.

The results show that the FBE formulation, in general, provided consistent predictions in relation to the experimental data. For all the points, except the top right position, the average error is 12.7%, which for structural fire engineering predictions is typically sufficiently accurate based on the high number of uncertainties. The error at the top right beam is 8mm, which translates to 57% due to the low baseline for comparison. It could be stated that on the left and right where deflections differ by only 3mm and 1mm respectively that the level of accuracy is in excess of what could reasonably be expected and this is partially coincidental, although it does show that the behaviour of the system has been captured. Overall, this is a novel contribution demonstrating that full structures can be analysed using independent slab methods coupled with an analysis of the main structural skeleton, as done by engineers at ambient temperature.

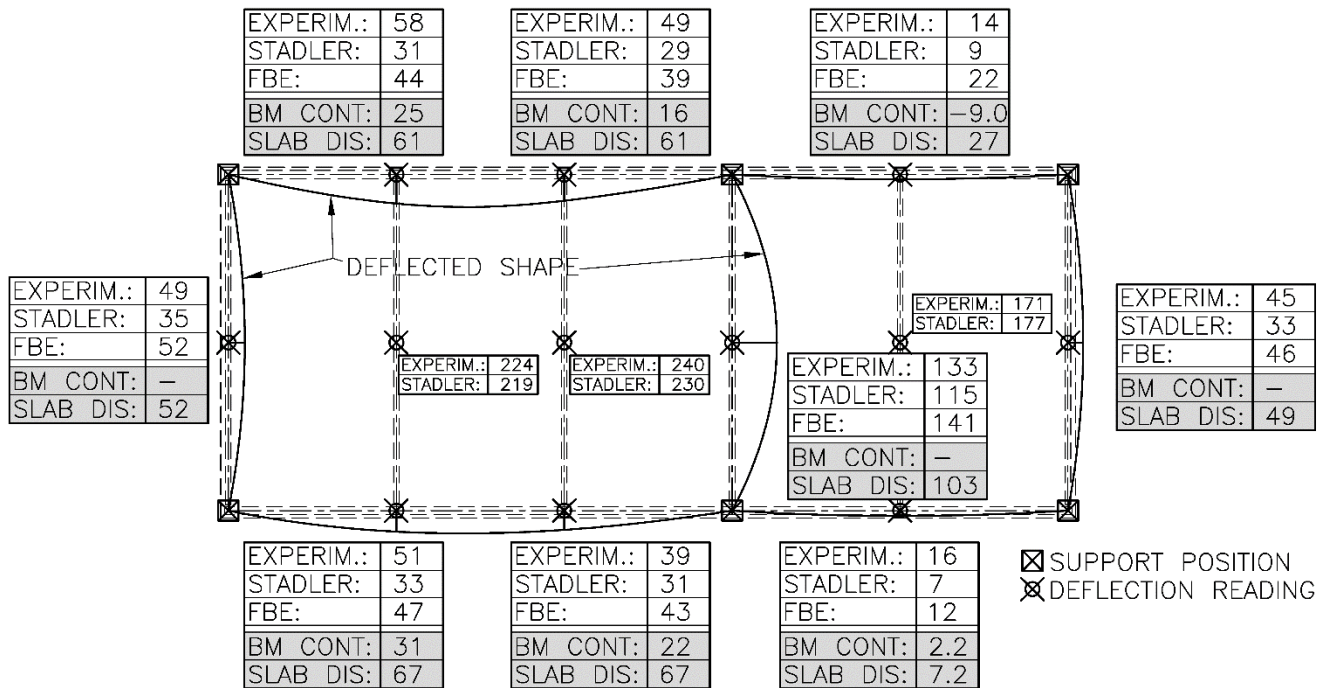


**Figure 6.16: Comparison of deflections between experimental data (EXPERIM.), predictions by Stadler (2012) and the FBE formulation (FBE). All readings are vertical deflections in mm. Additional results from the FBE model are provided considering top & bottom beams as continuous (BM CONT) and the slab as discontinuous (SLAB DIS)**

The difference in primary beam deflections between Stadler and the experiment is 34% on average, with the former being consistently lower. This could be due to a large number of factors. It is interesting to note that the central deflections correspond well to experimental data, although these are directly influenced by the perimeter beams where there are significant differences between experimental and predicted results. Stadler's Abaqus model can account for the behaviour of both the slab and the beams, which the FBE model cannot. However, it can be easily observed that significantly more modelling time is required to create the Abaqus model and include the sub-routines, whereas in this research the models were set up in as little as 10-15 minutes each.

For the top and bottom beams it can be seen that FBE deflections differ significantly from each other when it is assumed that full continuity between members is achieved (BM. CONT), with deflections being much lower than the original FBE configuration. This is as expected since additional stiffness has been created in the system through member continuity. With the top left beam spanning a greater distance than the top right beam, but with them carrying similar loads, it causes hogging on the right hand side. Hence, the negative, upward deflection occurs. The average error between experimental and continuous FBE beam predictions is 76.2%, significantly higher than the original FBE configuration. The continuous beams have a single degree of static indeterminacy, thus the analysis was manually iterated until convergence was obtained. Changing stiffnesses leads to a redistribution of force, which in turn changes stiffnesses, necessitating the iterative

technique. For more complex structures iterative methodologies would need to be built into the software to avoid manual intervention.

The scenario of no slab continuity, which changes yield line loading, leads to: (a) higher deflections of the top and bottom beams as they carry additional load, (b) a small increase in the deflection on the right side, and (c) lower deflections of the intermediate beam. These changes are intuitively expected based on the load patterns. With load patterns being difficult to predict as structural arrangements become more complex it can be observed that results can vary from the original readings by between 7.8% (right edge) and 58% (bottom left side, right hand reading) depending on the yield line pattern assumed. When beams carry additional load there is a combined effect of both the secant bending stiffness being reduced and mechanical loads increasing, both leading to higher deflections.

## 6.7 Conclusions

From this chapter it can be seen that the FBE formulation can be successfully applied to predict the deflections of a number of structural systems including a steel beam, reinforced concrete slab, composite beams and a full composite slab system. Eleven different beams from four different sets of experiments were considered. The FBE formulation describes the deflection of structural elements to a sufficient level of accuracy, sometimes replicating observed deflections closer than alternative methods. However, with the level of uncertainty and number of assumptions inherent to fire engineering design a scatter of results should be expected for any model.

Deflections predicted by the FBE formulation for the simply-supported steel beam typically closely matched those in the literature. At very low levels of stiffness the commercial software used experienced convergence issues. However, it was found that this occurs at conditions where Bernoulli beam assumptions have been violated and at stiffnesses lower than experienced even in severe fires.

Deflections predicted by the model for the single span concrete slab and the experiments by Wainman & Kirby were typically higher than those recorded in experiments. However, FBE results are comparable, or closer, to experimental measurements than predictions in the literature. The over-estimation of deflections could be due to a number of factors, with the temperature profile of the concrete possibly being one the largest contributors, although material properties may also play a part. Further case studies need to be investigated to verify this. Other factors that may influence results include the amount of tension stiffening that occurred in actual tests, boundary conditions, non-uniform heating, experimental errors and other such factors.

It is important to note that the FBE formulation was able to predict the runaway deflections indicating failure of Test 16 at the correct standard fire time, showing that not only deflections but runaway failure may be predicted. From the moment-stiffness graphs presented in Chapter 7 it would be possible to estimate when failure is likely to occur based on the forces that a cross-sections would be required to sustain. .

It was demonstrated that slab systems in fire can be analysed as decoupled slab panels along with separate structural frames consisting of primary beams, which is a novel contribution. It was also shown that assumptions regarding beam or slab continuity played a significant role in the Second Munich Test. Boundary conditions are often difficult to accurately define in any real structure, yet have an influence larger than most other assumptions. Hence, in any analysis it may be necessary to consider different plausible assumptions for boundary conditions to determine how load distribution would affect results. Thereafter, conservative assumptions could be made to design structural members. Assumed slab yield line patterns significantly influenced loading of primary beams in the analysis of a composite slab system in fire.

With the simplicity of the FBE formulation used it would be possible to conduct additional parametric studies on systems relatively quickly such that any potentially non-conservative assumptions could be identified. This will now be considered in the following chapter. In general engineers do not have the luxury of having test results and the simple geometries of these case studies with which to work. Thus, the ability to consider multiple scenarios quickly can enhance the design approach of engineers.



## 7 Chapter 7: Parametric Investigation

### 7.1 Introduction

In the previous chapter structures were analysed using input parameters available in the literature. The selection of input parameters likely plays a more significant role in the accuracy of the results obtained than the numerical modelling procedure employed for analyses. Hence, this chapter seeks to illustrate the influence of design variables on beam properties by conducting a parametric study and sensitivity analysis of the main variables influencing behaviour, such as: temperature, temperature gradients, fire exposure times, material strengths, level of tension stiffening, concrete tension capacities and width of concrete flanges. The vertical deflection of a structural element in fire is typically the primary experimental result which researchers try to replicate when developing and calibrating new prediction models or methods. With the destructive nature of full-scale fire tests it is difficult to measure strains, lateral deflections or any other data that requires access to a structure during testing. Hence, the properties most influential in terms of deflections of beams, namely bending stiffness ( $EI_{\theta}$ ) and Resultant Thermal Strain Moment (RTSM), are explicitly investigated in what follows. The primary objective is to show how  $EI_{\theta}$  and  $M_{\theta}$  vary with changing inputs, by changing one input parameter at a time, such that it can be understood how any uncertainties regarding input parameters may affect predicted deflections. Furthermore, changes in stress and strain distributions across the height of sections are important and investigated, as these lead to the changes calculated in section properties.

The parametric studies have been presented such they build upon each other. The main parametric investigations conducted are: (1) Behaviour of a **steel beam** with varying: (i) temperature and temperature gradients, and (ii) axial / restraining forces. This investigation is followed by considering (2) a **normally reinforced concrete slab** considering: (i) stress and strain profiles to provide an insight into structural behaviour, (ii) concrete tensile behaviour and tension stiffening, (iii) compressive strength, (iv) temperature profiles, and (v) the influence of axial restraint. The concrete slab and steel beam are then combined and (3) the resulting **composite slab** is investigated in terms of: (i) stress and strain profiles, (ii) concrete tensile behaviour and tension stiffening, (iii) the width of concrete flange acting compositely with the steel beam, and (iv) the influence of axial restraint.

The composite slab investigated is composed of an IPE 240 beam with a concrete slab, with properties similar to that encountered in the case studies. Although the configurations investigated in Chapter 6 are all unrestrained, simply-supported structures the methodologies developed in this research are suitable for restrained structures where thermal expansions can induce high axial forces. Thus, the influence of restraining axial forces on beam properties is also covered in this chapter. High tensile and compressive forces are applied to cross sections to simulate restraint, and the resulting properties plotted. Member properties are determined according to the methodology presented in Figure 3.17. It must be understood that only *cross-*



*sectional properties* are being investigated in this chapter, neglecting local buckling. Furthermore, a cross-section in isolation is neither restrained nor unrestrained, rather it is analysed based on the forces applied to it that result from global building analyses. Global analyses are affected by thermal expansions, mechanical forces and restraint. Hence, forces applied to cross-sections simulate any structural restraint present.

At the end of this chapter a summary of the parametric study is presented along with a discussion highlighting how parameters should be considered. It must be noted that with the large number of design variables encountered for each beam results will vary as configurations change, although the results below provide a good indication of general trends. In this chapter the trends in cross-sectional properties with changing input parameters is of greater significance than values initially specified. This chapter develops upon the material models and eccentric beam formulation of earlier chapters, illustrating how they function, and informs how validation studies could have been influenced by parameters selected.

### 7.1.1 Academic contribution

The benefit of the FBE formulation is that by determining a single bending stiffness ( $EI_\theta$ ), RTSM ( $M_\theta$ ) or other such properties the influence of variables can be more easily identified relative to more complex methods. This contribution is novel in that it provides designers and researchers with (a) a better understanding of how results may vary if there is uncertainty regarding design variables, (b) shows which factors are most critical, and (c) highlights some results which may initially seem counter-intuitive but occur due to the interaction of various non-linear properties. The presentation of stresses and strains over the height of a section in fire is also novel, as such results are typically not presented in the literature. By visualising cross-sectional stress and strain profiles encountered structural behaviour for beams can be more readily identified and explained.

## 7.2 Considering material properties and their effects

The total deflection of a beam,  $\Delta_{total}$ , is composed of both mechanical,  $\Delta_{mech}$ , and thermally induced,  $\Delta_\theta$ , components. The total deflection of a beam with uniform properties across its length will thus be (when approximated as a linear system):

$$\Delta_{total} = \Delta_{mech} + \Delta_\theta = f\left(M, N, \frac{1}{EI_\theta}, \frac{1}{EA_\theta}\right) + f\left(M_\theta, N_\theta, \frac{1}{EI_\theta}, \frac{1}{EA_\theta}\right) \quad (7.1)$$

where the bending stiffness ( $EI_\theta$ ) and axial stiffness ( $EA_\theta$ ) are functions of both the mechanical and thermal effects along with the material properties of the beam, i.e.:

$$EI_\theta = f(M, N, M_\theta, N_\theta, \text{Material properties at } \theta) \quad (7.2)$$

The change in  $EI_\theta$  and  $M_\theta$  will be plotted for each parametric study. It should be understood that for cases governed primarily by thermal effects the mechanical deflection contribution ( $\Delta_{mech}$ ) may be negligible, whereas for structures with higher mechanical loading this plays a significant role, as is the situation in Test

16 of Section 6.5. It is important to note this because in some of the parametric investigations  $EI_{\theta}$  and  $M_{\theta}$  increase or decrease at approximately the same rate. In a system where  $\Delta_{mech}$  is small total deflections would then be relatively unaffected as selected material parameters change, whereas for high  $\Delta_{mech}$  the total deflection will vary proportionally to  $EI_{\theta}$ . In most typical commercial and residential type structures the magnitude of the mechanical deflection is generally significantly lower than that caused by thermal effects (Sanad et al. 2000). This is influenced by the fact that at the fire limit state a reduced imposed load is used, in the order of 0.30 to 0.80 of the characteristic value (BSI 2002b), as opposed to 1.5 to 1.6 times the imposed loads at the ultimate limit state.

To be consistent with the case studies carried out in the previous chapter the mean values of material properties have been used, rather than characteristic values, as discussed in Chapter 5. If design calculations were carried out for determining ultimate resistances, rather than deflections, then design values (i.e. characteristic values modified by partial safety factors) would be more appropriate.

### 7.3 Parametric study of a steel beam

To isolate that structural behaviour which is directly affected by the properties of a steel beam the change in stiffness with temperature and temperature gradient is covered in this section for the IPE 240 section shown in Figure 7.1. The graphs produced assume no residual stresses to be present in sections, as generally done in the literature. The behaviour of structural steelwork at high temperatures is more predictable than concrete, as discussed in Chapter 5.

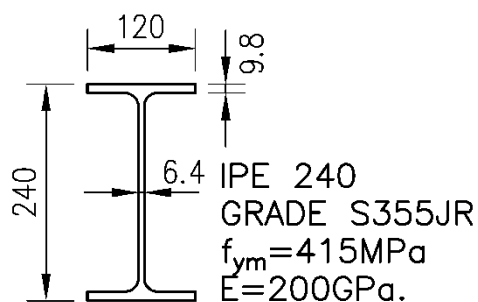


**Figure 7.1: IPE 240 used for the parametric study**

#### 7.3.1 Temperature and temperature gradients

Figure 7.2 shows the change in bending stiffness of the IPE 240 section with differing temperature gradients across the height of the section. The temperature gradient is the difference between the temperatures of the top and bottom flanges. The web temperature is set as the average of these temperatures. The figure shows that stiffnesses generally reduce at approximately the same rate, since the overall average temperature of each section remains the same for a particular web temperature. However, at around 500°C there is the greatest difference in results because of the ratio of change in reduction factors for  $E_{\theta}$  and  $f_{y,\theta}$  according to EN 3-1-2 (BSI 2005b), and the change in RTSL according to Figure 5.6. For the higher temperature gradients the hotter

bottom flange has a proportionally lower stiffness than the top flange due to the non-linear decrease of the material properties. At 500°C the beam with a 300°C gradient has a stiffness 29.3% lower than that with no gradient. As stiffnesses of the flanges change the NA also shifts. For the beam with the 300°C gradient the NA position has sifted 64.6 mm upwards by the time the web temperature reaches 1030°C. This represents a change in NA position of 26.9% of the height of the section, which is a substantial variation.

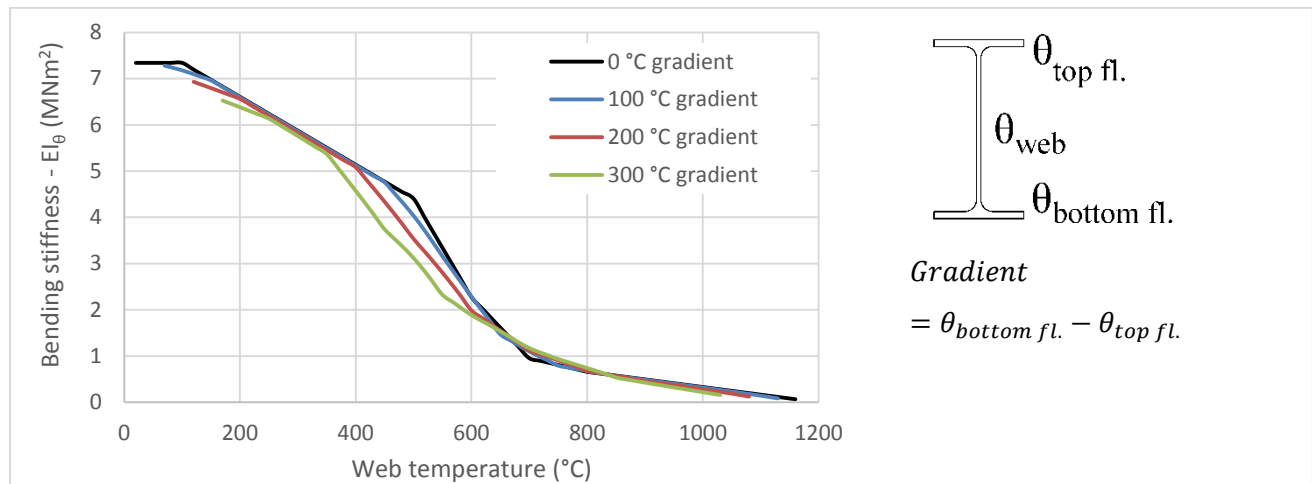


**Figure 7.2: Change in bending stiffness of the IPE 240 with different temperatures and temperature gradients. The average temperature of each beam is the same at each specific web temperature.**

The influence of temperature gradient on both bending stiffness and RTSM is illustrated in Figure 7.3. In this figure the temperature of the web is constant at 400°C, with the difference in flange temperatures being the value of the gradient. Thus, for this figure the average section temperature remains constant for the entire graph but the section properties change significantly with increasing temperature gradient. The bending stiffness decreases with temperature in approximately the same trend as that of the reduction factor for the Young's modulus of steelwork, as shown in Figure 5.4. Here the RTSM has a more unusual trend, which is due to the combined influence of the increasing thermal elongation and decreasing material stiffness. The average rate of material stiffness degradation of all elements exceeds that of steel elongation at a temperature gradient of 500°C (i.e. top flange at 150°C, web at 400°C, and bottom flange at 650°C), which is why  $M_\theta$  increases no further. This is based on the phenomena as previously explained and shown in Figure 5.6. At a temperature gradient of 600°C the temperature of the bottom flange reaches 700°C at which point the phase change occurs, leading to the change in graph slope.

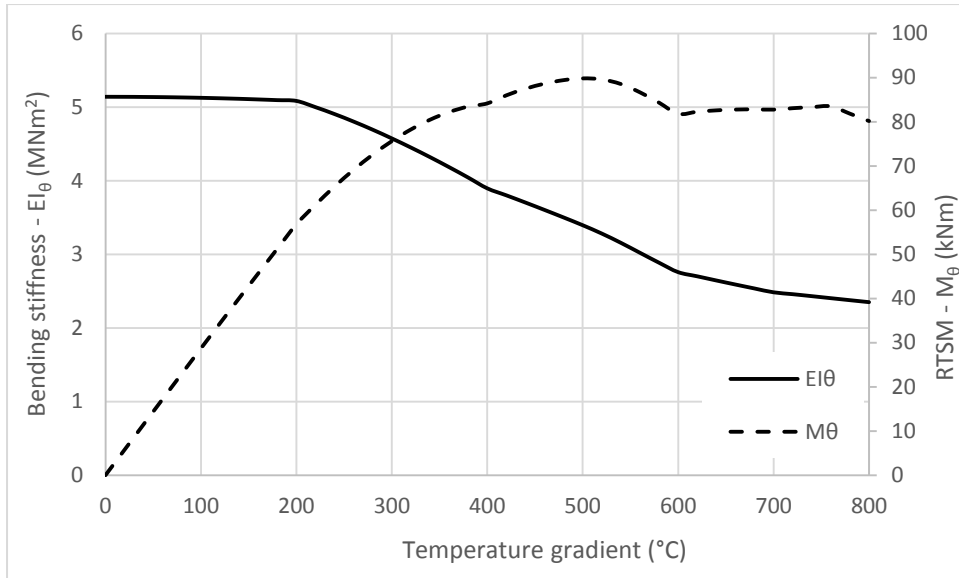


**Figure 7.3: Change in bending stiffness and RTSM for the IPE 240 with varying temperature gradients and web at 400°C**

If the web temperature was set higher the onset of the change in RTSM slope would occur at a lower gradient. In the following chapter it can be seen that temperature gradients in excess of 300°C are unusual, although average temperatures in excess of 600°C are certainly possible for unprotected steelwork. Overall, as would intuitively be expected, there is an increasing RTSM with increasing temperature gradient, but this reaches a maximum value that depends of the ratio of Young's modulus to elongation for all constituent materials at their respective temperatures.

### 7.3.2 Axial / restraining forces

The change of bending stiffness against applied mechanical axial load is shown in Figure 7.4 for the IPE 240 at uniform temperatures of 20°C, 400°C, 600°C and 800°C. At 600°C a mechanical moment of 50 kNm is applied, or a temperature gradient of 300°C, to illustrate the effect of non-uniform stress distributions. An axial load in a beam in fire may be induced either by external forces or by restraint. A RTSL will result in an internal compressive force of the same magnitude for a fully restrained beam.

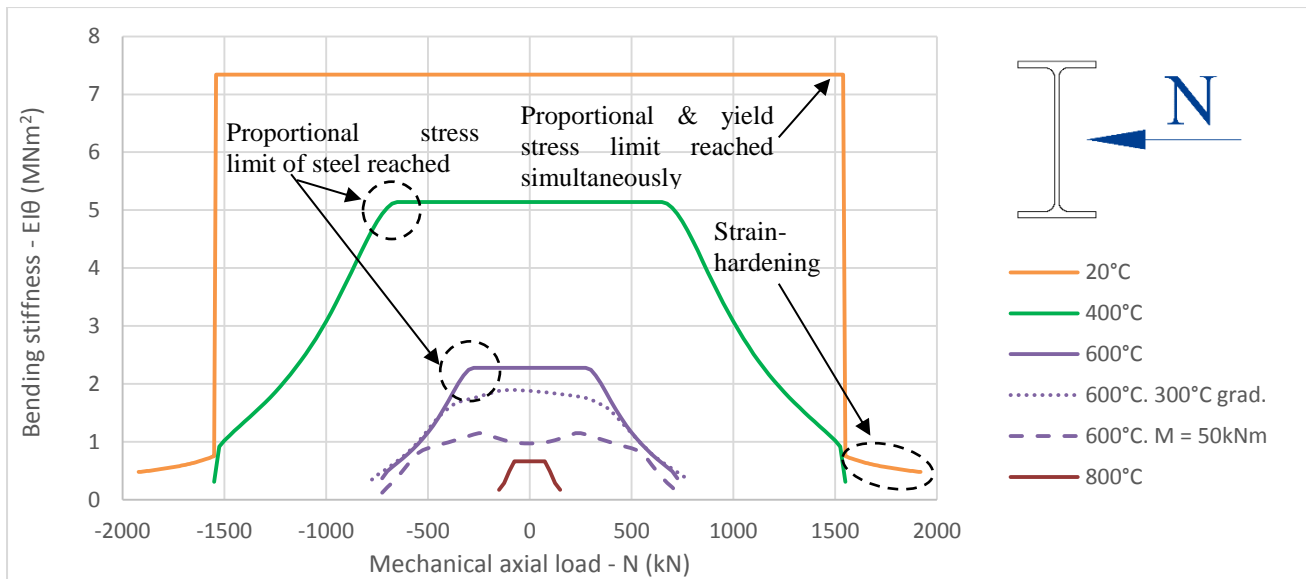


**Figure 7.4: Graph of bending stiffness against mechanical axial load for the IPE 240 beam. For the graph compression is negative.**

With the steel having the same behaviour in tension and compression the graphs are symmetrical about the 0kN mechanical axial load line for the cases when there are uniform stress distributions. It can be observed that for the case with the 300°C gradient the graph is no longer symmetrical. The same applies for when the 50 kNm mechanical moment is applied, although the asymmetry is less pronounced. The central plateau of the graphs end when the proportional stress limit of the steel has been reached and secant material stiffnesses start reducing accordingly with increase in axial load/stress. At ambient temperature the proportional limit is reached at the same time as the yield load, resulting in the sudden reduction. After the steel has reached the yield strain (see Figure 5.5) the capacity continues to increase due to strain hardening, although stiffness is significantly reduced. Above 350°C EN 3-1-2 predicts no strain hardening to occur so the 400°C graph does not follow the same trend beyond  $\pm 1600$  kN as the ambient temperature model. For the heated members the bending stiffness decreases by 56% as the temperature increases from 400°C to 600°C. When yield stresses are reached the beam can no longer sustain any additional axial load and failure ensues. With the inclusion of a mechanical moment or a temperature gradient (which causes RTSMs) the stresses at the outer fibres increase leading to a progressive onset of plasticity and generally lower stiffnesses, as can be seen for the 600°C graphs with the applied moment and temperature gradient.

It is interesting to note the change in steel yield load ( $C_{y\theta} = Af_{y\theta}$ ) and RTSL of an IPE 240 cross-section at different temperatures when no load is applied to it ( $N = 0$  kN), as shown in Table 7.1. Due to the peak in equivalent thermal stress (ETS) at 500°C the RTSL decreases with increasing temperature from 400°C to 800°C, whilst the yield load capacity of the section correspondingly decreases from 1388 kN to 153 kN. The RTSL as a proportion of yield load varies, being 195% at 400°C and 78.4% at 800°C. Hence, at 400°C material yielding would occur if there is an internal load 51% of the fully restrained value, and at 600°C the

load would need to be 34% of the fully restrained value. At 800°C no yielding would occur for a restrained section due to the significantly reduced RTSL value. This highlights both the potentially large magnitude of equivalent thermal forces along with the non-linear trends in material and thermal behaviour that occur.

Steel temp. (°C)	$f_{y\theta}$ - Yield Strength (MPa)	Free thermal strain (-)	$C_{y\theta}$ - Steel yield load (kN)	RTSL (kN)	$\frac{RTSL}{C_{y\theta}}$ (%)	$\frac{C_{y\theta}}{RTSL}$ (%)
400	355	0.0052	1388	2706	195%	51.3%
600	166.9	0.0084	652	1936	297%	33.7%
800	39.1	0.011	153	120	78.4%	128%

**Table 7.1: Comparison of yield load against RTSL for different temperatures of the unloaded IPE 240**

The implications of the results above are that fully restrained steel beams may buckle when heated without any load applied to them. Structures need to be designed to accommodate such effects to prevent failure. At high temperatures significant material degradation leads to reduced RTSL/M forces. However, at this stage mechanical loading effects may become more dominant as stiffnesses are significantly reduced.

#### 7.4 Parametric study of a concrete slab

The slab shown in Figure 7.5 will now be investigated to determine the influence of design parameters. The width has been selected to match that used in the composite beam parametric study in Section 7.5, such that results between the studies can be compared. The slab is 1500mm wide, with C25/30 concrete and 8mm diameter bars at 200mm centres with 30mm cover. The temperature profile across the thickness of the slab is determined using the FEA model presented in Section 5.3.4, which is based upon the standard fire, with the fire applied from below only.

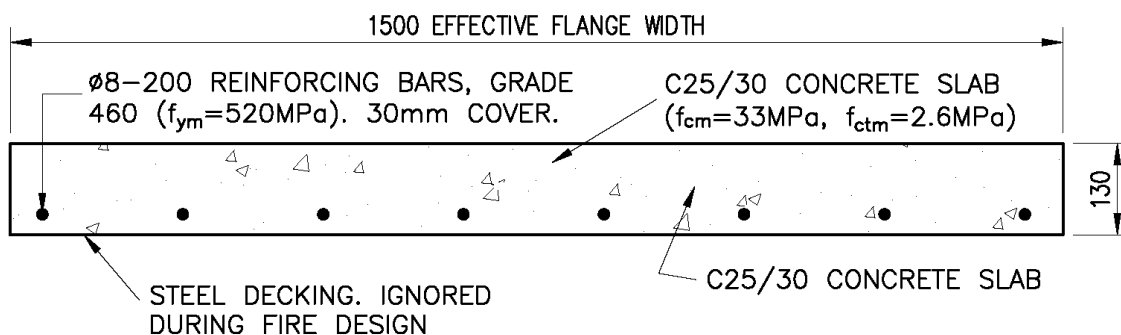


**Figure 7.5: Concrete slab used for the parametric study with reinforcement placed on the bottom**

It is important to note that for this case study and the following study on a composite slab the properties calculated for cross-sections are *independent of the load path followed*. This means that a small section of concrete that cracks in an earlier iteration may become uncracked in a later iteration and carry load again. For the FBE model it is possible to make materials properties either (a) path dependent or (b) path independent, with the former meaning that once an element of concrete has cracked it cannot become uncracked and carry load again. The reason that the load path of cross-sections has not been considered is that it introduces an

additional variable that is difficult to quantify independently and to identify its influence. In any structure various load paths could be followed depending on how mechanical loads are applied, the behaviour of connections and the spread of fire. For instance if a beam is restrained it will initially go into compression as it heats up, resulting in all concrete remaining uncracked, whereas an unrestrained beam may experience significant cracking initially. This issue is a topic requiring future research.

#### 7.4.1 Stress and strain profiles

##### **Stress profile at ambient temperature**

Before commencing with the parametric study of this slab it is important to understand the stress-strain profile over the thickness of a slab at ambient temperature as this provides insight into how design parameters influence results. As a simple verification exercise Figure 7.6 presents the stress distribution across the height of a 200x500 deep reinforced concrete beam at failure due to pure moment, when considered with the proposed prediction model. The beam has three 25mm diameter bars with 30mm cover at the bottom, and material parameters are as shown in Figure 7.5. Tensile capacity has been ignored to produce the “textbook” stress profile shown in Figure 7.6 (SABS 2000). The neutral axis occurs at 342mm above the base. This figure highlights how the typical compression block shape is captured by the prediction model. As the beam is made deeper the stress block will become more constant in the upper portion. Conversely, this stress profile is often lost in thinner slabs in fire where: (a) the neutral axis is near the top of the section, (b) non-uniform thermal actions cause a very complex stress-strain state as will be explained below, (c) tension capacity is considered, and (d) material properties vary across the height of the section due to temperature profiles. The influence of such factors on stress-strain profiles will now be illustrated.

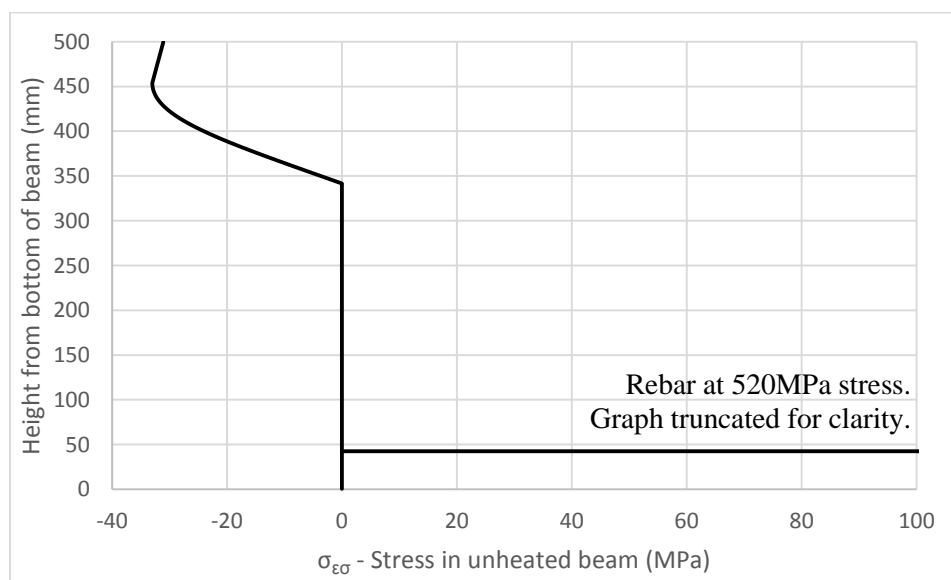


**Figure 7.6: Stress profile in a 200x500 deep reinforced concrete beam at failure**

### ***Stress and strain profiles in fire***

The stress-strain behaviour of the 130mm thick slab will now be considered when exposed to a 30, 60 and 120 minute standard fire, but when no mechanical load is applied. The predicted temperature profiles for the different exposure times are as shown in Figure 7.7. The thermal strain profiles follow approximately the same trends as the temperature profiles.

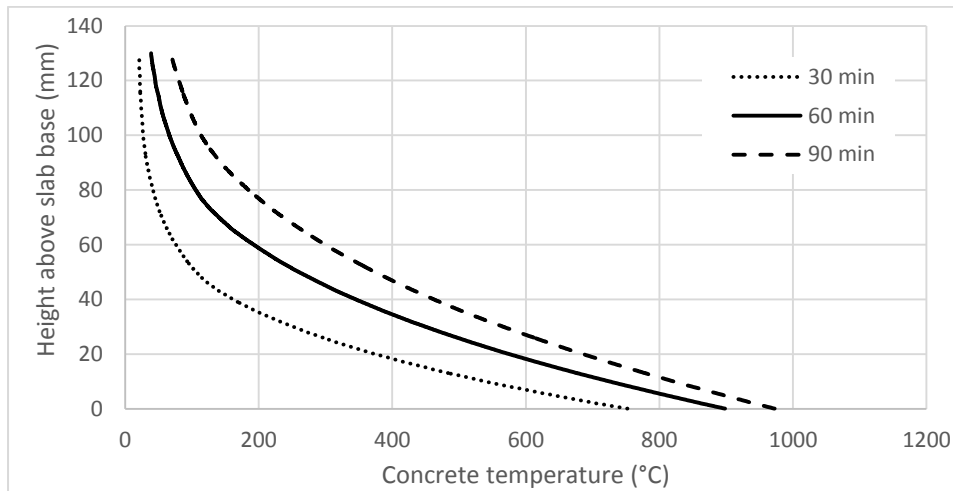


**Figure 7.7: Graph showing temperature over the height of the 130mm slab when exposed to different periods of a standard fire**

The thermal strains cause both RTSLs, due to net elongations, and RTSMs, due to temperature gradients. The concrete has a temperature dependent stress-strain curve (see Section 5.3.2) leading to changes in both strength and stiffness over the depth of the section. The total strains resulting from the RTSL/MS are shown in Figure 7.8 for the 60 minute exposure time. The NA occurs 97.6mm above the base of the slab. The position of zero strain does not coincide with the NA due to the RTSL causing axial strain. The total strain graph illustrates how the assumption of plane sections remaining plane is enforced. In this case almost the entire section has elongated due to thermal forces, except for the uppermost 2.1mm. The concrete thermal strain has a constant maximum value for the lowest 11.6mm because the concrete has reached temperatures in excess of 700°C. Above 700°C EN 2-1-2 predicts a constant elongation of 1.4% for siliceous concrete, as shown in Figure 5.11. The thermal strains decrease above this height as the temperature declines until almost zero strain at the top of the section. The mechanical strains caused by internal cross-sectional restraint are then calculated as the difference between the total and thermal strains, as per Equation 3.2, giving the unusual mechanical strain trend shown. The lowest 24.3mm and uppermost 4.6mm are in compression, while the remainder of the section is in tension.



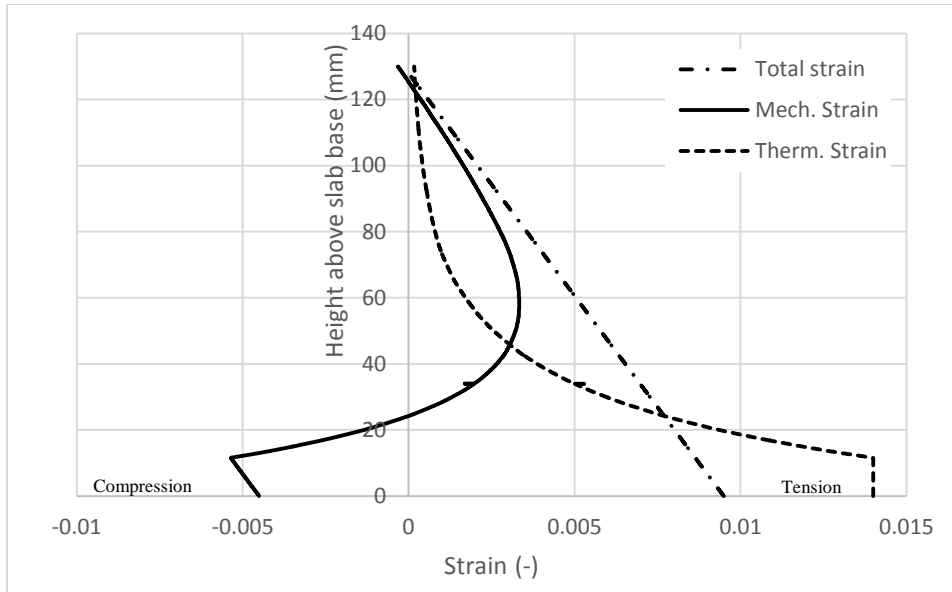


**Figure 7.8:** Graph showing the total, mechanical and thermal strains over the height of the 130mm slab for a 60 minute standard fire exposure time

Figure 7.9 shows the change in mechanical strain over the height of the slab for all three fire exposure times, while Figure 7.10 presents the change in secant Young's modulus values for these sections. Based on mechanical strains and temperatures the mechanical stress profiles are calculated, as shown in Figure 7.11. For the central region the strains have exceeded the cracking strain of the concrete, thereby causing failure. Hence, there is the zone of zero stress and zero stiffness between approximately 30mm and 120mm of the height. The entire compression block is carried within the upper 4-10mm, leading to the localised high stiffness. The influence of (a) material degradation, (b) thermal forces, and (c) differing mechanical strains cause the lower 30mm to have a very irregular stress pattern.

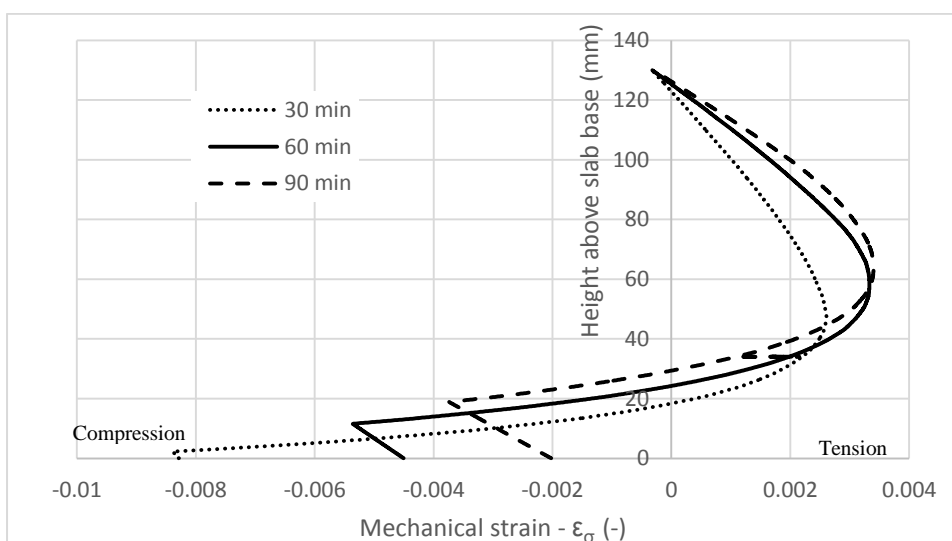


**Figure 7.9:** Mechanical strains over the height of the 130mm slab for different standard fire exposure times.

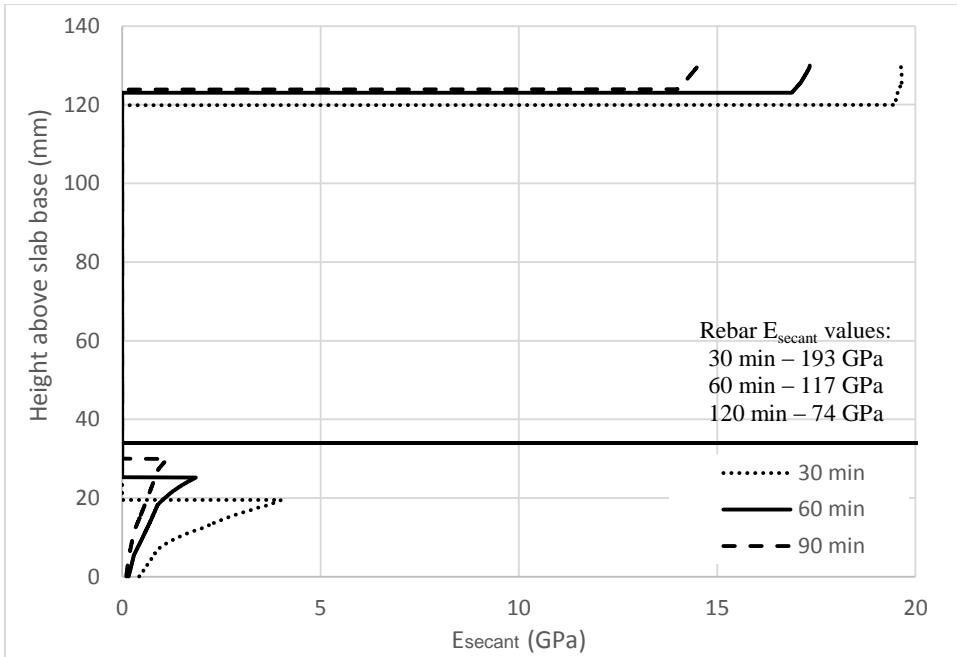


**Figure 7.10:** Graph showing secant Young's modulus values over the height of the slab at different fire exposure times

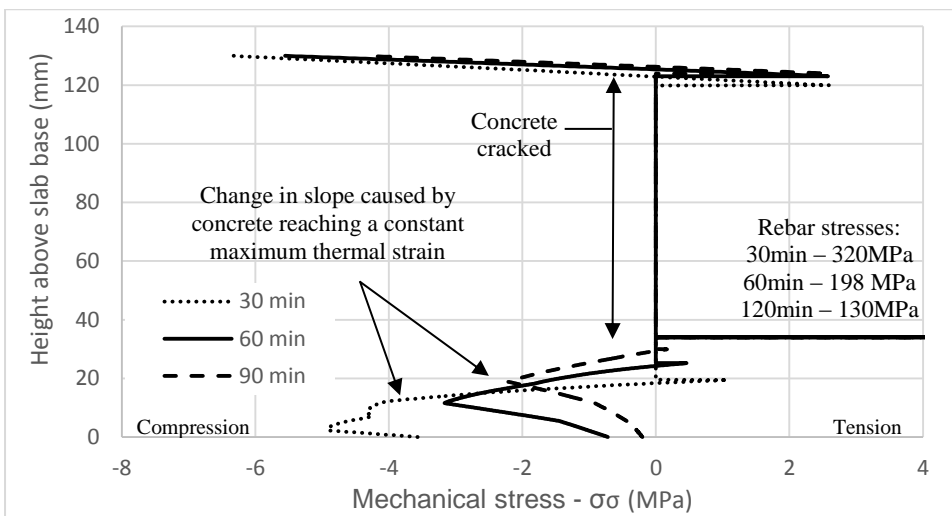


**Figure 7.11:** Graph showing the internal stresses caused by mechanical strains over the height of the 130mm slab when exposed to different periods of a standard fire.

The trends observed in Figure 7.11 are typically not included in research publications. However, stress profiles observed can be easily verified by considering simple static equilibrium of a cross-section, and this has been performed in the FBE model. The above stress and strain profiles are novel for illustrating the behaviour of reinforced concrete when exposed to thermal effects. When concrete tension capacity, mechanical loads and tension stiffening are included the stress-strain profiles explained above are complicated further. Hence, there can be unusual perturbations in graphs as different limits of stress, thermal elongation, cracking strains, tension stiffening and compressive capacity are reached. In spite of such non-linear

behaviour the graphs presented in the forthcoming sections are relatively consistent, while perturbations are highlighted.

The change in slab properties with varying input parameters will now be addressed that the stress-strain state of a heated slab has been illustrated. The behaviour discussed below should be considered in light of the stress and strain profiles given above.

#### 7.4.2 Concrete tensile capacity and tension stiffening

The structural behaviour of a slab undergoing bending is influenced by the tension capacity and level of tension stiffening that occurs, as addressed in Chapter 5. In this section slabs with the following properties are considered: (a) slabs with neither tension capacity ( $f_{ctm} = 0$ MPa) nor tension stiffening (TS), (b) for  $f_{ctm} = 2.6$ MPa (based on a C25/30 concrete) but no TS, and (c) for  $f_{ctm} = 2.6$ MPa and the inclusion of TS. The change in bending stiffness and RTSM with increasing standard fire time exposure is shown in Figure 7.12 for the slab configurations when no mechanical forces have been applied to it.

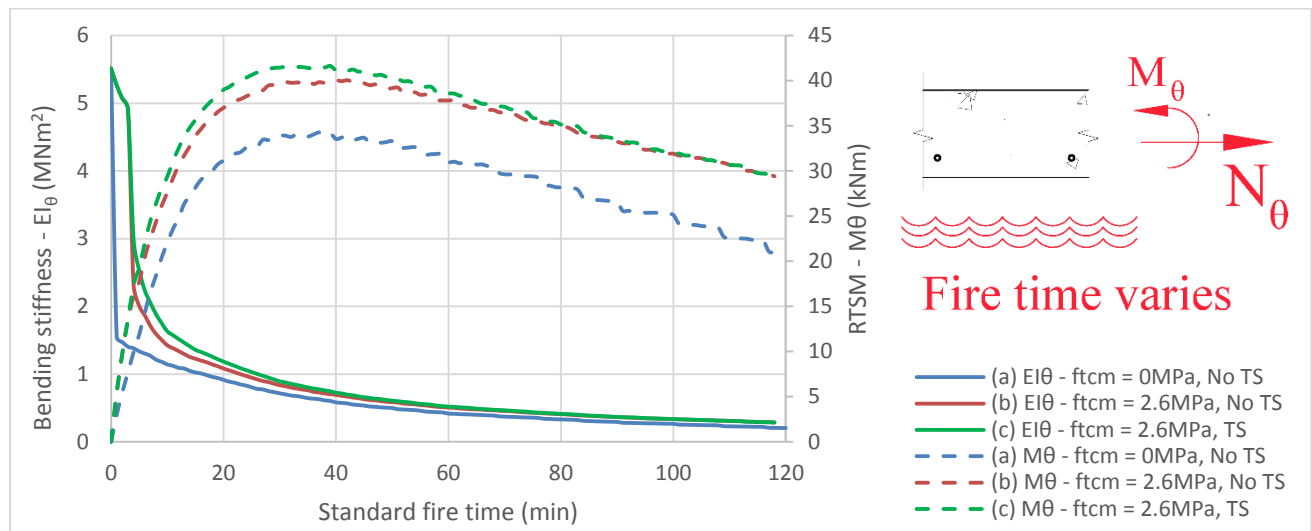


**Figure 7.12: Graph of bending stiffness and RTSM against standard fire time for the concrete slab with no applied mechanical forces, with (a) neither tension capacity ( $f_{ctm} = 0$  MPa) nor tension stiffening (TS), (b) for  $f_{ctm} = 2.6$  MPa but no TS, and (c) for both  $f_{ctm} = 2.6$  MPa and TS.**

From Figure 7.12 it can be seen that the lowest stiffness and thermal moments are obtained when no tensile capacity or tension stiffening (TS) are assumed, as per (a). Initially bending stiffnesses increase significantly when concrete tensile capacity is included, as per (b), but this influence decreases as the slabs heats up and RTSMs induce cracking. A further increase in stiffness and thermal moments is observed in (c) when tension stiffening is also included. With the rebar being in the lower hotter zone of the slab an increase in the slab's effective stiffness causes a higher thermal thrust from the rebar resulting in the net increase in thermal moments. The magnitude of the difference between calculated bending stiffnesses for (a) and (c) vary with time. This difference is 250% at 3 minutes, 33% at 15 minutes and then stays approximately constant at 25% between 30 and 90 minutes, increasing to 38% at 120 minutes. The difference in curves (b) and (c), due to

inclusion of tension stiffening, varies with time between 29% at 4 minutes, to 6.8% at 30 minutes and 0.5% at 90 minutes. With the slab being thin only a small area of concrete is available to provide tension stiffening, according to Figure 5.20. It can be seen for the composite slab parametric study conducted below that the influence of tension stiffening increases as the neutral axis migrates outside of the concrete slab of the composite beam, and the area available to provide tension stiffening increases. This is because the stress profile in the concrete slab becomes more uniform, as the NA of the section occurs within the steel section, leading to a lower stress gradient.

The rate of increase in  $M_{\theta}$  versus decrease in bending stiffnesses for configurations (a) to (c) is approximately the same, as illustrated by Figure 7.13. For this figure the slab with properties above is considered as a 3m long cantilever with no loading, but exposed to the same standard fire temperatures. Deflections are calculated as per Case Study A in Section 4.3.1. It can be seen that except for the initial 3 minutes the curves follow almost identical trends. At 3 minutes the difference between (a) and (c) is 48%, which reduces to 7% at 10 minutes and 2% at 30 minutes. From these results it can be concluded that the analysis of this particular slab would not be sensitive to assumptions regarding tensile properties, provided that mechanical deflections are limited. This is a positive result in terms of fire engineering prediction models as often tension and tension stiffening behaviour in concrete is difficult to take into account, as explained in Section 5.3.2, and consequently generally excluded from models. However, with a difference in bending stiffness of between 25% and 38% between 30 and 120 minutes mechanical deflections would vary depending on whether tensile capacity and tension stiffening are included or not. Overall these results highlight why it is possible that prediction models in the literature may accurately replicate the deflections of experiments in spite of not fully capturing the stress-strain profiles of members.

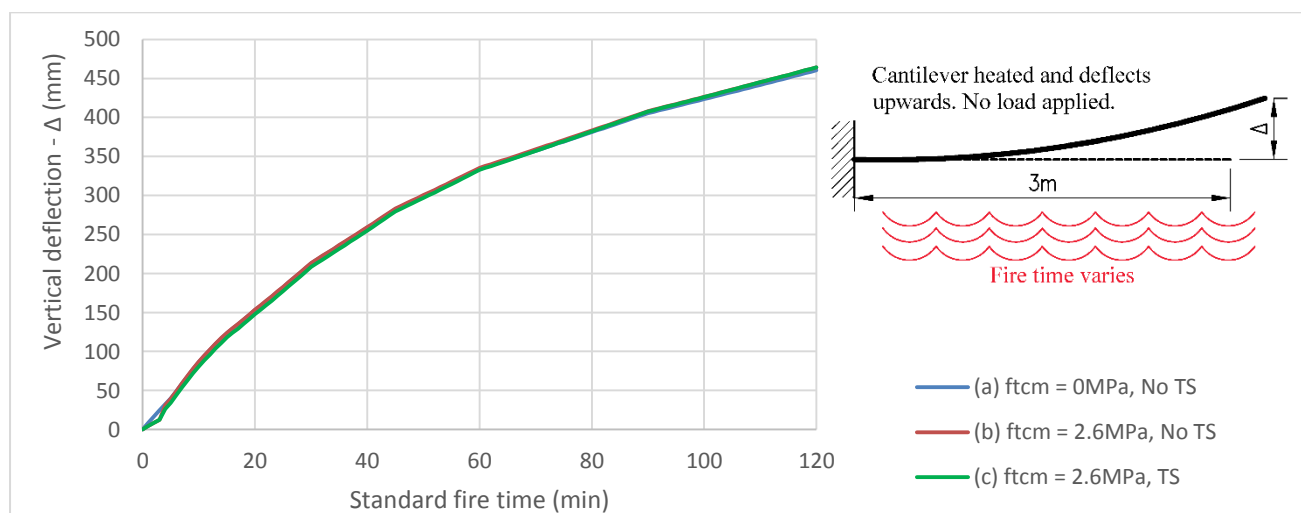


**Figure 7.13: Deflections of a 3m long cantilever slab with varying tensile properties when heated in a standard fire**

This variation in behaviour is further illustrated in Figure 7.14 which shows the change in bending stiffness and  $M_{\theta}$  against applied mechanical moment for the 130mm slab, when exposed to a constant 60 minute fire. It

can be seen that properties all reduce with increasing applied forces, and they reduce at approximately the same rate. The reduction in stiffness is due to the applied mechanical moments causing higher stresses which leads to lower secant stiffnesses. After 15kNm the onset of concrete crushing causes the discontinuity in slope.

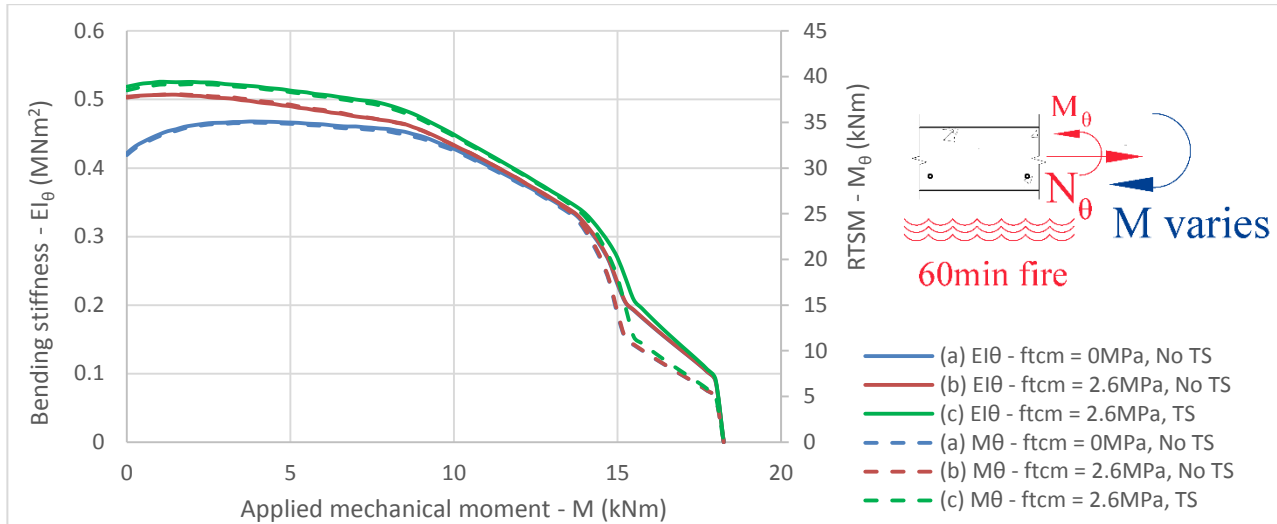


**Figure 7.14: Graph of bending stiffness and  $M_\theta$  against applied mechanical load for the 130mm concrete slab**

Somewhat different behaviour is observed when the applied mechanical moment is plotted against both the axial stiffness and the RTSL of the cross-section, as shown in Figure 7.15. The axial stiffness follows a different path from that of the bending stiffness, reaching a peak at around 10kNm with a much more sudden decrease at failure. The initial increase is caused by the increasing mechanical moment causing additional concrete in the upper and middle portions of the slab to experience strains below cracking strains, thus resulting in a larger cross-section carrying load and contributing to axial stiffness. However, since such areas are in the cooler middle and upper sections they contribute negligibly to the RTSL. The RTSLs follow the same trend as the thermal moments. If the slab was uniformly heated the trends followed would be very different. This behaviour relating to the change in axial properties is of great importance when restrained beams are considered.

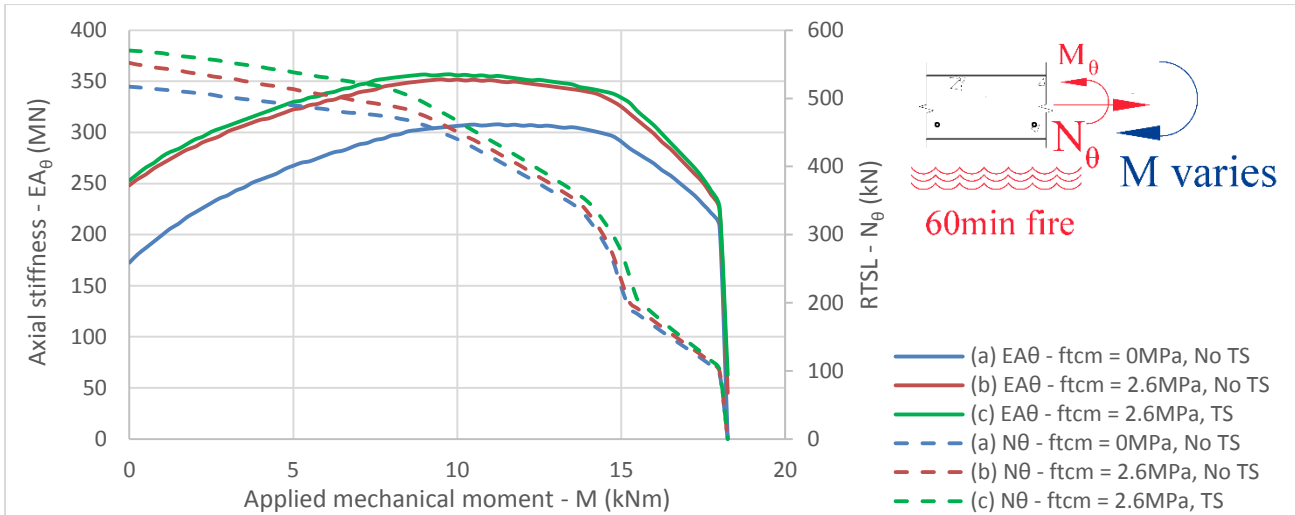


**Figure 7.15: Graph of axial stiffness and thermal axial force against applied mechanical load for the concrete slab**

### 7.4.3 Concrete compressive strength

Concrete in a slab is generally assumed to fail at the cylinder strength, and this property is typically obtained from tests or based upon mix designs. However, due to rebar and containment from concrete elements surrounding a structural section it is possible for the section to experience stresses higher than cylinder strengths before failure occurs, as discussed in Section 5.3.2. Furthermore, there is often scatter in compressive test results obtained versus those expected at the time mix design is done. In light of this Figure 7.16 is a graph showing the change in bending stiffness and thermal moment with increasing concrete strength ( $f_{cm}$ ) for fixed fire exposure times of 30 and 60 minutes, while  $f_{cm}$  remains constant at 2.6 MPa. An additional configuration is included at 30 minutes where  $f_{cm}$  is a function of the cylinder strength as per EN 2-1-2 (BSI 2005a). In this graph a mechanical moment of 10kNm has been applied throughout and the remaining parameters are as per Figure 7.5.

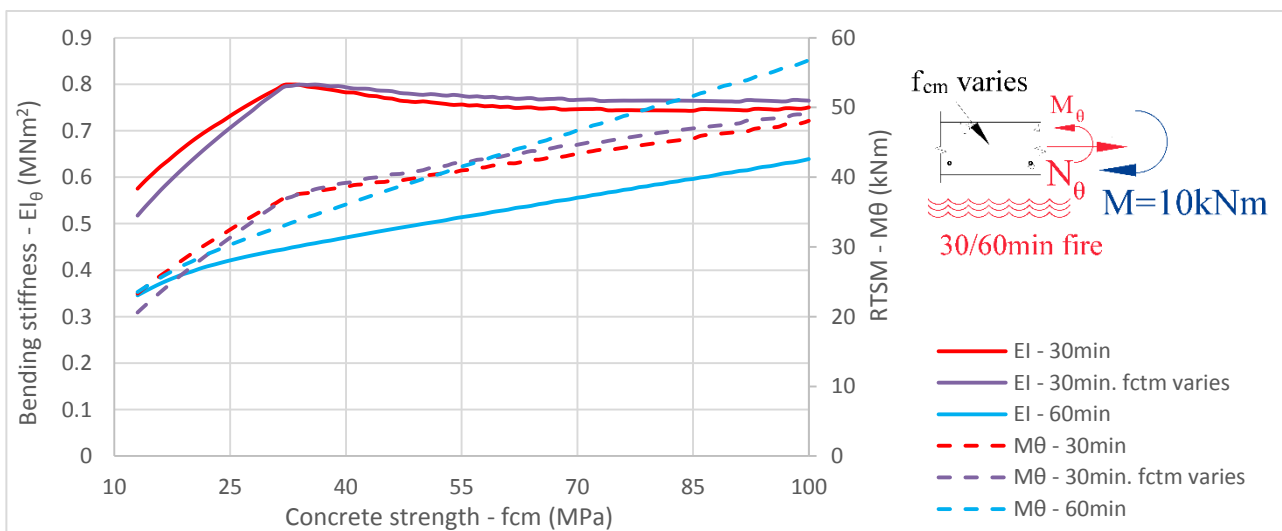


**Figure 7.16: Graph of bending stiffness and  $M_{\theta}$  against concrete strength**

For the slab exposed to the 30 minute fire there is an initial stiffness increase until a cylinder strength of 32MPa is reached. After this point the bending stiffness starts decreasing. This decrease is due to the significant increase in  $M_{\theta}$  which causes higher stresses in materials, thus reducing secant stiffnesses in the upper portion of the slab. It can be seen that when the tensile strength is a function of the compressive strength the stiffness is lower until 33MPa, at which point the tensile strengths of the configurations with constant  $f_{ctm}$  and varying  $f_{ctm}$  are equal. After this point the latter graph has a higher tensile strength, and a higher resulting higher stiffness, as would be expected. The trend for slab with the 60 minute fire exposure time does not have the same peak at 33 MPa, instead it has a less notable change in slope at 19MPa.

From the above it can be observed that stiffnesses and thermal forces do not necessarily vary at the same rate as concrete strength changes. Hence, it can be understood that the use of an incorrect value of concrete strength would lead to errors in predicted deflections, with the magnitude varying depending on the trends presented. Between 30MPa and 50MPa (a feasible magnitude of error for the situation when characteristic strength values are used rather than test results) the difference in bending stiffness for the 60 minute slab is 14% while the RTSM is 23%. For the 30 minute slab the differences are -2.2% and 12.5% respectively. Hence, deflection values predicted by models will vary depending on the concrete strengths selected, and how much containment effectively occurs during experiments.

#### 7.4.4 Temperature profiles

For most experiments reported in the literature the temperature profile across the depth of a concrete section is not declared, and for all real-world designs is not known. Hence, it is necessary to use one of the various models available for predicting the temperature of concrete, as discussed in Section 5.3.4. In this section the following slab temperature models have been included: (a) EN 2-1-2 (BSI 2005a), (b) EN 4-1-2 (BSI 2005c), (c) equations from Wickström (1986), and (d) the finite element analysis (FEA) proposed in Section 5.3.4. As previously discussed other models such as those summarised by Gao et al (2014) could be utilised. This section highlights the influence of differing temperature profiles on results. EN 2-1-2 and EN 4-1-2 only provide temperature profiles for the first 100mm through a slab. Hence, the case study was adjusted to 100mm thick to avoid extrapolating EN tabulated data and adding any additional uncertainty regarding inputs. Furthermore the EN codes only provide temperatures from 30 minutes onwards, so times prior to this have not been plotted for (a) and (b).

For the different prediction models a comparison of the resulting bending stiffness,  $EI_{\theta}$ , and RTSM of the 100mm thick slab with increasing exposure to the standard fire is shown in Figure 7.17. Initially the RTSMs increase rapidly. The maximum RTSM is reached when the rate of material stiffness degradation exceeds thermal elongation. In general it can be seen that there is good agreement in the trends between the graphs. The predicted difference in RTSM when applying the EN 2-1-2 or EN 4-1-2 temperature profiles is 21% at 120 minutes. As previously discussed in Section 5.3.4, the difference is presumably due to the EN empirical curves being based on observations from different slab thicknesses. The proportional increase between RTSM

and bending stiffness between the four temperature curves is relatively similar. At 30 minutes if the slab was considered as a 3m long cantilever, as in Section 4.3.1, the vertical deflection is 264 mm for EN 2-1-2, 284 mm for EN 4-1-2, 297 mm for Wickström's profile, and 303 mm for the FEA.

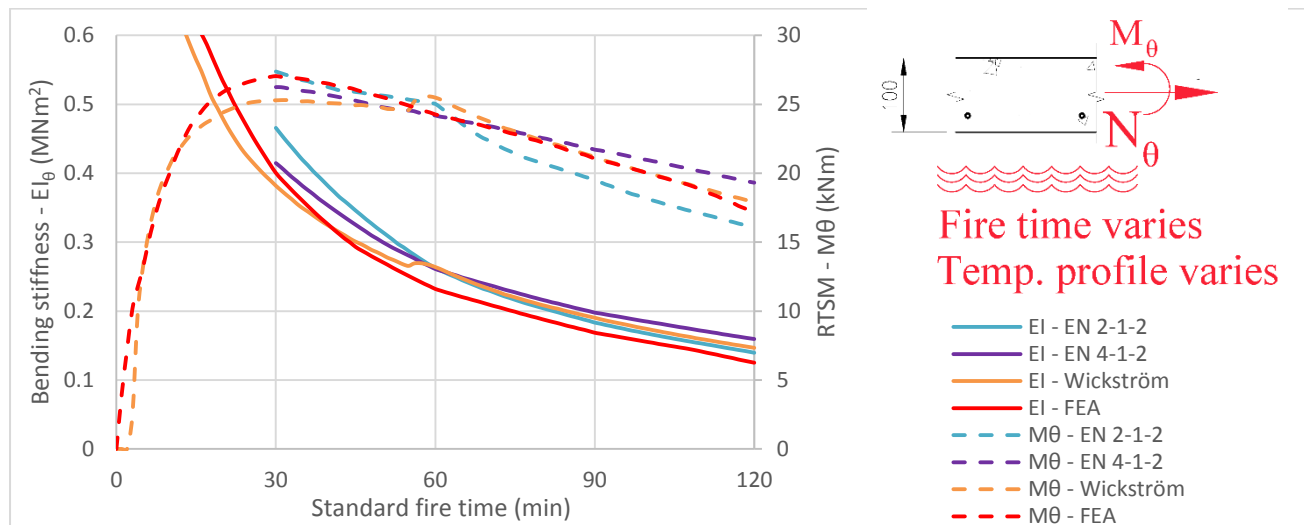


**Figure 7.17: Graph of bending stiffness and  $M_{\theta}$  against standard fire time exposure for different temperature profiles in a 100mm thick slab**

The localised increase in  $EI_{\theta}$  and RTSM at 56 minutes when using Wickström's profile is not a function of the temperature profile itself, but rather caused by the stress-strain condition at that specific time, and could also occur with any of the other curves. At this time the increasing temperatures of the lowest concrete areas result in a higher curvature moment which causes concrete at 94mm from the base to have strains within the cracking limit, thus suddenly becoming uncracked and providing additional stiffness. A similar phenomenon occurs with the EN 2-1-2 graph at this point, although it is less pronounced.

From the above it can be seen that depending on what temperature profile is selected structural moments can vary between being negligibly different and 20-25% different. This difference is exacerbated when slabs with non-uniform profiles are analysed, as is the case for ribbed slabs, or when "real" fire models are considered. It should be noted that temperature plays a significant role in the design process but is often difficult to define accurately.

#### 7.4.5 Axial restraint

Axial restraint will lead to compressive forces in the slab as it tries to expand. To simulate restraint mechanical axial loads are applied to the 130mm thick slab. The change in stiffness with increasing axial compressive load is shown in Figure 7.18. Compressive loads are shown as negative values, following the sign convention used throughout this research. The case with the slab at ambient temperature (0 min) along with those corresponding to 15, 30, 60 and 90 minute fires are shown. For the ambient temperature case the stiffness progressively decreases as mechanical axial load increases, with the graph following the non-linear concrete stress-strain curve trend of Section 5.3.2. For the cases which have been exposed to fire there is



partial tension in the slab due to the lower portions expanding, this leads to cracking across sections, following Section 7.4.1. Thus, as compressive forces increase the stiffness rises to a maximum as tensile forces are overcome and sections progressively become uncracked, after which the stiffness decreases in a similar trend to that experienced at ambient temperature. The graphs are shown up to the point of failure.

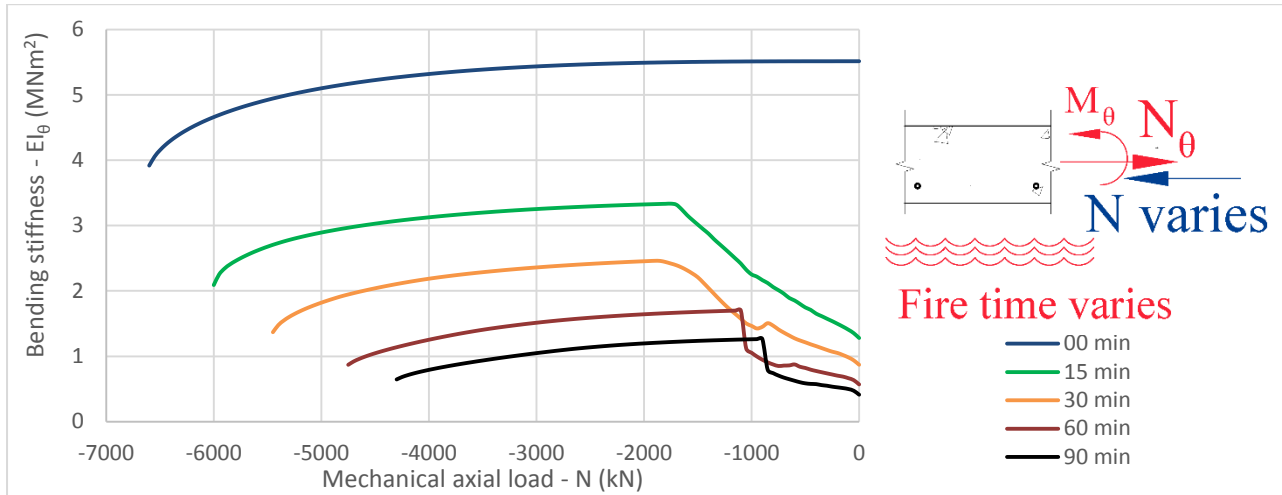


**Figure 7.18: Change in bending stiffness with applied axial compressive load for the concrete slab. For the graph compression is negative.**

Figure 7.19 plots the change in RTSL with increasing axial load. The RTSLs increase and vary as mechanical forces increase. This is due to the fact that as compressive forces increase stiffnesses rise due to sections becoming uncracked. Additional heated concrete can then contribute to thermal forces. The sudden increase in RTSL for the 60 and 90 minute graphs occur when a significant amount of concrete changes from cracked to uncracked in a single step. The maximum RTSL for the slab exposed to the 90 minute fire is 2246kN, which occurs for a 900kN compressive axial load. At this point the entire slab has gone into compression. After this the stiffness decreases as portions of the concrete enter the descending branch of the stress-strain curve, as per Figure 5.10. This maximum RTSL is 370% higher than initial value for the same slab. Hence, it can be seen that structures can be very sensitive to restraint, and large forces can be induced.

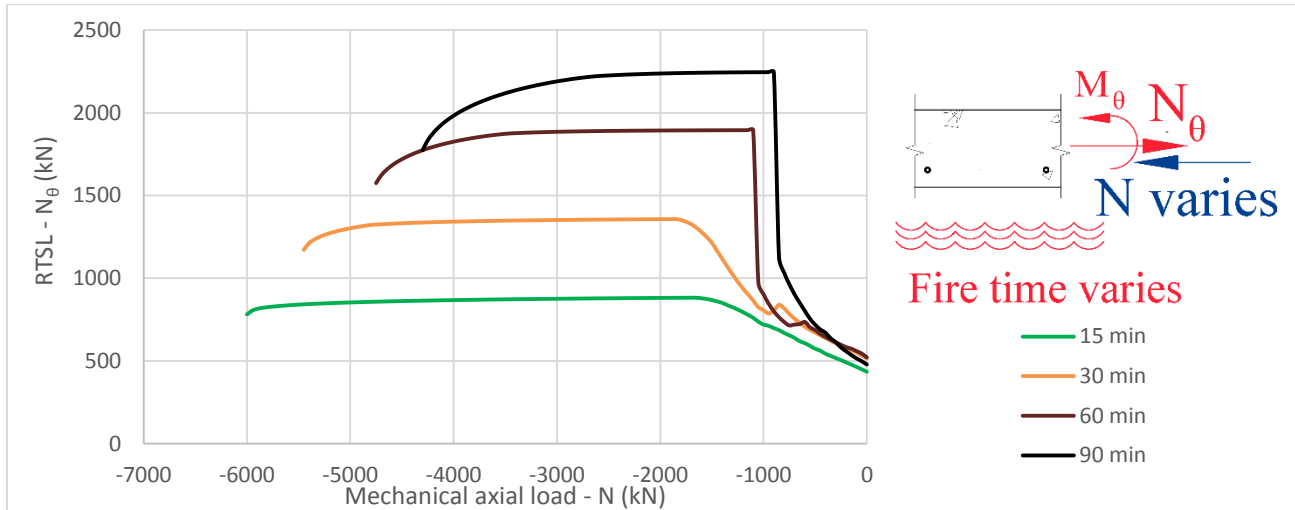


**Figure 7.19: Change in RTSL,  $N_\theta$ , with increasing applied axial load for the concrete slab**

Table 7.2 summaries the initial (no axial load) and maximum values of bending stiffness and RTSL for the different configurations. For the slab the net axial elongation will be positive until mechanical axial forces exceed RTSL values (i.e.  $|N| > |N_\theta|$ ). Full axial restraint occurs when  $N + N_\theta = 0$ . The mechanical axial load required to induce full restraint is also listed in Table 7.2. Due to the maximum RTSL plateaux that occur in Figure 7.19 full restraint may occur at the maximum RTSL. From Table 7.2 it can be seen that stiffnesses typically reduce with increasing fire exposure time, and the magnitude of mechanical force required to induce full axial restraint also increases with fire exposure time.

Std. Fire Time (min)	$EI_\theta$ (MNm <sup>2</sup> )		RTSL (kN)		$N$ required to provide full axial restraint (kN):
	Initial	Max.	Initial	Max.	
00	5.51	5.51	-	-	0
15	1.28	3.33	435	882	-610
30	0.870	2.46	515	1358	-831
60	0.569	1.70	521	1894	-1894
90	0.412	1.26	478	2246	-2233

**Table 7.2: Summary of thermal stiffness, RTSL and axial restraint load for the 130mm slab exposed to different standard fire times.**

## 7.5 Parametric study of a composite beam

This study has been conducted on the composite beam cross-section shown in Figure 7.20, which combines the 130mm slab and IPE 240 beam considered in Section 7.3 and 7.4 respectively. The ambient temperature ultimate limit state bending resistance of this section is 270kNm using the South African standard SANS 10162-1 (SABS 2011b) and characteristic strengths. If the beam is fully utilised at ULS with permanent and imposed loads being of approximately the same magnitude, as can occur in composite structures, the fire limit state bending moment will be around 123kNm. This is based upon a quasi-permanent load combination factor

of 0.3 for the imposed loading according to EN 1990 (BSI 2002a). In this section a moment with a positive magnitude refers to one that causes the bottom of the section to go into tension, i.e. a sagging moment.

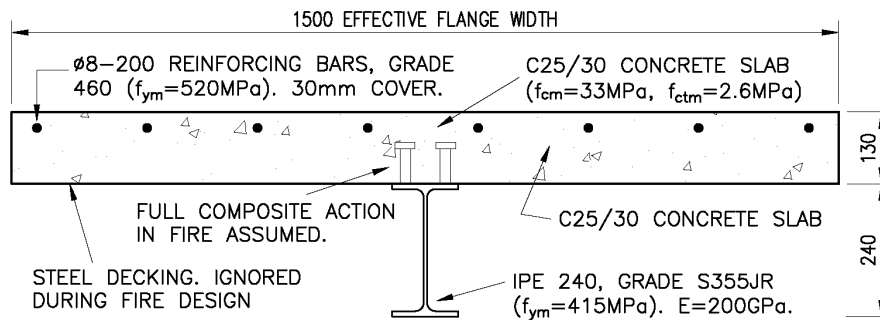


**Figure 7.20: Cross-section considered for the parametric study based on a typical office block beam size**

In this section the temperatures of the flanges and web of the steel beam have been determined according to the guidelines in Section 4.3.4.2.2 of EN 4-1-2 (BSI 2005c), which provides heat transfer equations for composite beams in fires. These guidelines assume the web and bottom flange to have the same constant temperature. Both an unprotected, or bare, steel beam configuration and a passively protected beam configuration have been considered. For the protected beam a 10mm contoured layer of perlite has been used to provide passive protection, and this provides approximately 60 minutes of fire resistance for the system considered when mean values are used. A thicker layer would be required to give the same rating when characteristic values are used. Concrete temperatures have been set according to the finite element generated profile of Section 5.3.4. The temperatures of the bare steel beam and passively protected beam are shown in Figure 7.21. For the passively protected section the steelwork initially heats up more slowly than the lowest portion of the concrete slab.

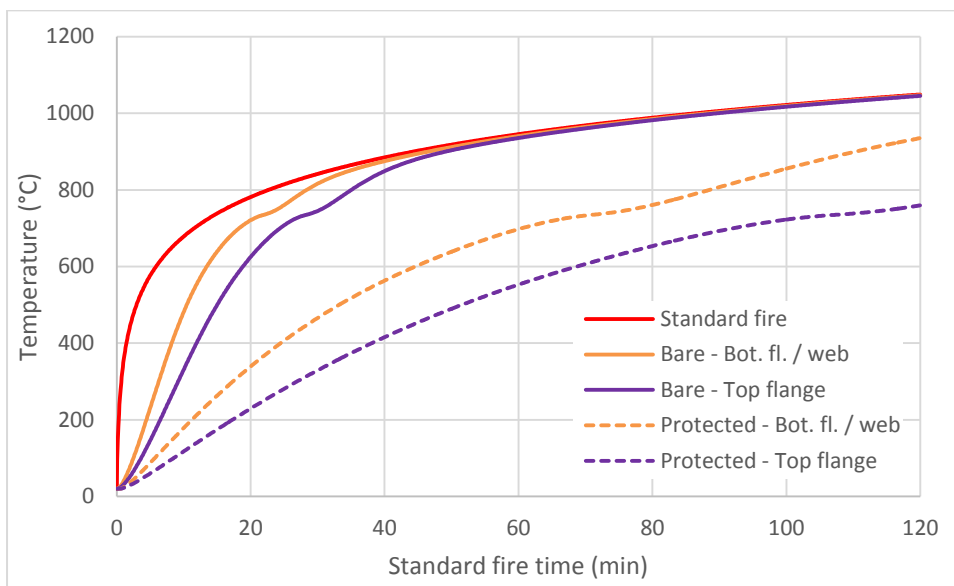


**Figure 7.21: Temperature of the top flange and bottom flange / web for the IPE 240 when exposed to a standard fire. Bare steel (Bare) and a 10mm layer of perlite passive protection (Protected) are considered.**

### 7.5.1 Stress and strain profiles

The behaviour of the beam in terms of stress and strain is now considered for both the unprotected/bare beam and the passively protected beam. For the unprotected beam concrete tensile capacity has initially been excluded to provide a simpler system for illustration purposes. Unless noted the beam has no external mechanical loading applied to it.

#### **Unprotected composite beam**

The change in mechanical, thermal and total strain with height for the composite beam with the bare steel beam is shown in Figure 7.22 assuming no tensile concrete capacity and exposed to a 30 minute fire. The cross-section on the right of the diagrams is provided to assist with visualising which parts of the section correspond to specific stresses and strains. In Figure 7.22 the thermal strains for the entire steel beam are constant because all temperatures exist in the phase change zone where the elongation is constant, as per Figure 5.1. Overall, the entire composite section has elongated due to thermally induced effects, as evidenced by the positive total strain. However, the mechanical strains show that the lowest 114mm of the steel beam and the upper 110mm of the slab are in tension while the remainder of the section is in compression. When a 45kNm mechanical moment is applied the strain profiles change to be as shown in Figure 7.23. This magnitude of bending moment is marginally below failure load, and has thus been included. In this scenario the maximum total strain has increased from 0.016 to 0.044, and the neutral axis has shifted from 266mm to 352mm above the bottom of the beam. The resultant mechanical stress profiles,  $\sigma_\sigma$ , over the height of the beam are shown in Figure 7.24.

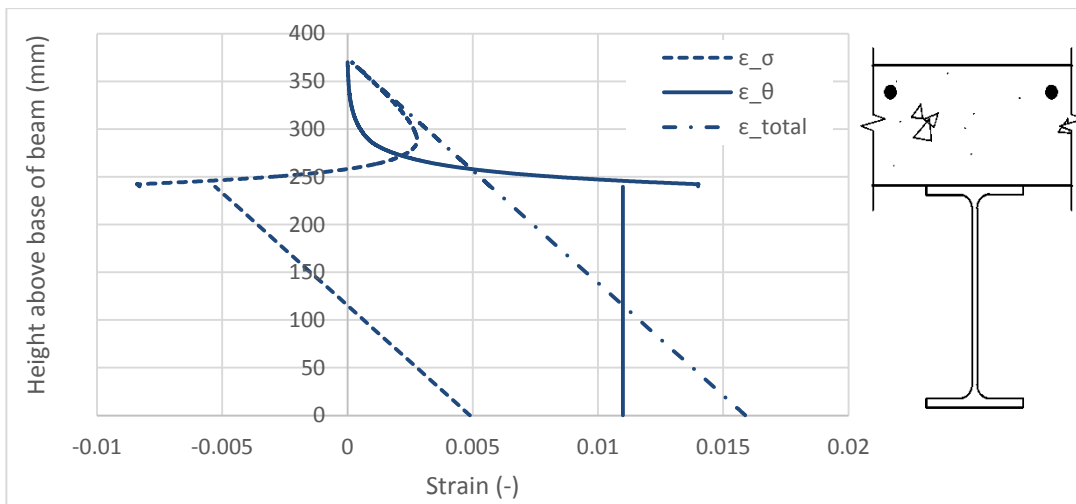


**Figure 7.22: Graph showing the total ( $\epsilon_{total}$ ), mechanical ( $\epsilon_\sigma$ ) and thermal strains ( $\epsilon_\theta$ ) over the height of the composite beam when exposed to a 30 minute fire and  $f_{ctm} = 0$  MPa**

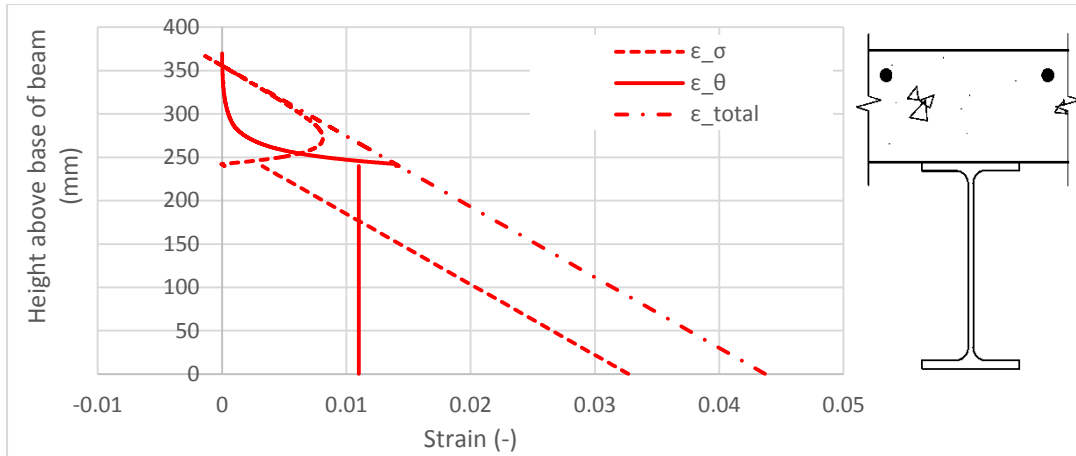


**Figure 7.23:** Graph showing the total ( $\epsilon_{total}$ ), mechanical ( $\epsilon_{\sigma}$ ) and thermal strains ( $\epsilon_{\theta}$ ) over the height of the composite beam when exposed to a 30 minute fire, a 45 kNm mechanical moment is applied and  $f_{ctm} = 0$  MPa

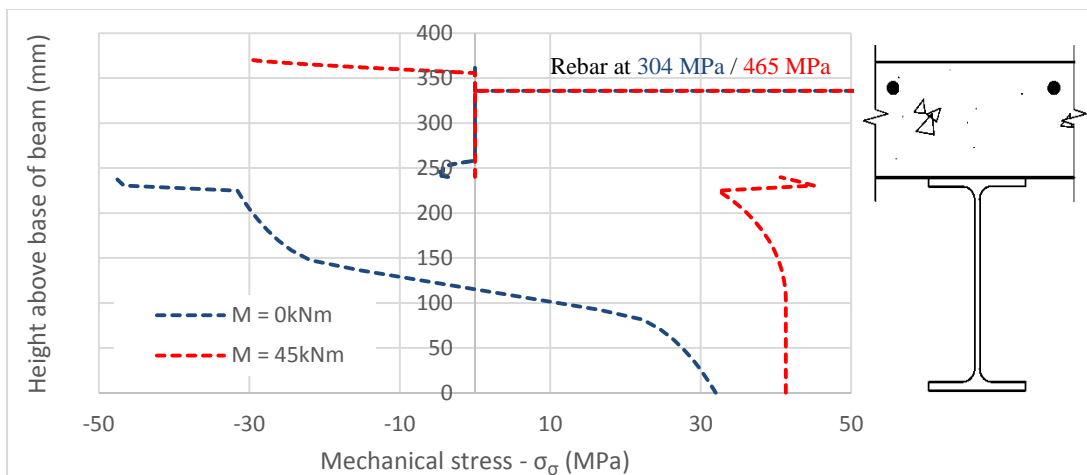


**Figure 7.24:** Graph showing the change in mechanical stresses,  $\sigma_{\sigma}$ , in the composite beam for mechanical moments of 0 kNm and 45 kNm respectively, with  $f_{ctm} = 0$  MPa

### ***Passively protected composite beam***

When the passively protected beam has the fire limit state load of 123 kNm applied to it after a 60 minute standard fire the resulting strains in the section are shown in Figure 7.25. The associated mechanical stresses,  $\sigma_{\sigma}$ , are shown in Figure 7.26. Temperatures are as per Figure 7.21. In this scenario tension stiffening and tension capacity have been included, although their influence is limited. When a beam nears the failure load the strains encountered are typically sufficiently high such that concrete fails in tension and in many cases rebar would also have fully yielded. This results in minimal influence from tension stiffening. For the beam configuration shown in Figure 7.25 the neutral axis occurs at 346mm above the bottom of the beam, leading to the rebar being in tension. From these figures it can be seen that only the upper 24mm of the section is in compression, and this zone has a pressure bulb of similar shape to that shown in Figure 7.6 (when enlarged and viewed in isolation). In this case the maximum concrete stress is reached. Except for a zone 1.1mm thick below the neutral axis (which is negligible and could conservatively be excluded) the remainder of the

concrete has failed in tension. Since the top flange is cooler than the bottom flange it has a higher yield strength, resulting in the increased induced-stress,  $\sigma_{\epsilon\sigma}$ , observed for the top flange.

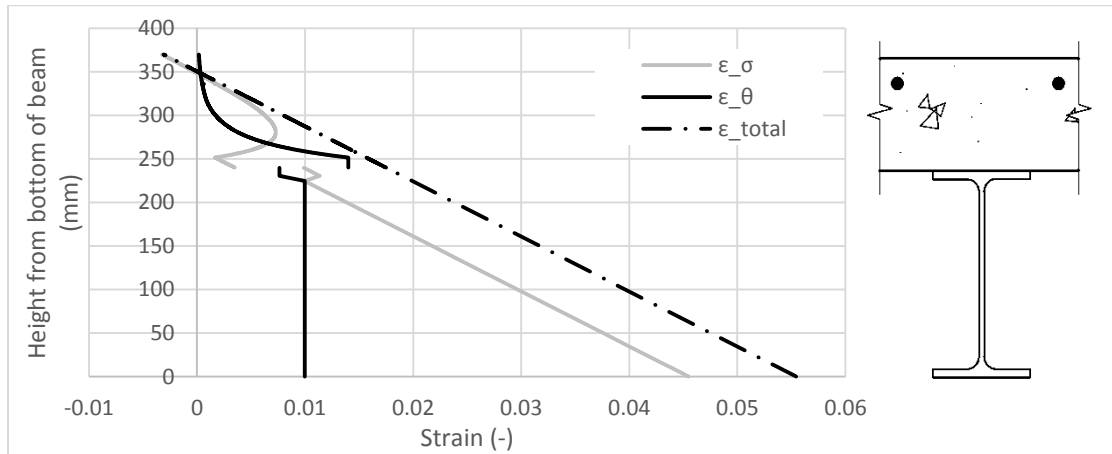


**Figure 7.25:** Graph showing the total, mechanical and thermal strains over the height of the composite beam

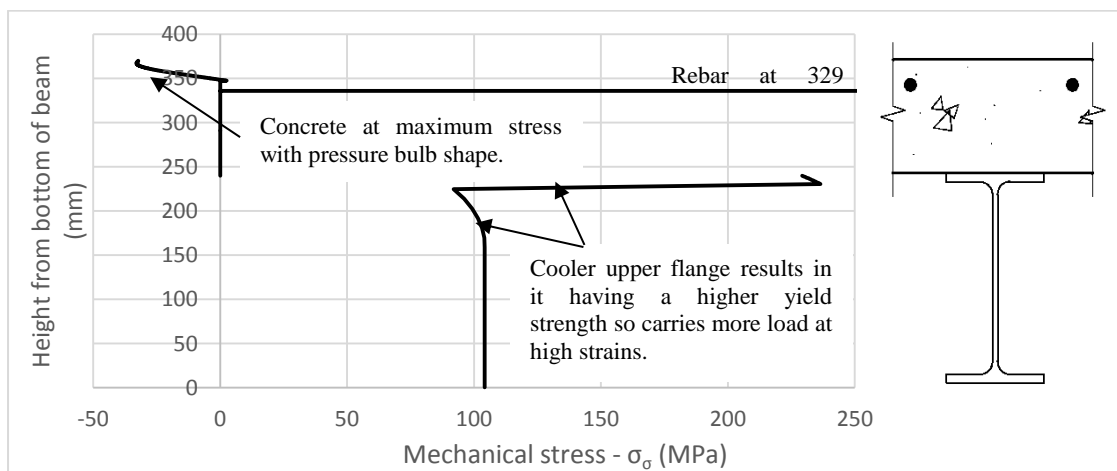
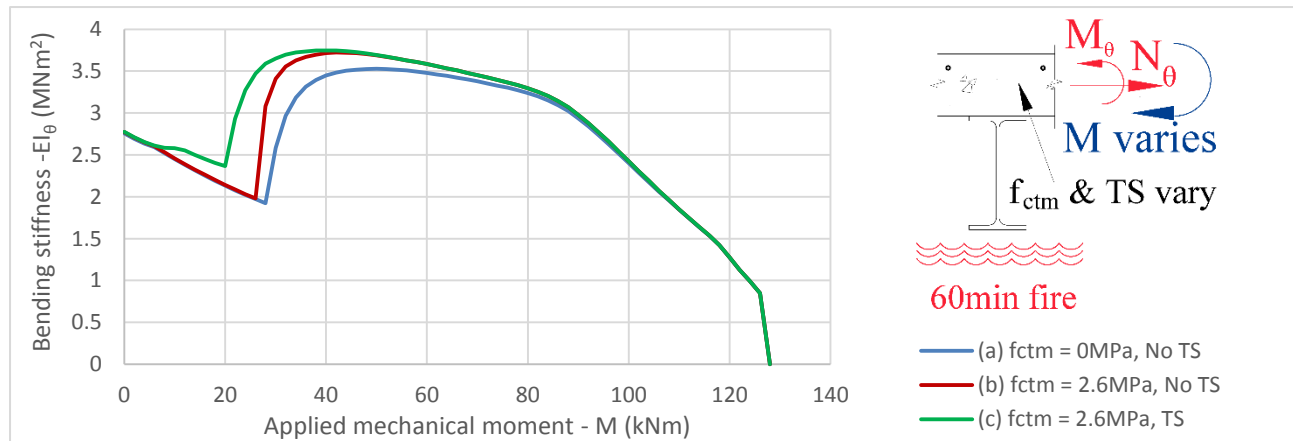


**Figure 7.26:** Graph showing mechanical stress over the height of the composite beam

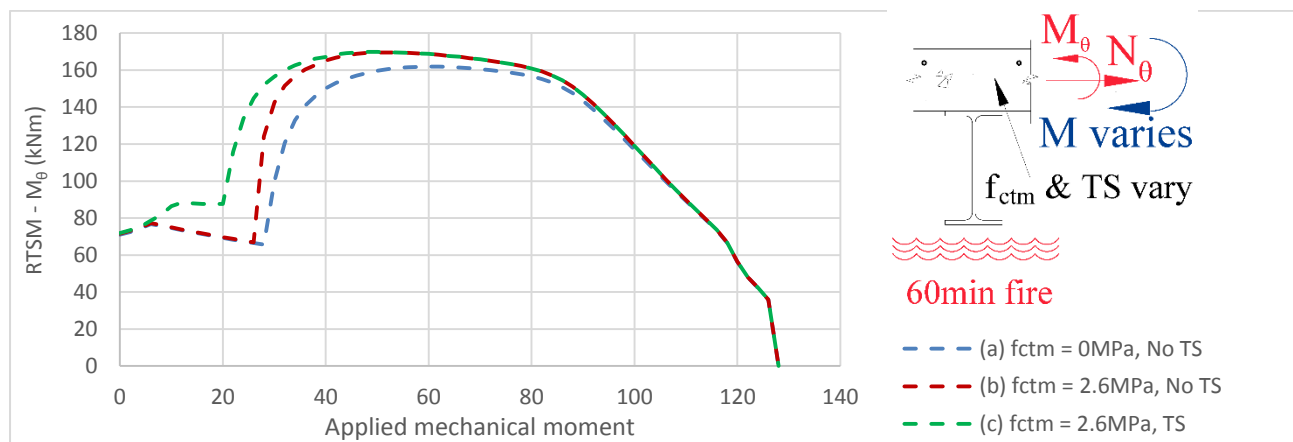
### 7.5.2 Concrete tensile capacity and tension stiffening

Figure 7.27 and Figure 7.28 show the change in  $EI_{\theta}$  and  $M_{\theta}$  for the composite slab with the passively protected steel beam when an increasing mechanical moment is applied to the cross-section. The cross-section has been exposed to a 60 minute fire. The same scenarios as investigated in Section 7.4.2 are presented, namely with (a) no tensile capacity, (b) tensile capacity but no tension stiffening (TS), and (c) both tensile capacity and TS. It can be seen that initially stiffnesses decrease as loads increase, due to the secant stiffnesses of materials decreasing. However, between 20 and 28 kNm the increasing moments cause the upper zone of the concrete to have strains limited to within cracking strains, thus becoming uncracked or even in compression. This leads to the sudden increase in both stiffness and RTSL/M. The maximum difference in

bending stiffness between (a) and (c) is 87% at an applied mechanical moment of 28 kNm. At this point the difference in  $M_\theta$  is 132%. Overall it can be seen that only in the range of 8 kNm to 45 kNm tension stiffening has an influence on behaviour, but outside of this range the influence is negligible. Once forces become sufficiently large concrete cracks fully or rebar yields, resulting in a negligible contribution from concrete tensile capacity or tension stiffening. With the fire limit state bending moment being in the order of 123 kNm there would be negligible influence of tension stiffening on properties at the mid-span of this beam, although near the supports of simply-supported beams tension stiffening would have an influence.



**Figure 7.27: Graph of bending stiffness against applied mechanical moment for the composite beam with the passively protected steel beam after a 60 minute fire, with (a) neither tension capacity ( $f_{ctm} = 0$  MPa) nor tension stiffening (TS) (b) for  $f_{ctm} = 2.6$  MPa but no TS, and (c) with both  $f_{ctm} = 2.6$  MPa and TS.**



**Figure 7.28: Graph of  $M_\theta$  against applied mechanical moment for the composite beam with the passively protected steel beam after a 60 minute fire**

If the cross-section is considered as a 3m long cantilever with a mechanical end point moment, as shown in Section 4.3.1, the deflection of the beam with increasing moment is as shown in Figure 7.29. This setup has been exposed to a 60 minute fire for all configurations. From this behaviour it can be observed that once again the change in  $M_\theta$  is offset by the change in bending stiffness. The maximum difference between the graphs is 9.6% at an applied moment of 12 kNm, whereas after 30kNm the difference between the graphs is negligible.

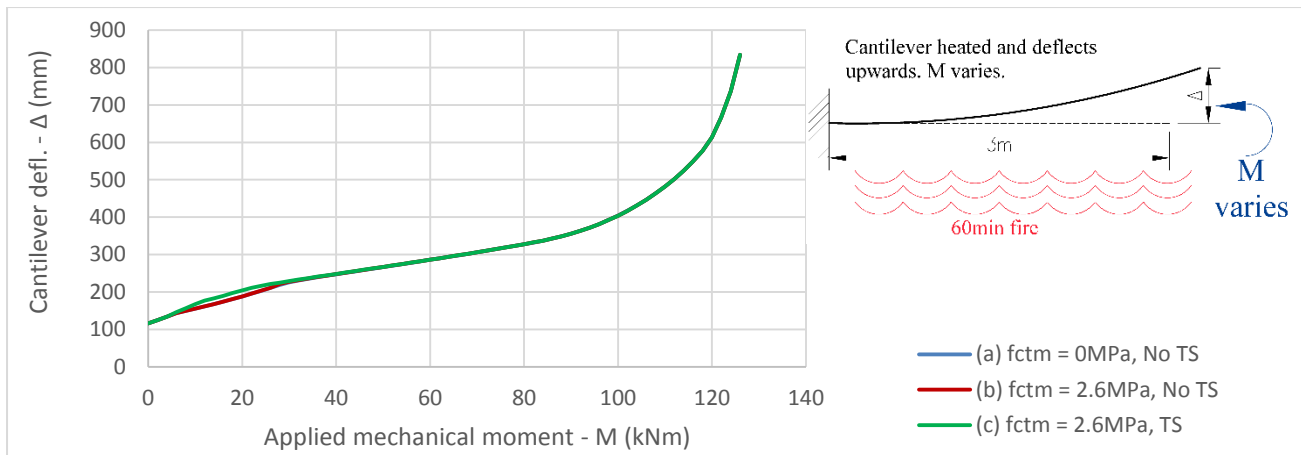


**Figure 7.29: Graph of deflection against applied mechanical moment for the composite beam after a 60 minute fire when considered as a 3m long cantilever with an end point moment**

For the different assumptions ((a) to (c)) of concrete tension behaviour the change in  $EI_{\theta}$  and  $M_{\theta}$  with increasing fire time for the composite slab with the passively protected beam is shown in Figure 7.30 and Figure 7.31. In this case no mechanical loads are applied, meaning that all stresses are thermally induced. In real-world scenarios there will always be some level of mechanical loading, although by excluding mechanical loads here the complex fire-induced behaviour can be more clearly shown. A number of factors interact to produce the unusual patterns observed, especially for Figure 7.31, which has been labelled to explain the phenomena encountered. This graph has been included to highlight how multiple structural materials and behaviours combine to influence results. Note that in these investigations all results are independent of the load path followed. A more uniform graph would be obtained if load path dependent properties were considered.

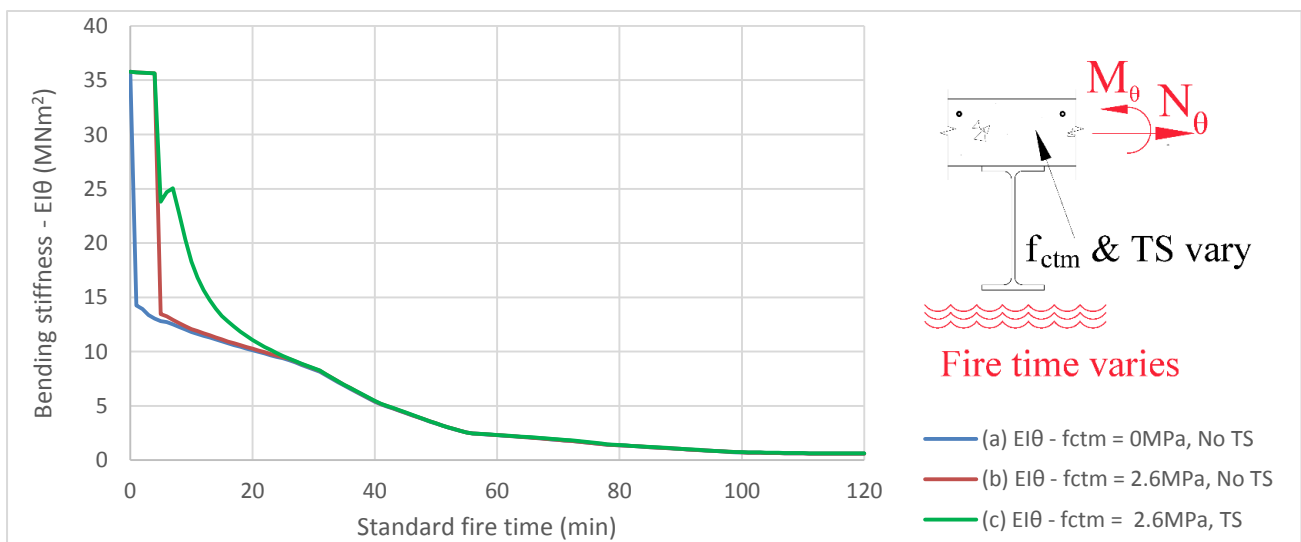


**Figure 7.30: Graph of  $EI_{\theta}$  against standard fire time for the passively protected composite beam**

With reference to Figure 7.31 the following are specific anomalies that occur on the graph:



- 1) Initially the steel beam heats up more slowly than the soffit of the slab due to the passive protection which absorbs energy around the steel beam. For case (a) where there is no tension capacity this results in a hogging moment in the early stages.
- 2) Cracking occurs for (b) and (c) once cracking strains have been exceeded. When outer fibres fail it results in a redistribution of stress as cracks propagate until equilibrium is restored. This results in the sudden decreases in both stiffness and  $M_{\theta}$ .
- 3) For (c) TS occurs after cracking, resulting in the increased overall section stiffness. Some of the stiffness of the cracked concrete is effectively added to the stiffness of the rebar, as discussed in Section 5.4.
- 4) As the rebar strains increase within the crack formation stage (see Figure 7.19) the secant stiffness of the rebar decreases while thermal forces increase due to increasing temperature. This results in the localised peak moment.
- 5) Thermal forces from the steelwork peak at 500°C (as per Figure 5.6) but this occurs at different times for the top flange and web/bottom flange (52 minutes vs. 33 minutes respectively, as per Figure 7.21). With the web and bottom flange having a more dominant influence on thermal moments their influence can be clearly observed from of the localised peak at 33 minutes.
- 6) As the neutral axis migrates upwards into the concrete section mechanical strains of the lower portions of the concrete decrease, causing some portions to become uncracked and exert forces again.
- 7) Changing forces cause the rebar to again be in a range of strain where tension stiffening occurs.

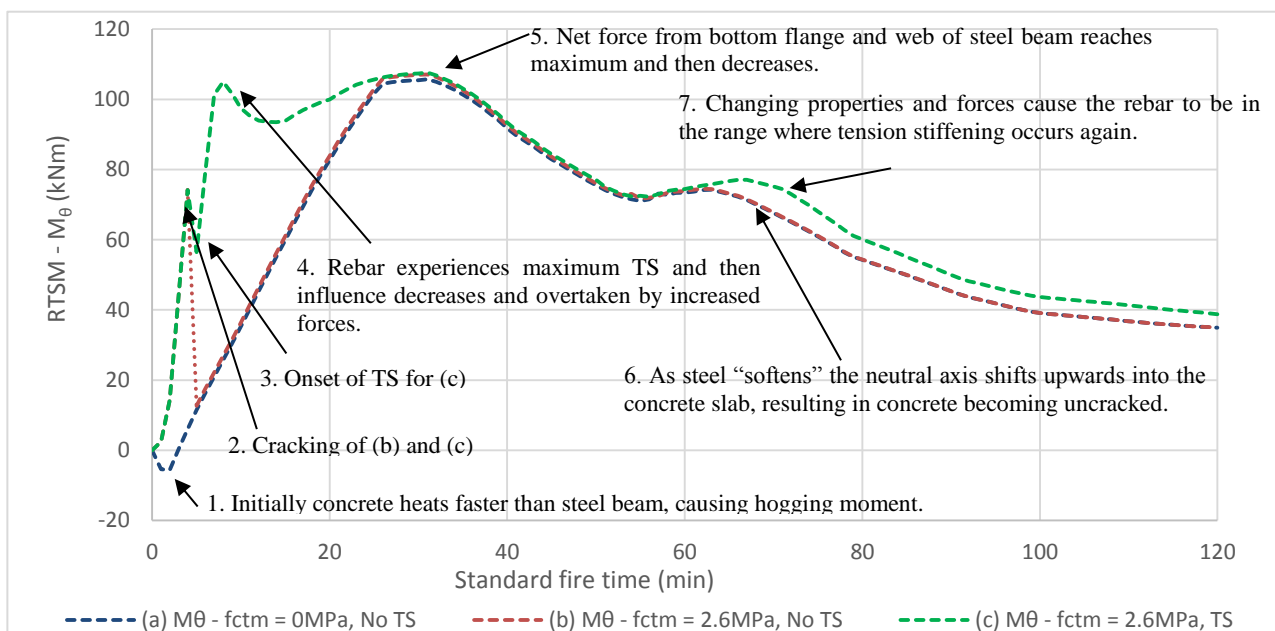


**Figure 7.31: Graph of  $M_{\theta}$  against standard fire time for the passively protected composite beam**

The above results highlight how very complex cross-sectional strain and stress states are created as fire loads are applied, even when no mechanical loads are present. However, it must be reiterated that in most structures the variation in forces will also cause varying section properties along the lengths of beams. This will mean

that the influence of localised phenomena for one portion of a beam, as observed above, may not be significant due to a limited contribution to overall results. For instance, even though for a simply supported beam the section at the supports, where bending moments are low, may experience one of the above phenomena, the total deflection of the beam is only marginally influenced if the rest of the beam is unaffected. Furthermore, it must be remembered that should properties be based upon load paths followed (as it ideally should be in a real structure) it would not be possible for sections to alternate between being cracked and uncracked (an exception to this could be for tensile cracks which close in compression).

To illustrate how the graphs shown above change when mechanical loads are applied consider Figure 7.32. The same configurations shown in Figure 7.31 have been analysed but with both the full fire limit state bending moment applied (i.e.  $M = 123$  kNm), and half of this moment (i.e.  $M = 61.5$  kNm). The case with the 123 kNm moment exhibits consistent trends as the upper sections of the concrete remains in compression throughout. The case with half this moment has different behaviour between 12 and 40 minutes. Here the two cases without tension stiffening ((a) and (b)), crack and exhibit significantly lower RTSMs. The case with tension stiffening follows the trend of the higher moment graphs more closely with no sudden changes. At 14 minutes for the case with  $M = 61.5$  kNm there is a 316% difference between the graph with no tensile capacity and that with tension stiffening. The difference in bending stiffness at this time is 116%. This variation in magnitude would lead to a difference in deflection results as moments are not fully offset by bending stiffnesses.

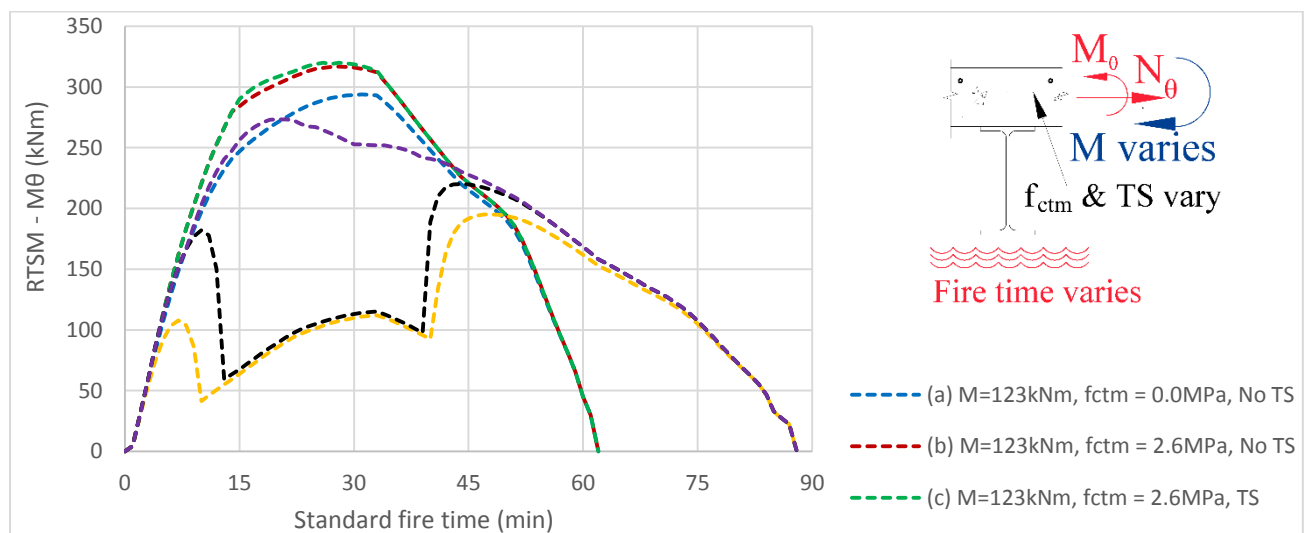


**Figure 7.32: Graph of  $M_\theta$  against standard fire time for the composite slab with varying mechanical moment and tensile properties**

### 7.5.3 Width of the concrete flange

As discussed in Section 5.3.6 the width of concrete acting compositely with a steel beam has not been extensively verified in fire, and typically ambient temperature guidelines are utilised. Clifton (2006) recommends using 60% of the ambient temperature width, whilst EN 4-1-2 (BSI 2005c) recommends the full

width. This section does not show which of these recommendations is more accurate (although pragmatically it would be more conservative and safer to use the former), but does indicate how deflections may fluctuate with changing concrete flange width assumptions. Figure 7.33 shows the change in bending stiffness and  $M_{\theta}$  against width of concrete flange acting compositely with the IPE 240 beam. Mechanical moments of 0 kNm, 61.5 kNm and 123 kNm have been applied, and a constant 60 minutes fire is applied throughout. It can be seen that the ratio of  $EI_{\theta}$  to  $M_{\theta}$  for the arrangements stays relatively consistent once sufficient material is present for loads to be carried. For the 61.5 kNm and 123 kNm configurations failure occurs for flange widths below 100 mm and 1000 mm respectively.

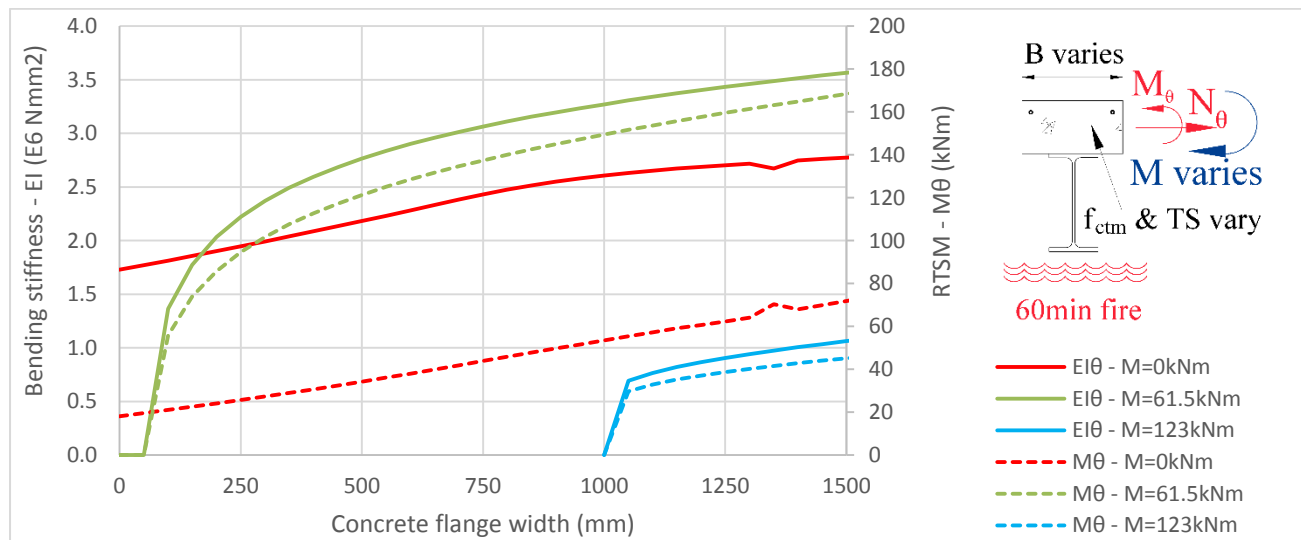


**Figure 7.33: Graph of bending stiffness ( $EI_{\theta}$ ) and RTSM ( $M_{\theta}$ ) against width of concrete flange acting compositely with the steel beam for various values of applied mechanical moment ( $M$ )**

If the cross-sections are considered as 3m long cantilevers as per Case Study A (Section 4.3.1) the deflections calculated are shown in Figure 7.34. In this figure it can be observed that when no mechanical loading is applied the deflection continuously increases as the flange width is made wider. This is because the RSTM increases more rapidly than the bending stiffness. When the 61.5kNm bending moment is applied the deflections initially decrease and then remain approximately constant. For the final case of the 123kNm bending moment deflections progressively decrease with time, and this continues even when the flange is made unrealistically wide, such as 7m. Thus, overall it can be seen that the influence of the flange width specified will depend on the magnitude of mechanical loads experienced by a system. For low levels of loading deflections may increase, whilst for high levels of loading deflections may decrease. Overall results are less sensitive to the width of the concrete flange assumed than may intuitively be expected.

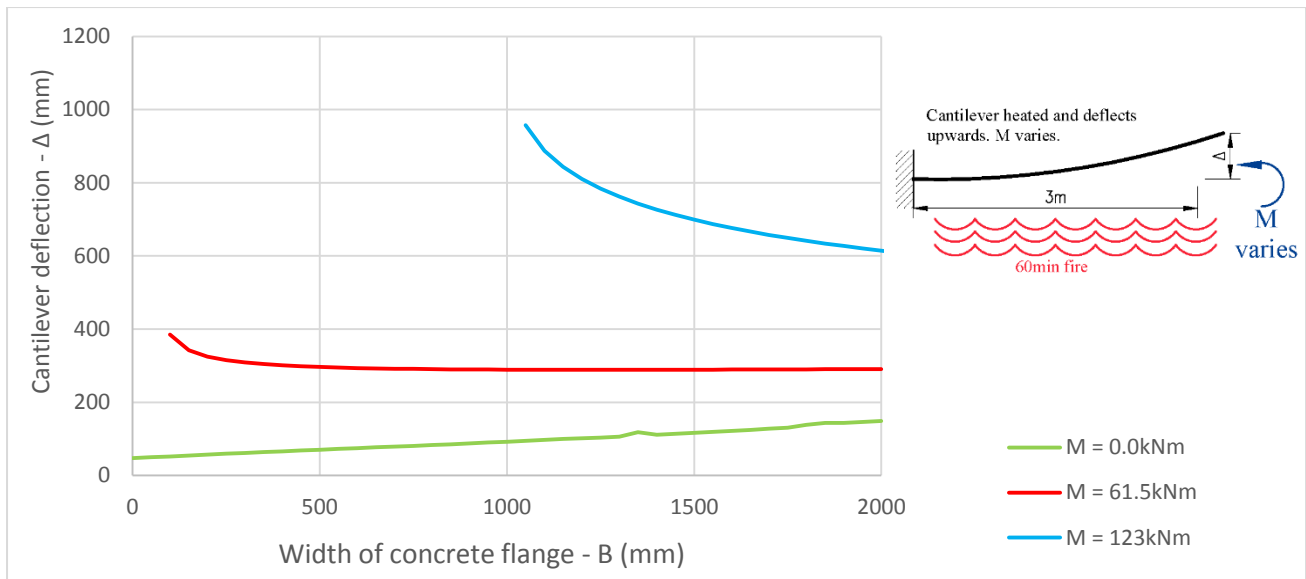


**Figure 7.34: Deflection of a 3m long cantilever subjected to an end point moment of 0kNm, 61.5kNm, and 123kNm with varying width of concrete flange acting compositely**

#### 7.5.4 The influence of restraint

As previously cited, Sanad et al (2000) note that the “effect of thermal expansion is generally ignored, even though it may swamp the effects of all other phenomena in a large highly redundant building under a local fire”. In this section the influence on  $EI_{\theta}$  and  $M_{\theta}$  of increasing the axial load on beams is demonstrated. By understanding the change in stiffness with applied axial load an understanding of how axial restraint influences material properties can be obtained. The change in bending stiffness with varying mechanical axial load is shown in Figure 7.35. Differing levels of mechanical moment are applied, as per the previous case studies. For all the systems a constant fire exposure time of 60 minutes is selected.

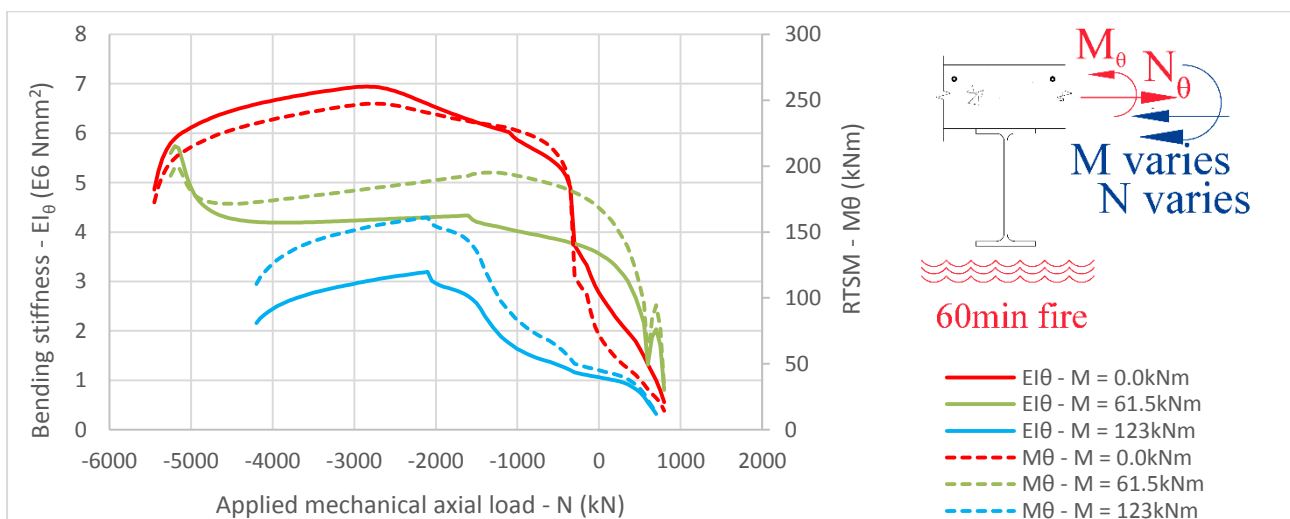


**Figure 7.35: Graph of bending stiffness and  $M_{\theta}$  against applied mechanical load for the composite slab with applied mechanical moments of 0.0kNm, 61.5kNm and 123kNm. For the graph compression is negative.**

For all the graphs it can be observed that there is a peak bending stiffness in compression, due to additional concrete being able to carry load. Bending stiffnesses and  $M_{\theta}$  follow approximately the same trends, although the ratio between these do vary. The magnitude of change in bending stiffness due to applied moment can be large, considering that for an applied compressive load of 1000kN there is a difference of 258% between the unloaded system and that with the 123 kNm mechanical moment. For a simply-supported beam the moment will vary from zero to a maximum along its length, re-emphasising the fact that the properties of a beam are not uniform, and all three graphs may apply to a single beam at different points along its length.

The perturbations seen are caused by similar factors as addressed in Section 7.5.2. However, for the graph with an applied moment of 61.5 kNm the increase in properties at +700kN tension is not at all linked to tension stiffening, but rather to concrete at the bottom of the slab failing. This failure causes the neutral axis to migrate upwards, resulting in the uppermost concrete being able to carry load in compression again, increasing stiffness. With increasing axial load the small zone carrying load is soon brought into tension and loses its strength.

## 7.6 Summary of results and conclusions

From this chapter it can be observed that results vary substantially depending on the parameters selected for design. However, often an increase in bending stiffness is accompanied by an increase in RTSM, resulting in calculated deflections being relatively unchanged. This is especially true when mechanical forces are low and deflection is governed primarily by thermal behaviour, as is often the case. The presentation of stress and strain profiles over the height of a beam's cross-section provides a novel insight into the mechanics of structural elements at high temperature.

For concrete or composite elements a number of factors influence calculated stiffnesses and thermal forces. These may reach peaks at different stages. Hence, it is not possible to provide broad characterisations regarding how changes in material or temperature parameters will always affect results. The advantage of the FBE formulation is that parametric studies can be carried out to better understand how uncertainties regarding design variables will influence a particular system. It must be emphasised that these results do not mean that structures *will* behave in the manner predicted by the graphs above, but rather that any *model* based on the parameters and methodologies as described in this research will be influenced by the trends predicted above. The exclusion or inclusion of factors such as concrete confinement, construction tolerances, and localised fluctuations in temperature will influence behaviour.

### ***Steel beam parametric study***

For the steel beam an important factor to note is that a peak RTSL is reached at 500°C, re-emphasising the results of Figure 5.6. This causes a decrease in thermal “forces” after this temperature. The trend of load-stiffness graphs follows the trend of the temperature-stress-strain curve selected. Significant softening occurs after the proportional limit (end of the elastic region) is reached at outer fibres, and failure occurs soon after

the outer fibres reach yield stress, except when strain hardening is included. The introduction of applied mechanical moments or temperature gradients causes asymmetry in load-stiffness graphs for axially loaded cross-sections, where hotter or more highly stressed zones have proportionally lower stiffnesses.

### ***Concrete slab parametric study***

For the concrete slab it was firstly shown that the prediction model captures the stress-strain profile of typical beams at ambient temperature when no tension is allowed in concrete. It was then shown that the combination of temperature profiles, thermal forces, mechanical forces, material degradation and the behaviour of reinforcing steel can cause unusual stress profiles over a beam's cross-section. The inclusion of tension capacity or tension stiffening can lead to changes in bending stiffness, although this is generally offset by an increasing RTSM. Changes in concrete strengths may cause deflections to decrease when stiffness increases are more dominant, while in other ranges RTSMs become more dominant causing deflections to increase.

Axial restraint leading to induced mechanical forces can significantly increase the stiffness of sections as the entire concrete slab goes into compression. There is typically a peak secant stiffness after which stiffnesses decrease due to the descending branch of the stress-strain curve of concrete being followed. Temperature profiles play an important role in the determination of the thermal forces and mechanical properties of concrete slabs. RTSM values varied by between zero and 25% depending on the temperature prediction model adopted. With this being one of the most difficult parameters to accurately define designers should be aware of the potential for variation in results depending on the temperature model selected.

### ***Composite beam parametric study***

Composite beams exhibit complex stress and strain profiles over the height of cross-sections due to varying material properties and temperatures of integration points. Expanding steel beams can place concrete into tension, thereby causing cracking and stiffnesses to decrease. For protected steel elements the concrete soffit may heat up more quickly especially during the initial stages of a fire. The interaction of multiple phenomena can cause localised effects and peak values of  $EI_{\theta}$  or  $M_{\theta}$ .

Results may be sensitive to the width of concrete flange assumed to be acting compositely with a steel beam. The ratio of bending stiffness to RTSM changes depending on the magnitude of applied loads where (a) for no applied moment the ratio decreased with increasing flange width, (b) for a mid-range moment the ratio stayed approximately constant, and (c) for high moments the ratio increased thus resulting in lower deflections with increasing flange width. Such results may seem counter-intuitive where in certain scenarios increasing flange width results in larger deflections.

The inclusion of axial forces to simulate restraint results in similar effects to that exhibited by concrete slabs alone. Maximum stiffnesses are achieved when sufficient compression causes entire sections to be uncracked. After maximum stiffness values are achieved stiffnesses decrease due to portions of concrete following the

descending branch of the stress-strain curve selected for concrete. If a linear ascending and descending branch were selected then different load-stiffness graph trends would be observed.

### ***General comments***

From this study a variety of structural phenomena have been identified. Results show that although tension stiffening and the tensile capacity of concrete do have an appreciable effect on individual beam properties, their effect is often counteracted by increased thermal forces. It is possible that in the design arena these results would justify the exclusion of tensile behaviour and tension stiffening, although more research is required to thoroughly investigate this aspect. The influence of restraint can result in significant changes in stiffness and RTSM/L values, therefore should be carefully considered. The presentation of stress and strain profiles across the height of sections provides novel insight into the structural mechanics of concrete slabs and composite beams in fire. Stress and strain profiles can be verified considering basic static equilibrium and the relationship between stresses and strains. This allows for the thorough interrogation of results which is often more difficult in three-dimensional FE models.

## 8 Chapter 8: Conclusions

### 8.1 Overview

This dissertation has provided a simplified method for the modelling of structures in fire as skeletal frames. The aim was to provide a structural engineering analysis tool that is suitable for structural engineering design requirements in practice, whilst having a sufficient level of accuracy when considering structural behaviour. A beam finite element incorporating eccentric, movable neutral axes (NAs), non-linear material properties, and temperature dependent behaviour has been developed and validated. The methodology is called the Fire Beam Element (FBE) formulation. Procedures have been developed for accounting for thermal strains through the application of pseudo “forces” called Resultant Thermal Strain Loads or Moments (RTSLs, RTSMs). The modelling procedures allow for structures to be analysed more easily than with advanced analysis models, while global structural behaviour can be considered which prescriptive methods do not account for. The FBE formulation has been generically formulated to account for any beam in fire where Euler-Bernoulli assumptions approximately hold. However, its application is not only limited to the field of structural fire engineering. An extensive discussion on material models and design uncertainties has been provided. A model for considering tension stiffening of reinforcing steel has been developed, based on modifying an existing ambient temperature model to account for material properties at elevated temperature. Four case studies were investigated to validate the FBE model against experimental and numerical data in the literature. The FBE model’s predicted deflections were comparable with methods cited in the literature, even for relatively complicated experimental setups. A series of parametric investigations has highlighted how structural behaviour is influenced by input variables selected, as discussed further below.

By combining the proposed FBE formulation with existing slab panel design methodologies (Clifton & Abu 2014) practitioners would be able to design entire structures in a manner similar to that at ambient temperature, with separate consecutive design of beams and slabs. This makes the design process significantly simpler and more suitable for codified design procedures, with a view to bridging the current divide between engineering practice and academic research.

### 8.2 Consideration of objectives

The objectives of the dissertation identified in Chapter 1 have been progressively addressed as follows:

- a) A step-by-step explanation has been provided in Chapter 3 considering and illustrating the fundamental structural mechanics of a beam exposed to fire. It has been shown how temperature effects and temperature gradients influence the strains, stresses and material stiffnesses within a cross-section. An iterative procedure for calculating the updated position of the NA of beams has been proposed. After the NA of a section has been found the bending and axial stiffnesses can be



determined, and included in analyses. If the position of the NA of a beam is known then thermal forces can be easily calculated about that position.

- b) Chapter 4 has proposed a mathematical finite element formulation for considering beams in fire. Matrix formulations are proposed which transfer the stiffness and load vector from the position that a beam is modelled about (i.e. the reference axis) to the updated NA position, or vice versa. This is done in a manner similar to the way in which the degrees of freedom of certain nodes in a finite element model can be slaved to master nodes.
- c) Numerical case studies, excluding thermal effects, have been conducted for structures where NAs shift by comparing results from the FBE formulation to finite element models using shell elements. Deflection, stress and strain results between the models compare favourably. Hence, it can be seen that structural behaviour has been adequately captured by the FBE formulation.
- d) Nonlinear material behaviour has been introduced based on the temperature-stress-strain material models discussed in Chapter 5. Various alternatives have been considered, highlighting the potential for variability in results based on assumed input parameters.
- e) A series of experimental tests, and one numerical case study, have been included for the validation of the FBE formulation, as presented in Chapter 6. The FBE formulation describes the deflection of structural elements to a sufficient level of accuracy, sometimes replicating observed deflections closer than alternative methods.
- f) The case studies investigated were carried out using subroutines coupled with a simple commercial finite element software package. This has highlighted how complicated structures with highly nonlinear behaviour can be analysed using software tools commonly available to structural engineers, provided that stiffness, NA and RTSL/M values are calculated separately. This is typically possible only for statically determinate / unrestrained structures, unless iterative procedures are manually performed.
- g) A detailed parametric study has been conducted in Chapter 7 where various design parameters have been adjusted and the resulting beam stiffnesses and resultant thermal forces plotted. Trends relating to the change in properties have been identified. For parameters such as concrete tensile strength or effective flange widths of composite slabs an increase in design stiffness is offset by an increase in thermal forces, thus resulting in negligible change in calculated deflections. The parameters with the highest level of uncertainty, and most difficult to accurately quantify, are those related to thermal effects and temperature loading. Unfortunately such parameters typically also have the largest effect on structural behaviour in fire.

## 8.3 Findings

### 8.3.1 *Modelling methodology*

The methodology proposed for analysing structures as skeletal frames is novel and provides a new approach for design engineers, whilst being similar to design methods used for ambient temperature design. Thus, the logic and principles employed could be more readily adopted within the structural engineering fraternity. The main concepts that engineers would need to become familiar with are (a) the need to update the NA position of a section, (b) the methodology for adjusting stiffness and load vectors to account for the eccentricity between the model reference axis and the NA position, (c) the calculation of combined bending and axial stiffnesses, and (d) the application of pseudo thermal forces using the RTSL/M calculations. All these procedures could be automated within custom coded software.

With the significantly reduced modelling times required for analysing skeletal structures it makes structural design more accessible for general buildings, rather than having it limited only to very expensive buildings where the modelling time can be justified. Results obtained from skeletal analyses (moments, axial loads and deflections) can be readily used for codified design, which is sometimes not the case for shell and volume element modelling methods where bending moments and axial forces need to be extracted from models and additional processing of data is required.

### 8.3.2 *Finite element formulation*

The formulation of a beam element that accounts for an eccentric, movable NAs is novel. The numerical simulations carried out show that the formulation yields approximately the same deflections as significantly more advanced shell element models with much larger numbers of degrees of freedom. A beam element accounting for eccentric NAs is not only suitable for fire analyses but also bridge decks, concrete wind towers and other such elements where the position of the neutral axis of an element changes along its length.

When the assumption of plane sections remaining plane is violated calculated results progressively become less accurate, with the FBE formulation typically underestimating deflections. Errors have generally been found to be relatively small (< 6%), although errors are proportional to the degree of cross-sectional distortion that occurs. In a real beam the calculated forces, especially bending moments, will generally vary over its length. Hence, even if one segment of an entire beam experiences localised distortions the overall behaviour is relatively unaffected. During the validation process of the FBE model it was observed that stress and strain profiles at positions of cross-sectional distortion (due to sudden changes in stiffness) differed between the Abaqus model, consisting of shell elements, and the FBE formulation. However, a small distance away from discontinuities structural behaviour and material strains become similar, once plane section assumptions are achieved again. This highlights how Euler-Bernoulli assumptions can be adopted in such analyses and still provide deflection predictions with a sufficient level of accuracy (within 0-10%, depending on the degree to which sections distort).

It is interesting to note the significant errors that occur when beam properties are not calculated about their updated NA positions. It is hypothesised that software systems which use beam elements to consider steel members in fire may be susceptible to such errors when there are temperature gradients over the height of a beam. Typical beam element formulations will not update NA positions when the hotter bottom section of a beam has a proportionally lower stiffness than the top cooler section.

### 8.3.3 *Experimental validation study*

The experimental case studies of Chapter 6 were used to validate the FBE model, by comparing predicted deflections to those measured during tests. FBE models were analysed in commercially available FE software coupled to subroutines to calculate member stiffnesses and RTSL/M values. A point that must be noted is that in structural fire engineering literature the experimental result which researchers seek to replicate is that of deflection, since due to the destructive nature of fire it is difficult to obtain material strains or other such data. From the parametric studies conducted it can be seen that two models with relatively different calculated stiffnesses may predict the same deflection, although internal forces may vary by a reasonable margin, due to the ratio of thermal forces to stiffness being the same. However, the challenge faced is that with the limited data available from tests it cannot be irrefutably stated which modelling system is more “correct”. This is an important consideration when interpreting results from models, and the insight provided regarding such behaviour is a contribution of this work.

In all case studies investigated the results from the FBE model were comparable with experimental results and those in the literature. This demonstrates that modelling structures in fire using skeletal frames is feasible and may be sufficiently accurate. The concrete slabs analysed in the second case study experienced phenomena such as spalling, moving moisture fronts and variable furnace temperatures (Ali et al. 2008) which any prediction model will not easily accommodate. It can be observed that for three identical slabs tested in a single furnace at the same time the final deflections of each slab varied due to factors such as spalling and moisture contents. In spite of such high levels of uncertainty the FBE formulation predicted deflections to a sufficient level of accuracy.

The runaway failure of Case Study 3 was also predicted by the FBE model. Hence, it can be seen that the proposed FBE model could possibly be used for estimating collapse loads. For failure to be more readily predicted it would be necessary to include routines in analysis programs for identifying lateral-torsional buckling and instability affects as these will generally not be identified by the FBE formulation in isolation. However, the same design philosophy is adopted for ambient temperature where analyses are conducted to determine elemental forces and then stability design is conducted based on code requirements. If it is found that a beam or column has insufficient resistance it must be increased in size or have additional passive protection applied to it.

It is important to note that even for the fourth case study investigated, consisting of an entire composite floor where tensile membrane action occurred, the FBE models used were able to predict deflections closer to

experimental results than a method designed specifically for tensile membrane action (Stadler 2012). However, it must be acknowledged that due to the aforementioned high levels of uncertainty at times this may be coincidental, as is the case for all prediction models. Also, the model in the literature was developed to account for floor design which the FBE formulation does not consider.

#### 8.3.4 *The application of engineering judgment*

With a large number of input parameters specified in models it would be possible to “calibrate” models to obtain results closer to experimental results. Engineering practitioners do not have such luxury and must base models on conservative estimates of input parameters. However, from the parametric studies it was shown that it is not always intuitive whether changing certain parameters will result in more or less conservative designs, necessitating sensitivity analyses in certain situations. Furthermore, with the high levels of uncertainty inherent in structural fire design there will always be a scatter in predicted fire loads, structural response and design forces. Temperature profiles play a significant role in overall structural behaviour, thus engineers should ensure that profiles selected are suitable and conservative for structures being designed. Parameters related to concrete properties are typically more variable than those for structural steelwork.

#### 8.3.5 *Composite beam concrete flange widths*

It has also been shown that the increasing the width of concrete flange width acting compositely with a steel beam may increase or decrease predicted deflections, as shown in Section 7.5.3. This is due to the change in ratio of bending stiffness to RTSM. However, in general it is seen that calculated deflections are not highly sensitive to the effective concrete flange width assumed, except where mechanical forces are dominant. This is beneficial for the modelling procedures employed as a width has to be specified by designers and codes provide limited guidance for structures in fire beyond what is recommended at ambient temperature.

#### 8.3.6 *Restraint against thermal expansion*

The presence of axial forces due to restraint has a significant influence on predicted cross-sectional properties, which will influence calculated deflections. This agrees with numerous publications in the literature that highlight how thermal expansion and restraint effects dominate behaviour, rather than the degradation of material properties (Sanad et al. 2000). For concrete elements axial and bending stiffnesses increase as increasing compression causes additional areas to become uncracked and carry load. This can lead to significantly higher thermal forces or stiffnesses than may otherwise be expected. However, after materials have reached their yield or crushing load stiffnesses decrease.

#### 8.3.7 *Stress-strain behaviour in beams in fire*

The parametric studies of Chapter 7 have provided novel insight into the stress-strain conditions of structural elements experiencing combined thermal and mechanical actions. In the literature the stress-strain behaviour over the height of a section is seldom plotted. By illustrating cross-sectional load carrying behaviour changes in stiffness and behaviour can be related to specific structural phenomena as explained in Figure 7.31. Such changes in stiffness are due to the interaction of factors such as temperature profiles, non-linear material

models, thermal expansion, cracking of concrete and changes in equivalent thermal stresses (ETSs). For instance the peak ETS for steelwork is reached at 500°C when EN 3-1-2 material properties are adopted. Furthermore, in composite beams steelwork typically expands more than concrete slabs, which causes internal restraint leading to compression in the steelwork and tension in the concrete. This tension can cause cracking when forces exceed concrete tensile capacity, which causes sudden changes in stiffness and stress-strain profiles at specific points on bending stiffness graphs. As the neutral axis of a section migrates it both increases and decreases strains in different portions of a cross-section, sometimes resulting in concrete sections that had cracked to carry compressive load once again, leading to changes in stress-strain profiles. This is influenced by the assumption of whether material properties are load dependent or independent, as discussed in Section 7.4.

### 8.3.8 *Concrete tensile capacity and tension stiffening*

The tension stiffening model developed is based upon verified ambient temperature mechanics. Behaviour has been extrapolated to high temperature by adjusting constituent material properties relative to temperature changes. It is shown in the parametric studies that the inclusion of tension stiffening can contribute significantly to bending stiffnesses in specific strain ranges, i.e. after cracking but before high strains where rebar has fully yielded. However, the increase in cross-sectional bending stiffness (due to the increased stiffness of the reinforcing steel) is also accompanied by an increase in thermal curvature forces. This is due to the fact that bottom reinforcing steel is typically exposed to elevated temperatures, so when it has an increased stiffness it results in an increased thermal thrust. The approximately proportional increase in bending stiffness and RTSM can lead to negligible change in predicted deflections. Such results possibly justify neglecting tension stiffening for simple models. However, it is acknowledged that even if predicted deflection results remain approximately constant, internal forces may change due to the inclusion of concrete tension capacity and tension stiffening. In most structures failure loads induce strains significantly beyond the range in which tension stiffening has an effect. Hence, it is hypothesised that failure loads will not be adversely affected by neglecting tension stiffening. However, prior to failure there may be discrepancies in calculated internal forces depending on whether tension stiffening is included or not.

## 8.4 Future research

A variety of novel methodologies and techniques have been developed in this work. However, the work has also highlighted the need for research in a number of areas. The most critical aspect to be pursued is the investigation of a variety of case studies, especially those in which restraint is present. The FBE formulation presented has the potential to account for such behaviour, but this needs to be developed. It must be investigated how thermal forces, three-dimensional behaviour and boundary conditions can be correctly included. Another important consideration is to investigate how the buckling of sections might be identified and included in the analysis procedure, beyond that which is accounted for by the geometric stiffness matrix.

The influence of 3D tensile membrane action may influence load paths in slabs and it should be determined whether it is fully accounted for by the yield line procedures proposed. For composite structures a valuable contribution for practicing engineers would be the direct linking of a tensile membrane behaviour routine for the design of slabs and secondary beams (Clifton & Abu 2014) with the FBE formulation for the design of primary beams. Since the deflection of primary beams influences the capacity of slab panels, while the failure pattern of slab panels influences yield line load patterns on primary beams, an iterative procedure could be introduced to design structures within a single system.

A topic of interest when considering restrained structures is the question: does the NA of a beam to column connection migrate with changing beam NA position, i.e. does the position of the resultant axial force applied by the connection into the beam change as the NA of the beam changes? It is hypothesised that this behaviour is dependent on the properties of the connection rather than the beam NA itself. However, such behaviour could cause substantial changes in restraining moments depending on how it is modelled. The properties of different connection types will have a significant influence on such behaviour.

Experimental testing is required to validate the tension stiffening model. A number of assumptions were made which need to be verified, especially those regarding the change in concrete behaviour at elevated temperature. Also, it is unclear whether the effective area of concrete contributing to tension stiffening remains the same in fire as it does at ambient temperature.

Currently insufficient literature is available regarding slippage in composite beams in a fire, and to what extent this influences behaviour. It would be possible to include empirical modification factors for bending stiffnesses to account for slippage, as outlined in Equation 2.4. Also, the FBE formulation could be developed to be applied to structural configurations not considered in this work such as timber structures and various new construction techniques. However, in elements where NAs do not significantly shift simpler methods could be employed, i.e. it would not be necessary to update beam stiffnesses to be about a new NA, rather properties could be calculated about the existing NA. With the generic formulation of the FBE it is hypothesised that composite floors consisting of cellular beams could also be considered by the proposed methodology. Cross-sectional properties and thermal forces would need to be adjusted for the holes in beams, and analyses would be suitable for primary beams not subject to buckling.

The parametric studies highlighted various trends in beam properties that are of interest. Future parametric studies should focus on entire structural frames and how results vary with changing input parameters. It may be shown that localised effects of one beam section become less important when multiple beams are considered. Non-linear springs to account for temperature-axial load-moment-rotation relationships can be included to investigate how various connection types influence results. This would complement research occurring in this field worldwide (Block et al. 2007).

When modelling full 3D structures it will be necessary to consider how the bending of a beam about its minor axis could be considered. This becomes a more important factor when structures analysed are only partially heated and cooler portions of the structure provide restraint based on bending about the minor axis of beams. For steel or concrete beams in isolation this is a relatively simple task. However, for continuous composite structures it needs to be tested whether calculating bending stiffnesses using the effective flange widths discussed in Section 5.3.6 would provide accurate results. It is hypothesised that the restraining effect of the cooler portions of a structure could be modelled by including high lateral stiffness for beams in 3D analyses.

## 8.5 Closing comments

From the discussion above it can be seen that a novel methodology and beam element has been proposed and validated in this dissertation for the analysis of structures in fire. It has provided a system that is suitable for design practitioners. This methodology could make rational structural fire design more accessible thereby leading to improved fire safety in structures, and reduced infrastructure costs if passive protection and fire safety systems can be more economically specified. The methodology has certain limitations in its application due to the underlying assumptions inherent to the beam element developed, as with all methods. However, these have been clearly identified and can be addressed in various manners. After addressing some of the factors requiring additional research the FBE methodology could potentially be introduced to industry as a commercial analysis tool. This would be especially beneficial if combined with floor slab design tools for structures in fire.

## 9 Appendix A – Concrete heat transfer model

As discussed in Section 5.3.4, various methods or tabulated sets of data are provided for determining the temperature of concrete across the depth of a slab. These are generally calibrated and provided for temperatures at standard fire times of 30, 60 and 120 minutes, and are based on slabs of different thicknesses, e.g. 100mm for EN 4-1-2 and 200mm for EN 2-1-2. The case studies investigated in this research typically involved results at less than 30 minutes at which point some of these available models could not be confidently extrapolated to suit, and for slab thicknesses other than those listed. Hence, a simple finite difference model based on the following input was generated:

- Heat transfer equations as per Drysdale (2011)
- Specific heat and density functions as per EN 2-1-2 (BSI 2005a)
- Radiation and convection parameters as per EN 1-1-2 (BSI 2002b)

It should be noted that by adjusting the input parameters of: moisture content, original density, surface emissivity, number of elements, magnitude of time step, configuration factor and surface convection heat fluxes (exposed and unexposed faces) it is possible to align results closer or further from the EN 2-1-2 or 4-1-2 curves. Final values selected are:

- Siliceous aggregate concrete with a moisture content of 3% and density of  $2300\text{kg/m}^3$ .
- Thermal conductivity at the lower limit according to EN 2-1-2.
- Coefficient of heat transfer on the exposed face of  $\alpha_c = 25\text{W/m}^2\text{K}$  and the unexposed face of  $\alpha_c = 9\text{W/m}^2\text{K}$ .
- Emissivity coefficient of 0.7 (BSI 2005c) for the fire and 0.8 for the concrete with a configuration factor of 1.0.

Note that with the non-linear, incremental nature of the thermal heat transfer analyses the size of the time steps and the number of elements over the cross-section of a slab have an influence on results. For slabs of around 100mm or thinner it was necessary to use a 2.5 second time step with 40 elements over the height of the section to ensure that stable solutions were obtained.

Refer to the temperature profile graphs provided in Figure 5.16 and Figure 6.14 for the results calculated using the procedure above.



## 10 Appendix B – Additional case study data

Additional data has been provided below for the numerical case studies (No. A - D) conducted in Chapter 4 and the experimental case studies (No. 1 - 4) conducted in Chapter 6. These tables have been provided to allow for the validation of models being developed by other researchers. Since not all details from all time steps at all positions can be listed only properties at specific times or load levels have been included.

### 10.1 Validation studies from Chapter 4

The structural properties listed in this section have been calculated and used in the software developed by the author, based on the principles developed in Chapter 4.

#### 10.1.1 Case Study A: IPE 200 cantilever with non-linear material properties

For Case Study A the properties are uniform across the length of the beam so only a single segment property has been listed at each load level. Both the stiffer and softer material models have been included. The neutral axis has been calculated relative to the centre of the beam.

Moment (kNm):	$E_0 = 200 \text{ MPa}$		$E_0 = 20 \text{ MPa}$	
	NA (mm):	$EI$ (MNm <sup>2</sup> ):	NA (mm):	$EI$ (MNm <sup>2</sup> ):
5	4.55	3.761	2.28	0.377
10	9.09	3.721	4.52	0.376
15	13.8	3.653	6.79	0.375
20	18.6	3.555		
25	23.6	3.424		

**Table 10.1: Case Study A - IPE cantilever – Properties for segments at different moments**

#### 10.1.2 Case Study B: Rectangular beam with material non-linearity

In the table below the properties of the first 16 segments of the rectangular beam are provided.

Sect. #	NA (mm):	EI (kNm <sup>2</sup> ):	EA (MN):
01	1.5	223.9	29.9
02	4.5	223.5	29.8
03	7.3	222.8	29.8
04	9.9	221.8	29.8
05	12.3	220.6	29.7
06	14.6	219.3	29.6
07	16.7	217.8	29.6
08	18.5	216.4	29.5
09	20.2	214.9	29.4
10	21.7	213.6	29.3
11	23.0	212.3	29.3
12	24.1	211.2	29.2
13	25.0	210.2	29.2
14	25.7	209.5	29.1
15	26.1	209.0	29.1
16	26.3	208.7	29.1

**Table 10.2: Case Study B – 5x300 Beam - Segment properties for a UDL of 10 kN/m**

### 10.1.3 Case Study C: Fixed-fixed IPE 200

For the IPE 200 properties of the first 16 segments are provided at the load of 10 kN/m below.

Sect. #	NA (mm):	EI (MNm <sup>2</sup> ):	EA (MN):
01	-17.1	3.622	551.8
02	-13.7	3.689	554.6
03	-10.5	3.738	556.7
04	-7.6	3.772	558.1
05	-5.0	3.793	559.0
06	-2.6	3.805	559.5
07	-0.5	3.810	559.7
08	1.5	3.808	559.7
09	3.2	3.803	559.4
10	4.7	3.795	559.1
11	6.0	3.786	558.7
12	7.1	3.777	558.3
13	8.0	3.768	558.0
14	8.7	3.761	557.7
15	9.1	3.756	557.5
16	9.3	3.754	557.4

**Table 10.3: Case Study C - Fixed-fixed IPE 200 - Segment properties for a UDL of 10 kN/m**

#### 10.1.4 Case Study D: Fixed-fixed rectangular beam with variation in material properties

For this case study the inner and outer sections have the same properties calculated for them due to the elastic material mode used.

Sect. #	NA (mm):	$EI$ (kNm <sup>2</sup> ):	EA (MN):
01-08	-50.0	225.0	45.0
09-16	0.0	562.5	75.0

**Table 10.4: Case Study D - Fixed-fixed 5x300 beam - Segment properties for a UDL of 10 kN/m**

## 10.2 Validation studies from Chapter 6

The structural properties listed below have been used in the commercial finite element software discussed in Chapter 6. Each overall beam was discretised into 16 segments (except as explained for Case Study 1), and numbered as shown in Figure 4.12 and Figure 4.16. Due to the symmetrical nature of the beams only the properties of the first 8 segments are listed. Neutral axes (NAs) are measured from the bottom of sections. For the results plotted in the main body of this dissertation the initial elastic deflections that occur before tests start have been subtracted from total results calculated using the properties below.

### 10.2.1 Case Study 1: Uniformly heated simply-supported steel beam

The following tables provide results at 300°C and 600°C when the beam has been discretised into 4, 8 and 16 segments.

Sect. #:	NA (mm):	$EI_{\theta}$ (MNm <sup>2</sup> ):	EA (MN):	$M_{\theta}$ (kNm):	$N_{\theta}$ (kN):
01	129.8	3.30	293.1	0.0	2461.4
02	129.8	0.31	40.3	0.0	338.6

**Table 10.5: Case Study 1 - Segment properties for the 4 segment beam at 300°C**

Sect. #:	NA (mm):	$EI_{\theta}$ (MNm <sup>2</sup> ):	EA (MN):	$M_{\theta}$ (kNm):	$N_{\theta}$ (kN):
01	129.8	4.31	362.4	0.0	3043.6
02	129.8	1.70	172.1	0.0	1445.5
03	129.8	0.47	58.0	0.0	487.0
04	129.8	0.25	32.6	0.0	273.7

**Table 10.6: Case Study 1 - Segment properties for the 8 segment beam at 300°C**

Sect. #:	NA (mm):	$EI_{\theta}$ (MNm <sup>2</sup> ):	$EA$ (MN):	$M_{\theta}$ (kNm):	$N_{\theta}$ (kN):
01	129.8	4.37	366.6	0.0	3078.8
02	129.8	3.99	340.8	0.0	2862.5
03	129.8	2.44	230.7	0.0	1937.9
04	129.8	1.17	126.6	0.0	1063.6
05	129.8	0.60	72.4	0.0	607.6
06	129.8	0.37	47.5	0.0	398.7
07	129.8	0.27	35.6	0.0	298.6
08	129.8	0.24	31.0	0.0	260.4

**Table 10.7: Case Study 1 - Segment properties for the 16 segment beam at 300°C**

Sect. #:	NA (mm):	$EI_{\theta}$ (MNm <sup>2</sup> ):	$EA$ (MN):	$M_{\theta}$ (kNm):	$N_{\theta}$ (kN):
01	129.8	3.30	293.1	0.0	2461.4
02	129.8	0.31	40.3	0.0	338.6

**Table 10.8: Case Study 1 - Segment properties for the 4 segment beam at 600°C**

Sect. #:	NA (mm):	$EI_{\theta}$ (MNm <sup>2</sup> ):	$EA$ (MN):	$M_{\theta}$ (kNm):	$N_{\theta}$ (kN):
01	129.8	4.31	362.4	0.0	3043.6
02	129.8	1.70	172.1	0.0	1445.5
03	129.8	0.47	58.0	0.0	487.0
04	129.8	0.25	32.6	0.0	273.7

**Table 10.9: Case Study 1 - Segment properties for the 8 segment beam at 600°C**

Sect. #:	NA (mm):	$EI_{\theta}$ (MNm <sup>2</sup> ):	$EA$ (MN):	$M_{\theta}$ (kNm):	$N_{\theta}$ (kN):
01	129.8	4.37	366.6	0.0	3078.8
02	129.8	3.99	340.8	0.0	2862.5
03	129.8	2.44	230.7	0.0	1937.9
04	129.8	1.17	126.6	0.0	1063.6
05	129.8	0.60	72.4	0.0	607.6
06	129.8	0.37	47.5	0.0	398.7
07	129.8	0.27	35.6	0.0	298.6
08	129.8	0.24	31.0	0.0	260.4

**Table 10.10: Case Study 1 - Segment properties for the 16 segment beam at 600°C**

### 10.2.2 Case Study 2: Single span 1200x200 concrete slab

Properties of the concrete slab are provided at both 30 minutes and 60 minutes below.

Sect. #:	NA (mm):	$EI_{\theta}$ (MNm <sup>2</sup> ):	$EA$ (MN):	$M_{\theta}$ (kNm):	$N_{\theta}$ (kN):
01	145.8	5.04	1076.3	92.3	741.0
02	147.9	4.96	1116.2	91.3	719.5
03	149.5	4.86	1144.1	89.8	697.6
04	150.8	4.75	1160.2	87.9	675.4
05	151.6	4.66	1165.2	86.9	662.1
06	154.3	4.29	1139.1	82.0	608.9
07	156.4	4.00	1118.6	78.0	568.1
08	158.3	3.72	1087.9	73.9	528.1

**Table 10.11: Case Study 2 – 1200x200 concrete slab - Segment properties at 30 minutes**

Sect. #	NA (mm)	$EI_{\theta}$ (MNm <sup>2</sup> )	$EA$ (MN)	$M_{\theta}$ (kNm)	$N_{\theta}$ (kN)
01	143.8	4.27	876.4	106.4	956.0
02	146.3	4.25	917.6	106.5	934.8
03	149.3	4.11	937.1	104.8	893.7
04	152.0	3.87	927.7	101.0	837.7
05	154.7	3.63	919.6	97.0	782.6
06	157.2	3.40	913.1	92.6	728.9
07	159.4	3.16	895.9	87.7	675.7
08	161.5	2.94	880.2	82.6	623.9

**Table 10.12: Case Study 2 - 1200x200 concrete slab - Segment properties at 60 minutes**

Temperatures measured in the reinforcing steel, as reported by Ali et al (2008), are provided in the figure below.

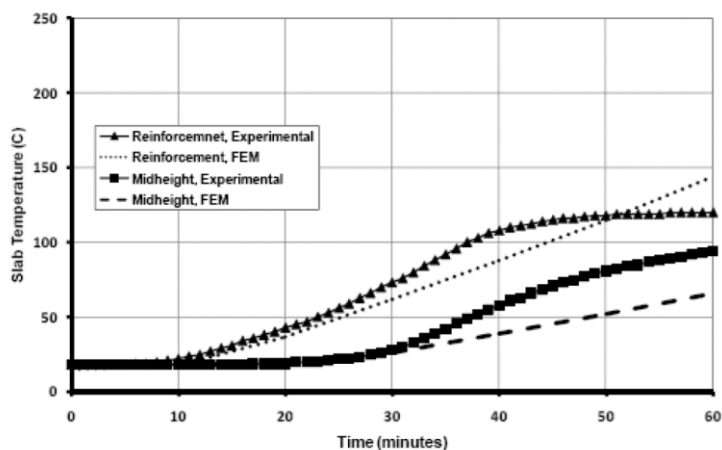


**Figure 10.1: Temperature data for the rebar of Case Study 2**

### 10.2.3 Case Study 3: Unprotected composite beams – “Test 15” and “Test 16”

For Test 15 and 16 segment properties at various times have been provided. Beams are symmetric about their midspan so only the properties for the first half of beams have been included.

#### Test 15

Sect. #:	NA (mm):	$EI_{\theta}$ (MNm <sup>2</sup> ):	EA (MN):	$M_{\theta}$ (kNm):	$N_{\theta}$ (kN):
01	173.3	9.49	724.4	177.5	3372.2
02	211.5	13.70	854.0	277.0	3265.1
03	241.3	14.75	956.8	314.6	3031.6
04	253.1	14.52	1003.5	318.2	2910.8
05	262.0	14.09	1042.5	316.0	2810.4
06	268.6	13.58	1072.4	310.7	2724.4
07	271.5	13.30	1086.3	307.2	2685.3
08	271.6	13.28	1086.1	306.8	2683.5

Table 10.13: Case Study 3 – Test 15 – Segment properties at 15 minutes

Sect. #:	NA (mm):	$EI_{\theta}$ (MNm <sup>2</sup> ):	EA (MN):	$M_{\theta}$ (kNm):	$N_{\theta}$ (kN):
01	230.0	2.27	370.7	52.9	2395.3
02	290.2	3.46	539.9	135.3	2205.3
03	304.3	3.71	639.0	155.8	2168.6
04	308.8	3.70	679.3	159.6	2142.9
05	311.9	3.63	710.1	160.6	2115.5
06	313.8	3.54	732.3	159.7	2092.5
07	314.6	3.49	742.7	158.8	2077.7
08	314.6	3.48	742.2	158.6	2076.6

Table 10.14: Case Study 3 – Test 15 – Segment properties at 30 minutes

Sect. #:	NA (mm):	$EI_{\theta}$ (MNm <sup>2</sup> ):	EA (MN):	$M_{\theta}$ (kNm):	$N_{\theta}$ (kN):
01	225.9	1.56	194.0	36.4	1452.4
02	311.9	2.41	395.2	113.8	1484.2
03	321.9	2.43	479.4	124.2	1530.7
04	325.4	2.34	507.4	123.7	1500.7
05	327.9	2.22	525.1	120.1	1447.9
06	334.1	1.85	496.0	99.7	1136.4
07	340.0	1.47	442.2	77.3	823.8
08	340.3	1.45	439.1	76.1	809.1

Table 10.15: Case Study 3 – Test 15 – Segment properties at 40 minutes

**Test 16**

Sect. #:	NA (mm):	$EI_{\theta}$ (MNm <sup>2</sup> ):	EA (MN):	$M_{\theta}$ (kNm):	$N_{\theta}$ (kN):
01	152.7	12.09	908.6	116.4	3261.9
02	161.6	11.46	888.5	116.0	3105.2
03	236.5	19.76	1207.2	277.1	2822.4
04	251.3	19.29	1283.6	284.9	2695.2
05	261.1	18.32	1333.8	281.4	2585.4
06	268.8	17.18	1370.1	273.1	2479.9
07	271.9	16.58	1381.1	267.5	2428.4
08	271.9	16.58	1381.1	267.5	2428.4

**Table 10.16: Case Study 3 – Test 16 – Segment properties at 9 minutes**

Sect. #:	NA (mm):	$EI_{\theta}$ (MNm <sup>2</sup> ):	EA (MN):	$M_{\theta}$ (kNm):	$N_{\theta}$ (kN):
01	167.0	8.62	666.0	136.2	3594.0
02	242.9	10.26	770.0	228.1	2851.8
03	274.3	10.44	930.3	259.1	2676.9
04	284.0	9.83	986.2	255.2	2570.3
05	290.6	9.17	1026.5	246.9	2470.7
06	295.2	8.49	1051.1	235.7	2379.9
07	297.0	8.14	1061.0	229.4	2335.2
08	297.0	8.14	1061.0	229.4	2335.2

**Table 10.17: Case Study 3 – Test 16 – Segment properties at 15 minutes**

Sect. #:	NA (mm):	$EI_{\theta}$ (MNm <sup>2</sup> ):	EA (MN):	$M_{\theta}$ (kNm):	$N_{\theta}$ (kN):
01	212.2	3.05	366.3	62.0	2361.0
02	298.7	4.77	660.9	176.0	2178.2
03	308.4	4.49	757.9	180.0	2181.1
04	311.8	4.19	785.6	174.7	2112.8
05	313.7	3.79	789.5	163.9	2007.0
06	322.8	2.58	636.1	110.8	1187.5
07	328.3	1.32	434.5	55.0	543.0
08	328.3	1.32	434.5	55.0	543.0

**Table 10.18: Case Study 3 – Test 16 – Segment properties at 23 minutes**

#### 10.2.4 Case Study 4: Munich Test 2

For the Munich Test 2 case study properties for all beams investigated are provided below at 40 minutes.

Sect. #:	NA (mm):	$EI_{\theta}$ (MNm <sup>2</sup> ):	EA (MN):	$M_{\theta}$ (kNm):	$N_{\theta}$ (kN):
01	155.7	4.94	777.2	58.9	2077.1
02	157.1	5.03	791.9	61.1	2090.7
03	158.5	5.13	806.1	63.5	2101.1
04	160.7	5.20	822.6	66.0	2107.2
05	165.0	5.08	834.0	67.7	2077.7
06	169.8	4.98	853.3	70.2	2052.5
07	173.7	4.95	873.2	72.8	2034.8
08	190.0	6.00	1035.9	99.8	2038.5

**Table 10.19: Case Study 4 – Munich 2 – Edge left - Segment properties**

Sect. #:	NA (mm):	$EI_{\theta}$ (MNm <sup>2</sup> ):	EA (MN):	$M_{\theta}$ (kNm):	$N_{\theta}$ (kN):
01	133.0	3.35	476.9	37.7	1847.8
02	218.6	5.99	1175.4	140.9	1868.8
03	230.0	5.39	1056.4	137.7	1758.8
04	234.7	4.73	1658.1	127.4	1618.9
05	231.5	4.08	1021.3	111.2	1396.7
06	234.8	3.74	1021.4	105.1	1292.4
07	238.4	3.35	987.3	95.9	1136.8
08	240.2	3.15	964.1	90.8	1055.2

**Table 10.20: Case Study 4 – Munich 2 – Intermediate - Segment properties**

Sect. #:	NA (mm):	$EI_{\theta}$ (MNm <sup>2</sup> ):	EA (MN):	$M_{\theta}$ (kNm):	$N_{\theta}$ (kN):
01	155.6	5.02	790.1	55.1	2024.4
02	156.8	5.10	802.5	57.0	2034.7
03	158.2	5.19	817.9	59.1	2047.9
04	159.6	5.29	832.3	61.3	2058.0
05	161.3	5.36	846.7	63.5	2064.0
06	164.0	5.31	855.9	64.9	2048.7
07	166.6	5.25	865.1	66.2	2034.5
08	167.8	5.23	870.2	66.8	2028.8

**Table 10.21: Case Study 4 – Munich 2 – Right left - Segment properties**

For the top and bottom beams the asymmetrical loading results in the overall beams not being symmetrical. Beams have been analysed still considering 8 different segment properties, except that properties now cover two sections at a time.



Sect. #:	NA (mm):	$EI_{\theta}$ (MNm <sup>2</sup> ):	EA (MN):	$M_{\theta}$ (kNm):	$N_{\theta}$ (kN):
01-02	200.8	15.45	1236.3	83.8	2835.1
03-04	205.9	16.17	1297.0	93.8	2885.3
05-06	211.8	17.03	1370.8	106.3	2934.5
07-08	213.8	17.33	1398.2	110.9	2950.7
09-10	212.9	17.19	1385.3	108.8	2942.8
11-12	209.2	16.65	1338.0	100.7	2914.0
13-14	204.6	15.99	1281.4	91.2	2873.1
15-16	200.4	15.40	1232.0	83.1	2830.9

**Table 10.22: Case Study 4 – Munich 2 – Edge top left - Segment properties**

Sect. #:	NA (mm):	$EI_{\theta}$ (MNm <sup>2</sup> ):	EA (MN):	$M_{\theta}$ (kNm):	$N_{\theta}$ (kN):
01-02	193.0	13.05	1037.0	114.8	3133.9
03-04	193.7	13.14	1043.5	116.4	3140.7
05-06	194.6	13.24	1051.5	118.1	3150.5
07-08	195.0	13.29	1055.1	119.0	3153.9
09-10	195.0	13.30	1055.6	119.2	3154.0
11-12	194.7	13.26	1052.4	118.4	3150.7
13-14	194.0	13.17	1046.0	116.9	3144.0
15-16	193.0	13.06	1037.3	114.9	3134.0

**Table 10.23: Case Study 4 – Munich 2 – Edge top right - Segment properties**

Sect. #:	NA (mm):	$EI_{\theta}$ (MNm <sup>2</sup> ):	EA (MN):	$M_{\theta}$ (kNm):	$N_{\theta}$ (kN):
01-02	200.2	14.97	1198.3	94.4	2978.3
03-04	205.0	15.62	1252.7	104.3	3026.3
05-06	210.4	16.40	1318.6	116.7	3073.3
07-08	212.4	16.67	1343.8	121.3	3088.9
09-10	211.5	16.55	1331.9	119.2	3081.3
11-12	208.2	16.07	1291.4	111.4	3055.9
13-14	203.9	15.48	1240.9	102.0	3017.4
15-16	200.0	14.94	1196.8	94.0	2978.0

**Table 10.24: Case Study 4 – Munich 2 – Edge bottom left - Segment properties**

Sect. #:	NA (mm):	$EI_{\theta}$ (MNm <sup>2</sup> ):	$EA$ (MN):	$M_{\theta}$ (kNm):	$N_{\theta}$ (kN):
01-02	193.5	14.46	1142.3	81.5	2647.6
03-04	194.5	14.59	1152.2	83.2	2656.6
05-06	195.4	14.72	1161.8	84.9	2665.4
07-08	195.9	14.79	1166.4	85.8	2668.5
09-10	196.1	14.82	1169.1	86.2	2671.2
11-12	195.5	14.74	1163.1	85.3	2665.6
13-14	194.7	14.63	1155.2	83.7	2659.5
15-16	193.5	14.46	1142.6	81.6	2647.7

**Table 10.25: Case Study 4 – Munich 2 – Edge bottom right- Segment properties**

## 11 References

- Abu, A.K. & Burgess, I.W., 2010. The effect of edge support on tensile membrane action of composite slabs in fire. In E. Batista, P. Vellasco, & L. de Lima, eds. *SDSS Rio 2010*. Rio de Janeiro, pp. 21–32.
- Alexander, M.G., 1985. Prediction of elastic modulus for design of concrete structures. *Civ Engr S Afr*, 27(6), pp.313–324.
- Ali, F., Nadjai, A. & Abu-tair, A., 2008. Experimental and Numerical Study on Performance of Concrete Slabs Subjected to Severe Fire. In *IAFSS NINTH INT. SYMP. FIRE SAFETY SCIENCE*, pp. 1255–1266.
- Ali, F., Nadjai, A. & Abu-Tair, A., 2010. Explosive spalling of normal strength concrete slabs subjected to severe fire. *Materials and Structures*, 44(5), pp.943–956. Available at: <http://www.springerlink.com/index/10.1617/s11527-010-9678-5>.
- Al-Jabri, K.S. et al., 2005. Moment – rotation – temperature curves for semi-rigid joints. *Journal of Constructional Steel Research*, 61, pp.281–303.
- Al-Jabri, K.S., 1999. *The behaviour of steel and composite beam-to-column connections in fire*. University of Sheffield.
- Almand, K.H., 2012. *Structural Fire Resistance Experimental Research - Priority Needs of U.S. Industry*, Quincy, MA: The Fire Protection Research Foundation.
- Anderson, K., 2011. *The effects of connections on structural behaviour in fire*. University of Edinburgh.
- ANSYS, 2016. ANSYS,
- ASFP, 2014. *The Yellow Book - Fire protection for structural steel in buildings 5th Edition* 5th ed., Hampshire, UK: Association for Specialist Fire Protection.
- Bailey, C.G., 2004a. Membrane action of slab/beam composite floor systems in fire. *Engineering Structures*, 26(12), pp.1691–1703.
- Bailey, C.G., 1995. *Simulation of the structural behaviour of steel-framed buildings in fire*. University of Sheffield.
- Bailey, C.G., 2004b. Structural fire design: Core or specialist design? *The Structural Engineer*, 82(May), pp.34–38.
- Bailey, C.G., 2002. Structural fire design of unprotected steel beams supporting composite floor slabs. In *II International Conference on Steel Construction*. Sao Paolo.
- Bailey, C.G. & Moore, D.B., 2000a. The structural behaviour of steel frames with composite floorslabs subject to fire: Part 1: Theory. *Structural Engineer*, 78(7), pp.19–27.
- Bailey, C.G. & Moore, D.B., 2000b. The structural behaviour of steel frames with composite floorslabs subject to fire: Part 2: Design. *Structural Engineer*, 78, pp.28–33.
- Bailey, C.G. & Toh, W.S., 2007. Small-scale concrete slab tests at ambient and elevated temperatures. *Engineering Structures*, 29(10), pp.2775–2791. Available at: <http://linkinghub.elsevier.com/retrieve/pii/S0141029607000466> [Accessed December 15, 2014].
- Bankoff, B., Lubken, U. & Sand, J., 2012. *Flammable Cities: Urban conflagration and the making of the modern world*, Madison, WI: University of Wisconsin Press.
- Bapat, A., 2009. *Influence of bridge parameters on finite element modeling of slab on girder bridges*. Virginia Polytechnic Institute. Available at: <http://scholar.lib.vt.edu/theses/available/etd-12132009-152410/>.
- Bathe, K.J., 2006. *Finite Element Procedures*, USA: Bathe, K.J.
- Beitel, J. & Iwankiw, N., 2008. Analysis of Needs and Existing Capabilities for Full-Scale Fire Resistance

- Testing. *Nist Gcr 02-843-1*, 1, p.86. Available at: <http://www.bfrl.nist.gov/866/pubs/NISTGCR02-843.pdf>.
- Benedetti, A. & Mangoni, E., 2007. Analytical prediction of composite beams response in fire situations. *Journal of Constructional Steel Research*, 63(2), pp.221–228.
- Bihina, G., Zhao, B. & Boucha??r, A., 2013. Behaviour of composite steel-concrete cellular beams in fire. *Engineering Structures*, 56, pp.2217–2228. Available at: <http://dx.doi.org/10.1016/j.engstruct.2013.09.002>.
- Bisby, L., Gales, J. & Maluk, C., 2013. A contemporary review of large-scale non-standard structural fire testing. *Fire Science Reviews*, 2(1), pp.1–27. Available at: <http://www.firesciencereviews.com/content/2/1/1>.
- Block, F.M. et al., 2013. Principles of a component-based connection element for the analysis of steel frames in fire. *Engineering Structures*, 49, pp.1059–1067. Available at: <http://dx.doi.org/10.1016/j.engstruct.2012.07.025>.
- Block, F.M. et al., 2007. The development of a component-based connection element for endplate connections in fire. , 42, pp.498–506.
- BSI, 2009. *BS 476: Fire tests on building materials and structures*, London: British Standards Institute.
- BSI, 2008. *BS 9999:2008 - Code of practice for fire safety in the design, management and use of buildings*, London: British Standards Institute.
- BSI, 2002a. *BS EN 1990:2002 - Eurocode 0 - Basis of structural design*, London: British Standards Institute.
- BSI, 2002b. *BS EN 1991-1-2: Eurocode 1 - Actions on structures part 1 - basis of design*, London: British Standards Institute.
- BSI, 2004. *BS EN 1992-1-1:2004 - Eurocode 2: Design of concrete structures - Part 1-1: General rules and rules for buildings*, London: British Standards Institute.
- BSI, 2005a. *BS EN 1992-1-2:2005: Eurocode 2: Design of concrete structures – Part 1-2: General – Structural fire design*, London: British Standards Institute.
- BSI, 2005b. *BS EN 1993-1-2:2005 Eurocode 3 - Design of steel structures, part 1.2: general rules—structural fire design*, London: British Standards Institute.
- BSI, 2011. *BS EN 1994-1-1:2004 - Eurocode 4: Design of composite steel and concrete structures - Part 1-1: General rules and rules for buildings*, London: British Standards Institute.
- BSI, 2005c. *BS EN 1994-1-2:2005: Eurocode 4: Design of composite steel and concrete structures - Part 1-2: General - Structural Fire Design*, London: British Standards Institute.
- Buchanan, A.H., 2001. *Structural Design for Fire Safety*, New York: Wiley.
- Budny, I. & Giuliani, L., 2010. A comparison between prescriptive- and performance-based approaches in fire safety design of structures. In *Handling Exceptions in Structural Engineering*. Rome: La Sapienza, pp. 1–20.
- Burgess, I.W. et al., 2015. *Vulcan*, Vulcan Solutions.
- Burgess, I.W., El Rimawi, J. & Plank, R.J., 1991. Studies of the behaviour of steel beams in fire. *J. Constr Steel Research*, 19, pp.285–312.
- C&CI, 2001. *Fulton’s Concrete Technology* 8th ed., Midrand: Concrete & Cement Institute.
- Cadorin, J.-F. & Franssen, J.-M., 2003. A tool to design steel elements submitted to compartment fires—OZone V2. Part 1: pre- and post-flashover compartment fire model. *Fire Safety Journal*, 38, pp.395–427.
- Cai, Y., Paik, J.K. & Atluri, S.N., 2009. Large Deformation Analyses of Space-Frame Structures , with Members of arbitrary Cross-Section , Using Explicit Tangent Stiffness Matrices , Based on a von Karman Type Nonlinear Theory in Rotated Reference Frames. *Computer Modeling in Engineering & Sciences*, 53(2), pp.117–145.

- CEC, 1988. Construction Product Directive, dated 21.12.1988. *Official Journal of the European Commission*, L40(12), p.89/106/EEC.
- Cedeno, G. a., Varma, A.H. & Gore, J., 2011. Predicting the Standard Fire Behavior of Composite Steel Beams. *Composite Construction in Steel and Concrete VI*, 41142(FEBRUARY 2011), pp.642–656. Available at: [http://ascelibrary.org/doi/abs/10.1061/41142\(396\)53](http://ascelibrary.org/doi/abs/10.1061/41142(396)53).
- Chan, T. & Chan, J., 1999. The use of eccentric beam elements in the analysis of slab-on-girder bridges. *Structural Engineering and Mechanics*, 8(1), pp.85–102.
- Chen, L. & Wang, Y.C., 2012. Efficient modelling of large deflection behaviour of restrained steel structures with realistic endplate beam/column connections in fire. *Engineering Structures*, 43, pp.194–209. Available at: <http://dx.doi.org/10.1016/j.engstruct.2012.05.030>.
- CISC, 2010. *CISC Commentary on CSA S16-09 Annex K Structural Design for Fire Conditions*, Ontario: Canadian Iron & Steel Institute.
- Clifton, G.C., 2001. *Collapse of the World Trade Centre Towers*, HERA.
- Clifton, G.C., 2013. Cost-effective fire resistant multi-storey steel structures. In *SteelFuture*. Johannesburg: SAISC.
- Clifton, G.C., 2016. *Fire Engineering Design of Multi-storey Steel and Composite Steel/Concrete Structures; Recommendations and Questions - Draft Version 2016/06/30*, Auckland.
- Clifton, G.C., 1996. *HEAR Report R4-83: Fire Models for Large Firecells*, Manakua City: HERA.
- Clifton, G.C., 2006. *R4-131:2006 Design of Composite Steel Floor Systems for Severe Fires*, HERA.
- Clifton, G.C. & Abu, A., 2014. *Modifications to the Application of the SPM:2006 Edition and Application to C/VM2*, Auckland.
- Coates, R.C., Coutie, M.G. & Kong, F.K., 1990. *Structural Analysis* 3rd ed., London: CRC Press.
- Cook, R.D. et al., 2001. *Concepts and Applications of Finite Element Analysis* 4th ed., Madison, WI: John Wiley & Sons.
- Crisfield, M.A., 1990. A consistent co-rotational formulation for non-linear, three-dimensional, beam-elements. *Computer Methods in Applied Mechanics and Engineering*, 81, pp.131–150.
- Crisfield, M. a. & Moita, G.F., 1996. A unified co-rotational framework for solids, shells and beams. *International Journal of Solids and Structures*, 33(1986), pp.2969–2992.
- CSA, 2009. *CSA S16-09 Design of steel structures*, Toronto: Canadian Standards Association.
- Dai, X. et al., 2016. Implementation of a new design travelling fire model for global structural analysis. In *9th International Conference on Structures in Fire*. Princeton, pp. 959–966.
- Dassault Systèmes, 2013. *Abaqus*, Providence, RI, USA: Dassault Systèmes.
- Deeny, S., 2010. *The implications of compartment fire non-uniformity for the membrane action of reinforced concrete slabs*. Edinburgh University. Available at: <http://hdl.handle.net/1842/5077>.
- Drysdale, D.D., 2011. *An Introduction to Fire Dynamics* 3rd ed., Chichester: John Wiley & Sons.
- ECCS, 2001. *Model Code on Fire Engineering*, Berne: European Convention for Constructional Steelwork.
- European Joint Research Program, 1999. *The behaviour of multi-storey steel framed buildings in fire*, Rotherham: British Steel plc.
- fib, 2010a. *Model Code 2010 - First Complete Draft - Volume 1* J. C. Walraven, ed., Lausanne: Federation Internationale du Beton (fib).
- fib, 2010b. *Model Code 2010 - First Complete Draft - Volume 2* J. C. Walraven, ed., Lausanne: Federation Internationale du Beton (fib).
- Fillo, L. & Benko, V., 2011. Example 5: Shear wall in office building. In *Design examples for strut-and-tie*

*models*. Lausanne: fib.

- Flint, G. et al., 2013. Recent Lessons Learned in Structural Fire Engineering for Composite Steel Structures. *Fire Technology*, 49(3), pp.767–792.
- Franssen, J.-M., 2005. SAFIR. A Thermal/Structural Program Modelling Structures under Fire. *Engineering Journal, AISC*, 42(3), pp.143–158.
- Franssen, J.M. & Vila Real, P.M.M., 2010. *Fire Design for Steel Structures*, Berlin: European Convention for Constructional Steelwork.
- Gales, J., Maluk, C. & Bisby, L., 2012. Large- scale structural fire testing- How did we get here, Where are we, and where are we going? In *15th International conference on experimental mechanics: Fire symposium*. pp. 1–22.
- Gao, W.Y., Dai, J.G. & Teng, J.G., 2014. Simple Method for Predicting Temperatures in Reinforced Concrete Beams Exposed to a Standard Fire. *Advances in Structural Engineering*, 17(4), pp.573–590.
- Gernay, T.G. & Franssen, J.M., 2012. A formulation of the Eurocode 2 concrete model at elevated temperature that includes an explicit term for transient creep. *Fire Safety Journal*, 51, pp.1–9.
- Gillie, M., Usmani, A.S. & Rotter, J.M., 2001. A structural analysis of the first Cardington test. *Journal of Constructional Steel Research*, 57(6), pp.581–601.
- Gimena, L., Gimena, F.N. & Gonzaga, P., 2008. Structural analysis of a curved beam element defined in global coordinates. *Engineering Structures*, 30(11), pp.3355–3364. Available at: <http://www.sciencedirect.com/science/article/pii/S0141029608002022> [Accessed February 5, 2015].
- Grünberg, J. & Göhlmann, J., 2013. *BetonKalender: Concrete Structures for Wind Turbines*, Berlin: Ernst & Sohn.
- Gu, T., 2016. *Effect of Edge Beam Deformations on the Slab Panel Method*. University of Canterbury.
- Gurley, C., 2008. Structural Design for Fire in Tall Buildings. *Practice Periodical on Structural Design and Construction*, 13(2), pp.93–97.
- Hozjan, T. et al., 2011. Fire analysis of steel-concrete composite beam with interlayer slip. *Computers and Structures*, 89(1–2), pp.189–200.
- Huang, Z., Burgess, I. & Plank, R., 2004. 3D Modelling of Beam-columns with General Cross-sections in Fire. In *Third International Workshop on Structures in Fire*.
- Huang, Z., Burgess, I.W. & Plank, R.J., 2003. Modeling Membrane Action of Concrete Slabs in Composite Buildings in Fire. II: Validations. *Journal of Structural Engineering*, 129(8), pp.1103–1112.
- Huang, Z., Burgess, I.W. & Plank, R.J., 1999. The influence of shear connectors on the behaviour of composite steel-framed buildings in fire. *Journal of Constructional Steel Research*, 51(3), pp.219–237.
- Huang, Z., Burgess, I.W. & Plank, R.J., 2000. Three-dimensional analysis of composite steel-framed buildings in fire. *Journal of Structural Engineering*, 126, pp.389–397.
- ISO, 1999. *ISO 834 Fire-resistance tests - Elements of building construction. Parts 1-12*, Geneva: International Organization for Standardization.
- Iu, C.K. & Chan, S.L., 2004. A simulation-based large deflection and inelastic analysis of steel frames under fire. *Journal of Constructional Steel Research*, 60, pp.1495–1524.
- Iu, C.K., Chan, S.L. & Zha, X.X., 2005. Nonlinear pre-fire and post-fire analysis of steel frames. *Engineering Structures*, 27, pp.1689–1702.
- Izzuddin, B., 2012. *ADAPTIC: User Manual*, London.
- JCSS, 2001. *Probabilistic Model Code - 12th Draft Edition*, Bygning, Denmark.
- Jiang, J., Usmani, A. & Li, G., 2014. Modelling of Steel-Concrete Composite Structures in Fire Using OpenSees. *Advances in Structural Engineering*, 17(2), pp.249–264.



- Kassem, A.T., Hassan, A.F. & Seddeek, M.M., 2009. Behavior of Composite Steel-Concrete Girders in Fire Condition. In *13 Int. Conf. on Aerospace Sciences & Aviation Technology*. Cairo, pp. 1–12.
- Kennedy, G. & Goodchild, C.H., 2004. *Practical yield line design*, Camberley: The Concrete Centre.
- Kodur, V., Dwaikat, M. & Dwaikat, M., 2008. High-temperature properties of concrete for fire resistance modeling of structures. *ACI Materials Journal*, 105(5), pp.517–527.
- Lamont, S. et al., 2006. Behavior of structures in fire and real design - a case study.pdf. *Journal of Fire Protection Engineering*, 16, pp.5–34.
- Lamont, S., 2001. *The Behaviour of Multi-Storey Composite Steel Framed Structures in Response to Compartment Fires*. University of Edinburgh.
- Law, A., 2016. The role of modelling in structural fire engineering design. *Fire Safety Journal*, 80, pp.89–94. Available at: <http://www.sciencedirect.com/science/article/pii/S0379711215300345>.
- Lennon, T., 2011. *Structural Fire Engineering*, ICE Publishing.
- Liao, F. & Huang, Z., 2015. An extended finite element model for modelling localised fracture of reinforced concrete beams in fire. *Computers & Structures*, 152, pp.11–26. Available at: <http://linkinghub.elsevier.com/retrieve/pii/S0045794915000449>.
- McAllister, T.P. et al., 2013. Overview of the Structural Design of World Trade Center 1, 2, and 7 Buildings. *Fire Technology*, 49, pp.587–613.
- Mensinger, M. et al., 2012. *Nutzung der Membran-wirkung von Verbundtrager-Decken-Systemen im Brandfall*, DAST-Forschungsbericht.
- Nadjai, A. et al., 2011. Full-scale fire test on a composite floor slab incorporating long span cellular steel beams. *Structural Engineer*, 89(21), pp.18–25.
- Nadjai, A. et al., 2007. Performance of cellular composite floor beams at elevated temperatures. *Fire Safety Journal*, 42(6–7), pp.489–497.
- Nadjai, A., Vassart, O. & Zhao, B., 2012. *MACS+ Engineering Background*, Arcelor-Mittal.
- Naili, E. et al., 2011. Experimental and Numerical Modelling of Cellular Beams with Circular and Elongated Web Openings at Elevated Temperatures. *Journal of Structural Fire Engineering*, 2(4), pp.289–300.
- Najjar, S.R., 1994. Three-dimensional analysis of steel frames and subframes in fire. , (March). Available at: <http://theses.whiterose.ac.uk/1861/>.
- Najjar, S.R. & Burgess, I.W., 1996. A nonlinear analysis for three-dimensional steel frames in fire conditions. *Engineering Structures*, 18(1), pp.77–89.
- NIST, 2005. *Final report on the collapse of the World Trade Center* Final report on the collapse of the World Trade Center. Rep. No. NCSTAR1, Washington DC.
- O’Loughlin, E. & Lay, S., 2015. Structural fire resistance: Rating system manifests crude, inconsistent design. *Case Studies in Fire Safety*, 3, pp.36–43. Available at: <http://www.sciencedirect.com/science/article/pii/S2214398X15000035>.
- Pettersson, O., Magnusson, S.E. & Thor, J., 1976. *Fire Engineering Design of Steel Structures*, Stockholm: Swedish Institute of Steel Construction.
- Prokon SCL, 2015. *Prokon Frame*, Pretoria: Prokon Software Consultants Ltd.
- Ranzi, G. & Bradford, M.A., 2007. Composite beams with both longitudinal and transverse partial interaction subjected to elevated temperatures. *Engineering Structures*, 29(10), pp.2737–2750.
- Rein, G., 2013. 9/11 World Trade Center Attacks: Lessons in Fire Safety Engineering After the Collapse of the Towers. *Fire Technology*, 49(3), pp.583–585.
- Retief, J. & Dunaiski, P., 2009. The Limit States Basis of Structural Design for SANS 10160-1. In J. Retief & P. Dunaiski, eds. *Background to SANS 10160*. Stellenbosch: SUN MeDIA, pp. 25–55.

- Rotter, J.M. et al., 1999. Structural performance of redundant structures under local fires. , 99, pp.2–1999. Available at: [http://www.civ.ed.ac.uk/research/fire/public\\_html/Cardington/TM1.pdf](http://www.civ.ed.ac.uk/research/fire/public_html/Cardington/TM1.pdf).
- Saab, H. a. & Nethercot, D. a., 1991. Modelling steel frame behaviour under fire conditions. *Engineering Structures*, 13, pp.371–382.
- SABS, 2000. *SANS 10100-1:2000 - The structural use of concrete - Part 1: Design 2.2.*, South African Bureau of Standards.
- SABS, 2011a. *SANS 10160: Basis of structural design and actions for buildings and industrial structures*, Pretoria: South African Bureau of Standards.
- SABS, 2011b. *SANS 10162-1 : 2011 The structural use of steel Part 1 : Limit-states design of hot-rolled steelwork*, Pretoria: South African Bureau of Standards.
- SABS, 2016. *SANS 10162-1 : 2016 SOUTH AFRICAN NATIONAL STANDARD - The structural use of steel Part 1 : Limit-states design of hot-rolled steelwork*, Pretoria: SABS.
- SABS, 2011c. *SANS 10400:2011 The application of the National Building Regulations* SABS, ed., Pretoria: SABS.
- SAISC, 2005. *Southern African Steel Construction Hand-book "The Red Book,"* Johannesburg: Southern African Institute of Steel Construction.
- Sanad, A. et al., 2000. Composite beams in large buildings under fire — numerical modelling and structural behaviour. *Fire Safety Journal*, 35(3), pp.165–188.
- SCI, 1991. *Investigation of the Broadgate Phase 8 fire*, Ascot.
- SFPE, 2008. *The SFPE Handbook of Fire Protection Engineering* 4th ed. P. J. DiNenno et al., eds., Massachusetts: NFPA.
- Shahabi, S.E.M. et al., 2016. Numerical analysis of channel connectors under fire and a comparison of performance with different types of shear connectors subjected to fire. *Steel and Composite Structures*, 20(3), pp.651–669. Available at: <http://koreascience.or.kr/journal/view.jsp?kj=KJKHEW&py=2016&vnc=v20n3&sp=651>.
- Stadler, M., 2012. Design of Composite Slab Systems in Case of Fire Using Simplified Finite Element Analyses.
- Stern-Gottfried, J. & Rein, G., 2012a. Travelling fires for structural design-Part I: Literature Review. *Fire Safety Journal*, 54, pp.96–112. Available at: <http://dx.doi.org/10.1016/j.firesaf.2012.06.003>.
- Stern-Gottfried, J. & Rein, G., 2012b. Travelling fires for structural design-Part II: Design methodology. *Fire Safety Journal*, 54, pp.96–112. Available at: <http://dx.doi.org/10.1016/j.firesaf.2012.06.011>.
- Stramandinoli, R.S. & La Rovere, H.L., 2008. An efficient tension-stiffening model for nonlinear analysis of reinforced concrete members. *Engineering Structures*, 30(7), pp.2069–2080.
- Su, M. & Zhang, B., 2013. *Strength and Stability of Slab Panel Support Beams: Project 156*. University of Auckland.
- Tata Steel & BCSA, 2013. *Steel Construction: Fire Protection*, Tata Steel & British Constructional Steel Association (BCSA).
- Tesar, C., 2008. *Zum Tragverhalten von Verbunddeckensystemen im Brandfall*. ETH Zürich.
- Thomson, G. & Preston, R.R., 1996. Towards harmonized standard fire resistance testing. *Fire Safety Journal*, 27(2), pp.91–112.
- Tian, Y., 2014. *The Tensile Membrane Action of Non-orthogonal Composite Slabs at Elevated Temperatures*. University of Sheffield.
- TNO DIANA, 2016. *DIANA*, TNO Delft.
- Twilt, L., 1994. Fires in Buildings: The Facts. In *Fire Safe Steel Structures*. Luxembourg: ECCS, pp. 1–11.



- Usmani, A.S. et al., 2000. *PIT Project: Behaviour of steel framed structures under fire conditions - Main Report*, Edinburgh.
- Wainman, D.E. & Kirby, B.R., 1988. *Compendium of UK Standard Fire Test Data (Unprotected Structural Steel - 1)*, Rotherham.
- Walls, R.S. & Viljoen, C., 2016. A comparison of technical and practical aspects of Eurocode 3-1-1 and SANS 10162-1 hot-rolled steelwork design codes. *Civ Engr S Afr*, 58(1), pp.16–25.
- Wang, Y.C. et al., 2012. *Performance-Based Fire Engineering of Structures* 1st ed., Spon Press.
- Wickstrom, U., 1986. *A very simple method for estimating temperature in fire exposed concrete structures*, Swedish National Testing Institute.
- Wickström, U., 1985. Application of the standard fire curve for expressing natural fires for design purposes. In T. Harmathy, ed. *Fire Safety: Science and Engineering*. Philadelphia: American Society for Testing and Materials, pp. 145–189.
- Wu, C., Li, T. & Clifton, G.C., 2012. *Testing of Slab Panel Method Program in Severe Fires*. University of Auckland.
- Yang, Y. & McGuire, W., 1986. Stiffness Matrix for Geometric Nonlinear Analysis. *Journal of Structural Engineering*, 112(4), pp.853–877.
- Zilch, K. & Zehetmeier, G., 2010. *Bemessung im konstruktiven Betonbau: Nach DIN 1045-1 (Fassung 2008) und EN 1992-1-1 (Eurocode 2)*., Springer Verlag.